A THESIS SUBMITTED FOR THE DEGREE OF

DOCTOR OF PHILOSOPHY

NUFFIELD DEPARTMENT OF OBSTETRICS AND GYNAECOLOGY

UNIVERSITY OF OXFORD

DEVELOPMENT OF MODELS AND METHODS TO ASSESS THE EFFICACY OF ANTI-CANCER DRUGS TARGETED TO THE MITOCHONDRIA

MICHELLE POTTER

MANSFIELD COLLEGE

TRINITY TERM 2014

'The most exciting phrase to hear in science, the one that heralds new discoveries, is not "Eureka!" ("I found it!") but rather "hmm...that's funny..."'

-- Isaac Asimov

Dedication

I am dedicating this thesis to Margaret Wallace who sadly lost her battle with cancer after five long years. Her courage, strength and determination to beat the disease were inspiring. During the difficult times in my research, she was always so encouraging despite everything that she was going through. Her passing has left an emptiness that can never be filled. Sleep tight Peggy xxxxxx

Acknowledgements

I really cannot believe I am writing my acknowledgements. The last three and a half years have been filled with highs and lows and at times I doubted that the end would ever arrive. I have thoroughly enjoyed my PhD, the good the bad and the ugly, but I am glad to be looking at it in the rear view mirror. I never expected it to be easy but I was a little under prepared for the emotional rollercoaster it turned out to be. Many people contributed to the success of this project in a variety of ways.

First and foremost, I would like to thank my supervisor Dr Karl Morten for his never-ending support and encouragement. I really could not have asked for a better mentor. His door was always open when it came to answering questions and getting advice.

From the Nuffield Department of Obstetrics and Gynaecology I need to extend a huge thank you to Bec and Jen for their expert flow cytometry advice and guidance. Thanks also to Tiff and Dionne who were always there when I needed a rant. I also

need to thank Dr. Tim Claridge, Department of Chemistry, for help with the NMR work and Dr. Andrei Tarasov, OCDEM, for the fluorescence imaging.

Thanks to the Williams Fund for supporting me through this project. Johanna and Peter Dodd are so committed to their cause and I wish them every success in their future endeavours to raise money for research into childhood cancers. I also need to acknowledge Luxcel Bioscience who provided the probes to measure metabolism.

On a personal note, I need to thank Danny for his patience, love and support over the last few years. I know at times I cannot have been the easiest to live with but he was always so understanding and supportive. I need to thank Mam and Dad for their never-ending support both financial and emotional; I promise I am finished studying and ready to get a real job. Thanks to Mary and Garry who were always on hand when I needed them whether it was a quick chat on the phone or a day at the spa to de-stress.

I need to say a huge thank you to Zahraa for being a great friend and the voice of reason when I needed it. Thanks also to Abdulla who always put a smile on my face. Thanks to Luned and Pam for the laughs we enjoyed in and out of the lab.

These acknowledgements are far from exhaustive so to all my wonderful family and friends your support and reassurance has been amazing and all that is left to say is "*Is brea liom sibh agus go raibh mile maith agaibh". Xxxx*

Abbreviations

αKG	α-ketoglutarate
18F-DG	18 Fluor-deoxyglucose
2D	Two-dimensional
2-DG	2-deoxyglucose
3-BP	3-bromopyruvate
3D	Three-dimensional
5-FU	5-fluorouracil
ACLY	ATP citrate lyase
ACU	Atmospheric control unit
ADP	Adenosine diphosphate
Akt	Protein kinase B (PKB)
AML	Acute myeloid leukaemia
ANOVA	One-way analysis of variance
ATP	Adenosine triphosphate
BBB	Blood brain barrier
BCA	Bicinchoninic acid
BSA	Bovine serum albumin
CAIX	Carbonic anhydrase nine
DCA	Dichloroacetate
DMEM	Dulbecco's modified eagle's medium
DNL	De-novo lipogenesis
ECL	Enhanced chemiluminescence
ECM	Extracellular matrix

EDTA	Ethylenediaminetetracetic acid
ETC	Electron transport chain
EtOH	Ethanol
FACS	Fluorescence activated cell sorting
FASN	Fatty acid synthase
FBS	Foetal bovine serum
FCCP	Carbonyl cyanide-4-(trifluoromethoxy)phenylhydrazone
FDA	Food and Drug Administration
FH	Fumarate hydratase
FMISO	18F-fluoromisonidazole
G-6-P	Glucose-6-phosphate
GAPDH	Glyceraldehyde 3-phosphate dehydrogenase
GBM	Glioblastoma multiforme
GLS	Glutaminase
GLUT	Glucose transporter
GSTZ1	Glutathione transferase zeta
Hif	Hypoxia inducible factor
HK	Hexokinase
HRE	Hypoxia response element
HRP	Horseradish peroxidase
IDH	Isocitrate dehydrogenase
IHC	Immunohistochemistry
LDH	Lactate dehydrogenase
L-glut	L-glutamine
MCT	Monocarboxylate transporter

MeOH	Methanol
MFI	Mean fluorescence intensity
MMP	Mitochondrial membrane potential
MTP	Mitochondrial transition pore
NADH	Nicotinamide adenine dinucleotide
NADPH	Nicotinamide adenine dinucleotide phosphate
NSCLC	Non-small cell lung cancer
PBS	Phosphate buffered saline
PDH	Pyruvate dehydrogenase
PDK	Pyruvate dehydrogenase kinase
Pen/Strep	Penicillin/Streptomycin
PET	Positron emission tomography
PFK	Phosphofructokinase
PFO	poly-9,9-diocylfluoene
PGM	Phosphoglycerate mutase
PHD	Prolyl hydroxylase
PI	Propridium iodide
PI3K	Phosphatidylinositol-4,5-bisphosphate 3-kinase
PKM2	Pyruvate kinase muscle type 2
pO_2	Partial oxygen pressure
PPP	Pentose phosphate pathway
PTEN	Phosphatase and tensin homolog
PtFPP	(Pt(II)-5,10,15,20-tetrakis-(2,3,4,5,6-pentafluorophenyl)-porphyrin)
RCCC	Renal clear cell carcinoma

ROS	Reactive oxygen species
RPM	Revolutions per minute
SD	Standard deviation
SDH	Succinate dehydrogenase
SDS-PAGE	Sodium dodecyl sulphate - polyacrylamide gel electrophoresis
TBS	Tris-buffered saline
TBST	Tris-buffered saline and tween 20
TCA	Tricarboxylic acid
TRF	Time resolved fluorescence
VDAC	Voltage dependent anion channel
VEGF	Vascular endothelial growth factor
VHL	Von Hippel Lindau
WHO	World Health Organisation

List of Figures

Chapter 1: General Introduction

Chapter 2: Profiling the bioenergetic phenotypes of paediatric and adult cancer cell lines

Chapter3: Investigating the potential of dichloroacetate as an anti-cancer therapy

Chapter 4: Measuring intracellular oxygen concentrations as a means of assessing cellular response to drugs that affect energy metabolism

Chapter 7: Supplemental Information

List of Tables

Abstract

Background: Malignant transformation of cells is typically characterised by aerobic glycolysis, resulting in supressed mitochondrial function, a state that helps resistance to apoptosis. This characteristic has been widely accepted as a hallmark of cancer and has been shown to be of critical importance in tumour development. The bioenergetic differences between normal and malignant cells are being exploited to identify potential cancer specific therapeutics. Improved in-vitro models are required to aid the identification and assessment of candidate drugs. In this project, we investigated the bioenergetic phenotypes of a panel of adult and paediatric cancer cell lines and evaluated the potential of 3D models as a platform for testing drugs that target cancer metabolism. We also investigated a novel method to assess mitochondrial function that enables the quantification of the level of oxygenation within the cell.

Results: The results presented in this thesis show that not all cancers display this aerobic glycolytic phenotype. We found that while some cell lines displayed the Warburg phenotype others displayed high levels of oxidative metabolism. These bioenergetic profiles need to be considered when deciding which anti-cancer drugs to use in a chemotherapeutic regime. If a bioenergetic pattern can be identified it may one day form the basis of a screening strategy for tumours. Dichloroacetate (DCA) is a small molecule PDK inhibitor that was investigated in this study. It was found to be relatively non-toxic to cells cultured in 2D but had improved toxicity when the cells were cultured in a 3D environment. Lastly, we evaluated a new oxygen sensing nanoprobe, Mito-Xpress Intra, and the results demonstrate its potential as a non-invasive means of measuring oxygen concentrations within the cell in real time as well as highlighting some striking differences between applied ambient and measured intracellular oxygen concentrations.

Conclusion: Our findings suggest that not all cancers display the characteristic glycolytic phenotype. They also highlight the importance of controlling oxygen and glucose levels when evaluating metabolism and when drug testing.

Table of Contents

CHAPTER 1

General Introduction

1.0 General Introduction

1.1 Cancer

1.1.1 History of Cancer

Cancer is one of the leading causes of death worldwide. The earliest evidence for cancer dates back to ancient Egyptian mummies in approximately 1600BC (Sudhakar, 2009). At the time, there was no treatment only palliative care. Throughout the centuries, there have been many theories about cancer. In the Middle Ages it was thought cancer arose when there was an imbalance of body fluids (blood, phlegm and bile). Before the 18th century, some believed cancer to be contagious and spread through parasites. Other theories included chronic irritation and trauma. By the middle of the 20th century, technological advances allowed researchers to gain deeper insights into the complexity of cancer. By this time, scientists were studying DNA and recognised that genes can be damaged and mutated by carcinogens. It was not until the 1970's that the importance of tumour oncogenes and tumour suppressor genes were realised (Sudhakar, 2009).

Cancer arises when cells divide uncontrollably as a result of mutations in tumour suppressor genes or oncogenes, epigenetic alterations such as methylation or histone modifications, errors in DNA proof reading or an inability to repair any damaged DNA. Each cancer arises from a single transformed cell or small group of cells. It is estimated that by the time a tumour is detected it can contain up to one billion cells (Hartnett M, M. and Goodridge H, S. 2009). Tumourgenesis is a multistep process

involving genetic mutations, in tumour suppressor genes and tumour oncogenes, as well as epigenetic factors. Cancer is not a single step event but rather a multi-layered and complex process. There are three general steps in this process: initiation, promotion and progression (Figure 1.1). Exposure to a cancer-causing agent (carcinogen) does not lead to the immediate production of a tumour. Following initiation, a period of latency and usually more carcinogen exposures cancers may arise.

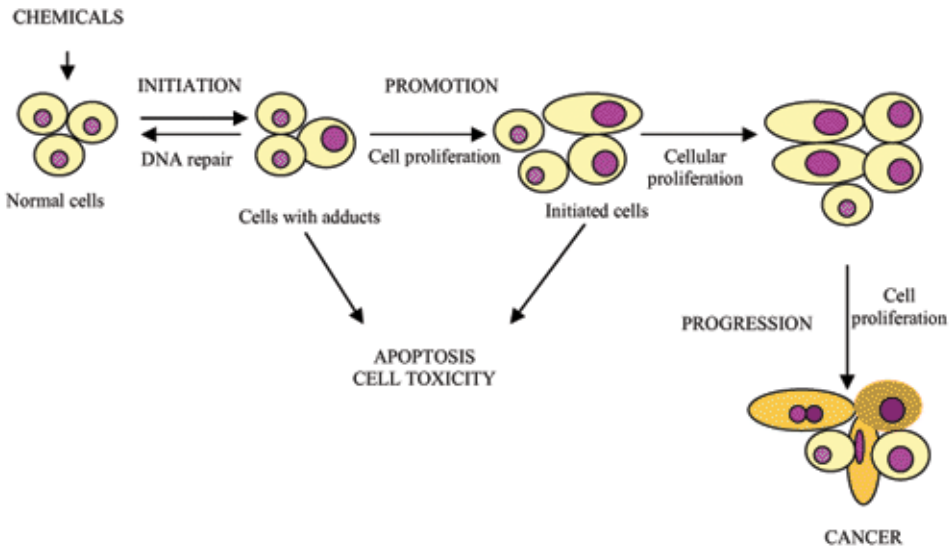

Figure 1.1: Process of carcinogenesis from initial exposure (initiation) through a period of latency to disease progression. (Oliveira et al., 2007)

1.1.2 Cancer Statistics

There are in excess of 200 cancer types. In the UK alone in 2011 more than 331,000 people were diagnosed with 159,000 succumbing to the disease (Figure 1.2) (CRUK statistics). Globally approximately 12.7 million people are diagnosed with cancer

each year. The frequency of occurrence predicts that 1 in 3 will get the disease in their lifetime (CRUK statistics). Medical advances have improved the survival rates with approximately half of all people diagnosed now surviving for at least five years. Throughout the last century the increase in incidence would suggest that the disease is becoming more prevalent however with advances in medicine and public health the most likely cause for the increase is that people are living longer, to an age when cancer is more likely to develop.

CANCER STATISTICS	Males	Females	Persons	Country	Year[4]
Number of new cases per year[1]	167,487	164000	331,487	UK	2010
Incidence rate per 100,000 population[2]	426.5	376.2	396.2		
Number of deaths per year	83,711	75,467	159,178	UK	2011
Mortality rate per 100,000 population[2]	200.9	146.7	169.9		
Five-year survival rate[3]	45.9%	56.4%	51.2%	England & Wales	2007
Ten-year survival rate[3]	39.3%	51.0%	45.2%		

1. Excluding non-melanoma skin cancer 2. European age-standardised 3. Adults diagnosed 4. Latest statistics available

Figure 1.2: Cancer statistics for the UK highlighting the number of new diagnoses in 2010, the mortality statistics in 2011 and the overall five and ten year survival rates from 2007 (Cancer Research UK).

In the UK, less than 1% of all cancers occur in children (aged between 0 and 14 years). This still equates to 1,600 diagnosed cases each year and 250 deaths. Leukaemia is the most common cause of childhood cancer followed closely by brain tumours (1 in 4 childhood cancers are brain tumours). In the 1970's the five-year survival rate for paediatric patients with brain and CNS tumours was 2 in 10 but the present day survival rates now stand at 7 in 10 (Cancer Research UK).

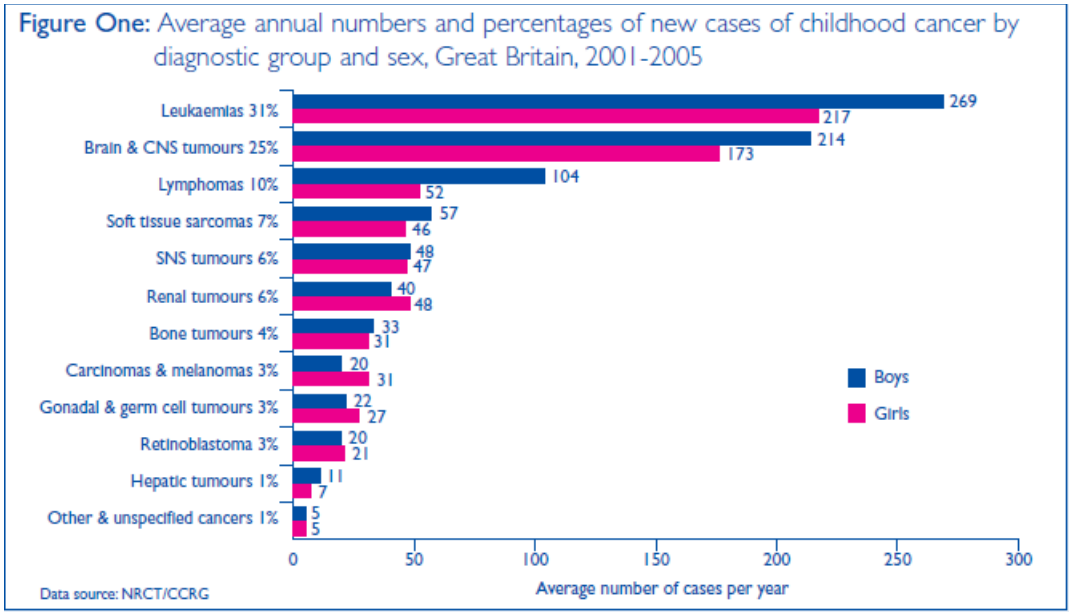

Figure 1.3: Incidence statistics for paediatric cancer cases in the UK between 2001 and 2005 (Cancer Research UK).

1.2 Therapies

The ideal cancer treatment will result in the eradication of all cancerous cells along with other localised tissues (pre-cancerous) that may be predisposed to tumour development. The three standard treatment approaches include surgery, chemotherapy (on its own or as an adjunct therapy) and radiotherapy. 1846 saw the birth of cancer surgery when surgeons began removing tumours and any localised lymph nodes. Surgery is not always a viable option particularly if the cancer has metastasised. New surgical techniques include laparoscopy (colon and bladder cancer) as well as cryo and laser surgery (liver and skin cancers) (Sudhakar, 2009). Radiation therapy has been used in the diagnosis and treatment of cancer since the early 1900's.

1.2.1 Chemotherapy

Chemotherapy is the backbone of cancer treatment and the concept of chemotherapy was devised during the Second World War at Yale University. The very first patient to undergo chemotherapy was a Polish man known only as "JD" who had lymphosarcoma that was unresponsive to radiation therapy. At the time nitrogen mustard was under investigation as a chemotherapeutic agent. In 1942, JD received nitrogen mustard daily and on the tenth day, a biopsy showed no tumour cells. Unfortunately, after stopping treatment his tumours returned and he died but this was a pivotal moment in the fight against cancer and has been described by many as the "Birth of Chemotherapy" (Christakis, 2011).

Chemotherapy today is still proving to be problematic as it is hard to identify an exploitable target that is unique to cancer cells and will not adversely affect healthy cells. Traditional chemotherapy drugs include cytotoxic agents that target cell division and these tend to have side effects on rapidly dividing non-cancerous cells including the epithelium cells in the GI tract, hence nausea is a common side effect of chemotherapy (Rang & Dale, 2007). Another common problem with current chemotherapy is the acquired multidrug resistance associated with some tumour types, which causes a decrease in the drug accumulation inside the cells and therefore negatively affects its efficacy (Szakacs et al., 2006). While there are numerous chemotherapy drugs that have been successful in the treatment of different types of cancer there is a great need to find new drugs/approaches for the management of the disease. The future of chemotherapy may lie in (i) new drugs (from natural sources or repurposed drugs), (ii) new combinations of drugs, (iii)

more targeted drug delivery (iv) co-administration of chemo-protective drugs to minimise the unwanted side effects or (v) a means of re-sensitising tumours and overcoming drug resistance (Rang & Dale, 2007).

Solid cancers are considered to have three distinct layers or compartments (Figure 1.4). The first layer is comprised of actively dividing cells with free access to oxygen and nutrients. The second layer will be hypoxic, nutrient deprived and made up of cells that are quiescent (in G0 phase). The inner layer is composed of necrotic cells and whilst the cells are not viable they do contribute to the overall tumour volume. The actively proliferating layer A contains the cells that are susceptible to chemotherapy drugs but this layer can comprise as little as 5% of the tumour volume. The hypoxic layer B is less susceptible to chemotherapy drugs and the cells within it are likely to emerge from their quiescent state and re-establish themselves as layer A following chemotherapy withdrawal (Rang & Dale, 2007).

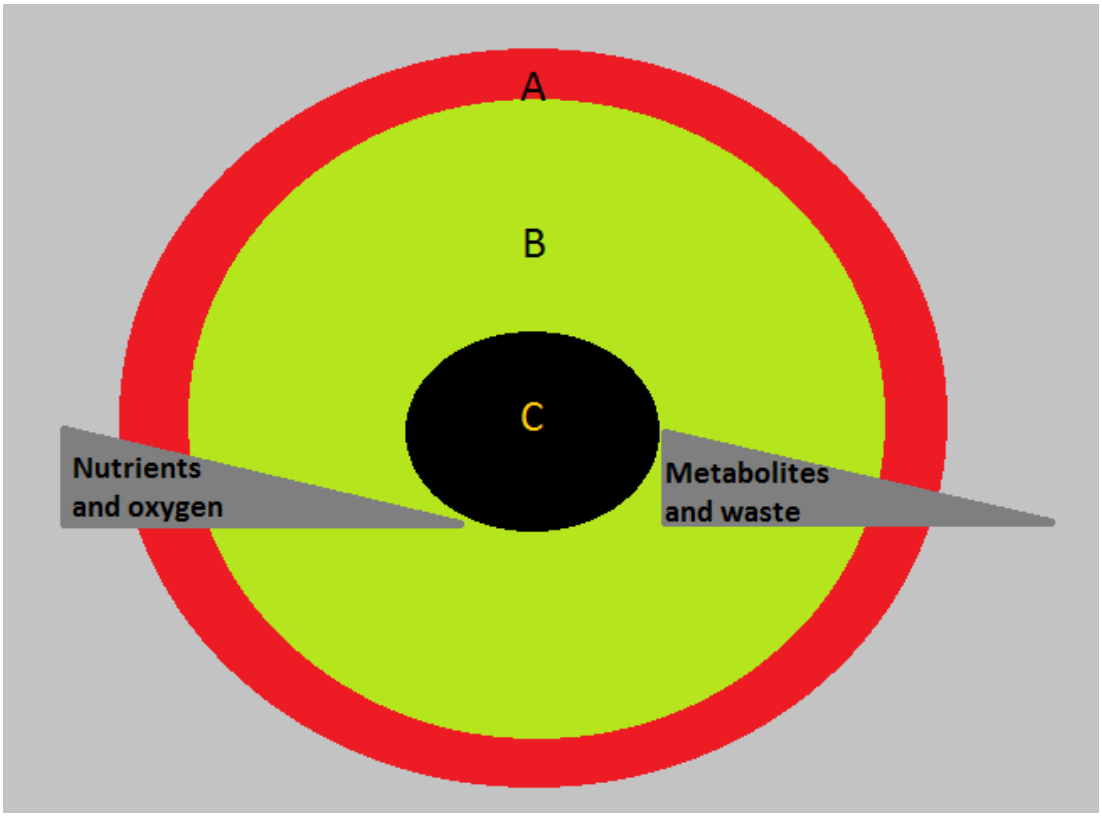

Figure 1.4: Solid tumours are composed of multiple layers. Depending on the size of tumours they are composed of layers consisting of a proliferating outer layer (A); a quiescent and hypoxic middle layer (B) and a necrotic central layer (C). Gradients of nutrients, oxygen and waste products are also present.

1.2.2 Drug development

The pharmaceutical industry is an incredibly regulated industry and the process of drug discovery and development is a complex, lengthy and focussed one (Rick, N.G. 2009). The drug discovery process generally starts with the identification of a new molecular target. Following target selection pharmaceutical companies spend anywhere from 2-3 years on average in the drug discovery stage in which they need to identify potential drug candidates. An initial drug screen may provide 100's of possible drug candidates with the number of potential candidates decreasing as drug

efficacy and toxicology is investigated. The drug development stage involves taking a lead compound and bringing it successfully through the pre-clinical and clinical testing procedures to the final registered product. Table 1.1 shows the steps involved in drug development. For some serious conditions or diseases where there is an unmet medical need the Food and Drug Administration (FDA) will sometimes fast track the process.

<table>
<tr><th>Drug

Discovery</th><th colspan="4">Drug Development</th><th>Regulatory

Approval</th><th>Phase IV</th></tr>
<tr><td rowspan="3">Lead discovery and optimisation</td><td>Preclinical</td><td colspan="3">Clinical</td><td rowspan="3"></td><td rowspan="3">Post market surveillance</td></tr>
<tr><td rowspan="2">In-vitro and in-vivo studies</td><td>Phase I</td><td>Phase II</td><td>Phase III</td></tr>
<tr><td>20-80 healthy volunteers</td><td>100-300 patients</td><td>Up to 3,000 patients</td></tr>
<tr><td>2.5 years</td><td>1.5 years</td><td colspan="3">5 – 7 years</td><td>1 – 2 years</td><td>Continuous</td></tr>
</table>

Table 1.1: Schematic of the steps involved in the process of drug discovery and the approximate length of time it takes to complete each stage.

In the past drug discovery was mainly accidental or random. Paul Ehrlich made pivotal discoveries in the early 1900's (Kaufmann, 2008) (Rang, 2006). He realised that if a chemical substance was is to be used in the body to treat diseases or disease causing organisms then they should have a high affinity for the causative agent and they should be non-toxic to the patient when used at therapeutic doses (Winau et al., 2004). This was Ehrlichs "magic bullet" theory; a toxin could be delivered that would selectively affect a particular target. Today the search for the magic bullet to

treat cancer continues with huge money invested in research and development. Unfortunately, new drugs are not being developed fast enough due to a more intricate and prolonged clinical trial process and problems identifying suitable drug targets (Rick, 2009). Two areas of research are focussing on finding new drugs or old drugs with new indications through (i) natural product screening and (ii) re-purposing.

1.2.2.1 Naturally derived drugs

For thousands of years natural products have been used to treat and prevent diseases. Today more than 50% of clinical drugs available originate from natural products or their derivatives (Gurib-Fakim, 2006; Tulp and Bohlin, 2004). Drugs derived from natural sources have proven to be extremely useful when treating diseases like cancer (Chin et al., 2006). Between the years 1998 and 2006, there were 592 natural compounds in preclinical development showing good anti-tumour potential (Mayer et al., 2010). Table 1.2 details some naturally derived anti-cancer drugs.

Drug	Origin	Mechanism of action	Cancer type	Reference
Vinblastine and vincristine	Madagascar periwinkle	Interfere with microtubule formation	Leukaemia, breast, lung, renal	(Nobili et al., 2009) (da Rocha et al., 2001) Mayer et al., 2010
Paclitaxel	Taxus brevifolia	Stabilise microtubule and prevent depolymerisation	Breast, head, neck, lung	
Doxorubicin	Streptomyces	Topoisomerase II inhibitor	Breast, small cell lung	
Trabectedin	Ecteinascidia turbinate	Not fully understood. Induces p53 independent apoptosis	Soft tissue sarcoma, ovarian. In phase II for breast, lung, prostate, paediatric	

Table 1.2: Examples of naturally derived drugs currently available for the treatment of cancer

1.2.2.2 Drug re-purposing

The huge R&D costs are extremely disproportionate to the amount of new drugs that successfully traverse the maze of drug development and make it from bench to bedside. In the US, it is estimated that it costs $1.8 billion dollars over 13 years to successfully bring a drug to the market. High failure rates, high costs and poor safety and efficacy are the reasons the new product pipelines are struggling to keep up with demand.

In 1988, James Black received a Nobel Prize for Medicine and Physiology and is noted for saying "*the most fruitful basis for discovering new drugs is to start with old drugs".* Re-purposing drugs has the potential to overcome the problems mentioned in the previous paragraph. The drug development time can be dramatically reduced (Figure 1.5) and because re-purposed drugs are already registered products there is

an abundance of safety and pharmacokinetic data that already exists for them (Gupta et al., 2013).

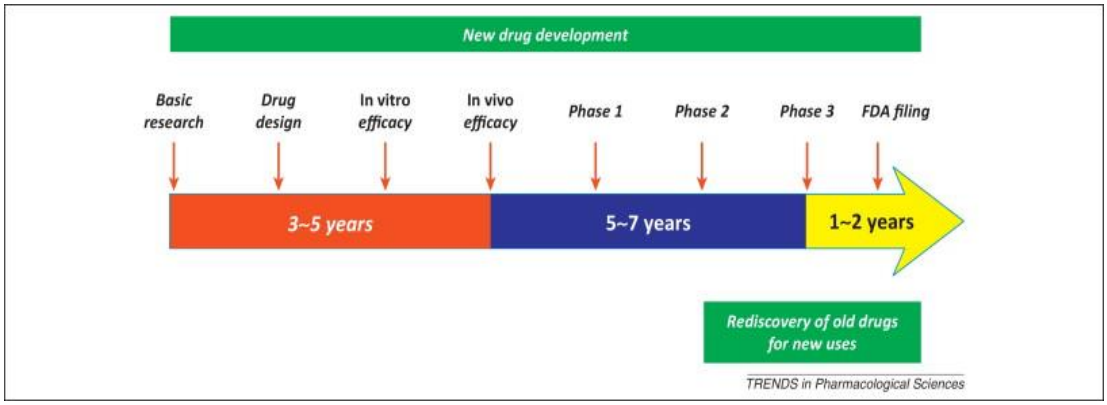

Figure 1.5: Drug re-purposing can be both cost and time effective (Gupta et al., 2013)

Approximately 90% of approved drugs have secondary indications for other diseases/conditions. Table 1.3 lists some of the most notable drugs that have demonstrated anti-cancer potential. Thalidomide was the centre of a scandal in the early 1960's when it was prescribed as an anti-emetic for pregnant mothers but was later demonstrated to have severe teratogenic toxicity. Its mechanism of action has been reported as anti-angiogenic and because of this it has a new indication in the treatment multiple myeloma. Other examples of drugs that had previously unknown anti-cancer potential include valproic acid (inhibits voltage dependent anion channel (VDAC) and has been shown to inhibit invasion, angiogenesis and metastasis) and aspirin (Gupta et al., 2013).

Dichloroacetate (DCA) has been used to treat lactic acidosis in patients with mitochondrial diseases but it is demonstrating potential as an anti-cancer agent

(Michelakis et al., 2008). DCA is the drug under investigation in this study and will be discussed later in section 1.6.

Drug	Original Use	New anti-cancer indication
Thalidomide	Anti-emetic in pregnancy	Multiple myeloma
Aspirin	Analgesic and antipyretic	Colorectal cancer
Valproic acid	Antiepileptic	Leukaemia and solid tumours
Celecoxib	Osteoarthritis and rheumatoid	Colorectal and lung cancer
Statins	Myocardial infarction	Prostate cancer and leukaemia
Rapamycin	Immunosuppressant	Colorectal cancer, lymphoma and leukaemia
Nitroxoline	Antibiotic	Bladder and breast cancer
Metformin	Diabetes mellitus	Breast, prostate and colorectal
Dichloroacetate	Lactic acidosis	Glioma, ovarian cancer
Minocyline	Acne	Ovarian cancer and glioma

Table 1.3: Examples of drugs that were developed for reasons other than chemotherapy but have shown potential as anti-cancer agents.(Gupta et al., 2013)

1.3 Hallmarks of Cancer

Advances in technology have helped in furthering our knowledge of the underlying molecular processes of this complex disease but there are still many unanswered questions. In 2000 a review article by Hanahan and Weinberg attempted to aid our understanding of cancer biology by identifying a series of cancer hallmarks (Hanahan and Weinberg, 2000). The six original hallmarks include uncontrolled proliferative signalling, resistance to apoptosis, initiating angiogenesis, acquiring replicative immortality, activating invasion and metastasis and evading growth suppressors (Figure 1.6).

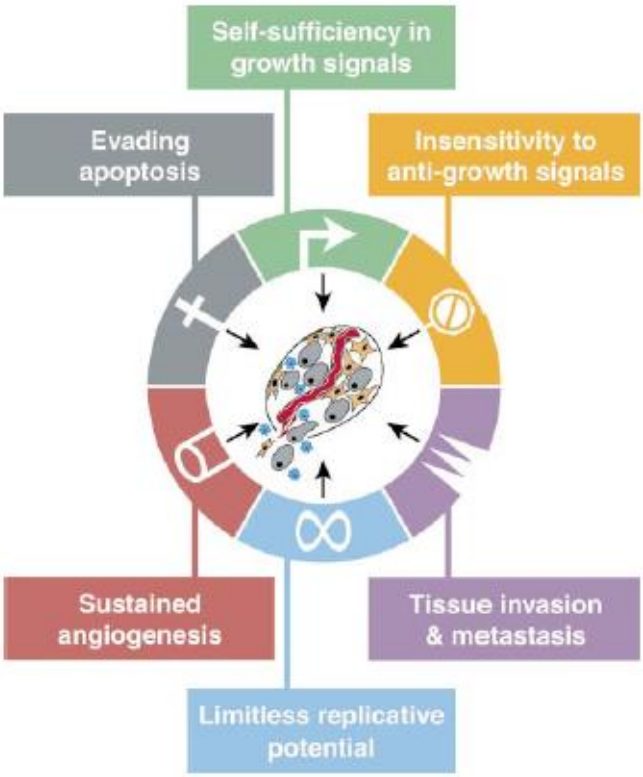

Figure 1.6: The hallmarks of cancer

Over the last decade, these hallmarks have been extensively studied and in 2011 they were re-evaluated. Hanahan and Weinberg revisited the original hallmarks and extended the list (Figure 1.7). In this latest review, metabolic reprogramming/deregulated cellular energetics was added as an emerging hallmark and potential anti-cancer target and forms the basis behind this thesis.

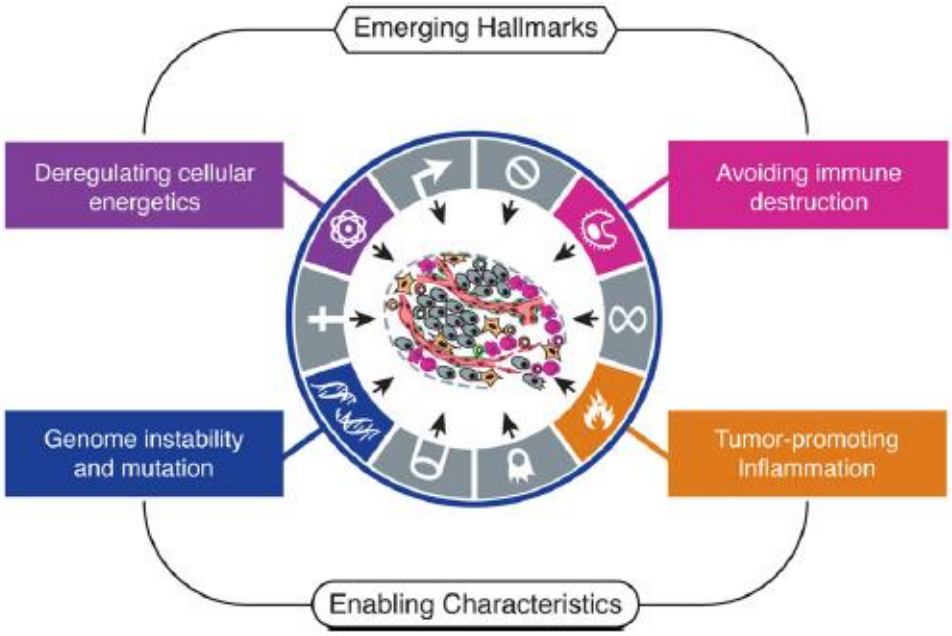

Figure 1.7: Emerging hallmarks of cancer include re-programmed metabolism and evading immune destruction (Hanahan and Weinberg, 2011)

1.4 Re-programmed cancer metabolism: An emerging hallmark

Uncontrolled proliferation is one of the essential characteristics of cancer. In order to sustain high levels of proliferation there needs to be a re-programming of energy metabolism in order to fuel and maintain such behaviour (Hanahan and Weinberg, 2011). The exact reasons behind the metabolic switch are not known but likely reasons include (i) sustaining high proliferative rates in hypoxia (Gatenby and Gillies, 2004) and (ii) evading apoptosis as a result of reduced mitochondrial function (Gogvadze et al., 2008). There has been reports of a correlation between invasiveness and glycolysis (Weinhouse et al., 1972). In order to effectively target cancer and develop effective therapeutic strategies it is crucial to understand the various aspects of metabolic reprogramming.

1.4.1 The Warburg Effect

When oxygen is present, normal cells will oxidise glucose in the mitochondria but in the absence of oxygen, glucose is converted into lactate. Otto Warburg first described in the 1920's that cancer cells utilised higher levels of glucose when compared to normal non-cancerous tissue. In addition to the high glucose consumption Warburg demonstrated the tumour cells had increased lactate production. The phenomenon of aerobic glycolysis has been termed the Warburg effect and this characteristic has since been observed in a variety of other tumour types including colorectal cancer (Sakashita et al., 2001), breast (Grover-McKay et al., 1998), lung (Wu et al., 2007) and glioblastoma (Lai et al., 2013; Michelakis et

al., 2010). From his observations, Warburg concluded that the mitochondria were dysfunctional (Warburg, 1956). The Warburg effect has proven to have clinical utility as it is believed to form the basis for 18F-DG PET imaging (Liu and Feng, 2012).

1.4.1.1 Glycolysis

Glucose is taken up by GLUT transporters and converted to glucose-6-phosphate (G-6-P) by hexokinase (HK). This is followed by a series of enzymatic reactions that concludes in the production of pyruvate. Lactate dehydrogenase A (LDHA) then converts pyruvate to lactate and recycles NAD+. Some pyruvate however will enter the mitochondria and be metabolised by the tricarboxylic acid (TCA) cycle and lead to ATP synthesis through the electron transport chain (ETC) and oxidative phosphorylation or the synthesis of anabolic precursors (amino acids and lipids) (Lunt and Vander Heiden, 2011). Normal cells predominantly use glucose oxidation to generate ATP but many cancer cells have been shown to use aerobic glycolysis as depicted in Figure 1.8.

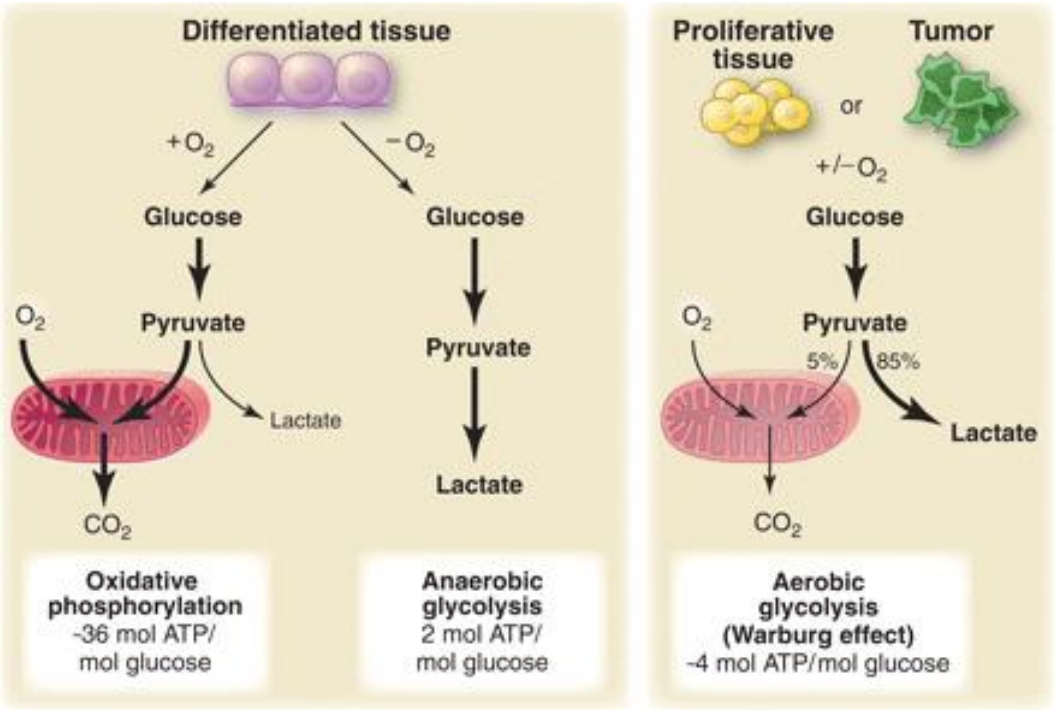

Figure 1.8: Differentiated tissues and cells generate their ATP through the process of oxidative phosphorylation. In times of low oxygen differentiated cells can use glycolysis. Tumour cells have been reported to use glycolysis even under aerobic conditions a phenomenon termed the Warburg effect after the man who made the original discovery. (Vander Heiden et al., 2009)

The fact that highly proliferative cancer cells rely on glycolysis for energy production is almost counter intuitive as glycolysis is an inefficient means of generating ATP (2 ATP molecules per glucose molecule) compared to Oxphos (36 ATP molecules per glucose molecule) (Phelps and Barrio, 2010). This inefficient means of ATP production would suggest that glycolysis has other important roles independent of ATP synthesis. Glycolysis has been proposed as a means of generating anabolic precursors for lipids synthesis, nucleotides and amino acids and also cofactor (NADH and NADPH) production all of which have important roles in the proliferation of cancer cells (Ward and Thompson, 2012a, b). Further benefits of aerobic glycolysis, include (i) increasing the survival chances of cancer cells when

the oxygen concentrations are variable as is the case in many tumours (ii) shuttling the glycolytic intermediates through the pentose phosphate pathway (PPP) and glutaminolysis will create NADPH (NADPH is important for macromolecule synthesis and as a cofactor for antioxidant defences), (iii) excessive lactate production causes a reduction in pH and therefore helps to break down ECM and encourages invasion and metastatic spread (Kroemer and Pouyssegur, 2008).

The enhanced glucose uptake observed in tumours and its subsequent utilisation in the glycolytic pathway leads to increased levels of intracellular lactate and an acidic pH. An alkaline pH inside the cell is crucial to its functioning and there are three regulatory systems in place to deal with intracellular acidification (i) sodium/hydrogen exchanger (NHE) (ii) CA9 which is a target of Hif and functions to convert CO_2 to bicarbonate (thereby preventing acidification under hypoxic conditions) and (iii) monocarboxylate transporters (MCT) which transport lactate from the cell interior to the extracellular environment (Schulze and Harris, 2012).

In the last decade, it is clear from the literature and indeed the results presented in this thesis that different tumour types (and indeed different populations within a tumour) have different bioenergetic alterations. The Warburg effect is not consistent across all tumours and the phenomenon of aerobic glycolysis has been challenged (Jose et al., 2011). Zu and Guppy reported in 2004 that ATP derived through glycolysis accounts for only 17% of the total ATP. This value was the average of a panel of 31 cell lines/tissues cultured in an in-vitro environment. In fact, the ATP generated through glycolysis was highly dependent on the cell type and could be as low as 0.31% (fibrosarcoma) and as high as 64% (hepatoma). The remaining

percentage of ATP is derived from oxidative phosphorylation in the mitochondria (Zu and Guppy, 2004). If this is true then why do tumours appear to have such high demands for glucose that allows them to be detected using PET imaging? A theory termed the reverse Warburg effect has been proposed that suggests the high glucose consumption and increased glycolysis rates may in fact be due to tumour-associated fibroblasts. Hydrogen peroxide is secreted from the cancer cells and leads to a cascade of events that culminates in mitophagy in the fibroblasts. This mitophagy will cause a reduction in the number of mitochondria and induce their subsequent switch from oxidative metabolism to glycolysis. The glycolytic fibroblasts produce and secrete excess lactate which the cancer cells take up and use as a mitochondrial energy substrate to generate the bio-molecules necessary to fuel biogenesis (Wallace, 2012). This "fibroblast-tumour metabolic coupling" causes the microenvironment to be glycolytic and possibly explains the PET signal. This co-operative relationship is similar to the relationship seen between neurons and glial cells in healthy brain tissue (Itoh et al., 2003).

There has been a huge increase in the interest of cancer metabolism in recent years and it is becoming more and more apparent that the Warburg effect is not found in all cancer types. This was realised as early as 1967 when Weinhouse reported that slow growing rat hepatoma cells were oxidative while the more proliferative hepatomas were glycolytic (Weinhouse, 1967).

Angiogenesis is also considered essential for tumour growth and progression and is another one of Hanahan and Weinberg's hallmarks of cancer (Figure 1.6). However, it has been reported that angiogenesis does not occur in all tumours and there exists

non-angiogenic tumours that get their blood supply by co-opting pre-existing blood vessels (Pezzella et al., 1997). Hu et al that has furthered this original observation and found that some aggressive cancers like non-small cell lung cancer (NSCLC) do not display sustained angiogenesis. They examined a panel of 30 angiogenic tumours and 12 non-angiogenic and found that there were distinct differences in the genes separating the two groups. Interestingly the non-angiogenic tumours were found to express higher levels of genes related to mitochondrial energy metabolism like NADH dehydrogenase [ubiquinone] 1 beta sub-complex subunit 6 (NDUFB6) a subunit of complex I (Hu et al., 2005).

1.4.2 Glutamine Metabolism

Glutamine is the most abundant amino acid found in blood and it is another important source of nitrogen, carbon and energy for cancer cells (DeBerardinis and Cheng, 2010). Glutamine has numerous roles including (i) glutaminolysis where it is partially oxidised to lactate and generates NADPH (ii) synthesis of non-essential amino acids (iii) ATP production through the TCA cycle and oxidative phosphorylation (iv) anaplerotic replenishment of TCA cycle intermediates (DeBerardinis et al., 2007; Lunt and Vander Heiden, 2011). Glutamine transporters and glutaminase have been reported to be up regulated in many cancer types (Gao et al., 2009). Glutamine metabolism therefore presents another possible therapeutic strategy in the fight against cancer.

1.4.3 Lipid Synthesis and Metabolism

In addition to an increased demand for glucose and glutamine, lipid synthesis is also an important factor in cancer cell metabolism. Most cells absorb lipids exogenously from the bloodstream (Schulze and Harris, 2012). Cancer cells have adapted their metabolism to produce lipids and fatty acids from de-novo lipogenesis (DNL). The exact function of DNL in cancer cells is unclear but is thought to be essential for the production of structural lipids. Endogenously derived phospholipids are crucial for rapidly diving cells to make up cellular membranes (Schulze and Harris, 2012). Another possible function of DNL is for energy production through β-oxidation. Lipids in the cancer cells may be a vital substrate during times where other nutrients are limited (Schulze and Harris, 2012). In glycolytic cells, β-oxidation is generally suppressed and when β-oxidation is activated glycolysis is suppressed. However, it has been proposed that it is possible for both pathways to be active simultaneously (Icard and Lincet, 2012).

Cytosolic acetyl co-A is central to lipid synthesis. Acetyl co-A comes from three sources glucose, triglycerides and proteolysis (Stillway L,W. 2009). The main source of acetyl co-A is from citrate that comes from glucose via PDH and the TCA cycle. Citrate is transported into the cytosol and converted to acetyl co-A by ATP citrate lyase (ACLY). In glycolytic cancer cells, where the pyruvate is converted to lactate and does not enter the TCA cycle, how is acetyl co-A produced? Recent publications have proposed glutamine as the source of acetyl co-A. Glutamine is converted to α-KG and converted to acetyl co-A through the action of IDH1. Alternatively, α-KG can be transported to the mitochondria and converted to citrate by IDH2, this citrate

is then transported to the cytosol and converted to acetyl co-A (Soga, 2013). Lipid metabolism may also prove to be a potential therapeutic target through inhibition key enzymes such as fatty acid synthase (FASN) or ACLY (orlistat and SB-204990 are in preclinical development against these targets) (Tennant et al., 2010).

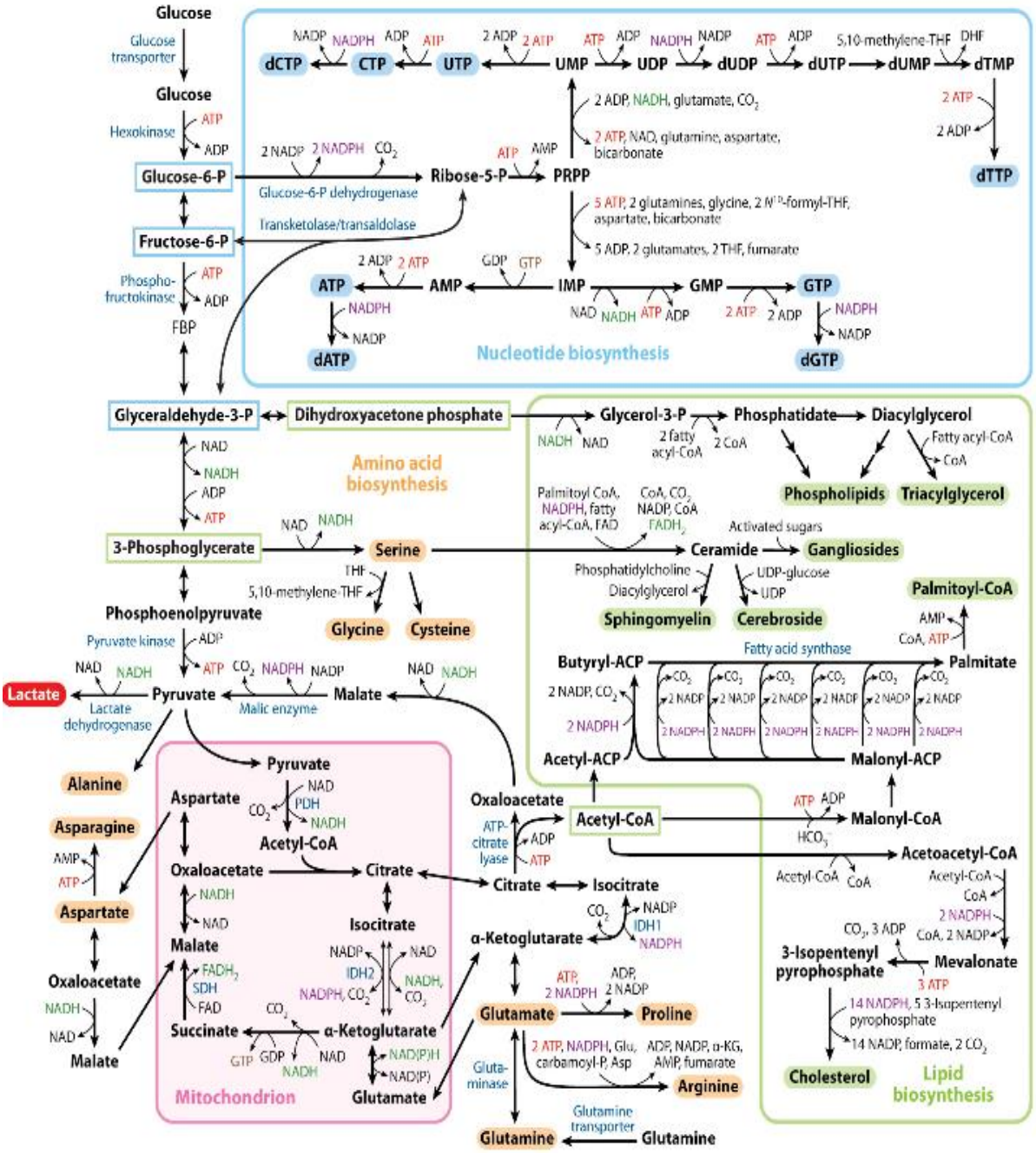

Figure 1.9: The complex role of aerobic glycolysis is highlighted in this image. (Lunt and Vander Heiden, 2011)

1.4.4 Mechanisms behind metabolic reprogramming

Cancer is well documented for its vast number of point mutations, deletions and over expressed genes. These mutations are fundamental to the development and progression of the disease. There are certain gene alterations/mutations that are directly involved in the metabolic reprogramming of malignant tumours. These include Hif1 and VHL, p53, c-MYC and PI3K (DeBerardinis, 2008; DeBerardinis et al., 2008; Soga, 2013).

Hypoxia Inducible Factor (Hif)

Hif1 plays an important role in gene regulation in reduced oxygen conditions. In normoxia Hif1α is hydroxylated by prolyl hydroxylases (PHD) and subsequently binds to the von Hippel Lindau (VHL) protein leading to ubiquitin mediated degradation by the proteasome (Stubbs and Griffiths, 2010). Hypoxia suppresses PHD. PHD requires various substrates including oxygen, Fe^{2+} and 2-oxoglutarate so inadequate levels of any of these will affect PHD ability to hydroxylate Hif1α. In addition, succinate and fumarate inhibit PHD. If PHD cannot hydroxylate Hif1α, it will not be marked for degradation. As a result, of this, Hif1α levels accumulate and form a dimer with Hif2α, this dimer interacts with the hypoxia response element (HRE) leading to activation of target genes involved in (i) glucose uptake (GLUT 1&3) (ii) glycolysis hexokinase II (HKII), aldolase A, phosphofructokinase1 (PFK1), glyceraldehyde 3-phosphate dehydrogenase (GAPDH), pyruvate kinase M2 isoform (PKM2), lactate dehydrogenase A (LDHA) (iii) the pentose phosphate pathway (transketolase) and finally (iv) the TCA cycle pyruvate dehydrogenase kinase 1

(PDK1) (Denko, 2008; Soga, 2013). Hif is known to directly affect a least 70 genes with many more being affected indirectly (Gatenby and Gillies, 2007). The target genes of Hif have the ability to promote glycolysis. It is worth mentioning that many in-vitro studies of hypoxia use high levels of glucose, which is likely to favour a glycolytic phenotype. Most cancers have regions of hypoxia where Hif1α is activated. However, it is also possible for Hif1α to be stabilised in normoxic conditions. Loss of VHL is common in renal clear cell carcinomas (RCCC) and glioblastoma multiforme (GBM) resulting in stabilisation of Hif1α and a subsequent increase in glycolysis (Gatenby and Gillies, 2007; Ivan et al., 2002; Ohh, 2006).

p53

The tumour suppressor TP53 is mutated in approximately half of all cancers (Liu and Feng, 2012). The classical role of p53 is in DNA damage repair and apoptosis (Vousden and Ryan, 2009). Emerging evidence demonstrates a role for p53 in metabolism. Wild type p53 generally keeps glycolysis rates under control by (i) inhibiting GLUT 1&4 (directly), GLUT 3 (indirectly through NFkB) and phosphoglycerate mutase (PGM) expression (ii) increasing the synthesis of cytochrome c oxidase 2 thereby enhancing Oxphos and (iii) supporting PTEN, by increasing its transcription, which leads to inhibition of PI3K and Akt. Loss or mutation of p53 therefore results in a loss of function and favours a glycolytic phenotype (Soga, 2013).

C-Myc

The oncogene c-MYC is over expressed in more than 70% of cancers (Soga, 2013). High c-Myc levels enhance glycolysis through the increased expression of GLUT transporters, pyruvate dehydrogenase kinase (PDK), hexokinase II (HKII), phosphofructokinase (PFK), Eno1 and lactate dehydrogenase (LDHA) (Dang et al., 2009a). Myc has also been shown to increase glutaminolysis by (i) up regulating glutamine transporters and (ii) decreasing miRNA's involved in the expression of GLS, which is the rate-limiting step in the process of glutaminolysis. The net result of this is promotion of glycolysis and glutaminolysis.

PI3K/Akt/mTORC1

Phosphatase and tensin homolog deleted on chromosome ten (PTEN) is a tumour suppressor frequently found to be mutated in cancer (loss of function). It negatively regulates the PI3K/Akt pathway by dephosphorylating and inactivating PIP3 (the second messenger of PI3K pathway responsible for the activation of Akt kinases) (Ortega-Molina and Serrano, 2013). The importance of PTEN in tumour metabolism was highlighted by Garcia-Cao who generated mice with increased PTEN expression (super PTEN mice) and found that the increased PTEN expression in the mice lead to reductions in glucose uptake and glycolysis. Super PTEN mice were also found to have reduced levels of GLS1 and subsequently displayed reduced glutamine consumption. GLS1 favours tumourgenesis while GLS2 is anti-tumourgenic (Garcia-Cao et al., 2012). Loss of PTEN leads to a series of events that culminates in the activation of Akt (important for cell growth survival, metabolism). Akt hyper-

activation has a direct effect on glycolysis as it increases the glycolytic enzymes (HKII and PFK1&2) and also the glucose transporters (GLUT 1&4) (Liu and Feng, 2012; Simons et al, 2011). PTEN mutations have also been found in many glioblastomas (Ortega-Molina and Serrano, 2013) and the activity of Akt correlates with the degree of glycolysis in glioblastomas (i.e. the higher the Akt activity the higher the glycolytic rate) (Simons et al, 2011).

Altered metabolic enzymes in cancer cells

In certain cancers, mutated metabolic enzymes serve as oncogenes and tumour suppressors. Isocitrate dehydrogenase 1 (IDH) is a cytosolic enzyme and IDH2 is a mitochondrial enzyme that catalyse the conversion of α-ketoglutarate (αKG) to isocitrate. Mutations in genes encoding these enzymes have been reported in >70% of low grade gliomas and secondary GBM (Parsons et al., 2008) and also in 10% of acute myeloid leukaemia (AML) cases (Dang et al., 2010). Mutations in these genes lead to a gain of function where the mutated enzymes produce 2-hydroxyglutarate (2-HG) (an oncometabolite). Accumulation of 2-HG inhibits α-KG dependent enzymes like PHD2 (leads to Hif stabilisation and increases glycolysis). Loss of IDH native function can also affect FA synthesis, reductive glutamine metabolism to α-KG and subsequent conversion to citrate and acetyl-coA depends on IDH functioning normally (Garber, 2010; Yan et al., 2009).

Succinate dehydrogenase (SDH) is an enzyme in the TCA cycle that generates reduced flavin adenine dinucleotide (FADH2) when it catalyses the conversion of succinate to fumarate. Paragangliomas and renal cell cancers have been associated

with mutations in the genes encoding SDH. Similarly, mutations in fumarate hydratase (FH), another TCA cycle enzyme that converts fumarate to malate, have been found in and are associated with leiomyomas and hereditary leiomyomatosis and renal cell cancer (HLRCC) (Dang, 2012). Mutations in SDH and FH cannot convert succinate and fumarate into fumarate and malate respectively and therefore succinate and fumarate accumulate in tumours with these mutations. Accumulation of these intermediates is reported to inhibit α-KG dependent PHD which can lead to Hif stabilisation and promotion of the glycolytic phenotype (Frezza and Gottlieb, 2009).

In addition to altered metabolic enzymes preferential expression of a particular isoform have been reported to be important in reprogrammed cancer metabolism. The most notable example of this is pyruvate kinase (PK), which converts phosphophenolpyruvate to pyruvate and is the last, rate-limiting, step in the glycolytic pathway. Pyruvate is at a cross roads between glycolysis and oxidative metabolism. Depending on the metabolic circumstances pyruvate can be shuttled into the mitochondria, it may go to FA biosynthesis, lactate production or it may be used for gluconeogenesis (Stillway L,W. 2009). Pyruvate kinase (PK) plays a key role in oncogenic metabolism. There are four isoforms of PK (liver, red blood cell and muscle type 1&2). PKM2 is of particular interest as it is over-expressed in cancer cells. PKM2 can be found as a dimer (low activity) or a tetramer (high activity). Dimeric low activity PKM2 leads to accumulation of upstream glycolytic intermediates that are shuttled into serine biosynthesis and into the PPP (Sutendra

and Michelakis, 2013; Wong et al., 2013). PKM2 can be switched between dimeric and tetrameric forms in cancer cells (Luo and Semenza, 2012).

1.5 Targeting cancer metabolism and the mitochondria as a therapy

As discussed previously cancer cells have different metabolic profiles compared to their normal counterparts and tissues from which they are derived. This has initiated research investigating the possibility of selectively targeting the aberrant cancer cell metabolism, which would result in minimal toxicity to healthy cells and normal tissue. There is a vast array of new chemotherapeutic drugs under investigation to target tumour metabolism (Tennant et al., 2010). Some of these are highlighted in Figure 1.10.

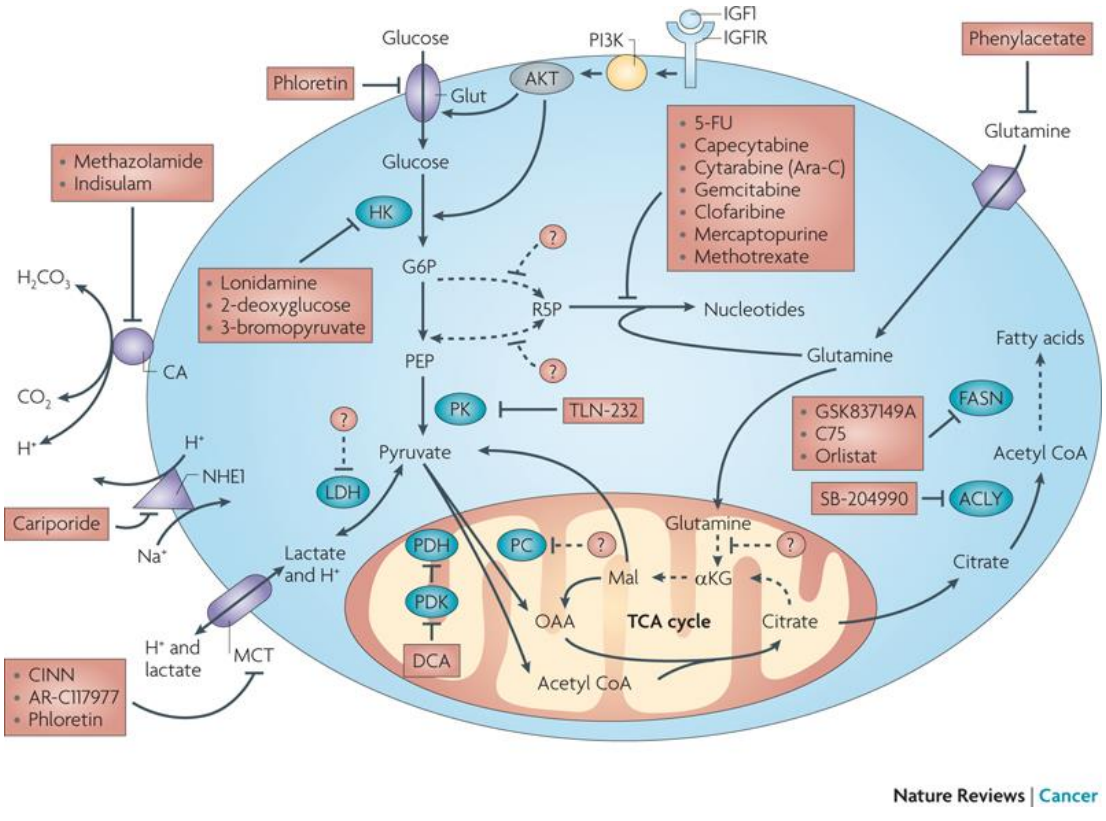

Figure 1.10: Compounds currently under investigation and in clinical trials for assessment of their effect on cancer metabolism. (Tennant et al., 2010).

It is clear from Figure 1.10 that there are numerous metabolic enzymes, which could be interesting anti-cancer targets with several studies now producing encouraging results (Tennant et al., 2010). Most studies are focussing on direct interference with the glycolytic pathway and glucose metabolism. Examples of drugs currently under investigation for their effect on cancer metabolism include: (i) 2-deoxyglucose (2-DG) and (ii) 3-bromopyruvate (3-BP) which target the first step in glycolysis involving HK. 2-DG has unacceptable toxicity associated with its administration and has its efficacy compromised when used at doses where side effects are acceptable (Singh et al., 2005). 3-BP has demonstrated toxicity to cancer cells (Mathupala et al., 2009). However, it is thought it has off target effects on other enzymes independent of its inhibition of HK that lead to its cytotoxicity to cancer cells. Dichloroacetate is a drug that has historically been used to treat lactic acidosis by restoring oxidative phosphorylation (Stacpoole, 1989) and is demonstrating potential as an anti-cancer agent. It is the drug that was focussed on in this thesis and is discussed in more detail in the next section.

1.6 Dichloroacetate

Mitochondria are crucial organelles that play a key role in cellular metabolism and biosynthetic reactions. Various studies have demonstrated that many cancer cells use glycolysis preferentially over glucose oxidation. It has therefore been hypothesised that restoring glucose oxidation in the cancer cells could potentially return a more "normal" cellular phenotype and may lead to their subsequent death when cells are subjected to cellular stress. Therefore, mitochondria are an exciting target in the field of cancer research. One particular drug that has been the subject of recent research focus for its ability to restore glucose oxidation via the mitochondria is dichloroacetate (DCA) (Mathupala, 2011).

1.6.1 Mechanism of Action

Dichloroacetate is a small molecule of 150Da (Figure 1.11) with high bioavailability (almost 100%) readily crossing the blood brain barrier (BBB). DCA can also be produced in-vivo as a metabolite of certain drugs including chloramphenicol (Stacpoole et al., 1998a; Stacpoole et al., 1998b). It is an analogue of pyruvate and is transported into the cell via the monocarboxylate transporter (MCT) and into mitochondrial matrix via the mitochondrial pyruvate transporter (Stacpoole et al., 1998a). DCA is an inhibitor of pyruvate dehydrogenase kinase (PDK) (Michelakis et al., 2008). PDK is responsible for the reversible phosphorylation of the E1alpha subunit of pyruvate dehydrogenase (PDH) leading to PDH inactivation (Papandreou et al., 2011). PDH is at the crossroads of mitochondrial metabolism as it is the rate

limiting step in the irreversible decarboxylation of pyruvate to acetyl co-A after which it enters the TCA cycle and results in ATP production (Zhao et al., 2013). As PDH controls carbon flow into the TCA and PDK regulates PDH, PDK is an attractive target for a therapeutic intervention that reactivates mitochondrial oxidative phosphorylation and potentially limits glycolysis.

DCA is a pyruvate analogue, which allows it to bind to the N-terminal regulatory site of PDK (usually occupied by pyruvate) and inhibit PDK activity thus preventing the phosphorylation of PDH (Knoechel et al., 2006; Papandreou et al., 2011). Once PDH is activated pyruvate is free to enter the mitochondria and this leads to increased glucose oxidation and restoration of mitochondrial membrane potential to levels seen in normal cells (Michelakis et al., 2008). This mitochondrial depolarisation leads to increased ROS levels and also cytochrome c and apoptosis inducing factor release from the mitochondria thus unlocking the cells from their state of apoptosis resistance (Figure 1.12) (Michelakis et al., 2008).

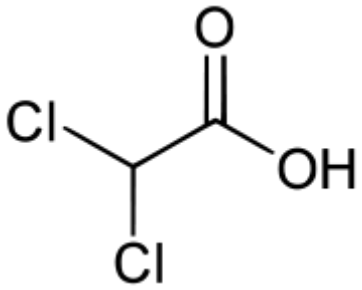

Figure 1.11: Structure of dichloroacetate

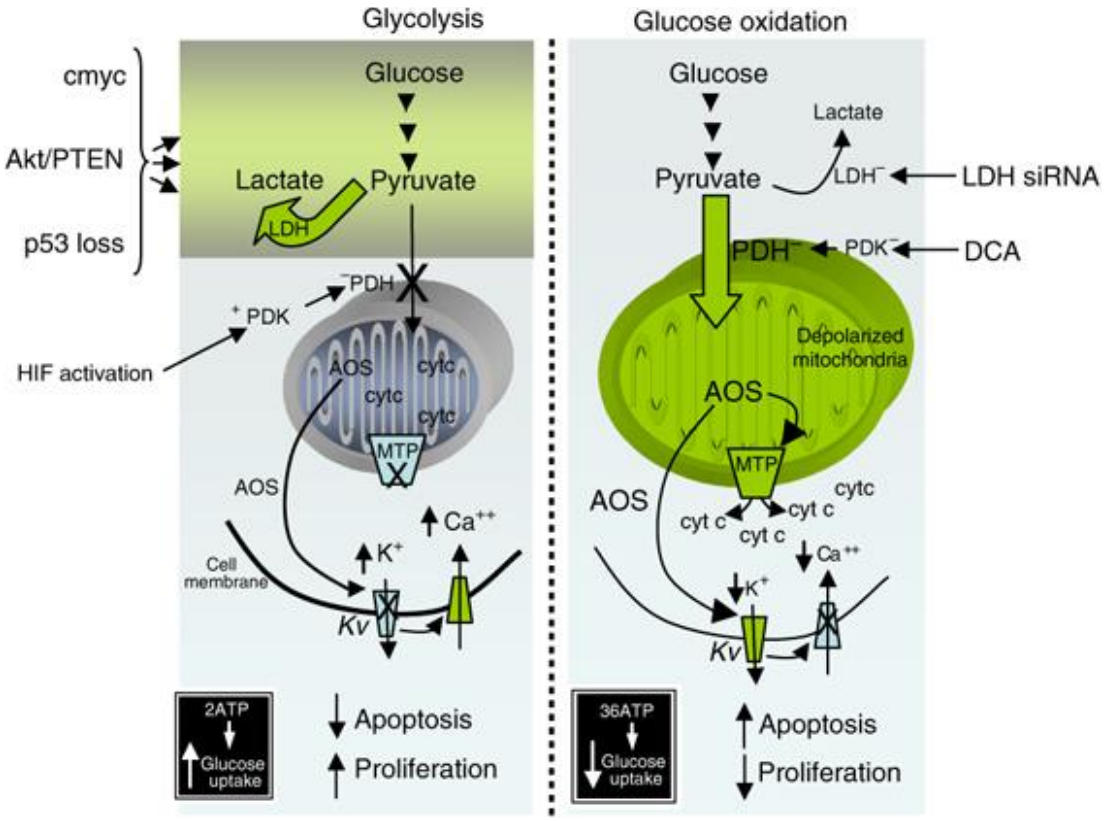

Figure 1.12: A glycolytic phenotype is associated with enhanced proliferation coupled with reduced mitochondrial function (decreased apoptosis). DCA restores the flux of pyruvate into the TCA cycle and releases the cell from its anti-apoptotic pro-proliferative state.(Michelakis et al., 2008)

1.6.2 Metabolism of DCA

The mitochondria are the site of action of DCA but they have also been reported as being the site of DCA metabolism (Li et al., 2011). DCA is de-chlorinated by glutathione S-transferase zeta 1 (GSTZ1) in the mitochondrial matrix to form glyoxylate (Figure 1.13). This intermediate then undergoes secondary metabolism by other mitochondrial enzymes before excretion (Anderson et al., 2004). DCA inhibits its own metabolism by reducing the expression and activity of GSTZ1 and chronic

exposure can lead to toxicity as the concentration is increased and there is reduced plasma clearance (Li et al., 2011).

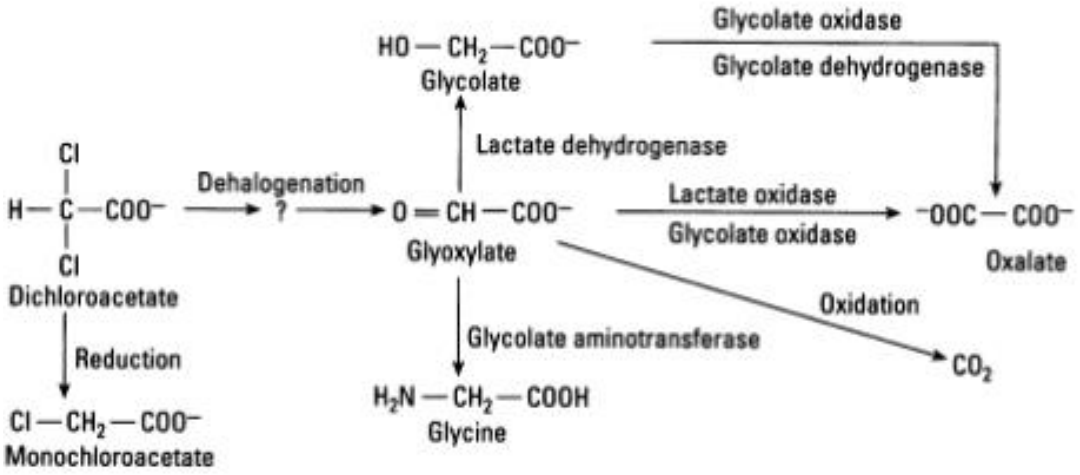

Figure 1.13: Metabolism of DCA

1.7 DCA and glioblastoma

1.7.1 Brain Tumours

The brain is a metabolically demanding organ that uses one fifth of the oxygen we inhale (Dominiczak M,H. 2009). The brain contains three main cell types (i) astrocytes (30%) (ii) oligodendrocytes (30%) and (iii) microglia (30%). Neurons only account for 10% of brain cells (Thompson E.J. 2009). Astrocytes are star shaped glial cells whose functions are (i) to surround neurons and keep them in position (ii) to supply nutrients and oxygen to neurons (iii) to insulate neurons from each other and (iv) to remove pathogens and dead neurons (Choi et al., 2012).

Gliomas are tumours that arise from glial cells and are the most common CNS tumours that affect children. The World Health Organisation (WHO) classifies gliomas as low grade (grade I and II) or high grade (grade III and IV). Grade I gliomas are pilocytic astrocytomas and these are generally cured upon surgical resection of the affected tissue. This tumour type has a more favourable prognosis because it is confined; gliomas graded II-IV are less confined and infiltrate surrounding tissue. While high-grade gliomas are not very common in children, they do occur and have a very poor prognosis. There is a great need for further treatment regimens for the management of gliomas (Katsetos et al., 2013).

Mitochondria play many important roles including production of reactive oxygen species, regulating apoptosis and contributing to ATP generation. Mitochondria are not the innocent bystanders they were once thought to be but rather active

participants in maintaining the biosynthetic ability of cancer cells (Frezza and Gottlieb, 2009). In gliomas mitochondria have been shown to have altered mitochondrial membrane potential, energy metabolism (Ordys et al., 2010) and mutated IDH (Garber, 2010).

1.7.2 Mitochondrial Dysfunction in Gliomas

As previously mentioned, cancer cells can adapt and switch their bioenergetic pathways in response to various stresses. Glioma cells have been reported as glycolytic and therefore assumed to generate their ATP from glycolysis however some glioma cell lines have been found to be highly dependent on their mitochondria to produce energy (Griguer and Oliva, 2011). Despite the finding of Griguer et al the accepted theory with gliomas is that they prefer aerobic glycolysis and have a dependency on glucose and FA metabolism. Non-malignant glial cells use glucose oxidation to generate ATP but can utilise ketones and fatty acids as substrates in the absence of glucose (Dominiczak M,H. 2009). Malignant glial cells cannot use these alternative substrates. Animal glioma models cannot sustain growth in the absence of glucose and with elevated ketones (β-hydroxybutyrate) (Ordys et al., 2010). Ketogenic diets have been proposed as a therapeutic strategy for gliomas as normal glial cells can metabolise ketones but the tumour cells will produce high ROS levels and undergo apoptosis (Katsetos et al., 2013).

IDH catalyses the conversion of isocitrate to a-KG. IDH1 is in the cytosol while IDH2 and IDH3 are localised to the mitochondria. IDH1 mutations have been found

in most astrocytomas graded II and III and secondary GBM (IV) (Katsetos et al., 2013). Gliomas without an IDH1 mutation have IDH2 mutations. IDH mutations are associated with better prognoses (Dang et al., 2009b; Myung et al., 2012).

1.7.3 Targeting the mitochondria in gliomas

Targeting the mitochondria and cell metabolism in gliomas is an active area of research. Tricyclic antidepressants can act on glioma mitochondria and initiate a caspase response (Higgins and Pilkington, 2010). Imipramine demonstrated anti-tumour activity in the U87MG glioma cell line by inhibiting the PI3K-Akt-mTOR pathway and inducing autophagy (Jeong et al., 2011).

DCA is also under investigation for the treatment and management of gliomas. As described earlier DCA inhibits PDK and PDK inhibition increasing PDH activity, TCA cycle intermediates, mROS and activating p53. Anti-proliferative and pro-apoptotic effects of DCA also lead to suppression of angiogenesis (Sutendra et al., 2013). There have been several clinical trials that have investigated DCA efficacy for patients with gliomas. These include:

1) Michelakis et al 2010 were the first group to use DCA for the treatment of cancer in humans, more specifically patients with glioblastoma multiforme (GBM). Five patients were recruited who had no other therapeutic options available to them. The study was originally designed to monitor the safety of the drug and not clinical efficacy. The results demonstrated that three of the

patients had clinical improvements and were alive 18 months after commencing the trial (Michelakis et al., 2010).

2) Dunbar et al 2013 conducted a Phase 1 clinical trial using DCA in adults with recurrent malignant brain tumours. They have suggested that the peripheral neuropathy induced by DCA may depend on it metabolism rate in-vivo. Its metabolism is dependent on patient age and haplotype variability in the glutathione transferase zeta 1 (bio transforms DCA to glyoxylate). Chronic use of DCA may be toxic to patients whose GSTZ1 haplotype extends the half-life. 15 patients were tested of which 7 were female and 8 were male. Two patients had metastatic disease and thirteen had progressive malignant gliomas (9 grade IV, 2 grade III anaplastic astrocytoma and 1 grade III oligodendroglioma). The study found that DCA treatment showed signs of disease stabilisation and that elucidating the GST zeta1 haplotype was important in managing toxicity (Dunbar et al., 2013).
3) There is an ongoing Phase I trial in Florida entitled "Study of the Safety and Efficacy of Dichloroacetate (DCA) in Glioblastoma and Other Recurrent Brain Tumours" NCT01111097 (clinicaltrials.gov)

1.7.4 DCA and other cancer types

The interest in DCA has been gathering momentum as a simple, cancer specific and cost effective treatment of glycolytic tumours. Studies carried out to date are too limited to draw solid conclusions on the potential efficacy of DCA but a review of the literature reveals that it is showing promise in a variety of cancer cell types.

The interest in DCA as a potential cancer therapeutic was initiated in 2007 by Bonnet et al when they showed it's inhibitory effect in lung cancer cells lines and xenografts (Bonnet et al., 2007). DCA has been shown to increase prostate cancer sensitivity to radiotherapy (Cao et al., 2008). When combined with standard the chemotherapeutic agent 5-fluorouracil (5-FU) it potentiates cell death in colon cancer cells (Tong et al., 2011). Also, in colon cancer cells it synergises with suldinac (a non-steroidal anti-inflammatory drug) (Ishiguro et al., 2012). Endometrial, breast and cervical cancers have also been reported to respond to DCA treatment (Sun et al., 2010; Wong et al., 2008; Xie et al., 2011).

Energy metabolism in tumours is showing promise as a potential therapeutic target. The exact perturbations in bioenergetic profiles vary widely between different cancers and probably within an individual tumour. Establishing the metabolic phenotype of a tumour and relating this to drug efficacy studies in cell culture models with a defined metabolic signature could prove extremely valuable as we move towards patient specific cancer treatment. The collaboration that exists between glycolysis and oxidative metabolism in cancer cells highlights the metabolic flexibility of tumours. Understanding how this flexibility occurs and how substrate concentrations in vivo encourages a particular metabolic phenotype and sensitivity to drug treatments are of fundamental importance in selecting the most appropriate metabolic therapy for a particular patient .

The scope of this thesis was to investigate a panel of adult and paediatric glioma cell lines and examine their reliance on the Warburg effect. By establishing their

bioenergetic phenotypes it was then investigated if there was a particular phenotype that would be susceptible to therapeutic intervention with DCA.

1.8 Aims of this thesis

1) Evaluate the bioenergetic phenotypes of established adult and paediatric cancer cell lines by measuring the rates of mitochondrial metabolism and glycolysis
2) Assess the effect of glucose concentration on the bioenergetic phenotypes
3) Investigate the effect of 3D culture on the bioenergetic phenotypes using 3D spheroids and Alvetex 3D scaffold systems
4) Evaluate the anti-cancer potential of drugs that target the aberrant metabolism of cancer (namely dichloroacetate and phenformin) and investigate if drug effects differ between 2D and 3D cultured cells

CHAPTER 2

PROFILING THE BIOENERGETIC PHENOTYPES OF PAEDIATRIC AND ADULT CANCER CELL LINES

2.0 Profiling the bioenergetic phenotypes of paediatric and adult cancer cells lines

2.1 Introduction

Normal healthy cells produce their ATP through the oxidation of glucose and lipids but it is a characteristic of cancer cells, that even in the presence of oxygen, glucose will be converted to lactate. Otto Warburg was the first to observe this aberrant metabolism of tumours. His observation was made in-vitro with tumour slices (Warburg et al., 1927). The mechanism behind the Warburg effect and its role in carcinogenesis was not well understood for many years but there is now a growing body of evidence suggesting that oncogenes could be driving this effect (Wu et al., 2007).

In this chapter we examined, the bioenergetic state of a panel of cancer cell lines by monitoring their oxygen consumption and extracellular acidification rates. The Mito-Xpress series of phosphorescent probes (Luxcel Biosciences) allows for the real time determination of these crucial parameters and allowed us to perform detailed bioenergetic analysis of the cells and investigate the existence of the Warburg effect. The overall aim of this thesis was to investigate the drug dichloroacetate, which modulates mitochondrial metabolism. Based on the mechanism of DCA it should have a greater impact on cancer cells displaying a glycolytic phenotype. Therefore, in this chapter we profiled a panel of cancer cells to establish which ones were glycolytic and more likely to respond to DCA treatment.

Cancer cell lines are extensively used to screen drugs (Ertel et al., 2006) but how much do we really know about their bioenergetic pathways or how chemotherapeutic drugs affects their metabolism. A recent publication by Gillet et al had some troubling findings (Gillet et al., 2011). They reported that cancer cell lines bear more resemblance to each other, irrespective of their origin, than to the clinical samples they are intended to model. When attempting to screen compounds that modulate metabolism it is important to understand how the cell line(s) used relate to the primary or secondary tumour you are attempting to model. By gaining a deeper understanding of aerobic glycolysis and its role in cancer would it be possible to devise a general screening strategy such that biopsy material from a tumour is bioenergetically profiled in order to select the most appropriate metabolic treatment? In addition, enhanced understanding of the metabolic phenotype of the cancer cell lines will allow for a better evaluation of the effects chemotherapeutic drugs have on these lines.

Also in this chapter we examine the effect of 3D culture on the bioenergetics of the cancer cells. Current approaches to study cancer cells in-vitro are lacking. 2D monolayer culture has numerous disadvantages including (i) it does not mimic the in-vivo environment of these cells and (ii) 2D cultures are generally exposed to un-physiological nutrient and oxygen levels all of which will greatly impact the metabolic profile.

2.2 Methods

2.2.1 Materials

All materials and reagents were purchased from Sigma Aldrich unless otherwise stated.

2.2.2 ATP Assay

Total cellular ATP levels were determined using the Cell Titer Glo ATP kit (Promega). Briefly, cells were seeded at 75,000 cells/well overnight in white 96 multiwell plates in various glucose concentrations. Immediately before ATP assessment FCCP, oligomycin, oxamate and 2DG were added to their appropriate wells and incubated for 45 minutes. Cell Titer Glo reagent was prepared and a volume equal to the volume in the wells was added. The plate was placed on an orbital shaker for 3 minutes followed by 10 minutes incubation at room temperature. Luminescence was monitored on the BMG FLUOstar Omega plate reader.

2.2.3 Hoechst Assay

Hoechst is a family of fluorescent cell permeable dyes that bind to DNA. A wash step to remove dead cells provides information on cell viability/number in the remaining live cell population. When cells were set up to measure oxygen consumption rates/acidification rates a parallel plate was also set up for a Hoechst

assay to allow cell number calculation and any effects caused by substrate derived growth differences to be normalised when oxygen consumption rates (OCR) and extra cellular acidification rates (ECAR) were calculated. 100µl of Hoechst working solution (1µg/ml) in media was added to each well and the plate was incubated for 25 minutes at 37^0C. Following incubation, the Hoechst solution was removed and the wells were carefully washed with 2 X 200µl PBS to remove unbound dye. 150µl PBS was added post washing and the plate was read in the BMG Optima in fluorescent end-point mode using Ex 350nm and Em 460nm with a bottom read.

*2.2.4 **Protein Determination***

Media was removed from the flask, cells were briefly washed in ice cold PBS. Protein was extracted scraping the cells from the flask using an appropriate volume (100-500µl depending on the confluency of the flask) of the following buffer: 50mM Tris-HCl pH 7.4, 150mM NaCl, 1mM EDTA, 1% Triton, 0.1% SDS, mini complement protease inhibitors – 1 tablet per 10mls (tablets from ROCHE), PhosStop inhibitor tablets – 1 per 10mls (tablets from ROCHE). The cell suspension was transferred to an Eppendorf and left on ice for 30 minutes. Samples were then centrifuged for 5mins at 13,000rpm, to remove cell debris and the supernatant collected for analysis. The Pierce® BCA Protein Assay Kit (Thermo Scientific) was used to determine the concentration of protein in the sample. Briefly, standards were made up according to the protocol laid down in the kit. 25µl standards and samples were added to a 96 well plate in triplicate. 200µl working reagent was then added to each well and the plates were allowed to incubate for 30 minutes before being read

on a plate reader. Sample protein concentrations were determined from the standard curve generated.

2.2.5 SDS-PAGE and Western Blotting

Cell lysates (20µg) were denatured by boiling at 100^0C for 5 minutes in the presence of 6X laemmli buffer (for 10 ml combine1.2g SDS (sodium dodecyl sulphate), 6mg bromophenol blue, 4.7ml glycerol, 1.2ml Tris 0.5M (pH6.8), 2.1ml dH_2O and 0.93g DTT). Following denaturation protein were resolved on SDS-PAGE gels (4-20%)(Pierce). A voltage of 130Vwas applied and gels were run for approximately 50 minutes. Proteins were next transferred to PVDF membrane (Immobilon-Fl, Millipore) activated in methanol using the wet transfer technique (Towbin buffer containing 25mM Tris, 192mM glycine and 10% v/v MeOH). The transfer was run either overnight at 10V at 4^0C or at 30V for 2.5 hours at room temperature. Loading and transfer efficiency was assessed using Ponceau S Solution (Sigma). Membranes were blocked for 2 hours using 5% w/v non-fat milk (Marvel) dissolved in 1X TBST (10mM Tris-HCl, 0.9% NaCl and 0.01% Tween). Primary antibodies were made up in the 5% milk-TBST solution and left overnight at 4^0C. Membranes were washed three times (3 X 15 minutes) using 1X TBST. Secondary antibodies were HRP conjugated (Dako) and made up in 1X TBST (without milk). Secondary antibody was left for 2 hours at room temperature. Membranes were washed as described earlier. Signal was detected using Pierce ECL kit and film (GE healthcare).

Antibody	Supplier
PDHE1α (pSer$^{293)}$	Calbiochem
Hexokinase II	Cell Signalling
PDK 1	Enzo Life Science
Hif 1α	Merck Millipore
GAPDH	Abcam
B-actin	Abcam

2.2.6 Spheroid Generation

Cells were washed and trypsinised to remove from flask. An ice-cold suspension of media containing 2.5 X 10^4 cells/ml and 2.5% Matrigel (BD Biosciences) was prepared. 200µl of this suspension (5000 cells) was added to each well of a 96 well Corning Ultra Low Attachment multiwell plate. The plates were centrifuged at 1800 rpm for 10 minutes and then incubated under standard culture conditions (5% CO_2). Initially after centrifugation cells form a concave shape structure in the well but once incubated overnight they adopt the characteristic spheroid morphology. However, this is only true for some cell types. Not all cells form typical spheroid structures. Images of the spheroids were taken at various time points and volumes were calculated using the formula $4/3\pi r^3$.

2.2.7 Alvetex Set-up

Alvetex 3D scaffolds were purchased from Reinnervate in a 96 well plate format. The scaffolds were activated with 70% ethanol, followed by two washes with sterile PBS and 150µl media before incubation for 1 hour. Cells were harvested, counted, and made up to 10^6/ml. The media in the scaffolds was removed and cells seeded in 100µl volume to give a cell density of 10^5/ml. Well volumes were topped up with media to give a final volume of 250µl. Cells were maintained in high glucose DMEM with daily media changes for 5 days. On day five media was removed, and cells were washed with glucose free media and replaced with DMEM containing various glucose concentrations. On day six, the media was replenished and on the morning of day seven prior to running the oxygen consumption and glycolysis assays.

2.2.8 NMR using U-^{13}C glucose

Cells were fed with DMEM supplemented with 2mM L-glutamine, 1mM pyruvate and 20mM D-[U-13C] glucose (UK Isotope) for 2 hours. After 2 hours cells were washed with ice cold PBS. Cells were then scraped over dry ice and extracted with a 55:35:10 mix of MeCN:MeOH:ddH_2O. Samples were vortexed and then centrifuged and the supernatant dried. Lyophilised products were then reconstituted in 50mM sodium phosphate buffer (pH 7) containing 500µM TMSP, 1.5mM sodium azide and 10% D_2O (Sigma).

13C NMR spectra were collected on a Bruker AVIII 700 spectrometer equipped with a He-cooled TCI cryoprobe with sample temperatures stabilised at 298K in 5 mm NMR tubes. Pulse excitation used a 3.6 µs (30^{o}) 13C pulse and power gated proton decoupling was achieved with a WALTZ-16 scheme employing 80 microsecond 1H 90^{o} pulses during the 0.8 s acquisition period. Data accumulations consisted of between 2000- 10240 transients per 1D spectrum. All spectra were processed using a 1Hz exponential line broadening (LB = 1 Hz). Spectra shown in this thesis were produced using the 1D ACD/NMR Processor Academic Edition.

2.2.9 Oxygen consumption and extracellular acidification assays

2.2.9.1 Background

Historically the Clark electrode has been used to monitor oxygen consumption (Clark et al., 1956) and extracellular acidification rate (ECAR) was measured by determining lactate levels or by using a micro-physiometer (Owicki and Parce, 1992). Luxcel Bioscience has developed probes that allow parallel OCR (MitoXpress-Xtra) and ECAR (pH-Xtra) measurements. These assays are carried out in real time on adherent or suspended cells in a microplate format (Hynes et al., 2009a). These probes enable us to gain a better understanding of the metabolism of cancer cells by monitoring the glycolytic and oxidative bioenergetic pathways. By making use of a variety of pharmacological modulators it allows us to monitor the dynamic interplay that exists between these two pathways and determine the metabolic phenotype of cell type being assayed (Wu et al., 2007).

*2.2.9.2 **Theory of Measurement***

The MitoXpress probe is oxygen sensitive and probe phosphorescence is quenched in high oxygen (Hynes et al., 2009a). Each well containing a cell monolayer or cells in suspension is sealed from the atmosphere using highly viscous oil. As the cells respire oxygen is depleted from the well resulting in an increase in probe signal. Drug induced changes in mitochondrial activity can be seen as changes in the probe signal overtime. The pH-Xtra probe works in a similar manner, as lactic acid is produced the pH decreases and the probe signal increases (Hynes et al., 2009b). The pH – Xtra probe provides data on the glycolytic activity of the cells by measuring the pH changes in the extracellular environment as a result of acidic metabolites being extruded from the cell be it lactic acid or carbonic acids (McDonald et al., 2012). This assay is not a sealed system as sealing it would result in bulk acidification and would not be a true reflection of lactic acid production. The plates are de-gassed before running the assay to allow residual carbon dioxide present in the cell culture media to leach out of the plastic, as this would interfere with the results. Figure 2.1 shows the experimental set up for these assays.

The OCR and ECAR rates are determined by (A) the metabolic activities of the cells but also (B) the number of cells present. The cell number/viability can be determined on the cells used to examine ECAR or on a separate plate run in parallel using a cell viability stain. Cell number cannot be determined on the cells used in the OCR measurement, as the viscous oil used to seal these samples does not allow for the recovery of the cells for further analysis; in this instance a parallel plate must be run to assess cell number.

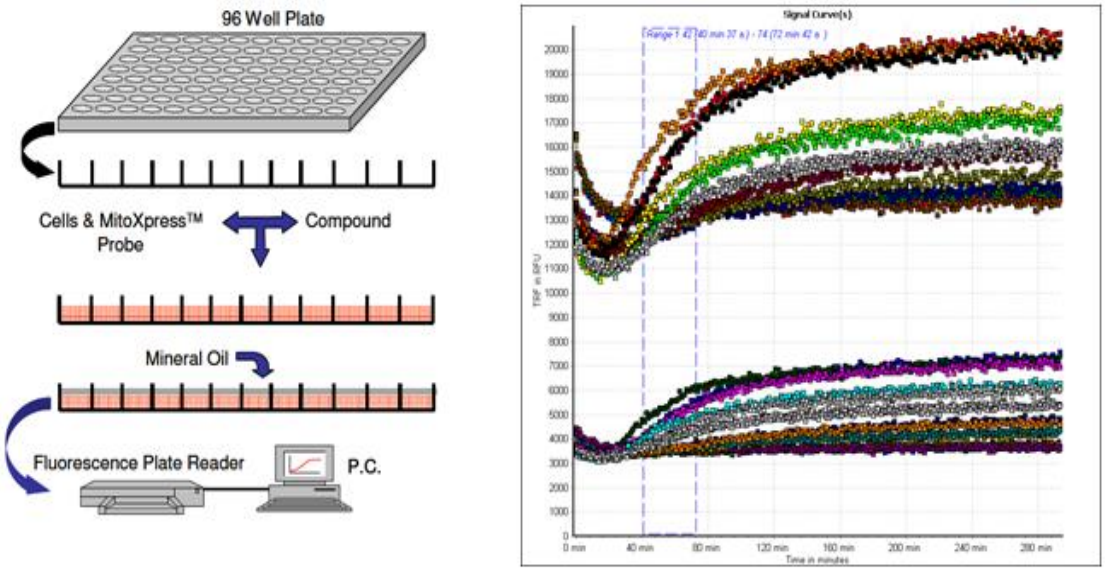

Figure 2.1: Experimental set-up of the oxygen consumption and pH assay (left) and an example of the raw data output (right).

The Mito-Xpress and pH-Xtra probes are measured using dual delay time resolved measurements. The delay times for the Mito-Xpress are 30 and 70µs and for the pH-Xtra are 100 and 300 µs. The data output using both of these probes looks like the example depicted in Figure 2.1. The raw data produced is a graph of time (x-axis) versus TR-F intensity (y-axis). These measured TR-F intensity signals need to be converted into phosphorescence lifetime values. Lifetime is the time that a molecule exists in an excited state before returning to the ground state it can provide information about the molecular microenvironment of a fluorescent molecule such as oxygen concentration and pH. The benefit of converting TRF intensity to lifetime is that the values are generally absolute, they are independent of the concentration of fluorophore added and this allows for better comparison between samples and between independent experiments. Lifetime is calculated using the following equation: lifetime = t2-t1/ Ln (D2/D1) [t=delay time, D=measured intensity value].

Once the lifetime curves are calculated it is possible to determine the oxygen consumption rates of the samples by looking at the difference (slope) in the lifetime values between two set time points.

2.2.9.3 Assay Protocol

Cells were seeded at 75,000 cells/well in DMEM containing the appropriate concentration of glucose, 1mM pyruvate, 2mM glutamine and 10% FBS and placed in a 5% CO_2 incubator at 37^0C overnight.

MitoXpress – Xtra: The following day 140µl fresh media was added to each well. MitoXpress-Xtra was reconstituted in 1ml molecular grade water. 10µl of this was added to each of the sample wells (H11 and H12 are control blanks and must not contain probe). 100µl HS oil was added to each well and the plate read using TRF at 37^0C and 18% oxygen on the BMG Labtech FLUOstar Omega (Ex 340 ± 50nm, Em 650 ± 50nm).

pH-Xtra: Following overnight incubation the plate was removed to a CO_2 free incubator for three hours to de-gas. Media was removed and cells were washed carefully (X3) in pH buffer (0.07M NaCl, 0.05M KCl, 0.8mM $MgSO_4$, 2.4mM $CaCl_2$ and appropriate concentration of glucose, adjusted to pH 7.4). Remove the final wash and add 140µl of pH buffer. Reconstitute one vial of pH-Xtra probe in molecular grade water and add 10µl to each well (leaving H11 and H12 as blanks). You do not add oil. Place in the reader and record TRF at Ex 340nm and Em 615nm.

2.2.10 The cell lines evaluated

As mentioned in the aims our interest lies in looking at anti-cancer drugs that target the mitochondria. Dichloroacetate is one such drug that has gained widespread interest over the last decade. In 2010 a small scale clinical trial was conducted on GBM patients and was found to improve overall survival in 3 out of the 5 patients treated (Michelakis et al., 2010). For this reason, we chose two high-grade GBM cell lines from ATCC, U87MG and M059K, to study the effects of DCA.

Histologically paediatric gliomas resemble their adult counterparts however, discrete differences exist between the two and a lack of childhood glioma cell lines has slowed down significant progress into a deeper understanding of the disease. Bax et al analysed a panel of paediatric glioma cell lines and compared them to some adult glioblastoma multiforme cell lines and found 93 differentially expressed genes that separated the two groups (Bax et al., 2009). The classification of brain tumours set out by the World Health Organisation (WHO) is based on the adult disease and it is not known how effectively this represents the diversity of the paediatric disease. All the paediatric lines used in this study have been derived from astrocytomas of various grades (I-IV). SF188 cells had high level amplifications of numerous known oncogenes including myc. KNS42 was not found to contain any amplification but rather a very re-arranged genome, UW479 and Res259 were found to contain deletions of CDKN2A/B. The Res186 cells are derived from the lowest grade (pilocytic astrocytoma) and these cells were found to contain the least complex genome however, they do harbour a homozygous PTEN mutation. Res259 and Res186 have been reported as being difficult to successfully culture in-vitro and have

been shown to contain mutations more commonly seen in higher grade tumours so it is possible that the genetic alterations reported in them have been acquired from in-vitro culture conditions (Bax et al., 2009).

As a comparison, two other paediatric cancer cell lines RD and RH30 were chosen (Rapa et al., 2012). These are derived from rhabdomyosarcoma tumours. RH30 cells are of the alveolar subtype, associated with a more metastatic phenotype (linked to ELMO and NELL1 up-regulation), and have been shown to display a glycolytic phenotype while the RD line is from a non-malignant tumour (Rapa et al., 2012). Previous studies have shown that RH30 is sensitive to the glycolytic inhibitor 2-DG while RD cells are not (Fan et al., 2008; Ramirez-Peinado et al., 2011)

Cell Line	Type	WHO Grade
SF188	pGBM, 8yr Male	4
KNS42	pGBM, 16yr Male	4
UW479	pAA, 13yr Female	3
Res 259	pDA, 4yr Female	2
Res186	pPa, 3yr female	1
U87MG	GBM	4
M059K	GBM, 33yr Male	4
RD	ERMS	Non malignant
RH30	ARMS	Metastatic

Figure 2.2: Table of the cell lines used in this research. SF188, KNS42, UW479, Res259 and Res186 are all derived from paediatric gliomas. U87MG (old (>p40) and early (p6) passages) and M059K cells are derived from adult GBM tumours. RD and RH30 cells are from rhabdomyosarcoma tumours.

The rhabdomyosarcoma cell lines RD and RH30 were selected from in house laboratory stocks that were originally purchased from the ATCC. The adult glioblastoma multiforme cell lines U87MG and M059K were provided by the Harris group, WIMM University of Oxford. The paediatric glioma cell lines SF188, KNS42, UW479, Res 259 and Res 186 were kindly donated by Dr. Chris Jones ICR, London. Cells were maintained in Dulbecco's modified eagles medium (4500μg/ml glucose), supplemented with 10% v/v foetal bovine serum, penicillin (100U/ml), streptomycin (100μg/ml) and L-glutamine (2mM). For low glucose experiments, cells were maintained in glucose free DMEM (Invitrogen) containing glutamine and supplemented with the desired concentration of glucose and 1mM sodium pyruvate (Sigma). Cells were maintained at 37^0C and 5% CO_2. When passaging cells were rinsed with PBS (Sigma) and trypsinised with 0.25% w/v trypsin-EDTA (Sigma).

2.3 Results

2.3.1 Assessing the bioenergetic phenotype of cancer cell lines 2D in-vitro culture

The environmental conditions of cancer cells in-vivo differ from in-vitro environments. High glucose Dulbecco modified Eagles medium (4500µg/ml) and high oxygen concentrations (21%) are not representative of the hypoxic and/or hypoglycaemic microenvironment of a tumour (Walenta et al., 2003). Cells grown in un-physiological conditions will have significantly altered metabolic programs (Gstraunthaler et al., 1999). For instance, the well-documented Crabtree effect results in a reduction in respiration when glucose levels are elevated (Crabtree, 1929). Glucose concentration can have a major impact on the bioenergetics of a cell and depending on the level of mitochondrial activity cells may respond differently to xenobiotics designed to target the mitochondria. Marroquin et al demonstrated that glycolytic HepG2 cells were resistant to some well-known mitochondrial toxicants like rotenone and antimycin-A when cultured under standard (high glucose) conditions. However, when glucose media was replaced with media containing galactose cells derived ATP from oxidative metabolism and sensitivity to the mitochondrial toxicants was restored (Marroquin et al., 2007). Using this approach, mild to moderate impairment of mitochondrial respiration can be identified. Impairments that may have been masked when cultured in high glucose (Aguer et al., 2011). This highlights the potential importance of controlling cell culture conditions

to better reflect the conditions in actual tumours in order to gain a deeper insight into cancer bioenergetics.

The effect of culture glucose concentration was assessed in the RD, RH30, old U87MG (>p40), new U87MG (approximately p5), M059K, SF188, KNS42, UW479, Res259 and Res186 cell lines in 2D by measuring oxygen consumption rates (OCR) and extracellular acidification rates (ECAR) under standard cell culture conditions i.e. 21% O_2 and 20mM glucose (Figure 2.3). To determine whether cell lines had the capacity to carryout oxidative phosphorylation when incubated with mitochondrial substrates, OCR and glycolytic (ECAR) capacities were also measured on the aforementioned lines in glucose free media (media containing pyruvate and L-glutamine as the only substrates).

All cells were cultured overnight in high (20mM) or low glucose (0mM) media before assaying OCR and ECAR. Glucose free media (containing pyruvate and glutamine) will drive the cells to use their mitochondria for energy production and therefore give an approximation of the maximal aerobic capacity. The OCR data shows that RH30, old and new U87MG, M059K and Res259 are capable of significantly increasing their mitochondrial respiration rates (Figure 2.3). The remaining lines show no significant differences in oxygen consumption between the two test groups (Figure 2.3). The ECAR data shows that all lines, except the Res259, have varying degrees of glycolytic activity that is significantly decreased upon the removal of glucose from the culture medium. The ECAR results were quite surprising because even the cells that were aerobic had significant reductions in ECAR upon glucose removal. In these cells both pathways appear to be active.

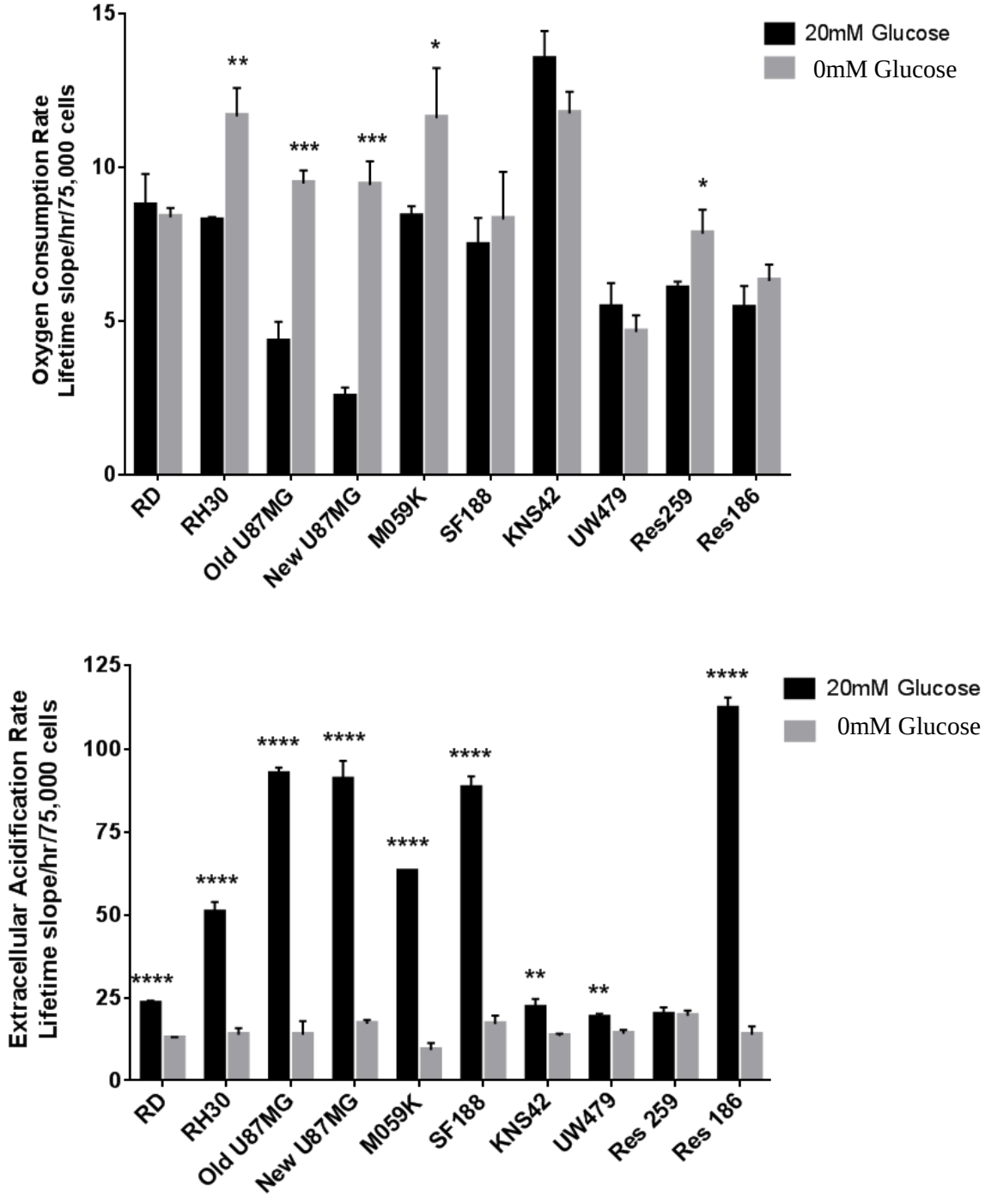

Figure 2.3: Preliminary metabolic profile of the cell lines. Cells were grown as a 2D monolayer on either on regular media (20mM glucose, 1mM pyruvate and 2mM L-glutamine) or on glucose free (same as regular media minus glucose). Cells were seeded in appropriate media at 75,000/well and left overnight. Oxygen consumption rates are shown in the top graph and extracellular acidification rates in the bottom graph. N = 3 and the error bars represent the standard deviation of the mean.

To better visualise the bioenergetics of the lines OCR was directly plotted against ECAR (Figure 2.4). What is clear from this figure is that a spread of bioenergetic phenotypes exists between the cells cultured on high glucose (20mM) media (Figure 2.4A). The RD, KNS42, UW479 and Res259 cells appear clustered in the left hand side of the graph having varying degrees of respiration coupled with relatively low levels of acidification. In the centre of the graph lie the RH30 and M059K cells that have considerable respiration rates and a more intermediate acidification rate. On the right side of the graph are the old and new U87MG, SF188 and Res186 cells that have reduced respiration rates and significant acidification rates. Also in this figure, we see how the profiles of the lines change in a glucose free environment. The cells become more aerobic and less glycolytic and this is reflected by the dramatic shift in the data points towards the left hand side of the graph (Figure 2.4B).

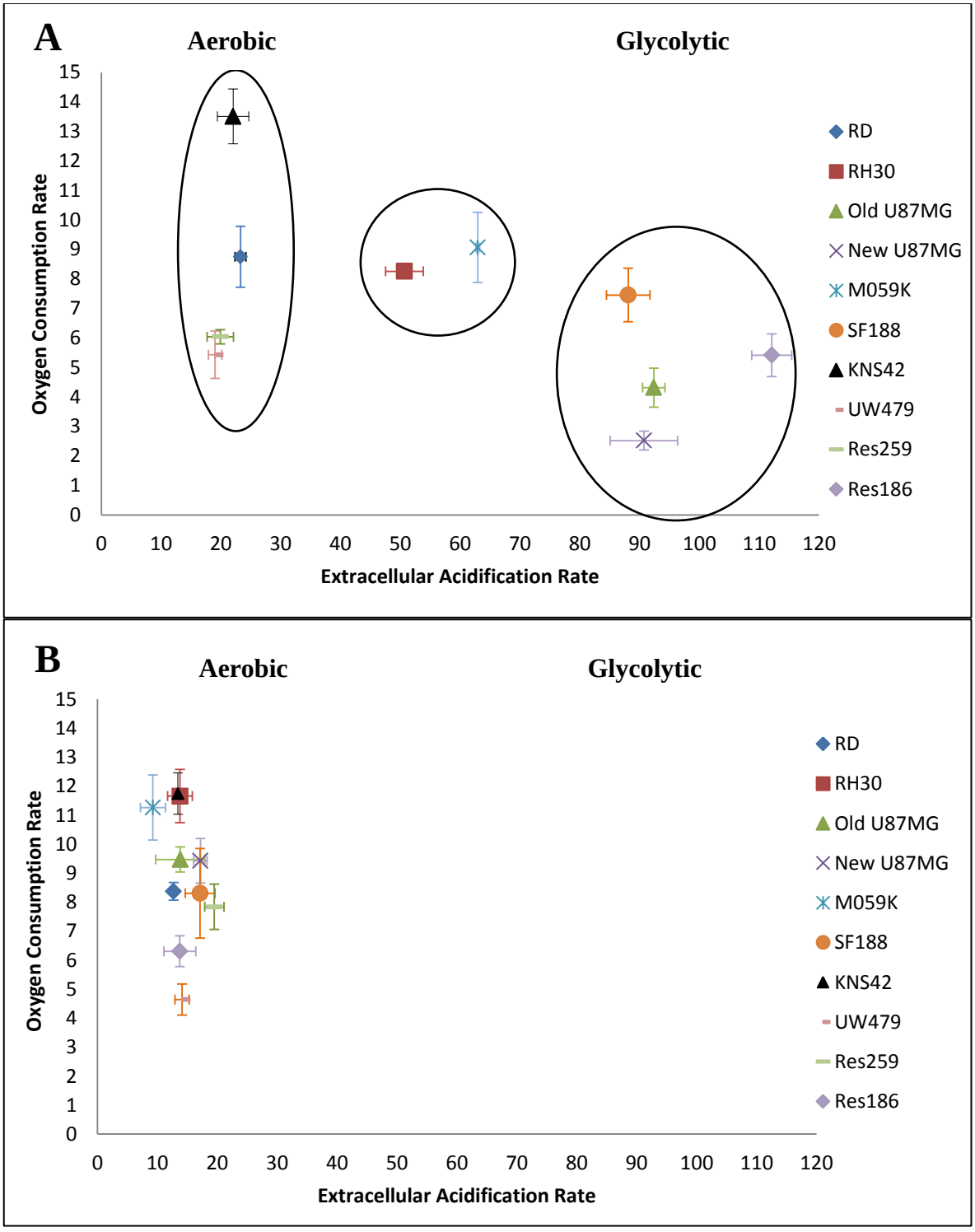

Figure 2.4: The relationship between oxygen consumption and acidification rate. High glucose (A) and glucose free (B). N = 3 and the error bars represent the standard deviation of the mean.

2.3.1.1 Rhabdomyosarcoma cells do not exclusively depend on the Warburg effect with RD and RH30 cells displaying distinct metabolic phenotypes

To try to gain a deeper understanding of the metabolism of the individual cell lines experiments were repeated using media with four different glucose concentrations. Basal rates of OCR and ECAR were determined for the lines on high 20mM, physiological 5mM (plasma levels) and low glucose 1mM (cellular levels) (Hirayama et al., 2009). 0mM glucose media containing 1mM pyruvate and 2mM glutamine was used to measure the maximum respiration rate and hence give an indication of maximal aerobic capacity of the cells. Cells grown in high glucose medium derive ATP from glycolysis and from glutamine-driven oxidative metabolism. Removal of glucose from the media forces the cells to down regulate glycolysis and ECAR and generate ATP almost exclusively from glutamine (Gohil et al., 2010).

The effects of pharmacological modulators of energy metabolism were also assessed. FCCP was used to uncouple the mitochondria from ATP synthesis which stimulates maximal mitochondrial respiration by disintegrating the mitochondrial proton gradient, oligomycin is an inhibitor of complex V and subsequently OXPHOS, oxamate inhibits LDH thereby inhibiting glycolysis (oxamate insensitive acidification is as a result of non-glycolytic acidification most likely through CO_2 (can be converted to bicarbonate and contribute to ECAR) (Wu et al., 2007) and 2-DG which is a glucose analogue that inhibits hexokinase and hence inhibits glycolysis (Abe et al., 2010; Zhang et al., 2011).

Figure 2.5 shows the response of RD and RH30 cells lines to the various glucose concentrations and pharmacological modulators. RD cells, which were previously shown to be aerobic (Figure 2.3), maintain the same OCR rates on 20, 5, 1 and 0mM glucose. They have significant glycolytic rates on 20 and 5mM glucose but this acidification is diminished on 1 and 0mM glucose (Figure 2.5). FCCP significantly stimulated both OCR and ECAR compared to 20mM glucose without FCCP. Oligomycin effectively reduced OCR rates and caused a compensatory increase in ECAR. The glycolysis inhibitors oxamate and 2-DG significantly decreased ECAR and had no significant compensatory effect on OCR further strengthening the theory that the RD cells are aerobic and making maximum use of mitochondrial respiration.

Unlike the RD cells, the RH30 cells required a switch to 1 and 0mM glucose conditions to increase cellular respiration (Figure 2.5). The basal ECAR of RH30 on 20mM glucose media was almost double that of RD. On 5mM glucose, the RH30 ECAR was significantly reduced compared to 20mM and at 1 and 0 mM glucose, the ECAR rates were very low. FCCP stimulated both OCR and ECAR. FCCP did not stimulate ECAR as much as it did in the RD cells. It has been reported that glycolytic cells have increased resistance to uncouplers (Harper et al., 2002). A lack/reduced effect of FCCP on glycolytic cells could be for various reasons including (i) glycolysis is already at max/near maximal capacity or (ii) the cells are not very reliant on Oxphos for ATP synthesis. Oligomycin reduced OCR but did not significantly stimulate ECAR adding strength to the argument that RH30 cells on high glucose are at maximal glycolytic capacity.

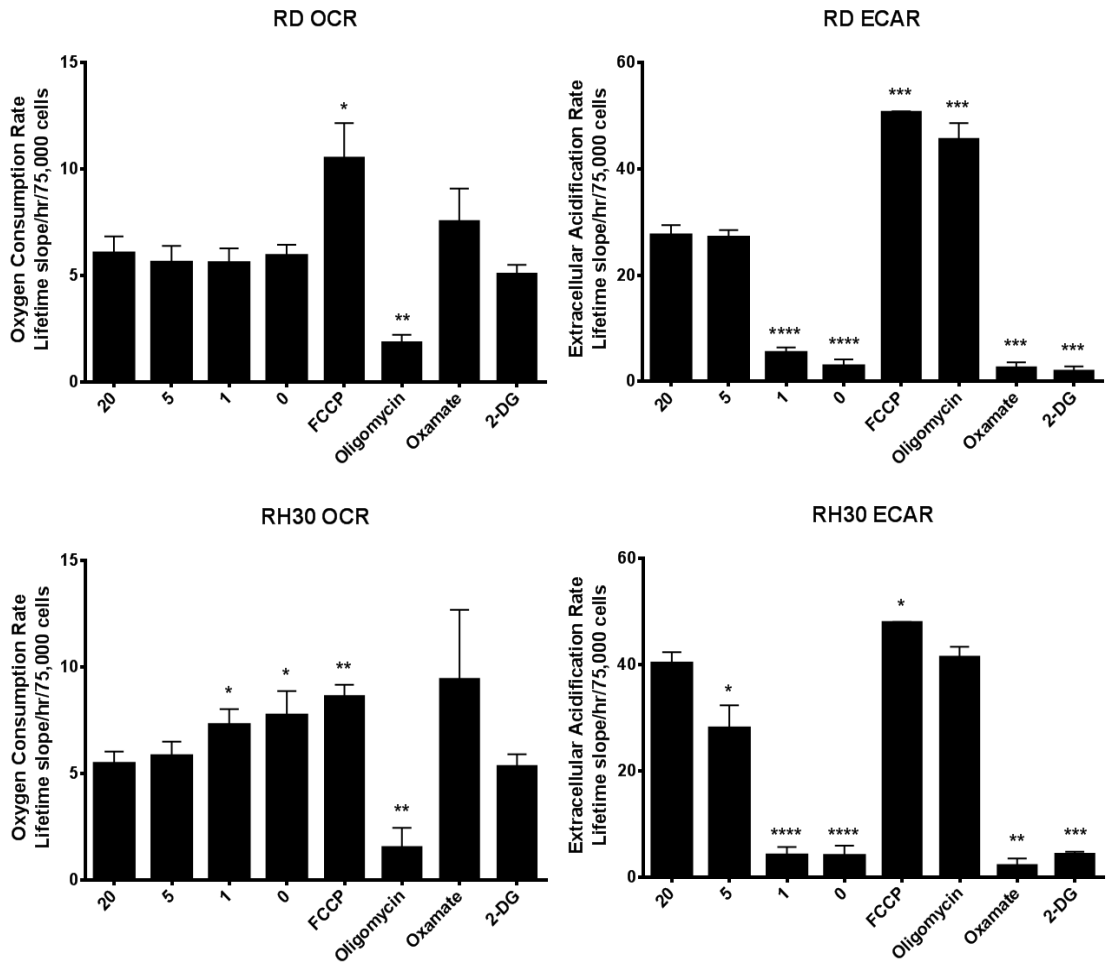

Figure 2.5: OCR and ECAR profiles of the rhabdomyosarcoma cell lines RD and RH30. Cells were assayed in media containing either 20, 5, 1 or 0mM glucose as well as 1mM pyruvate and L-glutamine. The cells treated with pharmacological modulators were grown on normal media (20mM glucose). Cells were seeded in appropriate media at 75,000/well and left overnight. Fresh media was added to each well prior to measurement and at this point 1µM FCCP, 1µM oligomycin, 100mM oxamate or 10mM 2-DG was added to the appropriate wells. N = 3 and the error bars represent the standard deviation of the mean.

2.3.1.2 Adult GBM cell lines show a greater reliance on aerobic glycolysis when cultured on high glucose

The old U87MG cells have very low rates of respiration on 20mM glucose. When glucose is reduced to more physiological concentrations (5mM) there is a significant increase in OCR. OCR further increases when glucose is reduced to 1mM and is at maximal capacity when glucose is removed completely (Figure 2.6). FCCP significantly increases the OCR compared to 20mM glucose but does not increase the OCR to same extent as the 1mM or 0mM glucose in the absence of FCCP. The ECAR profile shows an inverse relationship to the OCR in that the ECAR decreases significantly, as the glucose concentration is reduced. Oligomycin does not significantly decrease OCR thus supporting the finding that respiration is extremely low in the cells on high glucose media but it does stimulate a significant increase in ECAR. Oxamate and 2-DG satisfactorily inhibit glycolysis but in this cell line (unlike the RD and RH30 cells) inhibiting glycolysis results in significant increases in OCR compared to 20mM glucose (Figure 2.6). The new U87MG cells were obtained from a new aliquot from ATCC are of a much earlier passage (p5) than the old U87MG cells (P> 45). Initial experiments using a new aliquot of U87MG cells showed them to have very high rates of OCR on high glucose media (supplemental Figure 7.1). The data shown in Figure 2.6, from new U87MG cells at a slightly later passage (p10), shows the cell line moving to a more glycolytic state on high glucose media with relatively high rates of OCR on high glucose media but with some induction of OCR when glucose levels are reduced. FCCP and oligomycin significantly increased ECAR in new U87MG cells but FCCP failed to increase

OCR, and similar to the old U87MG oligomycin did not significantly reduce OCR. Oxamate and 2-DG significantly decreased ECAR resulting in a significant compensatory increase in OCR above basal rates (20mM glucose). On high glucose media when treated with 2-DG the more glycolytic cells should show the greatest reduction in ECAR and if mitochondria are functioning normally then the cells should be able to compensate for this inhibition by increasing OCR. If OCR does not increase it could be that (i) cells have adequate ATP (ii) the mitochondria are dysfunctional or (iii) they are unable to use metabolise glutamine for ATP synthesis.

M059K cells significantly increased their OCR between 5 and 1mM glucose (Figure 2.6). FCCP had no effect on either OCR or ECAR. Oligomycin significantly decreased OCR but did not significantly increase ECAR. The ability of the new U87MG and M059K cells to increase their OCR in the presence of FCCP was not apparent. This could be interpreted that these cells have a weakened aerobic capacity however; they were able to increase respiration on reduced glucose and glucose free media. This is suggestive that the FCCP in these lines is possibly having other effects due to its “non-classical” response on OCR.

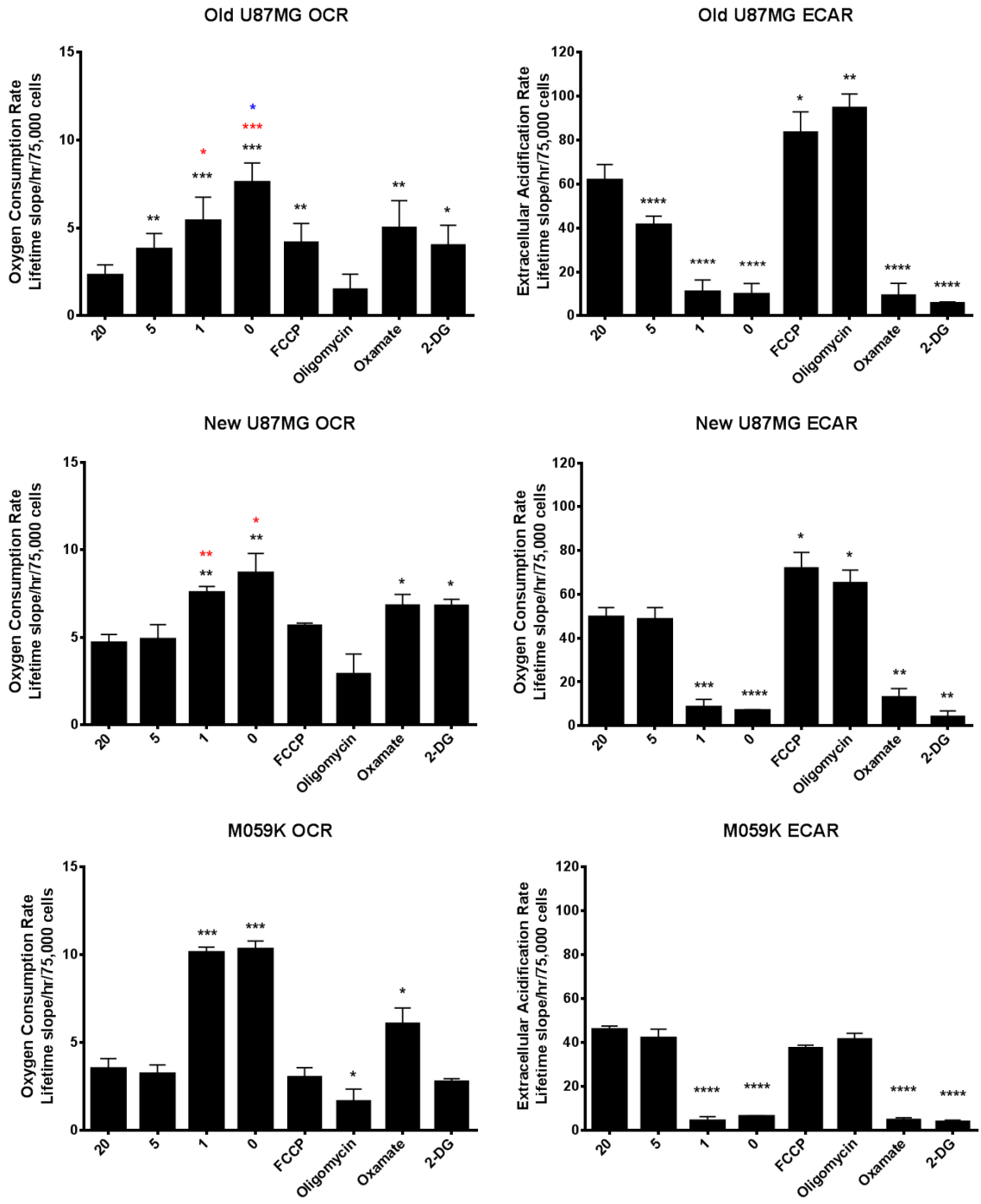

Figure 2.6: OCR and ECAR profiles of the adult GBM cell lines old U87MG, new U87MG (p10) and M059K. Cells were assayed in media containing either 20, 5, 1 or 0mM glucose as well as 1mM pyruvate and L-glutamine. Cells treated with pharmacological modulators were grown on normal media (20mM glucose). Cells were seeded in appropriate media at 75,000/well and left overnight. Fresh media was added to each well prior to measurement and at this point 1µM FCCP, 1µM oligomycin, 100mM oxamate or 10mM 2-DG was added to the appropriate wells. N

= 3 and the error bars represent the standard deviation of the mean. * compared to 20mM glucose, * compared to 5mM glucose, * compared to 1mM glucose.

2.3.1.3 High grade paediatric glioma lines display active mitochondrial respiration in combination with considerable levels of glycolysis

The high grade paediatric gliomas SF188, KNS42 and UW479 were assessed next and they appeared to be at maximal respiratory capacity on all glucose concentrations as no significant increases in OCR were obtained by reducing/removing the glucose (Figure 2.7). FCCP significantly increased the respiration in the grade IV gliomas, SF188 and KNS42, but not the grade III UW479. The basal OCR rates of UW479 were almost double that of the other two lines and potentially explains the lack of effect of FCCP, this line is very aerobic on high glucose media. The ECAR rates in the SF188 cells decrease significantly, as glucose is reduced but neither FCCP nor oligomycin are capable of stimulating ECAR beyond the basal rate seen at 20mM glucose (Figure 2.7). FCCP did not significantly increase ECAR in KNS42 cells. Interestingly, 2-DG significantly decreased OCR in the KNS42 while oxamate in these cells had no effect on OCR (Figure 2.7). The reason for the 2-DG decrease is unclear. FCCP and oligomycin induced a threefold increase in UW479 ECAR. This dramatic increase induced by FCCP and oligomycin adds strength to the argument that the UW479 cells rely heavily on oxidative metabolism as they dramatically increase glycolysis to meet their ATP demands when respiration is inhibited (oligomycin) or uncoupled (FCCP).

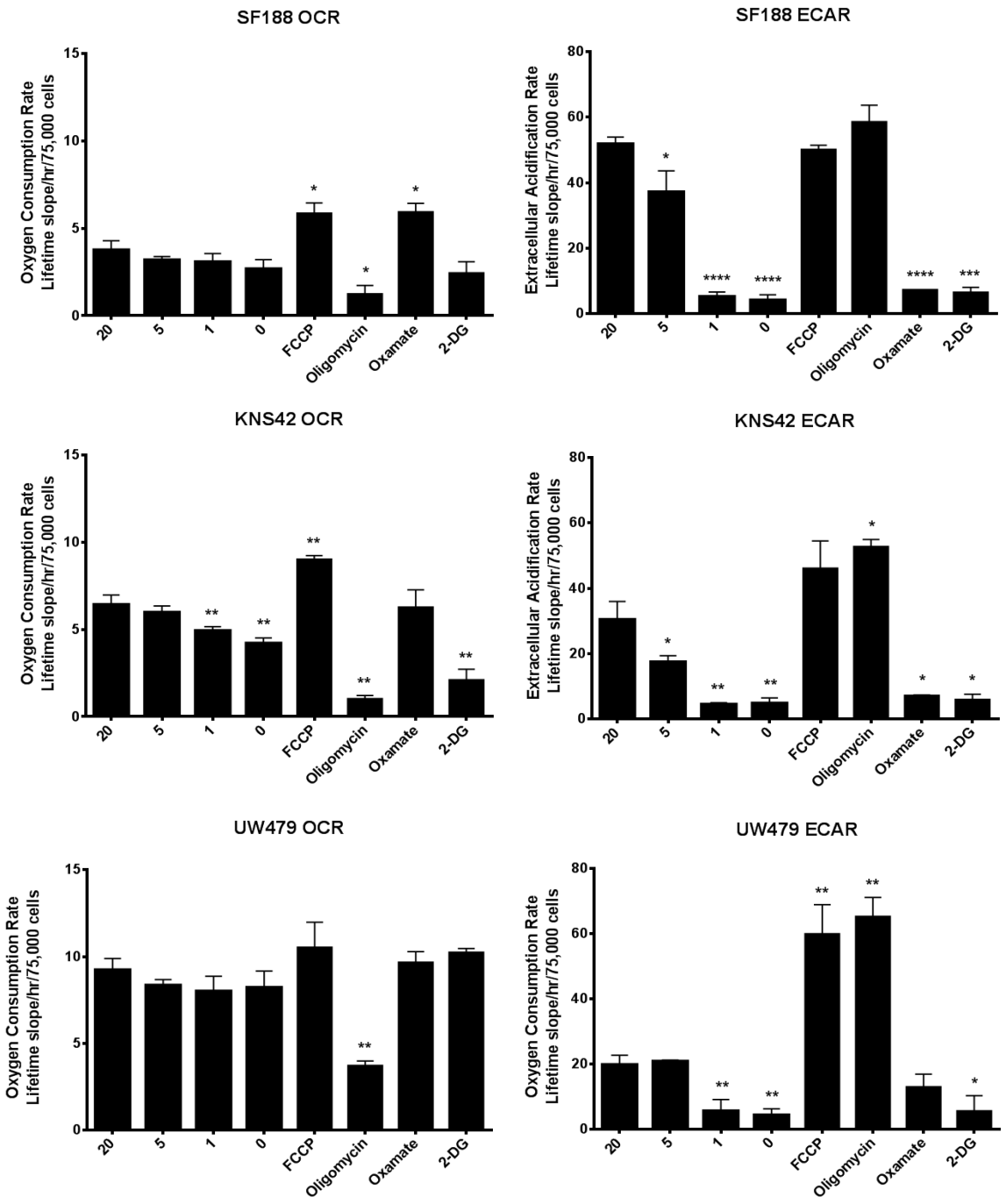

Figure 2.7: OCR and ECAR profiles of the high-grade paediatric gliomas SF188, KNS42 and UW479. Cells were assayed in media containing either 20, 5, 1 or 0mM glucose as well as 1mM pyruvate and L-glutamine. The cells treated with pharmacological modulators were grown on normal media (20mM glucose). Cells were seeded in appropriate media at 75,000/well and left overnight. Fresh media was added to each well prior to measurement and at this point 1µM FCCP, 1µM oligomycin, 100mM oxamate or 10mM 2-DG was added to the appropriate wells. N = 3 and the error bars represent the standard deviation of the mean

The low-grade glioma Res259 cells significantly increased their respiration rates on 0mM glucose Figure 2.8. FCCP, oxamate and 2-DG also induced significant increases in OCR. ECAR was considerably reduced on 1 and 0mM glucose as well as the glycolysis inhibitors (oxamate and 2-DG) while FCCP and oligomycin stimulated ECAR significantly Figure 2.8. Bax et al has shown that this cell line has a PTEN deletion that they hypothesised is just an artefact that has been acquired through in-vitro culture and is not generally seen in patients' in-vivo. PTEN is known to suppress glycolysis and glutaminolysis and this mutation could explain the extremely high acidification rates we see for this line (Liu and Feng, 2012). Unfortunately, due to culturing issues the Res186 cell line could not be assessed beyond the initial preliminary experiment shown earlier (Figure 2.3).

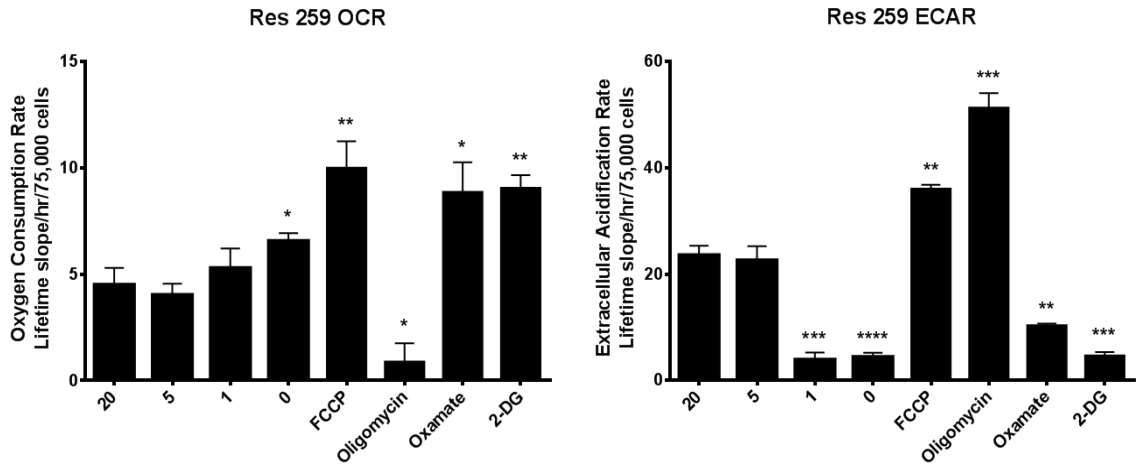

Figure 2.8: OCR and ECAR profile of the low-grade paediatric glioma Res259. Cells were assayed in media containing either 20, 5, 1 or 0mM glucose as well as 1mM pyruvate and L-glutamine. The cells treated with pharmacological modulators were grown on normal media (20mM glucose). Cells were seeded in appropriate media at 75,000/well and left overnight. Fresh media was added to each well prior to measurement and at this point 1µM FCCP, 1µM oligomycin, 100mM oxamate or 10mM 2-DG was added to the appropriate wells. N = 3 and the error bars represent the standard deviation of the mean

2.3.1.4 Normalising OCR and ECAR data

The experiments for the OCR and ECAR data depicted earlier were all set up with the same number of cells seeded however even with a short overnight incubation the cells will grow at different rates to each other and the glucose concentrations may also affect the cell growth within a particular line. A Hoechst stain was used to assess cell number immediately prior to running the OCR and ECAR assays and the data was subsequently normalised to the Hoechst data. The Hoechst data highlighted some expected and unexpected results. The RD, RH30, old U87MG and M059K cells unsurprisingly all had lower cell numbers on the reduced glucose and glucose free media (Figure 2.9). What was interesting is that the aerobic paediatric high-grade gliomas appeared to increase cell number on the reduced glucose and glucose

free media (Figure 2.10). The SF188 and KNS42 cells had significantly increased cell number on glucose free media (containing glutamine and pyruvate only). The UW479 cells were trending towards an increase but it was not significant. The Res259 cells were unaffected by glucose concentration in the media.

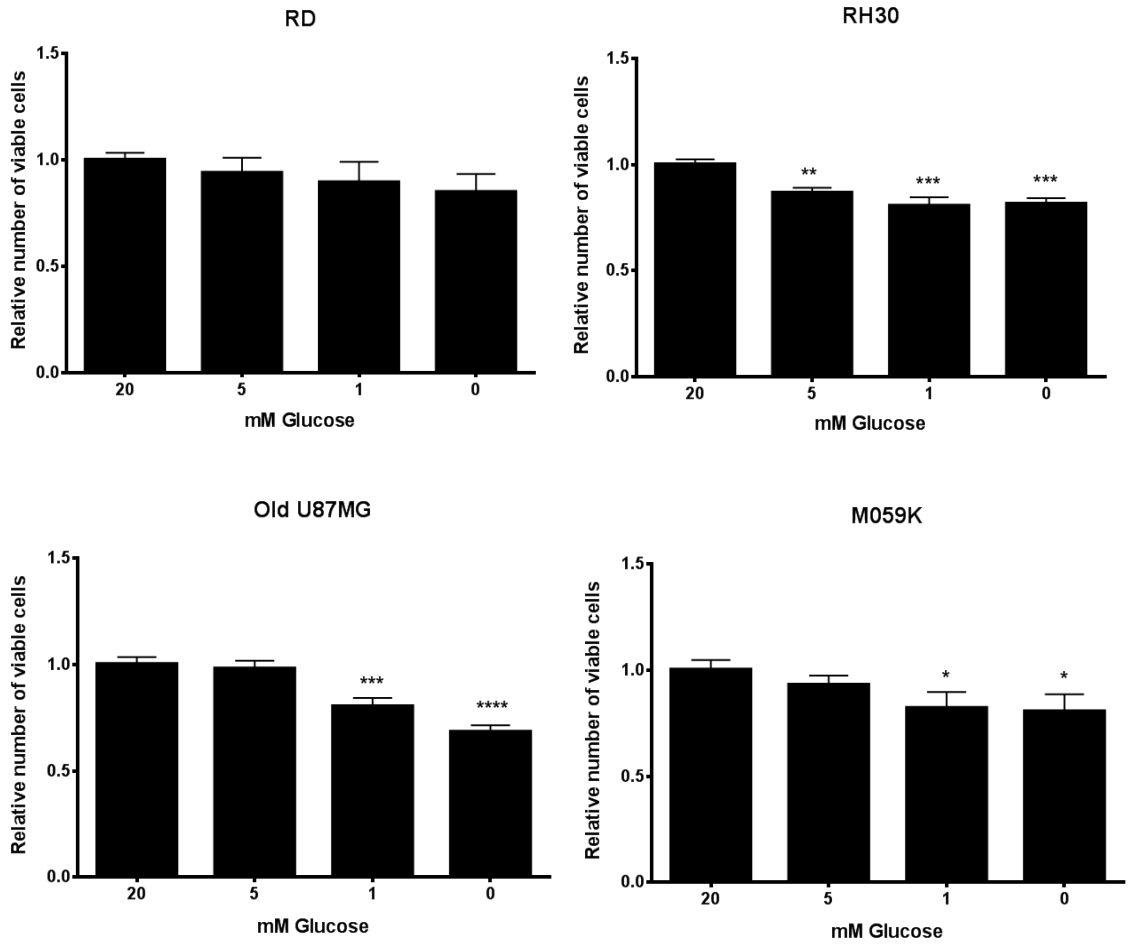

Figure 2.9: Cell number data for RD, RH30, Old U87MG and M059K cells. Cells were seeded at 75,000 cells/well and left overnight in various glucose, as per OCR ECAR method. When cell number was assessed using the Hoechst stain there is a decrease in cell number for cells exposed to decreasing glucose (n=3)

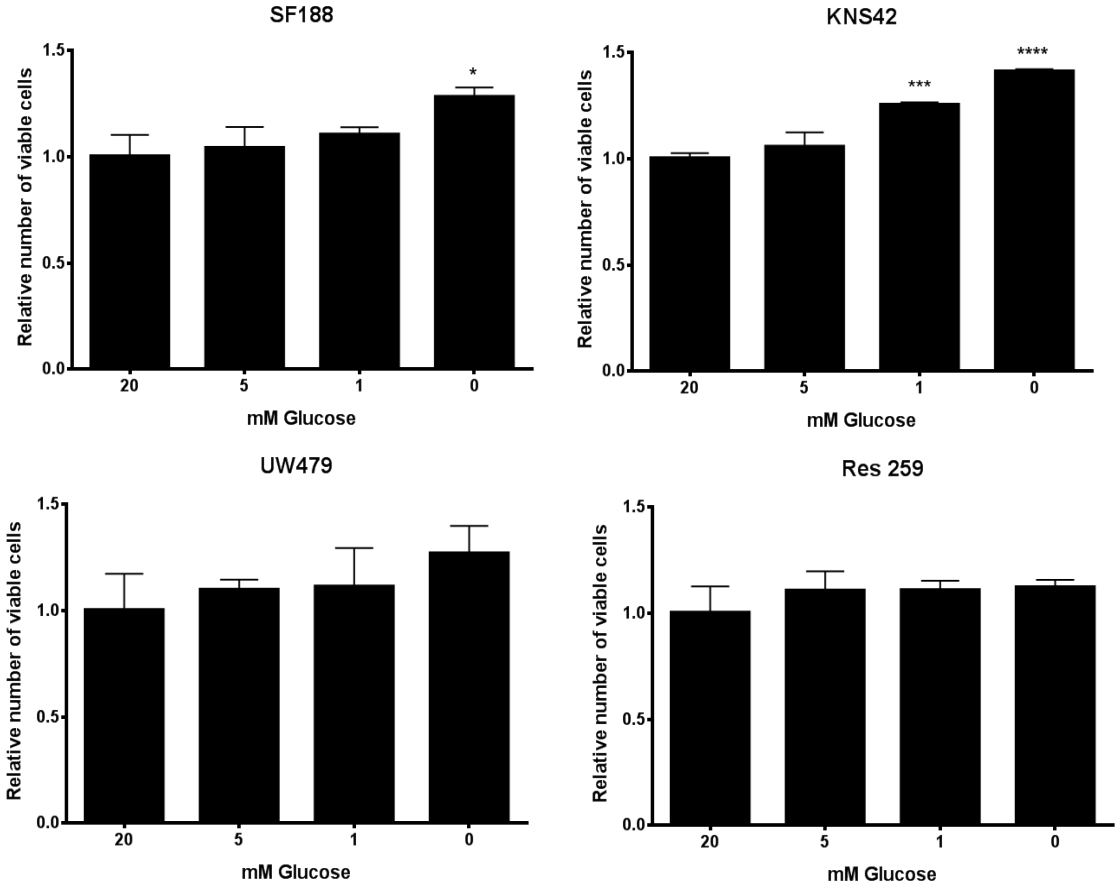

Figure 2.10: Cell number data for SF188, KNS42, UW479 and Res259 cells. Cells were seeded at 75,000 cells/well and left overnight in various glucose, as per OCR ECAR method. When cell number was assessed using the Hoechst stain there is an increase in cell number for cells exposed to decreasing glucose (n =3)

2.3.1.5 Effect of glucose and mitochondrial modulators on ATP levels

The OCR ECAR data suggests that some of the cells lines have a degree of plasticity and depending on the circumstances can switch readily switch from oxidative metabolism to glycolytic metabolism but the effect on ATP of decreasing the glucose levels and adding mitochondrial modulators remained unknown.

ATP levels were determined using the Promega kit cell titer glow. Cells were set up as with the OCR, ECAR and Hoechst assays, 75,000/well overnight in the

appropriate media and the following morning the media was replaced and inhibitors/uncouplers were added for 45 minutes prior to running the assay. The ATP data has been normalised to Hoechst and is presented as a percentage relative to the ATP level in the control (20mM glucose).

RD cells have significantly increased ATP levels on 1mM and 0mM glucose (Figure 2.11). RH30 cells have significantly higher ATP levels on 1mM glucose, FCCP appears to lower the ATP levels although not significantly (Figure 2.11). Old U87MG cells have significantly reduced ATP levels when exposed to uncoupler (Figure 2.11). FCCP dissipates the proton gradient, which can result in a loss of membrane potential. To maintain the membrane potential complex V can be reversed so that it hydrolyses ATP. In order to survive the cells would need to quickly restore the ATP pool by up-regulating glycolysis (Nicholls and Budd, 2000). As the cells are very glycolytic without the added stress of an uncoupler it is likely the U87MG cells cannot up regulate glycolysis any further and as such ATP is depleted (Figure 2.11).

Oxamate inhibits LDH so that glycolysis cannot continue through to lactate. Oxamate caused a decrease in ATP levels of the old U87MG cells. It has already been demonstrated that U87MG cells can be forced to use their mitochondria and we see in Figure 2.11 that U87MG cells grown on 0mM glucose maintain their ATP levels.

LDH is inhibited by oxamate. Pyruvate cannot be converted to lactate and similarly lactate cannot be converted back to pyruvate. Perhaps this inhibition of lactate to pyruvate and subsequent utilisation of pyruvate could account for reduced ATP.

Interestingly the oxamate decrease is only seen in the cells exhibiting high rates glycolysis U87MG, M059K, SF188 and Res259. However, RH30 cells, which are also glycolytic, did not exhibit an oxamate induced ATP reduction. Some have reported that the oxamate effect goes beyond LDH, and actually limits pyruvate entry into mitochondria (Martin-Requero et al., 1986). Another possible reason is that 45 minutes exposure time before ATP measurement is not enough time to switch to fully maximise oxidative metabolism.

M059K cells show a similar profile to the U87MG, they have a decreased ATP with FCCP although not significant and a portion of the ATP pool is sensitive to oxamate.

RD, RH30, old U87MG and M059K all experienced a significant drop in ATP levels when treated with 2-DG. This was a little unexpected as it was assumed that by inhibiting glycolysis the cells would use the other substrates to maintain ATP and support OXPHOS similar to the response seen in the 0mM glucose samples. The cells treated with 2-DG had only been exposed to 2-DG for 45 minutes while the cells on 0mM glucose had an overnight incubation to adjust so perhaps the dramatic loss of ATP was as a result of the cells not switching over their metabolism to the new substrates in a shorter time frame. It would be interesting to have a longer 2-DG treatment and assess the effect on ATP would it recover.

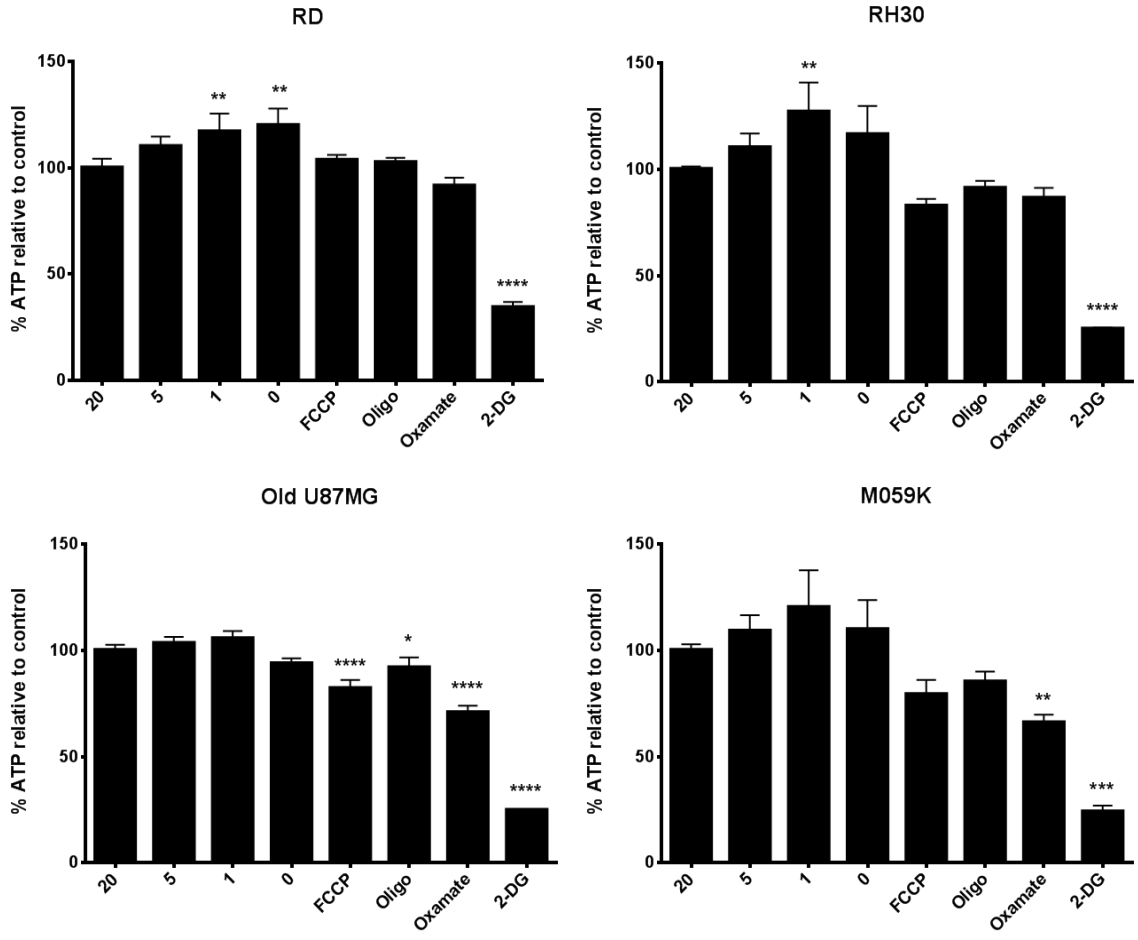

Figure 2.11: ATP levels in RD, RH30, old U87MG and M059K cells cultured overnight in various glucose concentrations with 75,000 cells seeded per well. Data is normalised to cell number (Hoechst) and ATP levels are relative to control cells grown on standard media (20mM glucose). Cells treated with mitochondrial modulators were grown on 20mM glucose and exposed to inhibitors/uncouplers for 45 minutes before measuring ATP.

SF188 cells maintained their ATP levels on all glucose concentrations, as well as FCCP and oligomycin treatments. Oligomycin was shown to significantly decrease OCR in these cells (Figure 2.7) and while removing the glucose did not increase their OCR rates, suggesting they are quite aerobic, they had considerable basal levels of glycolysis. So perhaps in this instance the ATP level is maintained solely through compensatory up-regulation of glycolysis. The oxamate ATP decrease is again

evident in the SF188 cells. KNS42 cells experienced a significant drop in ATP levels when glucose was removed, this is consistent with the decrease seen in OCR rates. It would seem that glucose has a major role to play in the bioenergetic function of this cell line. FCCP also caused a reduction in ATP most likely due their over reliance on mitochondrial oxidative phosphorylation and an inability to increase glycolysis, oligomycin reduced ATP but not as much as one might have expected for cells that rely so heavily on oxidative metabolism. Oxamate did not affect the ATP levels adding strength to the argument that these cells are highly oxidative. ATP levels in UW479 cells were unaffected by everything except 2-DG. The glycolytic Res259 cells experienced ATP decreases when treated with oxamate and 2-DG as has been seen in all the other glycolytic lines examined thus far in this study.

Inhibition of hexokinase by the glucose analogue 2-DG caused significant ATP depletion in all lines (>50%) but did not completely eliminate the ATP levels. Possibly reasons for this include 1) there was not enough time to switch over metabolism so there is an initial decrease before ATP levels can be restored, 2) glutamine and the TCA cycle are sustaining the remaining levels or 3) glycogen was mobilised to restore the glycolytic pathway downstream of the hexokinase inhibition.

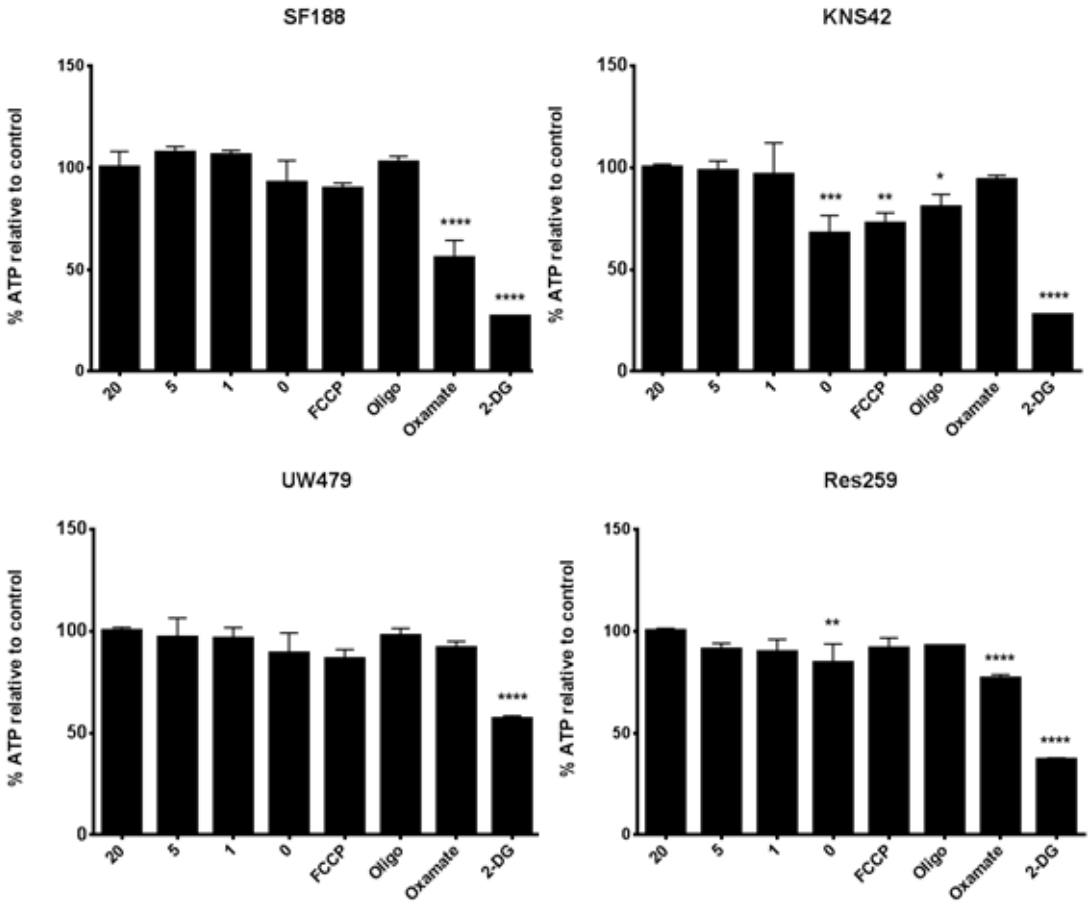

Figure 2.12: ATP levels in SF188, KNS42, UW479 and Res259 cells cultured overnight in various glucose concentrations with 75,000 cells seeded per well. Data is normalised to cell number (Hoechst) and ATP levels are relative to control cells grown on standard media (20mM glucose). Cells treated with mitochondrial modulators were grown on 20mM glucose and exposed to inhibitors/uncouplers for 45 minutes before measuring ATP.

2.3.2 Assessing the metabolic phenotype of cells grown in 3D systems

2.3.2.1 Spheroid Metabolism

Current methods for assessing cell metabolism and screening new chemical entities to treat cancer are based upon cancer cell lines grown in 2D monolayer culture, which is physiologically distinct from 3D tumours and tissues from which the cells

are derived (Yamada and Cukierman, 2007). The non-physiological, artificial environment of cell monolayer based assays for drug discovery can lead to low predictability when drugs move into clinical trials (Nirmalanandhan et al., 2010). To better understand the in-vivo behaviour of cancerous tumours 3D cell culture models should be utilised.

A spheroid model was investigated as it is more comparable to the in-vivo scenario in terms of complex architecture, more physiological cell-cell and cell-matrix interactions, tight junctions that allow for cell to cell communication as well as functioning as a barrier to mass transport (Mehta et al., 2012). Spheroids are characterised by having high density and closely packed cells and as the spheroids expand and grow it leads to concentration gradients of oxygen and glucose as well as carbon dioxide and waste products thereby leading to a heterogeneous cell population containing sub-populations of necrotic, hypoxic, quiescent and proliferating cells, similar to in-vivo tumours (Khaitan et al., 2006). The interactions between cells in a 3D environment have been shown to change expression of RNA and protein (Hirschhaeuser et al., 2010).

The 2D bioenergetic profile of the cell lines have been described earlier in this chapter but it is unknown what effect, if any, a 3D environment will have on the energetic status of the lines.

The first 3D model investigated were spheroids utilising BD Matrigel™ Matrix and ultra-low adherent multiwell plates so that the cell-cell interactions will favour cell-surface ones and thereby enhance the spheroid assembly (Lin and Chang, 2008). The

intention was to assess the energy metabolism status, of all the cell lines, cultured as spheroids. However, the M059K, SF188, UW479 and Res259 cells all formed tiny spheroids that did not proliferate and expand during a 7 day culture period and as such were deemed unsuitable to work with. RD, RH30, U87MG and KNS42 spheroids were selected for metabolic assessment as these grew well in the spheroid model.

The MitoXpress O_2 assay has only been described so far as being applicable for use in 2D cell culture. Preliminary studies showed that OCR can also be measured for spheroids using as few as 6 spheroids per well (data not shown). As with any model system, 3D spheroids have their advantages and disadvantages. One of the major disadvantages studying OCR and ECAR in spheroids is that an extremely large number of them were required. Approximately 500 would be required to assess the OCR and ECAR of spheroids on high (20mM) and no (0mM) glucose only with an n=3. Picking and selecting spheroids is time consuming with media changes and the scale of production increasing experimental variability. For these reason only four cell lines forming good spheroids where selected for the OCR/ECAR spheroid study. The four lines were chosen based on (i) their ease to produce uniform spheroids and (ii) for the metabolic phenotype they displayed in 2D. In this pilot experiment, we wanted to look at each of the phenotypes observed in 2D and take a representative sample from across the range. The lines assessed were RD and KNS42 (aerobic in 2D), RH30 (intermediate metabolism) an old U87MG (very glycolytic in 2D).

All the spheroids were cultured in normal media (20mM glucose, 1mM sodium pyruvate and 2mM L-glutamine) for 5 days. On the 6^{th} day they were transferred to

assay plates (black, clear bottom, 96 well plates). They were left to adhere overnight and the following day the media was changed and the spheroids were either maintained on normal media (20mM glucose, 1mM sodium pyruvate and 2mM L-glutamine) or changed to glucose free media (1mM sodium pyruvate and 2mM L-glutamine). Images of the spheroids in the wells were taken immediately before running the metabolic assays (Figure 2.13). The RD, old U87MG and KNS42 spheroids attached loosely to the wells (enough to make changing the media easy) however, the RH30 cells once attached to the wells proliferated quite rapidly to occupy the entire surface of the well almost to the point where the spheroids lost their spheroid shape. This was quite surprising, as when these cells grow in 2D they do not proliferate very rapidly (Rapa et al., 2012).

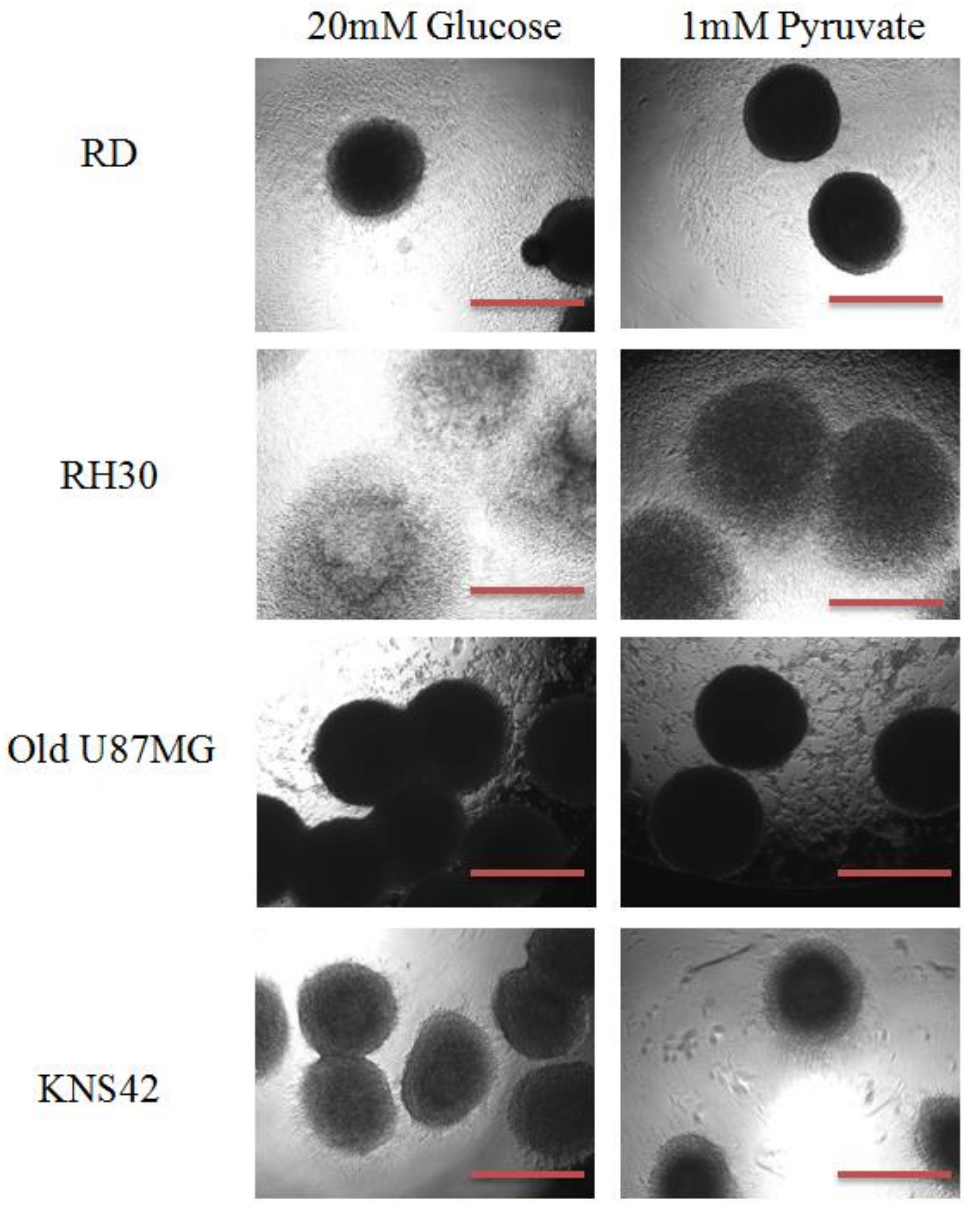

Figure 2.13: Spheroid images before measuring their OCR and ECAR rates. After 5 days 12 spheroids were transferred into each well of a black clear bottom 96 well plate and allowed to adhere overnight then imaged. Scale bars represent 1000µm. Spheroids cultured in glucose free media contained 1mM pyruvate and 2mM glutamine.

The OCR profiles obtained for the cells in 3D spheroids (Figure 2.14) resemble their 2D profiles (Figure 2.3). RD spheroids do not increase their respiration when glucose is removed suggesting they are significantly aerobic in the presence of glucose. RH30 and old U87MG can both up regulate their respiration when glucose is removed as was seen in 2D and KNS42 spheroids are aerobic and have the highest basal OCR of all the lines.

The ECAR profiles for the spheroids are quite interesting. The RD and KNS42 cells were shown to have low basal ECAR in 2D (as was seen in Figure 2.3). However, when cultured as spheroids there is a large increase in acidification for both lines on high glucose media (Figure 2.14). The KNS42 spheroids have more than double the ECAR rate of the RD spheroids and is comparable to the ECAR rates observed for the U87MG spheroids (Figure 2.14)

If OCR is plotted against ECAR it becomes apparent that the profile of the RH30 and KNS42 spheroids has changed (Figure 2.15). In 2D RH30 cells had intermediate levels of acidification while the KNS42 cells had negligible levels. In spheroids RH30 and KNS42 are as glycolytic as the old U87MG spheroids. When glucose is removed from the spheroids the RD and KNS42 spheroids maintain the same level of respiration but have reduced acidification levels while the RH30 and old U87MG spheroids increase respiration and reduce acidification. This is seen in Figure 2.15 by the data points shifting diagonally towards the left hand side of the bottom graph. It is important to note that it is most likely only the cells in the outer layer of the

spheroids are contributing to the respiration and acidification recorded.

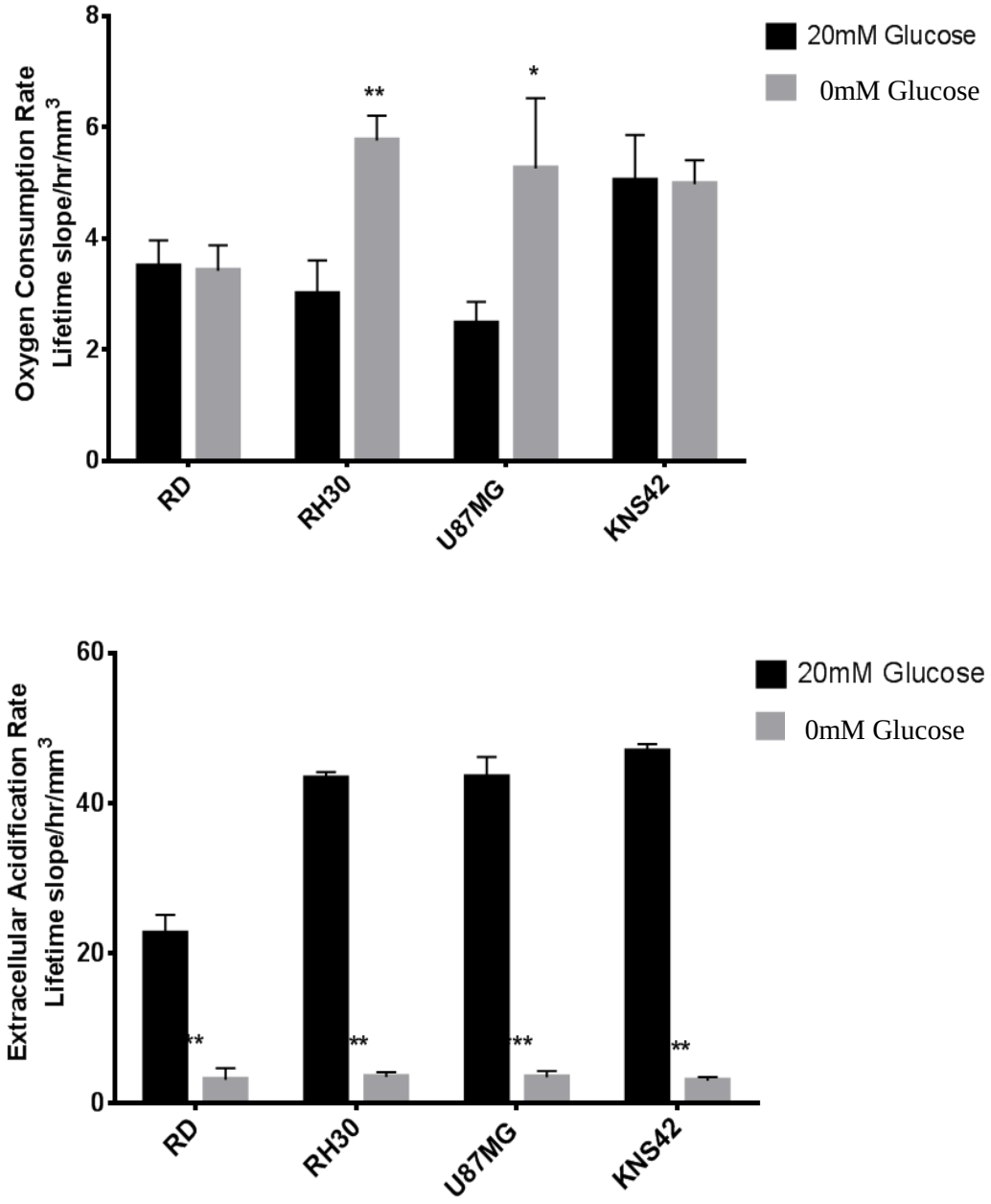

Figure 2.14: Metabolic profile of the RD, RH30, Old U87MG and KNS42 cells grown as 3D spheroids. Spheroids were cultured in round bottom plates for 5 days, transferred to black clear bottom plates overnight and the following day assay media was added which either contained high glucose (20mM glucose, 1mM pyruvate and L-glutamine) or no glucose (same as normal minus glucose). Oxygen consumption rates are shown in the top graph and extracellular acidification rates in the bottom graph. N = 3 and the error bars represent the standard deviation of the mean.

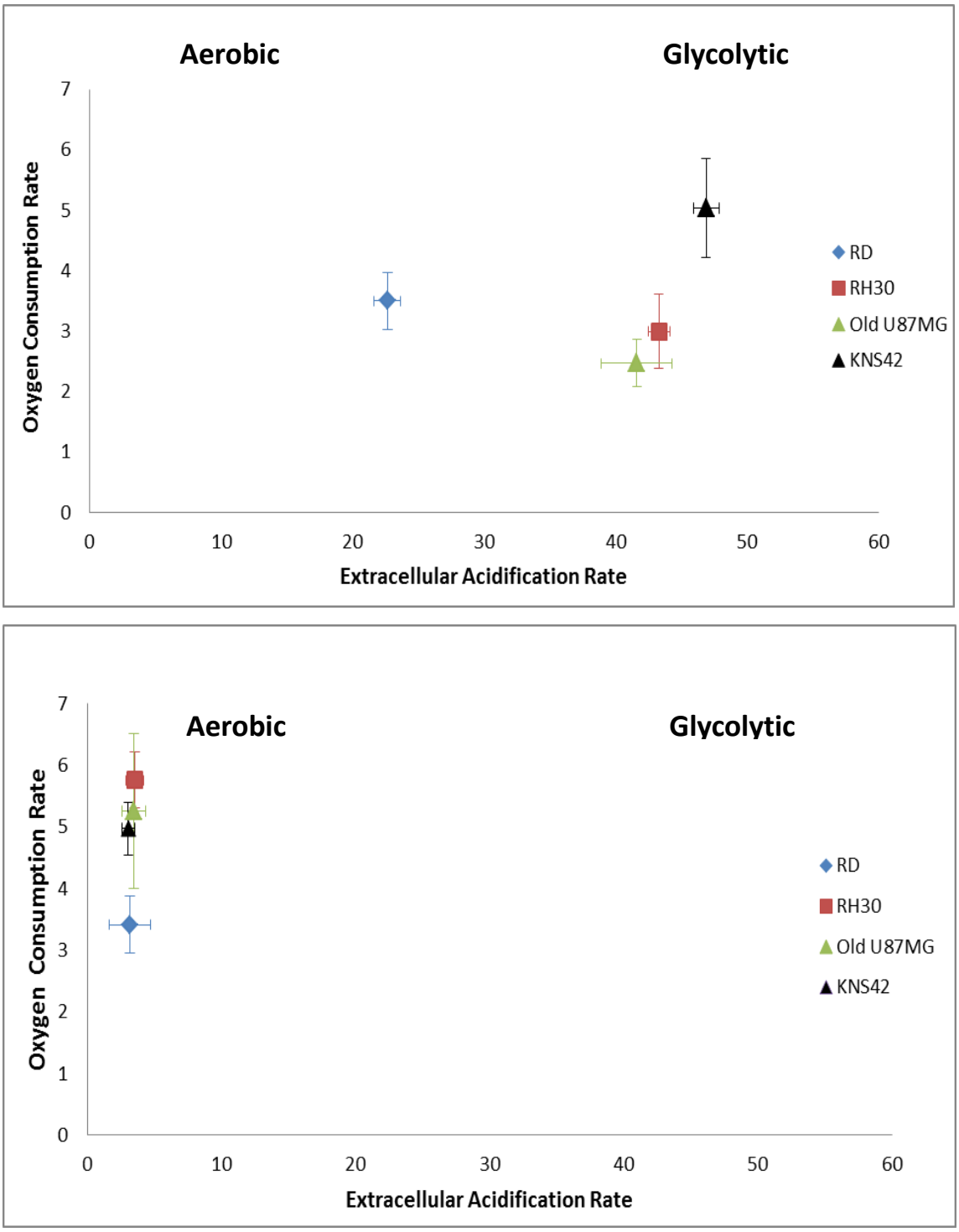

Figure 2.15: Bioenergetic profile of spheroids grown on normal media (20mM glucose) (top) and glucose free media (bottom). This OCR ECAR figure depicts the relationship between oxygen consumption and acidification rate. N = 3 and the error bars represent the error of the mean

2.3.2.2 3D Alvetex Metabolism

Another promising system for culturing cells in 3D is the Alvetex scaffold (Reinnervate Plc). This is a new commercially available polystyrene scaffold that has the same chemistry as standard cell culture plates, allowing direct comparison between the 3D and 2D monolayer culture. Alvetex® is a vastly porous polystyrene scaffold created for 3D cell culture (Figure 2.16). Cells cultured in an Alvetex scaffold regain a more natural tissue-like morphology. This impacts on cellular function and allows cells to behave in a more physiologically relevant manner. The scaffolds are just 200µm thick, which is important to ensure sufficient diffusion of gases, nutrients and waste products between the cells and cell culture medium, whilst enabling 3D cell growth. This is approaching the diffusion limit for many molecules including oxygen but depending on the scaffold format you chose and the cell density the cells may never be more than 100µm from nutrients and oxygen. The scaffold is designed in such a way that greater than 90% of it is free space allowing cells to easily move into and grow in the scaffold. The scaffold materials are similar to that used in 2D culture and are designed to be inert (Knight et al., 2011). They do not contain any proteins of ECM of animal origin (unlike the matrigel spheroids). Studies using the Alvetex scaffold have not been widely published as it is a relatively new product to the market however one study has reported that it improves the viability of primary hepatocytes and the 3D environment induces changes in some of the cytochrome-P450 enzymes that allow for better predictions to be made in drug metabolism screening programs (Schutte et al., 2011).

The aim was to compare the properties of the new 3D scaffold system to the established 3D spheroid model. Alvetex is more user friendly than the spheroid model; it is easier to feed the cells and as the scaffold is fixed it is far less labour and time intensive to set up assays and change the culture media. The Alvetex system theoretically has the potential to allow experiments to be set up under defined oxygen and nutrients conditions with all cells in the 3D scaffold exposed to the same levels of oxygen and nutrients. In a spheroid nutrient and oxygen gradients are dependent on the metabolic properties of the cells and the size of the spheroids.

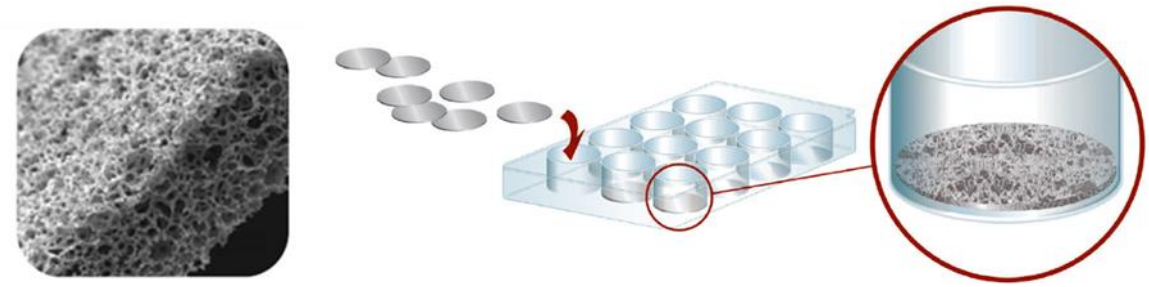

Figure 2.16: SEM of cross-section through Alvetex. Cells proliferate and fill the space created

Due to the fact that this is a more relatively high throughput 3D system (as opposed to spheroids) all the lines investigated in 2D were re-investigated in 3D Alvetex (apart from Res186 due to culturing issues). A complicating factor with this system is that, contrary to what the manufacturers say, it is really quite difficult to visualise the cells once they are seeded in the scaffold. A preliminary experiment was conducted where cells were seeded at various densities and their proliferation into the scaffold monitored over a period of a week. It was difficult to see exactly how far into the scaffold the cells had grown (without fixing, embedding and sectioning the scaffolds). Neutral red staining as suggested by the manufacture was uniform throughout the well and the cells were avidly consuming glucose as the media

required daily changes. From this it was decided that 100,000 cells initial seeding density was appropriate for all the cells lines for a 7 day culture period (data not shown).

The RD and RH30 cells were cultured for 5 days on normal media (20mM glucose, 1mM pyruvate and 2mM L-glutamine) and the media was replenished daily. The media was replaced on day 6 with DMEM containing 1mM pyruvate and 2mM glutamine and 20, 5, 1 or 0mM glucose overnight. Before assaying on day 7 fresh media was added to all wells. OCR and ECAR data has been normalised to total protein levels (mg).

2.3.2.3 RD cells when cultured in Alvetex show a more glycolytic phenotype than was previously observed in 2D or 3D spheroids cultures

When cultured in this system the RD cells showed a surprising result in that they significantly increased their respiration rates once the glucose was reduced to 5mM and below and their ECAR dropped when glucose was reduced to 5mM (Figure 2.17). This was not seen for the cells grown either in 2D or in spheroids (Figure 2.5 & Figure 2.14). Is it possible that these cells are more differentiated when cultured on this scaffold. RD cells are tumour cells derived from muscle. They fail to withdraw from the cell cycle and go through terminal differentiation to myotubes. (Ostrovsky et al., 2002) These RD cells have been used in a study by Vergani et al to study muscle defects (Vergani et al., 2007). They reported that differentiation from myoblasts to myotubes involves a bioenergetic shift from glycolysis to oxidative phosphorylation. In contrast to this, we see a shift from oxidative phosphorylation to

glycolysis. It is not certain what is happening to the cells but the change in their bioenergetic profile suggests they have altered metabolism in this 3D structure on high glucose. This could be investigated further by carrying out immunoblotting or immunohistochemistry to look at specific muscle marker proteins. The basal ECAR of RD cells on 20mM glucose was significantly higher than for the RH30 which again is the opposite of what is seen in the other two model systems. RH30 cells grown on Alvetex maintain their "glycolytic phenotype" (Figure 2.17).

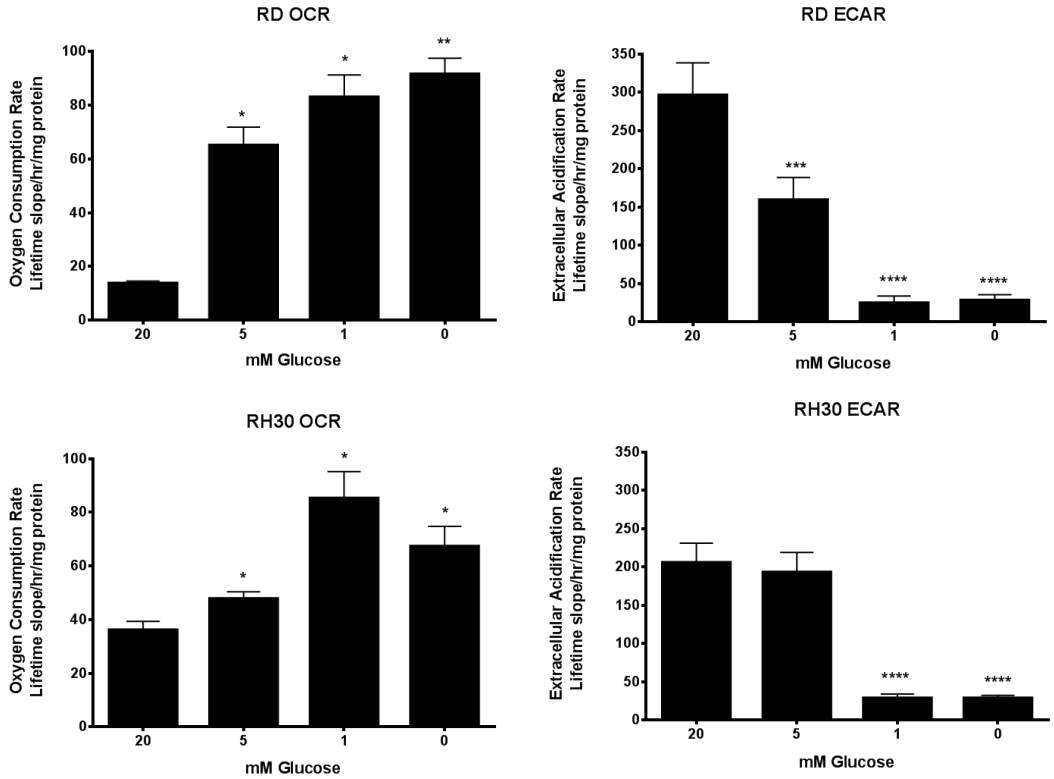

Figure 2.17: OCR and ECAR profiles of RD and RH30 cells cultured in the 3D Alvetex scaffold. Cells were assayed in media containing either 20, 5, 1 or 0mM glucose as well as 1mM pyruvate and L-glutamine. The cells treated with pharmacological modulators were grown on normal media (20mM glucose). Cells were seeded in at 100,000/well and fed every day for 5 days. On the sixth day, the media was changed to assay media (various glucose concentrations) and incubated overnight. Fresh media was added to each well prior to measurement. N = 1 and the error bars represent the standard deviation of the mean of triplicate wells.

2.3.2.4 U87MG cells achieve maximum respiration rates on higher glucose concentrations compared to 2D

The old U87MG bioenergetic profile also changes when the cells are cultured in Alvetex. In 2D, there is a gradual increase in respiration each time the glucose is reduced but in the Alvetex the cells reach maximal respiratory capacity somewhere below 20mM glucose and above 5mM (Figure 2.18). A possible reason for this could be that the cells were avidly consuming the glucose and if glucose levels in the media were depleted this would increase the rate of respiration. Interestingly at 5mM glucose while there is maximal aerobic respiration there is no negative effect on ECAR, this most likely rules out limited glucose as the reason for the increased OCR and suggests the cells are carrying out higher rates of glycolysis and more mitochondrial glucose oxidation. The increased OCR in the 5mM glucose sample could be due to better utilisation of glutamine and pyruvate. The acidification rate is unchanged compared to 20mM glucose. The M059K cells maintain a profile similar to 2D culture, they increase aerobic respiration and decrease their acidification somewhere between 5 and 1mM glucose Figure 2.18.

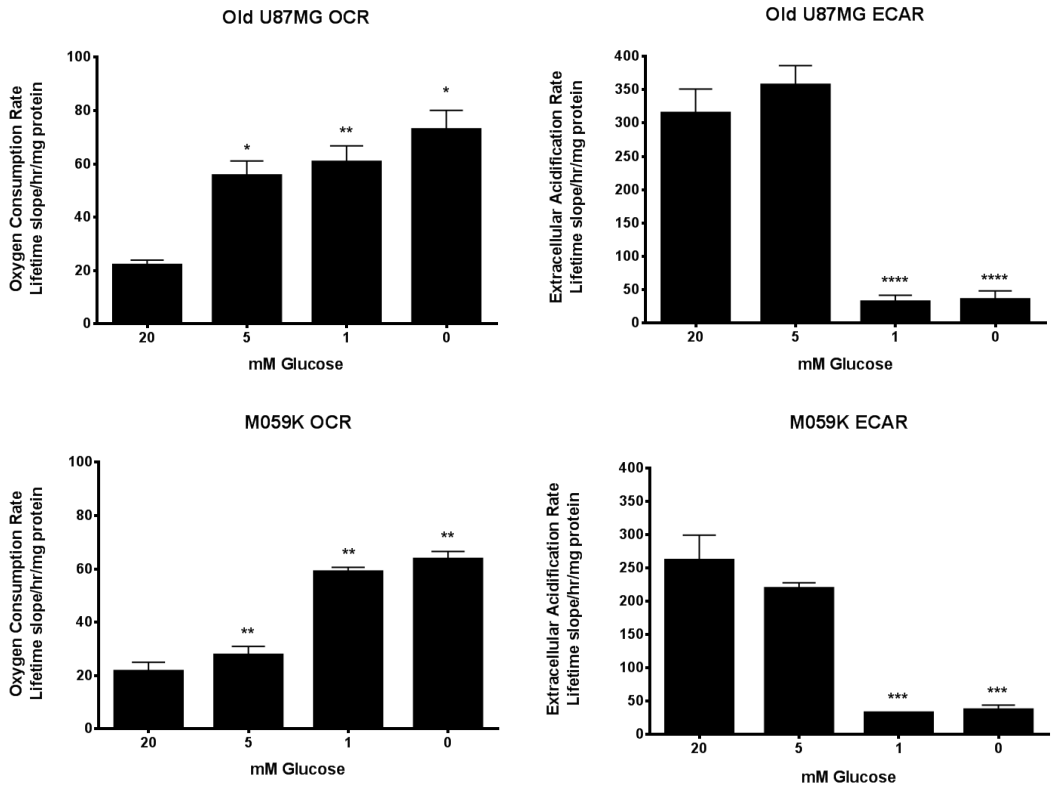

Figure 2.18: OCR and ECAR profiles old U87MG and M059K cells cultured in the 3D Alvetex scaffold. Cells were assayed in media containing either 20, 5, 1 or 0mM glucose as well as 1mM pyruvate and L-glutamine. The cells to be treated with pharmacological modulators were grown on normal media (20mM glucose). Cells were seeded in at 100,000/well and fed every day for 5 days. On the sixth day the media was changed to assay media (various glucose concentrations) and incubated overnight. Fresh media was added to each well prior to measurement. N = 1 and the error bars represent the standard deviation of the mean of triplicate wells.

2.3.2.5 High grade paediatric gliomas have markedly different metabolic phenotypes in Alvetex compared to 2D

The SF188 grade IV glioma cells were shown to carryout high levels of mitochondrial glucose oxidation in 2D as decreasing the glucose could not further increase the rates of respiration (in addition they also had surprisingly high basal levels of acidification (Figure 2.7). In Alvetex, SF188 oxygen consumption rates can be increased almost two-fold when glucose is removed from the media indicating a change in their bioenergetic profile (Figure 2.19). Similarly, they have high ECAR rates on 20mM glucose, which deceases as the glucose is reduced. KNS42 cells experience an unexpected and significant decrease in their respiration rates when cultured on 1mM glucose but on glucose free media their rates are equivalent to the basal rates on 20mM glucose. It is unknown why this decrease occurs. This experiment was only conducted once so further repeats are required to draw more solid conclusions from this data. The UW479 cells remain aerobic as in the 2D model but there is a non-significant trend towards decreased respiration on the lower glucose concentrations. Res259 cells retain a profile consistent with their 2D profile (Figure 2.20).

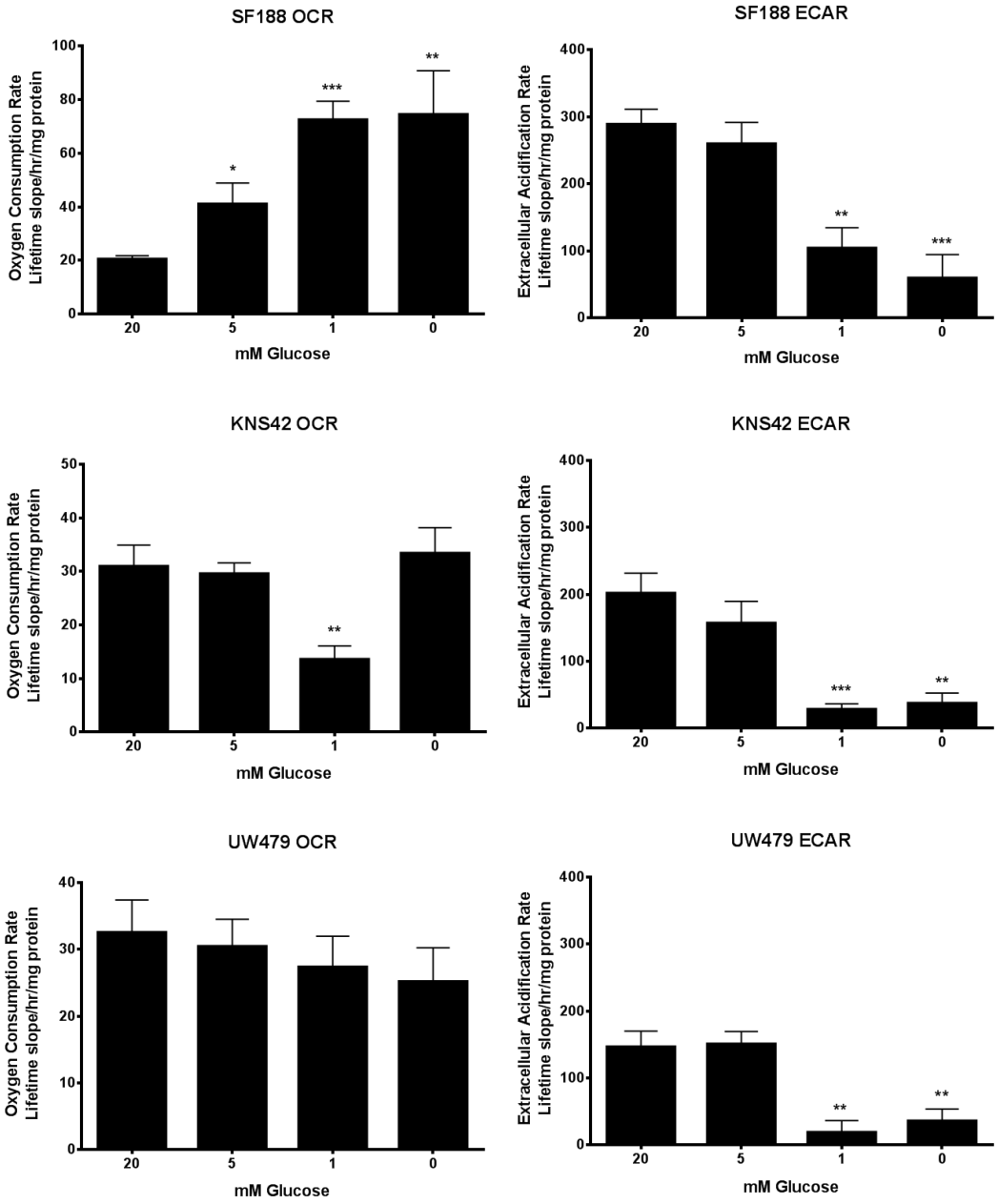

Figure 2.19: OCR and ECAR profiles SF188, KNS42 and UW479 cells cultured in the 3D Alvetex scaffold. Cells were assayed in media containing either 20, 5, 1 or 0mM glucose as well as 1mM pyruvate and L-glutamine. The cells to be treated with pharmacological modulators were grown on normal media (20mM glucose). Cells were seeded in at 100,000/well and fed every day for 5 days. On the sixth day the media was changed to assay media (various glucose concentrations) and incubated overnight. Fresh media was added to each well prior to measurement. N = 1 and the error bars represent the standard deviation of the mean of triplicate wells.

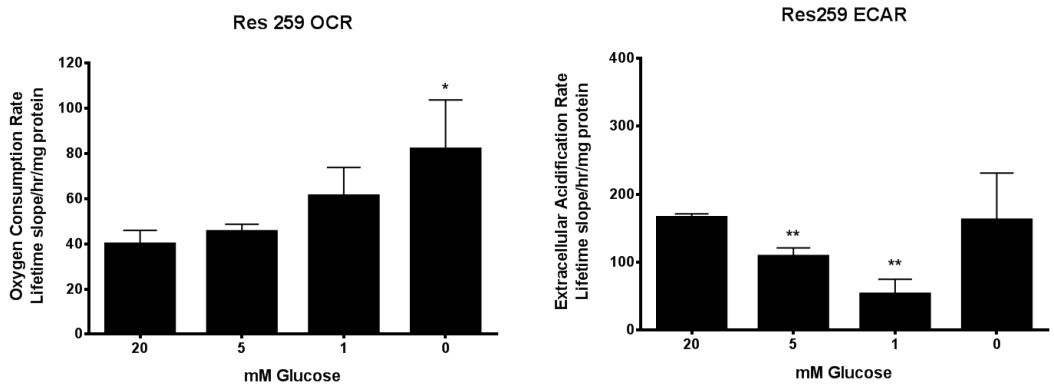

Figure 2.20: OCR and ECAR profile of Res259 cells cultured in the 3D Alvetex scaffold. Cells were assayed in media containing either 20, 5, 1 or 0mM glucose as well as 1mM pyruvate and L-glutamine. The cells treated with pharmacological modulators were grown on normal media (20mM glucose). Cells were seeded in at 100,000/well and fed every day for 5 days. On the sixth day the media was changed to assay media (various glucose concentrations) and incubated overnight. Fresh media was added to each well prior to measurement. N=1 and the error bars represent the standard deviation of the mean of triplicate wells.

As mentioned previously it is extremely difficult to visualise the cells in this system and it is difficult to quantify cell number. Therefore, as a means of normalising the data from the metabolic assays protein was extracted from the wells and the total protein extracted (in mg) was used to normalise the OCR ECAR data (Figure 2.21). The protein in each well was extracted in a small volume of extraction buffer and replicate wells were pooled in order to get a large enough volume to run the samples through a BCA assay. Once collected as a measure of how well the extraction went more buffer was added to each well and these samples were analysed for protein. The second extractions were found to contain little or no protein (data not shown). This highlights that the protein extraction works well in this system with all the protein being collected.

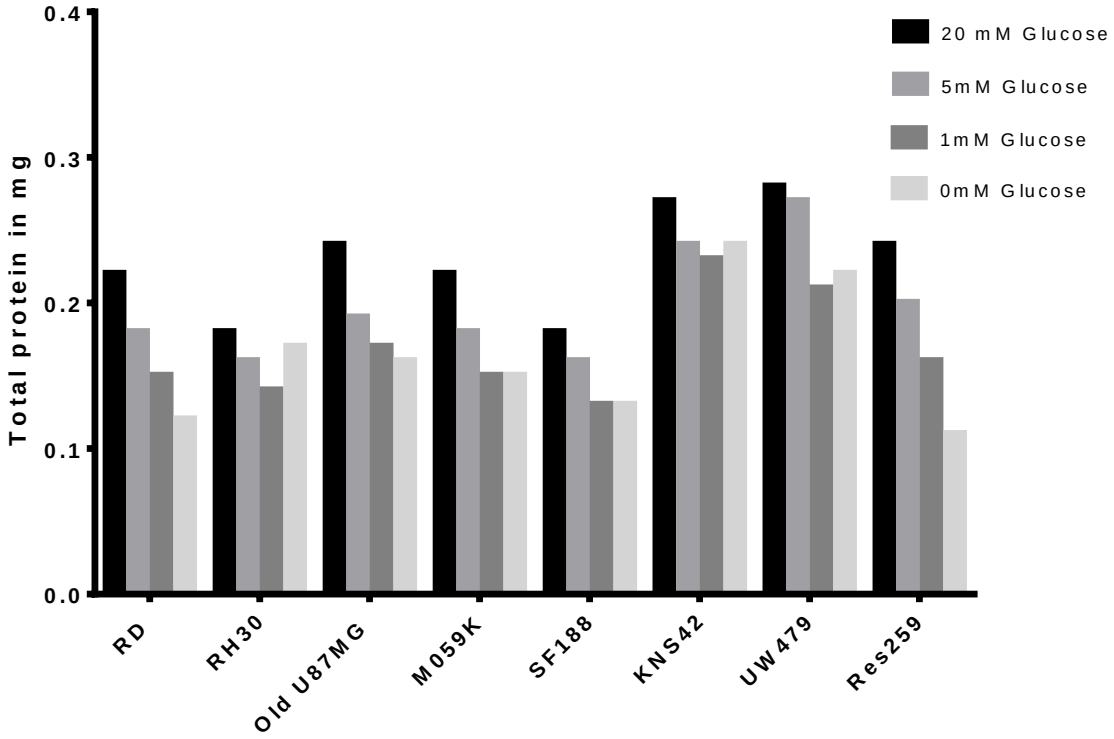

Figure 2.21: Total protein concentrations harvested from the Alvetex scaffold from all cell lines on various media types. Proteins were harvested immediately after metabolic assays were completed.

All the lines follow the same expected trend of decreasing protein concentration following overnight exposure to reduced glucose conditions. It is of interest to note that the paediatric gliomas that demonstrated improved viability under low glucose in 2D with the Hoechst assay do not follow the same trend in the Alvetex system.

2.3.3 Comparison of metabolism in the three model systems

The three model systems investigated show interesting differences in how energy metabolism can be altered when cultured in a different environment. Figure 2.22 shows how the three systems compare to one another. The most obvious differences

between them are that KNS42 cells become more glycolytic in spheroids. The RH30 cells also increase their acidification rates in spheroids but are less glycolytic in the Alvetex and the RD cells display a glycolytic phenotype on high glucose in the Alvetex scaffold.

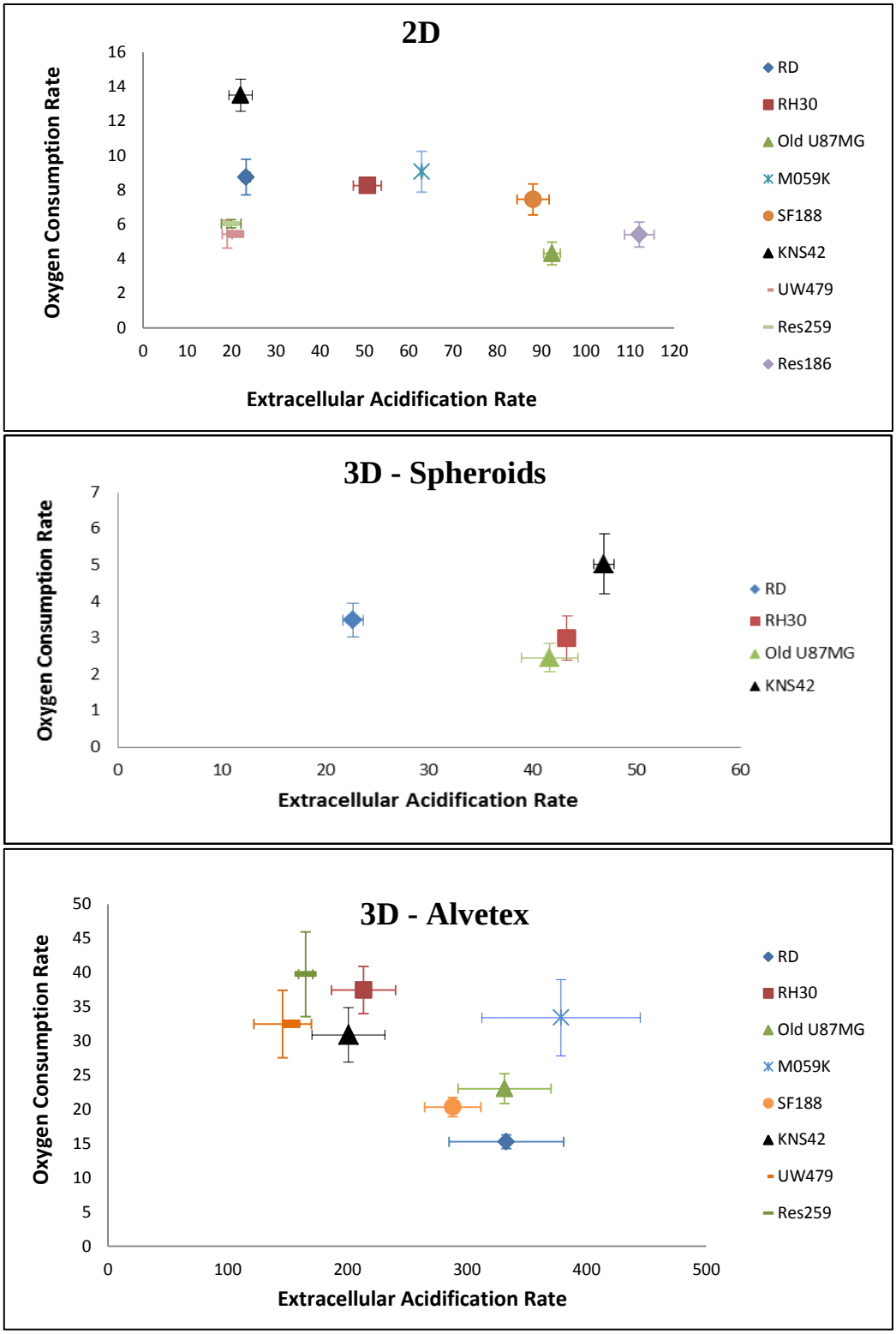

Figure 2.22: Bioenergetics profile of the cells grown on 20mM glucose in 2D (top), spheroids (middle) and Alvetex (bottom).

2.3.4 Can the bioenergetic profiles observed be explained?

Given that each type of cancer varies in its genetic mutation profile is it possible that there is a common mechanism to explain why some cells display the Warburg phenotype on high glucose media under high oxygen conditions and others do not? PET scans show an increased uptake of glucose in tumours due to over expression of GLUT transporters and historically increased glucose uptake has been associated with supporting the Warburg effect (Zu and Guppy, 2004). However, high glucose uptake does not automatically equate to increased glycolysis and reduced mitochondrial metabolism. The increased glucose uptake could be for conversion to lipids. In addition, over expression of these glucose transporters cannot be assumed to correlate with increased metabolic flux. Each enzyme in the glycolytic pathway makes a different contribution to metabolic flux. Therefore, only the enzymes involved in the rate limiting steps of the pathway can influence glycolysis. Key rate limiting enzymes include hexokinase (HK), phosphofructokinase (PFK) and pyruvate kinase (PK) (Diaz-Ruiz et al., 2011). HKII is the main isoform up regulated in cancer and gliomas in particular (Wolf et al., 2011). It interacts with the mitochondrial membrane and as such has direct access to ATP generated from Oxphos, therefore functional mitochondria are essential to maintain high rates for glycolysis (Mathupala et al., 2009). While the Warburg effect is the long term re-programming of metabolism, the Crabtree effect is a more short-term phenomenon where cellular respiration decreases in response to increased glucose (Crabtree, 1928). The mechanism underlying the Crabtree effect remains unclear.

It has been assumed that increased glucose uptake is due to an activated glycolysis pathway and a subsequent suppression of oxidative metabolism. This assumption is being challenged with emerging evidence highlighting that cancer cells can be oxidative or glycolytic (Wallace, 2012).

Changes in the rate limiting enzymes in the glycolytic pathway such as hexokinase (HKII) could possibly explain the increased glycolysis associated with the Warburg effect. HKII interacts with voltage dependent anion channel (VDAC) on the outer membrane of the mitochondria. When HKII interacts with the mitochondria it utilises ATP derived from oxidative metabolism demonstrating that in order to maintain high glycolytic rates the mitochondria must remain functional (Mathupala et al., 2006). In this study Hexokinase levels were assessed using western blotting and found to be highly expressed in the cell lines that displayed high ECAR rates with the exception of SF188 (Figure 2.23).

Pyruvate is a key player in both glycolysis and oxidative metabolism (Sutendra and Michelakis, 2013). It can enter the mitochondria and help to drive the ETC or it can complete the glycolytic pathway in the cytosol and be converted to lactate. If pyruvate does not enter the mitochondria then the TCA activity is decreased and this can happen if the gate-keeping enzyme PDH is inhibited. PDH is regulated by phosphorylation and is inactivated when phosphorylated by PDK and PDK is up regulated in many cancer types (Papandreou et al., 2011). PDK1 expression was assessed in all lines but there was no correlation seen between the expression of PDK and the glycolytic capacity of the cells (Figure 2.23). However, westerns only

measure total protein levels and do not provide information on the activity of the enzyme.

Normoxic stabilisation of Hif is thought to contribute to the Warburg effect, as Hif is responsible for the up-regulation of many glycolytic enzymes and over expression of glucose transporters. PDK1 is also regulated by Hif (Kim et al., 2006) and similar to the PDK1 Hif expression in the cell lines showed no correlation between levels of protein expressed and how glycolytic the cells were under normoxia (21%) and high glucose (20mM).

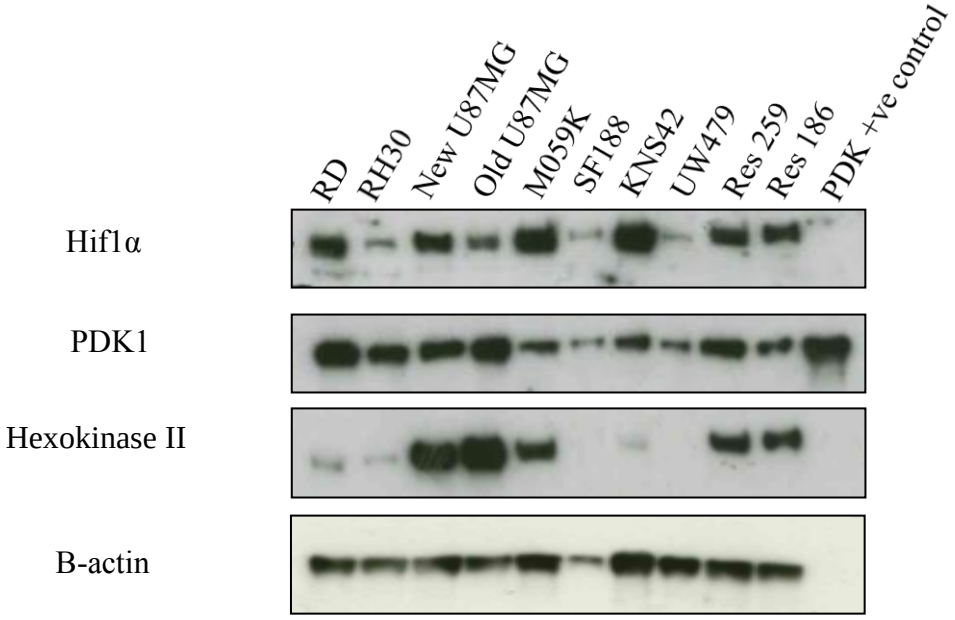

Figure 2.23: Hif1a, PDK1 and HKII levels were assessed in all the lines (cultured in 2D under high glucose conditions) and HKII expression was found to be increased in the lines that displayed glycolytic phenotypes.

Hexokinase II and PDK1 were also assessed in protein extracted from spheroids (Figure 2.24). PDK1 was expressed in RD, RH30, old U87MG and KNS42 at similar levels seen in 2D. Interestingly, HKII was expressed in all spheroids despite RD and KNS42 cells not expressing HKII in 2D culture. RD and KNS42 were shown

previously to have increased ECAR (glycolysis) rates in spheroids (Figure 2.14) that may correlate with the HKIII up-regulation observed by immunoblotting (Figure 2.24). As total spheroid protein extracts were immunoblotted the increased HKII observed could link to high levels of expression within a subpopulation of the spheroid structure. Future investigations should carry out immunohistochemistry (IHC) on fixed sections from spheroids to determine whether local changes in protein levels occur. As glucose and oxygen gradients exist across the spheroid and the core is likely to be necrotic it is highly likely that expression differences in proteins involved in energy metabolism will be observed.

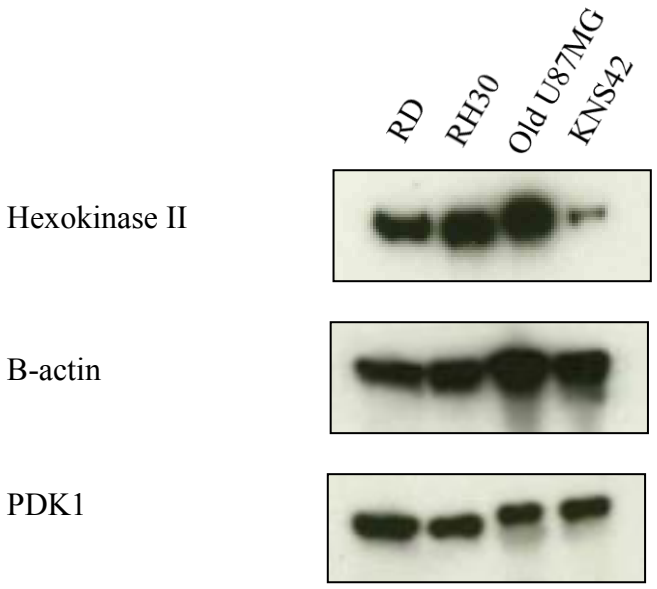

Figure 2.24: Hexokinase is up regulated in RD and KNS42 cells when cultured as spheroids

2.3.5 NMR Metabolomics Analysis

In this study, we have shown that the RD, SF188, KNS42 and UW479 cancer cell lines display an aerobic phenotype in standard culture conditions (5-20mM glucose) in 2D and the remaining lines (RH30, old U87MG, M059K and Res259) all have the

capacity to change to a more aerobic phenotype when glucose levels are reduced . To further investigate the glycolytic and Oxphos profiles of these lines C13-labelled glucose was used to trace the fate of glucose through cellular energy metabolism. It was not feasible to do this for all the lines so an aerobic line (RD) and glycolytic (U87MG) on high glucose media were assessed as examples of the two types of cancer energy metabolism observed in our 2D models.

Metabolomics is a field of study that is closely related to genomics and proteomics. It gives information on the activity of enzymes by looking at the metabolites produced by them. The metabolome is a collection of every metabolite produced by chemical reactions in a biological system and metabolomics is the study the metabolites produced in these reactions. Metabolomics involves the use of analytical instrumentations such as NMR and MS based techniques to enable the identification of the chemical "fingerprints" produced during and after various cellular processes. Metabolomics does not give insight into the dynamics of the processes merely a snapshot of the cell at a particular time.

2.3.5.1 U-^{13}C glucose labelling to investigate cell metabolism

Cells were grown to 90% confluency before removing their regular growth medium, washing with PBS and replacing with medium containing l-glutamine, pyruvate and 20mM U-^{13}C glucose for 2 hours. Extracts were harvested as per methods section and analysed by 1D NMR, in collaboration with Dr. Tim Claridge, Dept. Chemistry.

The basis of NMR is that nuclei in atoms can behave like magnets. When these nuclei are in an externally applied magnetic field, they will align with the field.

Radiofrequency (RF) waves are then applied and the nuclei will absorb some of their energy and change direction so that they are aligned against the magnetic field. Once the RF is stopped, the nuclei return to their ground energy state and emit radiation that is characteristic of each nuclei. Each nucleus in a molecule is affected and influenced by its neighbouring nuclei (in a phenomenon known as coupling). This coupling can also be measured and allows the structure of the metabolite to be identified by looking at specific nucleus within the molecule and its relative location within the molecular structure (Pitt A. and Kolch W. 2009). 13C will resonate at a specific frequency, depending on the chemical environment and the proximity of other carbon nuclei; spin-spin coupling will result. Peaks are generated for the different nuclei with each peak separated by a coupling constant, which tells you about the distance between the signals. By looking at the distance between the peaks and the chemical shifts, the metabolite can be identified and its specific labelling pattern linked to the pathway that produced it.

^{13}C-NMR of the U87MG (glycolytic) and RD (aerobic) cell extracts revealed many similarities between the two cell lines with spectra showing multiple of peaks ^{13}C labelled metabolites Figure 2.25. At first glance, the two profiles look almost identical. It is only when each section of the spectra are studied in more detail that several differences become apparent.

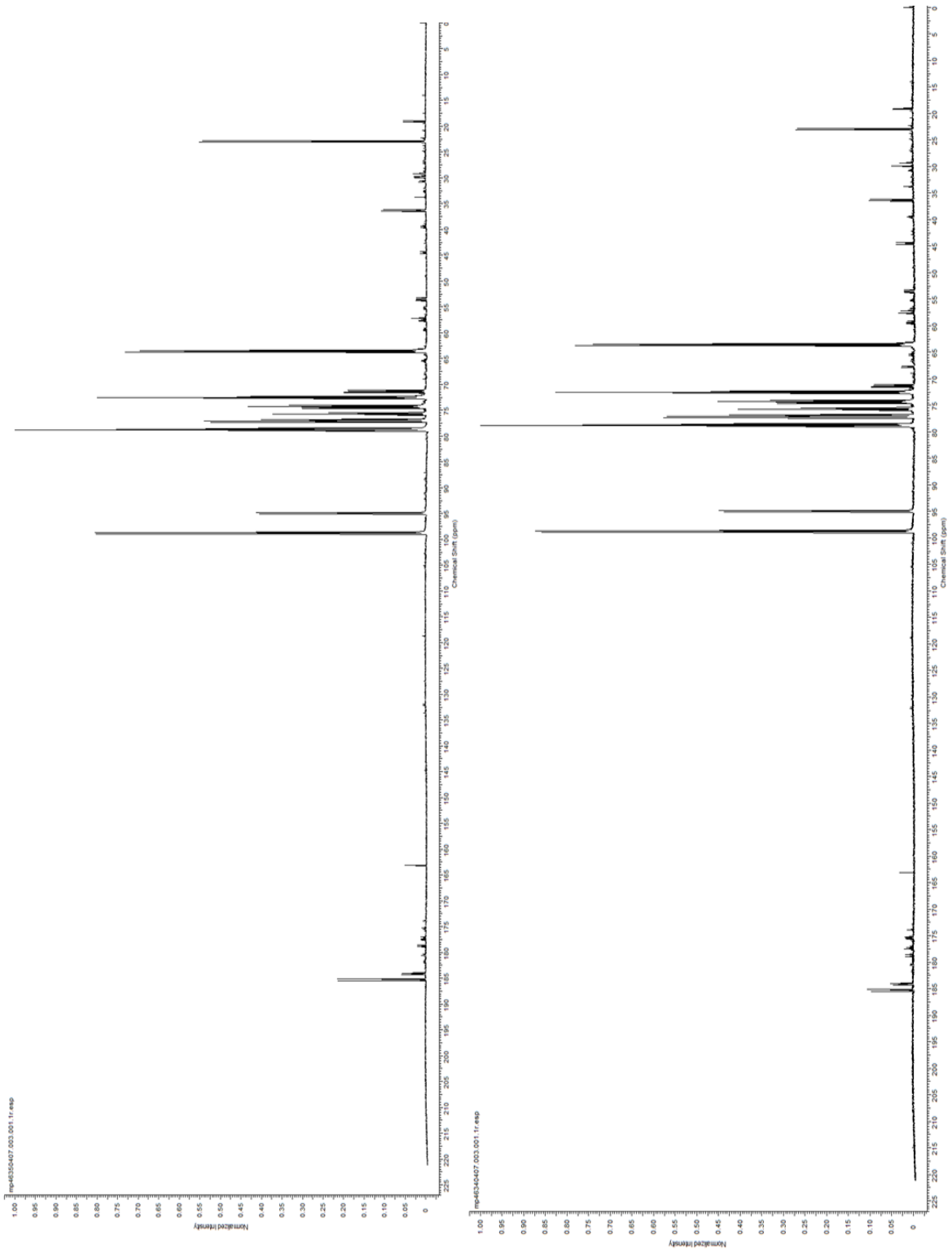

Figure 2.25: Whole 1D NMR spectrum of U87MG cells (top) and RD (bottom). Both spectra share many similar peaks.

In Figure 2.26 the potential fate of universally labelled glucose is illustrated depicting how it is metabolised through the glycolytic pathway to lactate or through pyruvate into the TCA cycle. Glycolysis will produce pyruvate and lactate molecules that are labelled in all three-carbon positions. If the TCA cycle is functioning normally, (active PDH) then after the first cycle glutamine and glutamate doublets labelled in the 4-5 position can be seen (Figure 2.26). This labelling can only occur if PDH and the TCA cycle result in glucose oxidation via the mitochondria. As the TCA cycle completes further cycles other multiplet labelling patterns are seen (in 3,4 and 5 carbon positions) and evidence of complete turnover of the cycle is confirmed by double doublets (quartets) in glutamine and glutamate C4 position (Marin-Valencia et al., 2012).

Closer examination of the spectra shows that there is significant TCA cycle activity in both cell lines (Figure 2.27, Figure 2.28, Figure 2.29 and Figure 2.30). Figure 2.27 shows glutamate 4-5 doublets in both U87MG and RD cell lines. The U87MG extract also shows double doublets (Q) which are generated from complete turnover of the TCA cycle. The RD extract contained the doublets but not the quartets and the reason for this is unknown. Nonetheless, TCA activity was seen in both lines. Glutamine 4-5 doublets were seen in Figure 2.28. Both lines had almost identical spectra in this region. Labelling demonstrates that there was de-novo synthesis of glutamine from labelled glutamate. Figure 2.29 and Figure 2.30 show further glutamine and glutamate labelling patterns suggestive of TCA cycle activity but there are also considerable differences between the two cell types. This will require further analysis in the future.

In Figure 2.30 glutamate at carbon 2 was shown to have 2-3 doublets in both cell lines. This labelling pattern is suggestive of anaplerosis (processes involved in replenishing intermediates for the TCA cycle). If pyruvate is carboxylated by PC this can give rise to the pattern we see (Fan et al., 2008).

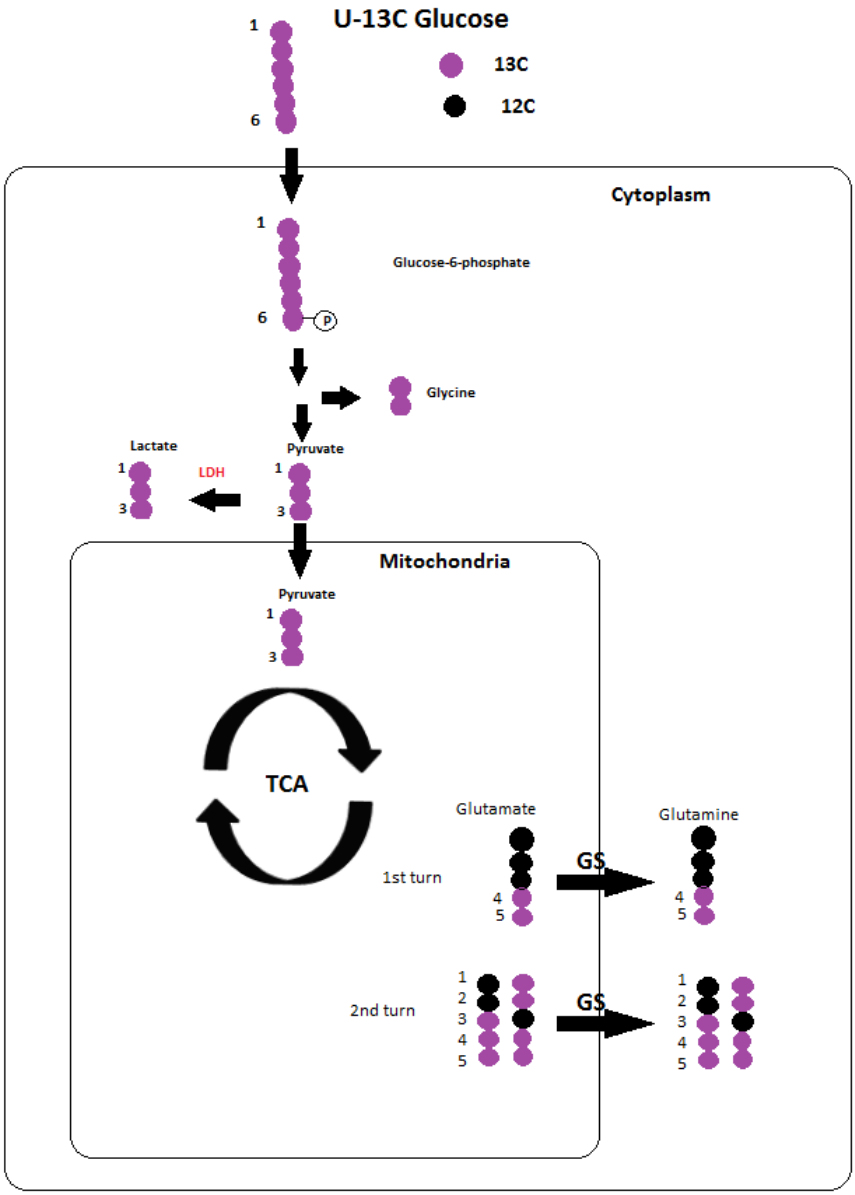

Figure 2.26: Schematic depicting the fate of U-^{13}C glucose in the cell (figure adapted from Marin-Valencia et al).

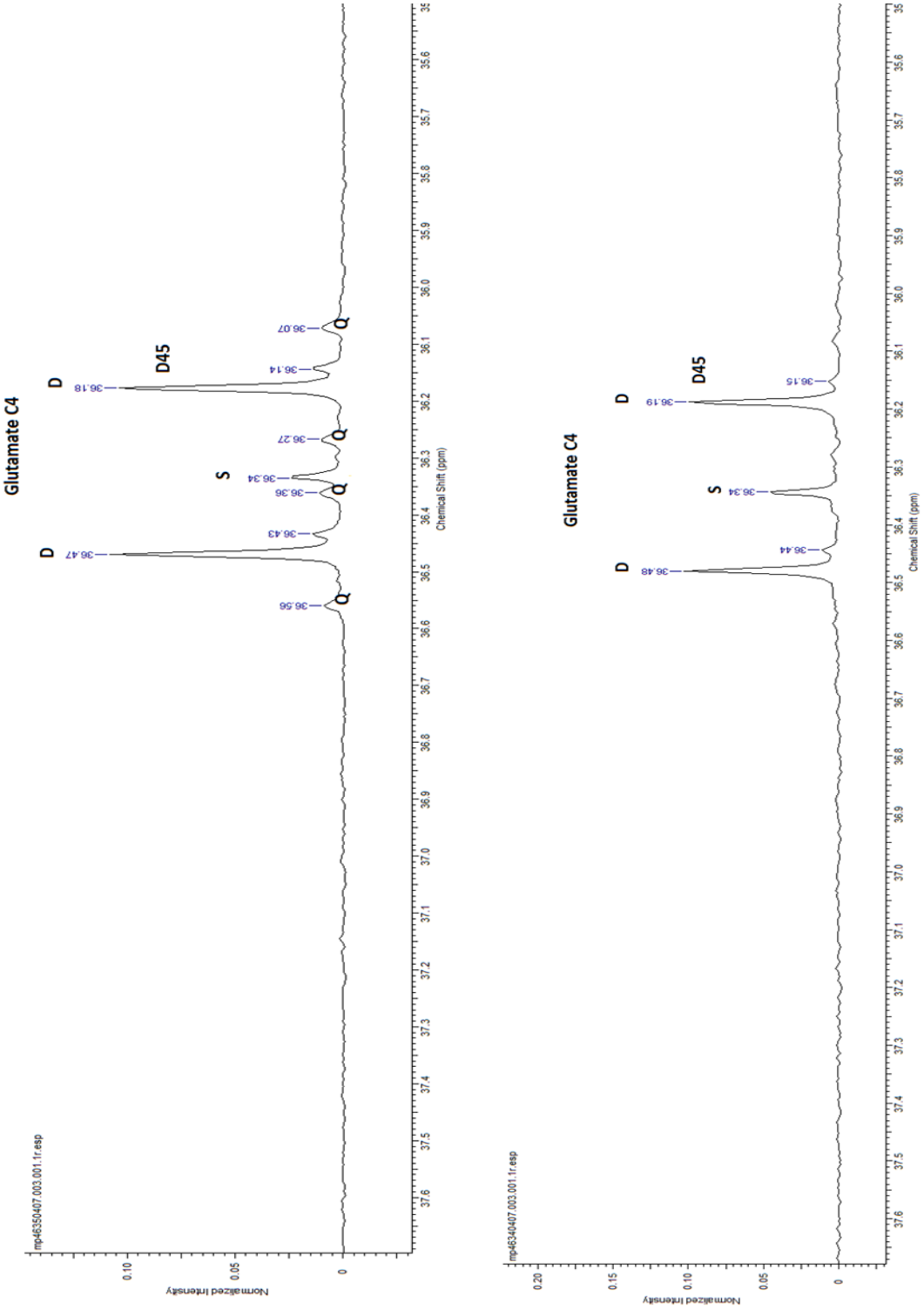

Figure 2.27: Part of a 1D NMR spectrum of U87MG (top) and RD (bottom) cells that were grown on U-13C glucose for 2 hours. Both spectra show glutamate 4-5 doublets at 36.19ppm.

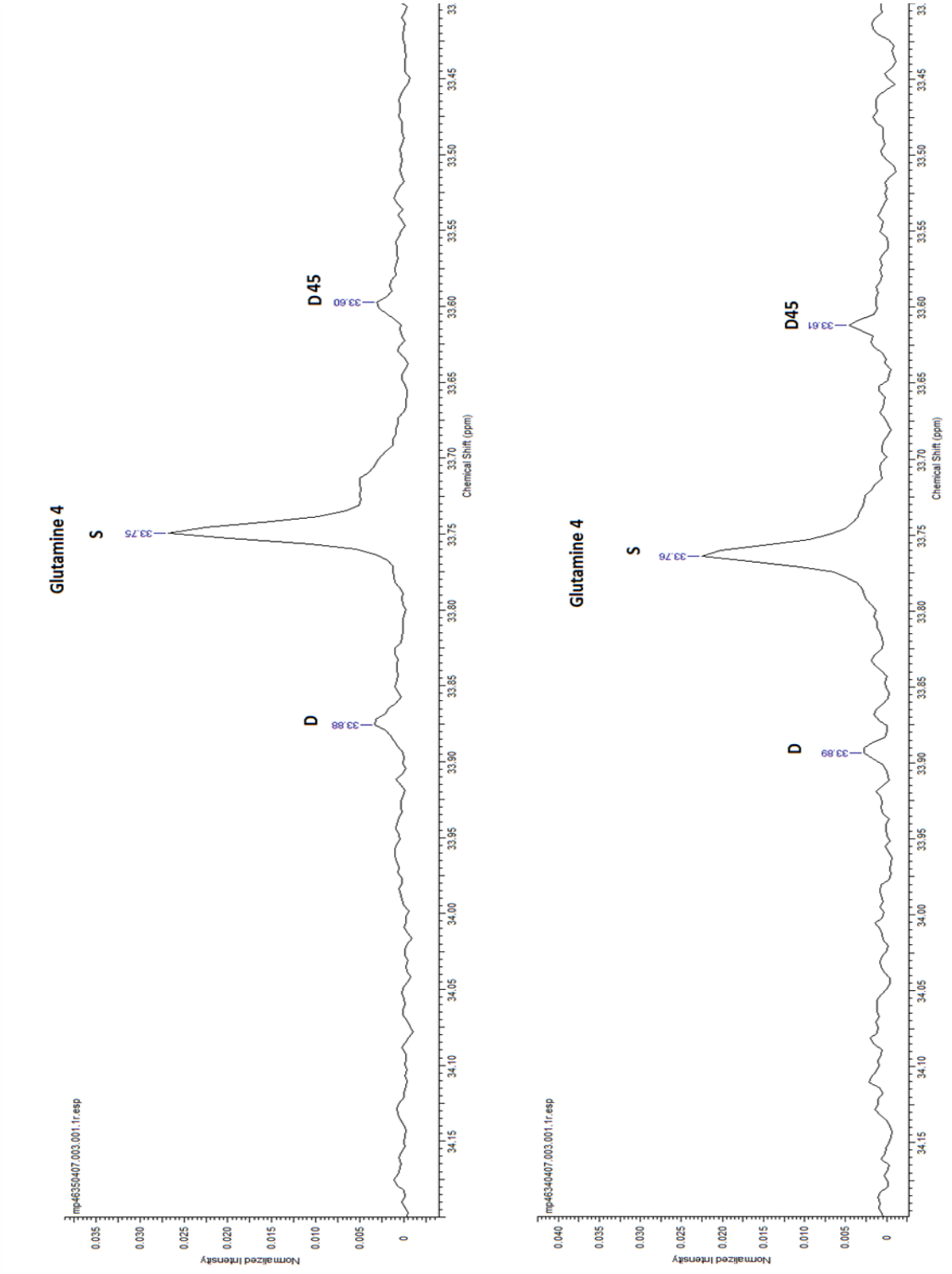

Figure 2.28: Part of a 1D NMR spectrum of U87MG (top) and RD (bottom) cells that were grown on U-^{13}C glucose for 2 hours. Both spectra show glutamine 4-5 doublets at 33.61ppm .

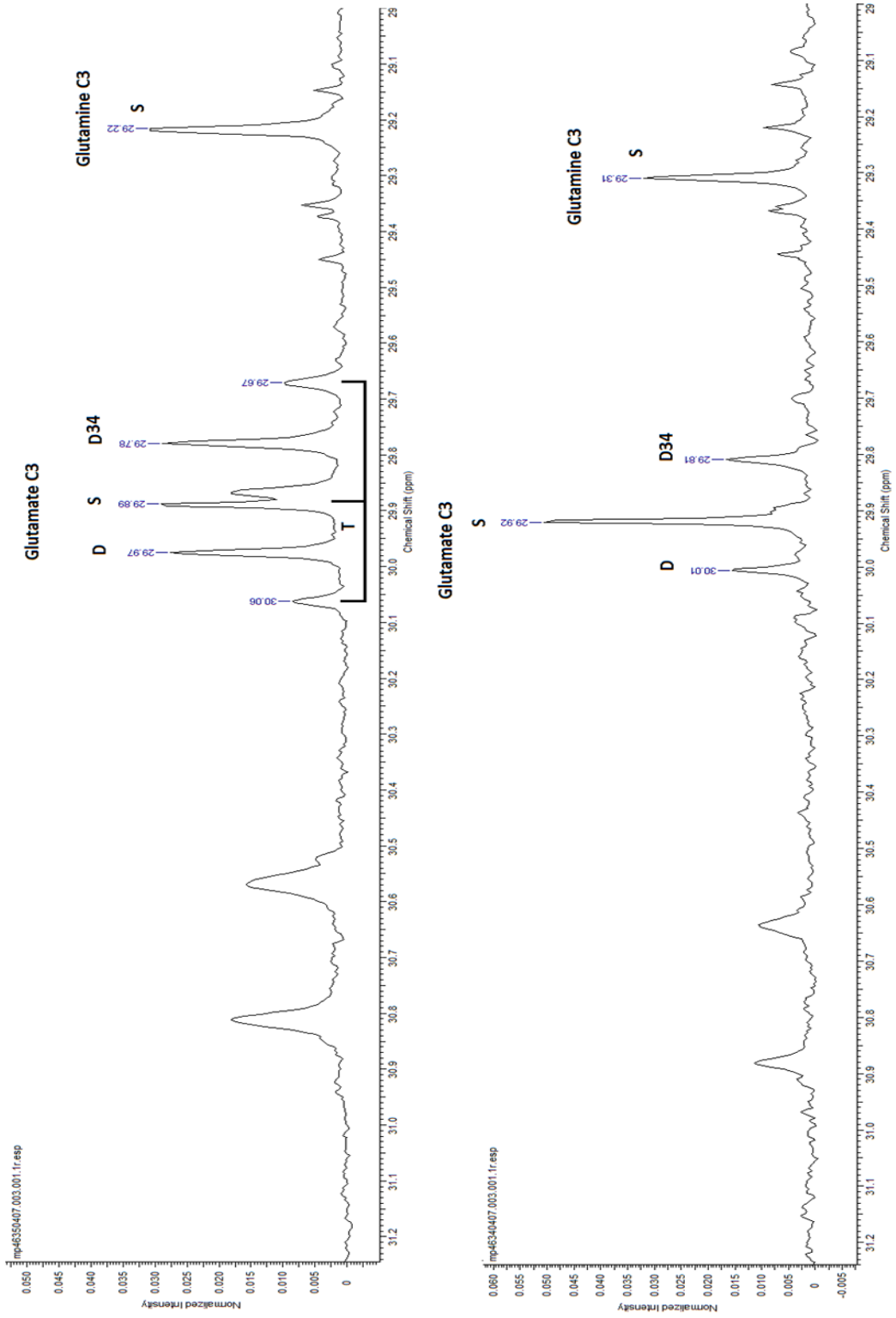

Figure 2.29: Part of a 1D NMR spectrum of U87MG (top) and RD (bottom) cells that were grown on U-13C glucose for 2 hours. Both spectra show glutamate 3-4 doublets at 29.78ppm.

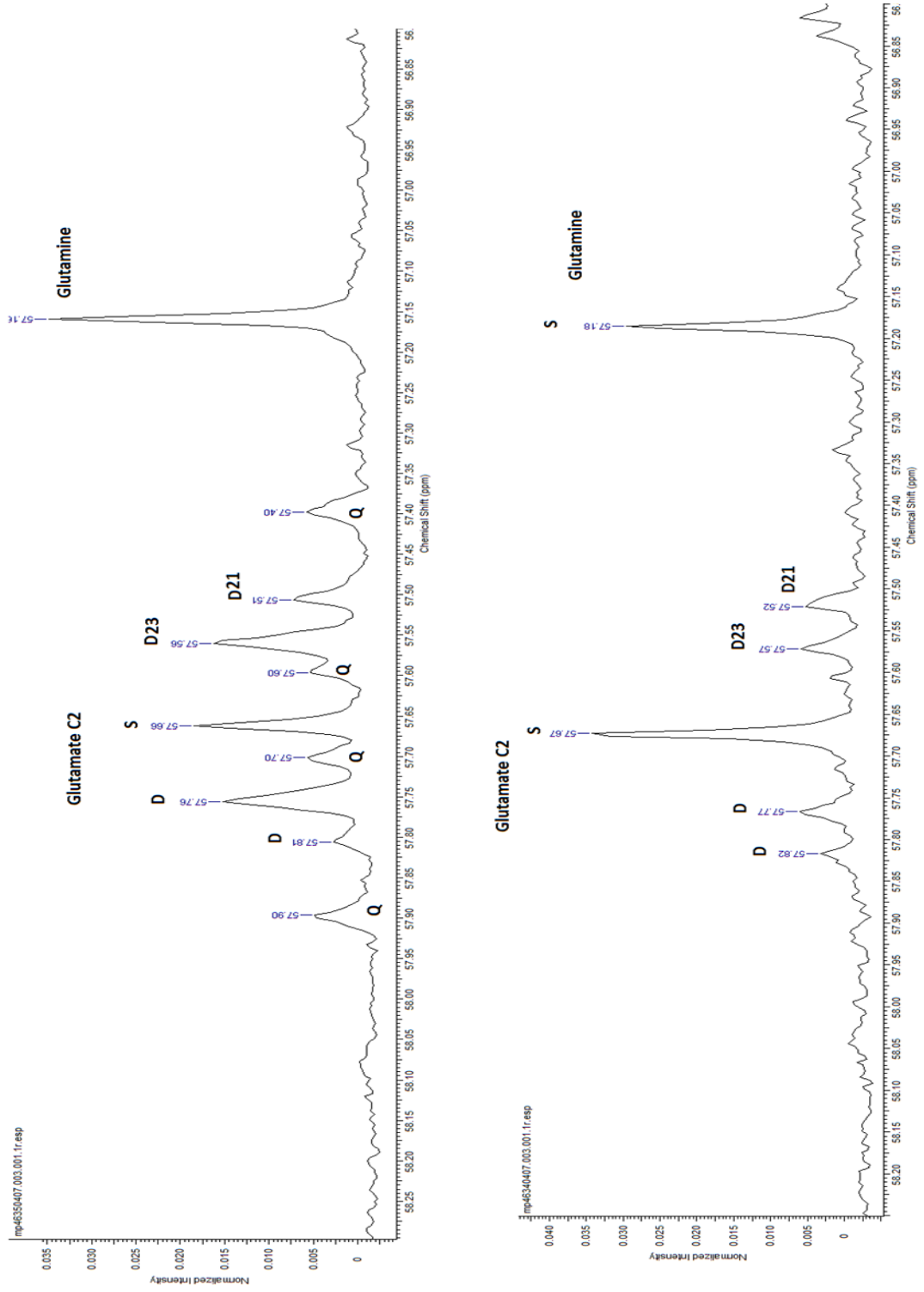

Figure 2.30: Part of a 1D NMR spectrum of U87MG (top) and RD (bottom) cells that were grown on U-13C glucose for 2 hours. Both spectra show glutamate 2-3 and 2-1 doublets as well as double doublets (Q).

As the data generated from the 2D metabolic assays (Figure 2.6) indicated the U87MG cancer line to be very glycolytic on 20mM glucose we anticipated finding very little in the way of TCA cycle intermediates and identifying large pyruvate and lactate peaks. Large lactate peaks were seen for the U87MG but also for the RD cell line, which had shown a more aerobic energy profile (Figure 2.31 and Figure 2.32). Considerable lactate peaks were also seen in the RD extract albeit slightly smaller peaks than the U87MG cells. As no internal standards were used in these experiments the concentrations of lactate cannot be quantified with peak sizes giving relative amounts The lactate peaks in the RD extracts were a little unexpected given their aerobic nature and low levels of ECAR. However, as the metabolic data earlier demonstrated although aerobic metabolism plays an important role in these cells glycolysis also contributes to the cells grown on 20mM glucose.

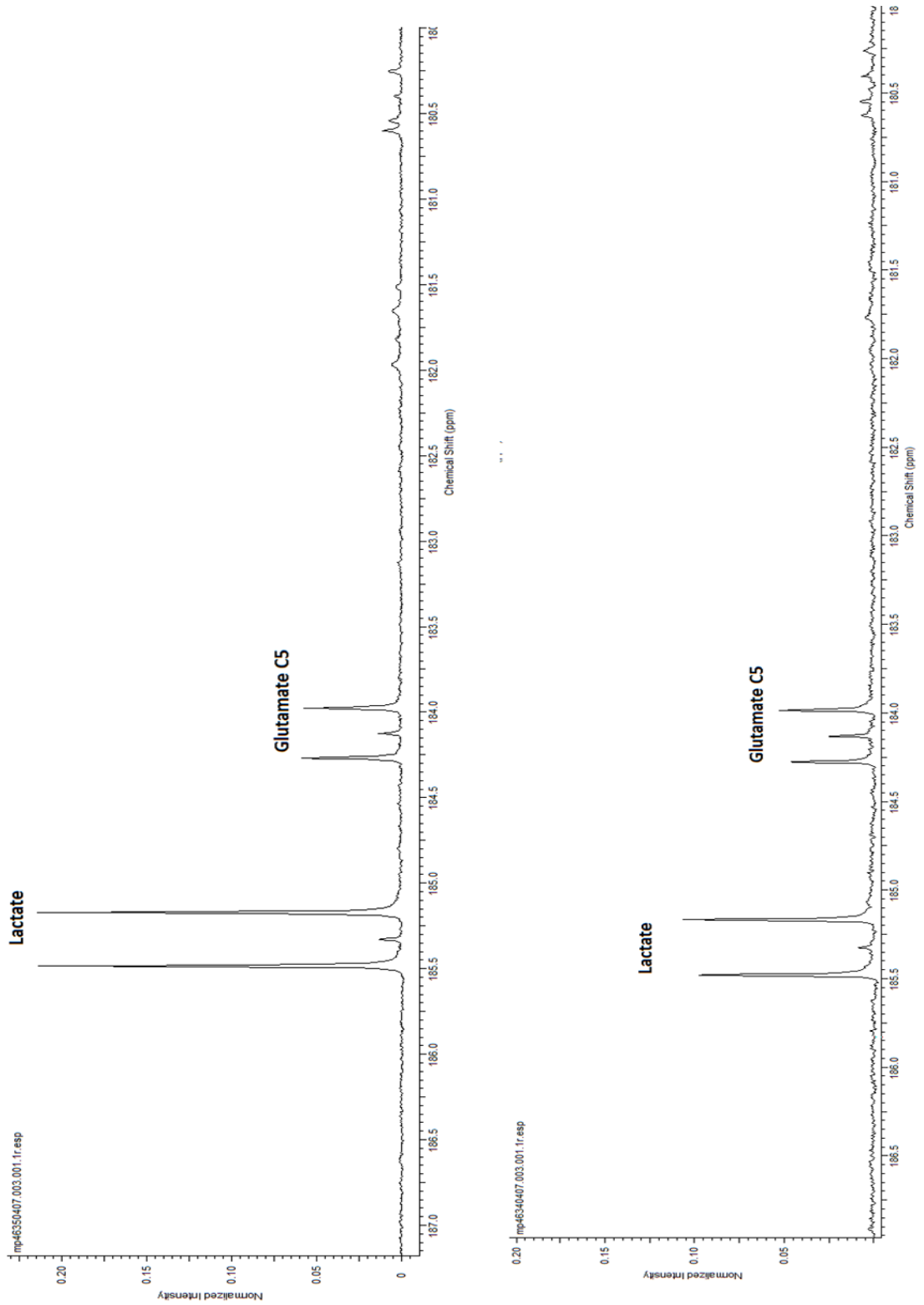

Figure 2.31: Part of a 1D NMR spectrum of U87MG (top) and RD (bottom) cells that were grown on U-13C glucose for 2 hours. Both spectra show significant lactate peaks around 185ppm.

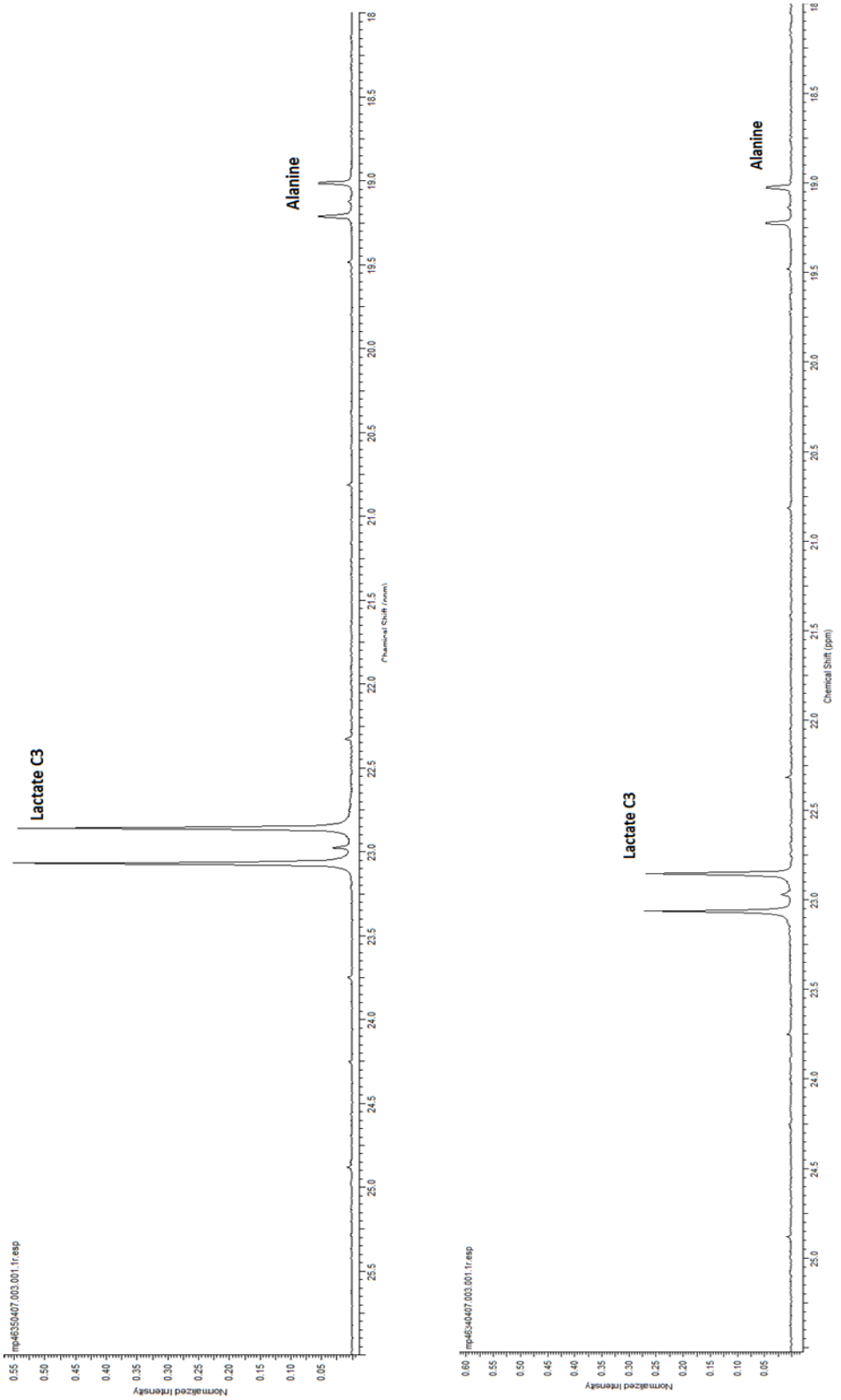

Figure 2.32: Part of a 1D NMR spectrum of U87MG (top) and RD (bottom) cells that were grown on U-13C glucose for 2 hours. Both spectra show significant lactate peaks around 23ppm

2.4 Discussion

2.4.1 2D bioenergetic profiles

By the mid 1900's cancer cells were known to have characteristic metabolic alterations as first identified by Otto Warburg in the 1920's. His early studies suggested the presence of mitochondrial dysfunction in cancer cells and an over reliance on glycolysis for ATP production. After this initial finding alterations in the rates of lipid synthesis and glutaminolysis were also realised and it is now accepted that reprogrammed cancer cell metabolism is a complex process.

While highly significant and clinically beneficial Warburg's original hypothesis was flawed as it stated respiration was inactive. Numerous studies have repeatedly demonstrated that this is not entirely true. Glycolysis is up regulated in several cancer types but in many cases, there is little evidence to suggest the presence of any mitochondrial dysfunction. However, there is always an exception that proves the rule. Petros et al reported that mitochondrial DNA (mtDNA) mutations can increase tumourgenicity but the mutations are acquired during the disease progression and are not the trigger (Petros et al., 2005). High levels of mtDNA mutations have been found in numerous cancers and complex I mutations are regarded as markers for thyroid oncocytic tumours (Chiaradonna et al., 2012). In the cancer cells, that do not contain mtDNA mutations, the respiratory capacity remains intact and the cells simply choose not to use their mitochondria for the purpose of ATP generation (Moreno-Sanchez et al., 2007). A possible reason for the preferred reliance on

glycolysis is that mitochondria are key players in the apoptotic pathway so by suppressing mitochondrial metabolism it promotes growth and survival in tumour cells (Wenner, 2012). In depth, knowledge of this re-programmed metabolism is crucial in order to develop and improve therapeutic approaches.

Some researchers have investigated the bioenergetic profiles of a small number of cancer cell lines, namely A549 and H460 cells. Wu et al examined these two lines and found them to have increased glycolysis and attenuated mitochondrial respiration but highlighted that it would be beneficial to increase the number of cell lines exposed to this type of analysis (Wu et al., 2007). By evaluating larger panels of cell lines patterns may emerge regarding their bioenergetic phenotypes that could help in the selection of therapeutic agents for potential anti-cancer effects.

We wanted to build on this theory and investigate the bioenergetic phenotype of a panel of eight different human cancer cells lines including two rhabdomyosarcoma lines RD and RH30, adult grade IV glioblastoma cells U87MG and M059K and paediatric gliomas SF188 (grade IV), KNS42 (grade IV), UW479 (grade III) and Res259 (grade II). The rates of glycolysis and oxidative phosphorylation in response to metabolic modulators/inhibitors were measured as were the effects of glucose concentration on the glycolytic and aerobic rates of the cell lines. The results of the 2D profiles are summarised below (Table 2.1).

Cell		5mM	1mM	0mM	FCCP	Oligomycin	Oxamate	2DG	Proposed phenotype (on high glucose)
RD	OCR	-	-	-	↑	↓	-	-	Oxphos
	ECAR	-	↓	↓	↑	↑	↓	↓	
	ATP	-	↑	↑	-	-	-	↓	
RH30	OCR	-	↑	↑	↑	↓	↑	↑	Glycolytic
	ECAR	↓	↓	↓	↑	-	↓	↓	
	ATP	-	↑	-	-	-	-	↓	
U87MG	OCR	↑	↑	↑	↑	-	↑	↑	Glycolytic
	ECAR	-	↓	↓	↑	↑	↓	↓	
	ATP	-	-	-	↓	↓	↓	↓	
M059K	OCR	-	↑	↑	-	↓	↑	-	Glycolytic
	ECAR	-	↓	↓	-	-	↓	↓	
	ATP	-	-	-	-	-	↓	↓	
SF188	OCR	-	-	-	↑	↓	↑	-	Oxphos
	ECAR	↓	↓	↓	-	-	↓	↓	
	ATP	-	-	-	-	-	↓	↓	
KNS42	OCR	-	↓	↓	↑	↓	-	↓	Oxphos (glucose dependent)
	ECAR	↓	↓	↓	-	↑	↓	↓	
	ATP	-	-	↓	↓	↓	-	↓	
UW479	OCR	-	-	-	↓	-	-	-	Oxphos
	ECAR	-	↓	↓	↑	↑	-	↓	
	ATP	-	-	-	-	-	-	↓	
Res 259	OCR	-	-	↑	↑	↓	↑	↑	Glycolytic
	ECAR	-	↓	↓	↑	↑	↓	↓	
	ATP	-	-	↓	-	-	↓	↓	

Table 2.1: Summary of cellular response (relative to high glucose 20mM) to various glucose concentrations and mitochondrial modulators in cells grown in 2D. Arrows indicate where a significant difference was observed.

There was a lack of consistency between the cell lines with only four of them displaying the anticipated "classical" Warburg phenotype. The metastatic and aggressive ARMS rhabdomyosarcoma cell line RH30 displayed a Warburg phenotype, on high glucose, with significant aerobic capacity while the non-malignant ERMS RD cell line demonstrated efficient oxidative metabolism. In response to uncoupling with FCCP and mitochondrial inhibition with oligomycin both lines also had significant glycolytic capacity. These results show that cells can rapidly adjust their energy metabolism in response to substrate availability. This metabolic plasticity underpins the difficulty in treating cancer cells and their ability to adapt to adverse conditions. Targeting glycolysis alone may not be sufficient to

generate a therapeutic response although inhibition of glycolysis will make the cells more susceptible to subsequent inhibition of mitochondrial respiration.

The adult glioblastomas are well documented for their high rates of glycolysis so the low basal OCR rates we saw on 20mM glucose were unsurprising. Inhibition of mitochondria with oligomycin did not decrease OCR supporting the finding that they are not oxidative. Lowering the glucose concentration increased the OCR in both the U87MG and M059K significantly and revealed very high maximal respiratory capacities. FCCP and oligomycin increased ECAR in the U87MG cells showing that although very glycolytic there is also a glycolytic reserve in these cells. FCCP and oligomycin did not increase the ECAR in M059K suggesting glycolysis was maximised in this line.

The paediatric glioma cell lines SF188, KNS42 and UW479 are not very common lines. They have not been extensively studied and have only been used previously in a small number of published studies. Their bioenergetics phenotypes have not been reported in the literature before. As mentioned previously paediatric tumours are classed according to guidelines that have been laid down to describe adult tumours but it is not known whether this truly reflects the childhood disease. If childhood glioblastomas, SF188 and KNS42, are expected to behave like the adult ones then one might expect to see high rates of glycolysis. However, in this study the paediatric glioblastoma lines all demonstrated high levels of oxidative metabolism under high glucose conditions that could be reduced upon inhibition of the mitochondria. The SF188 cells also had high rates of glycolysis suggesting both glycolysis and Oxphos are equally important to this line. Interestingly while the KNS42 cells were very

oxidative they relied heavily on glucose as they could not maintain their OCR rates when glucose was removed. UW479 proved to be the most oxidative of all the lines with the highest basal OCR rates but they also displayed significant glycolytic capacity when the mitochondria were inhibited/uncoupled. Apart from KNS42, all the cell lines demonstrated metabolic plasticity, they were capable of switching from oxidative metabolism to glycolysis or vice versa whilst maintaining ATP levels. These findings highlight that the cells have intact and functional mitochondria and that in the case of the RH30, U87MG, M059K and Res259 cells respiration is merely suppressed under the high glucose conditions used in culture media. This poses the question could the Warburg effect observed in cancer cell lines in culture be an artefact of the high glucose concentration used in standard culture conditions? Physiological glucose concentrations are in the 5mM range so in a tumour depending on the level of vascularisation the glucose concentration is expected to be considerably lower. Assuming a tumour has a glucose concentration of approximately 1mM from our results we can expect the basal OCR rates of RH30, U87MG and M059K cells to increase significantly. M059K cells cultured on 1mM glucose have the same rates of oxygen consumption as those cultured on no glucose.

The NMR data has highlighted that there is a significant amount of glucose oxidation in glycolytic U87MG cell line. The metabolomics profile obtained from this line is contrary to popular opinion that these cells have inactive mitochondria. In 2010 Michelakis et al published a study detailing how targeting glycolytic GBM tumours might be an effective therapy using a drug called dichloroacetate that works to restore oxidative metabolism (Michelakis et al., 2010). Most research into potential

therapies for GBM is progressing on the basis that these cancer cells are highly glycolytic (Hao et al., 2010; Lai et al., 2013). However, in 2012 Marin-Valencia et al studying human orthotopic GBM tumours which had no prior adaptation to cell culture (i.e. the cells were directly transplanted from patients into mice) showed that when glucose and glutamine tracers labelled were used to identify metabolic intermediates GBM tumours had a surprising amount of oxidative metabolism and TCA cycle activity (Marin-Valencia et al., 2012). Our results comply with the Marin-Valencia study suggesting that glucose is oxidised by mitochondria in the U87MG cell line on high glucose media but it is not coupled to ATP production by the respiratory chain. Even though glucose enters the TCA cycle and is oxidised, very low levels of oxygen are consumed by the mitochondria suggesting a disconnect between products of the TCA and the mitochondrial respiratory chain in the presence of high glucose. The metabolomics data coupled with the data from the metabolic assays suggests that both glycolysis and glucose oxidation are equally important for these U87MG cells perhaps glycolysis providing ATP and glucose oxidation providing intermediates for macromolecule synthesis. The study by Marin-Valencia et al also reported that all their tumours had similar metabolic phenotypes despite them having different mutation statuses in EGFR and PTEN. In this study U-13C glucose metabolomics analysis has proved a useful tool to gain deeper insight into the metabolic pathways at work in two very energetically distinct cell lines. It was surprising to see high mitochondrial activity in what has previously been regarded as a glycolytic cancer line. While the mitochondria in U87MG cells are not being utilised for energy it is clear that they are active in their TCA cycling presumably as

a means meeting the biosynthetic demands required to provide accelerated growth (Fan et al., 2008).

This finding highlights the pitfalls in the current view of tumour metabolism. Targeting glycolysis may not be sufficient to kill cancer because they have active PDH and TCA cycle activity that can be further increased to compensate for impaired glycolysis. In addition, the Warburg effect, at least in this study, is highly influenced by the concentration of glucose in the culture media. In-vivo when cells are exposed to much lower levels of glucose glycolysis rates are likely to be very low while Oxphos rates could be much higher. Oxygen levels in-vivo will affect cancer cell metabolism with hypoxia up regulating genes involved in glycolysis. As many hypoxia studies investigating metabolism have been carried out in high glucose media the influence of genes like Hif over the effects of high glucose in culture media are far from clear.

The idea that cancer cells are glycolytic in-vivo may not be correct, as the cells examined in this thesis are oxidative when cultured under appropriate glucose conditions that better reflect the in-vivo scenario. A potential problem with our study design is that cellular bioenergetics were assessed under hyperoxic conditions of 21%. If we are assuming low glucose levels in the tumour we should also account for reduced oxygen availability. In the future, it would be beneficial to repeat these experiments under reduced oxygen conditions in a perfused system to allow for more regulated control over substrate and oxygen levels. Under low oxygen conditions, Hif is activated and causes over expression and up-regulation of many enzymes and transporters consistent with the Warburg phenotype.

The hypothesis of a purely glycolytic cancer phenotype is being challenged (Moreno-Sanchez et al., 2007) with many glioma cell lines reported as having mitochondrial function (Martin et al., 1998). Extreme glycolysis is not seen in all tumours types and for that reason, it may be inappropriate to consider it a hallmark. By assessing a panel of cancer cell lines from a number of different tumour types, we hoped to establish and demonstrate their glycolytic dependency but instead we have uncovered a variety of bioenergetic phenotypes. Our results demonstrate a dynamic interplay between oxidative metabolism and glycolysis a metabolic flexibility that has been observed in cervical, breast and pancreatic cancer also (Jose et al., 2011).

It was hoped that by establishing the phenotypes of these lines it might be possible to determine if there was a pattern emerging that may one day form the basis of screening patient tumours to determine their metabolic signatures in order to establish the most appropriate anti-cancer agent to target that phenotype. As we have seen in this study the cancer cells display a certain metabolic plasticity and are insensitive to inhibition of glycolysis or oxidative metabolism alone highlighting the need for a two-pronged therapeutic strategy where both pathways are targeted. By inhibiting glycolysis and forcing cells to rely on oxidative metabolism it would sensitise the cells to mitochondrial inhibition.

The in-vitro cell culture environment lacks homeostatic regulation that can affect cell metabolism. Metabolism of in-vitro cells may not be a true representation of the tissue from which the cells were derived. In an attempt to address this issue 3D cultures of the lines investigated here were also evaluated and are discussed below.

2.4.2 3D bioenergetic profiles

As discussed earlier there are many limitations using current standard 2D culture approaches. In order to gain a more accurate understanding of cancer cell metabolism and to assess drug effects in a more physiological setting better culture models are necessary. The results presented in this chapter provide insight into the different bioenergetic profiles which can be observed when cells are cultured in 2D compared to different 3D model systems.

The RD and KNS42 lines hinted at a more aerobic based metabolism when cultured in 2D as seen by high OCR, low ECAR and low HKII expression but switched to a more glycolytic phenotype when cultured as spheroids. In these spheroid structures the RD and KNS42 lines had increased basal ECAR rates coupled with increased HKII expression (HKII had been undetectable when cultured in 2D). HKII was only seen in 2D in the lines that displayed glycolytic profiles. HKII has been reported as vital for the Warburg effect in human GBM (Wolf et al., 2011). By reducing HKII, using siRNA, Wolf et al were able to restore oxidative metabolism and increase sensitivity to the cell death inducers radiation and temezolomide (TMZ). Their HKII depleted xenograft model also demonstrated a marked reduction in proliferation and angiogenesis. GBM are very heterogeneous tumours with moderate levels of hypoxia. They have been shown to exhibit almost a threefold increase in glycolysis when compared to healthy brain tissue. Normal non-malignant brain typically expresses HK1 but HKII is over expressed in GBM. Hif1a regulates many enzymes involved in glycolysis including HKII. The Wolf study showed that by targeting glycolysis through inhibiting of HKII Oxphos was restored which also resulted in

decreased ECAR (Wolf et al., 2011). Therapy for GBM may lie in targeting HKII however, increased Oxphos, as observed in this thesis, may not necessarily be detrimental on its own.

By establishing and implementing more complex 3D in-vitro models it will hopefully serve to better recapitulate the in-vivo microenvironment. Cells in tumour spheroid models have been shown to exhibit different morphology and expression profiles compared to 2D cultures. In this study, we also see differences in the bioenergetic profiles between 2D and 3D. Despite the many advantages of the spheroid model it is still rather simplistic in that it contains only one cell type and is not a true representation of the microenvironment. The future of 3D models may lie in a more biomimetic model consisting of multiple cell types contained in an appropriate matrix with a perfused rather than static environment to better control nutrient and oxygenation levels.

The data presented in this chapter has shown the importance and effect of nutrient availability on the metabolism of cancer cells with the results highlighting the differences between cancer cell types. The successful application of in-vitro models to assess the efficacy of drugs relies on the extent to which the model represents the relevant characteristics of the in-vivo scenario. Despite the obvious difficulties associated with trying to reproduce all in-vivo characteristics in an in-vitro model system, the use of 3D systems could help to bridge the gap. In vivo drug efficacy is a multi-factorial and complex sequence of physiological events that are rarely recapitulated in molecular detail in simplified in vitro models.

The idea that all cancer cells suppress their mitochondria and exclusively use glycolysis for ATP production is attractive because it provides a selective means of targeting cancer as normal cells do not rely on glycolysis. However, Warburg's original experiments and many subsequent experiments have been conducted in cells ex-vivo under non-physiological culture conditions. We have demonstrated that not all cancer cells rely on glycolysis except when mitochondria are inhibited. Those cells that display the Warburg phenotype have high levels of hexokinase and this might explain the increased rates of glycolysis.

In summary, care needs to be taken when moving forward with strategies that target cancer metabolism. Warburg made a remarkable observation all those years ago but his conclusions were mechanistically flawed. In order to make substantial contributions in tackling cancer metabolism it is imperative that we fully understand the metabolic pathways and their relationships in their entirety.

CHAPTER 3

INVESTIGATING THE POTENTIAL OF DICHLOROACETATE AS AN ANTI-CANCER THERAPY

3.0 Investigating the potential of dichloroacetate as an anti-cancer therapy

3.1 Introduction

Cancer cells are characterised by numerous features including their high proliferative capacities. If the tumour vascularity supplies inadequate levels of nutrients and oxygen, this enhanced proliferation can generate hypoxia. Hypoxia activates hif1a, which favours a glycolytic phenotype (Denko, 2008). PDK is a target of Hif1a and is induced when hif1a is transcribed. PDK1 is the main PDK isoform induced and is responsible for the phosphorylation and subsequent inactivation of PDH. The net result of which is reduced pyruvate entry and oxidation in the mitochondria (Papandreou et al., 2011). DCA is currently under investigation for its anti-tumour potential as it inhibits PDK activity and prevents the phosphorylation of PDH resulting in increased pyruvate oxidation by the mitochondria. The increase in TCA cycle activity induced by DCA has been shown to increase the intermediates of the TCA cycle, increased ROS, increase mitochondrial transition pore (MTP) opening, release apoptotic factors (AIF and cytochrome C) and activate p53 (Dhar and Lippard, 2009; Sutendra and Michelakis, 2013). The net result of this should be reduced tumour growth. In this chapter, we examine the effect of DCA in our panel of cell lines in 2D and 3D spheroid model systems.

3.2 Chapter Aims

- Assess the cytotoxicity of dichloroacetate on paediatric and adult glioma cell lines grown in standard 2D in-vitro culture
- Assess if dichloroacetate efficacy changes when cells as cultured as a 3D structure

3.3 Methods

3.3.1 Materials

All materials and reagents were purchased from Sigma Aldrich unless otherwise stated.

3.3.2 Cell Culture

See section 2.2.10

3.3.3 Propridium Iodide

Propridium Iodide (Sigma Aldrich) was used to determine cytotoxicity. Propridium iodide is impermeable to cells provided the cell membrane is intact. In dead/dying cells where the plasma membrane is compromised PI enters the cells and binds to exposed DNA. Once bound its fluorescence is enhanced 20-30 fold.

Cells were seeded at a specified density (usually between 10,000 and 30,000 per well depending on the length of drug exposure) in 150µl of media and allowed to adhere overnight. Once adherent 200ul fresh media was added and the cells were treated with 50µl of various doses of DCA or phenformin and left for 24, 48 or 72 hours. The untreated controls received 50µl of media. The dead cell control was set up by

adding 100µM menadione to the cells overnight to induce maximal death and use as a 100% cytotoxicity control.

Following drug incubation, a 25µM PI working solution was made up in media from a 1.5mM stock solution. 50µl of this working solution was added to each well, using a multichannel pipette, to give a final concentration of 5µM and the plate was incubated for 25 minutes at 37^0C. Following incubation the plate was read on a BMG Optima plate reader in fluorescent, end point mode with an Ex 540-20 and Em 620-10.

Once the PI fluorescence was determined the media was removed (to remove the dead cells) and it was replaced with media containing Hoechst to assess the number of viable cells left attached. See 3.3.4.

3.3.4 Hoechst

Hoechst is a family of fluorescent cell permeable dyes that bind to DNA and give information on cell viability/number. The plate from the PI assay was re-used to assess the number of viable cells remaining following DCA, phenformin and DCA & phenformin treatment. A 1µg/ml Hoechst working solution was made up in media from a 2mg/ml stock solution. 100µl of Hoechst working solution was added to each well and the plate was incubated for 20 – 30 minutes at 37^0C. Following incubation, the Hoechst solution was removed and the wells were carefully washed with 2 X 200µl PBS to remove unbound dye. 150µl PBS was added post washing and the

plate was read in the BMG Optima in fluorescent endpoint mode using Ex 350nm and Em 460nm with a bottom read.

3.3.5 Oxygen Consumption Rate

Oxygen consumption assay was performed as detailed in 2.2.9.3. Briefly, the Mito-Xpress probe was measured using dual delay time resolved measurements with Ex TR-exl filter (380nm) and Em TR-em^2 (650nm) and delay times of 30 and 70µs. Cells were seeded at 50,000 cells/well in a black clear bottom 96 well plate and left to adhere before adding DCA for 24 hours. Following treatment 10µl probe was added to 140µl fresh media and covered with 100µl high sensitivity oil before placing in the reading and collecting data over the course of a 7 hour period.

3.3.6 Extracellular Acidification Rate

The pH assay was performed as detailed in 2.2.9.3. Briefly, the probe was measured using dual delay TRF measurements (Ex 340nm and Em 615-10nm, delay times 100 and 300µs). Cells were seeded at 50,000 cells/well in a black clear bottom 96 well plate and left to adhere before adding DCA for 24 hours. Following treatment plate was de-gassed, cells washed in pH buffer. 140µl fresh buffer and 10µl of pH-Xtra probe were added to each well (except blanks) and the plate was read over the course of a few hours.

3.3.7 Spheroid Generation

Cells were washed and trypsinised to remove from flask. An ice-cold suspension containing 2.5 X 10^4 cells/ml and 2.5% Matrigel (BD Biosciences) was prepared. 200µl of this suspension was added to each well of a 96 well Corning Ultra Low Attachment multiwell plate. The plates were centrifuged at 1800rpm for 10 minutes at 4^0C and then incubated under standard culture conditions (5% CO_2 & 21%O_2).

3.3.8 Growth Curves

Spheroids were seeded as outlined above and images were taken over the course of a week. Spheroid diameters were measured and total spheroid was calculated from this using the equation $4/3\ \pi r^3$.

3.3.9 PI and Annexin V

3.3.9.1 Background

Apoptosis is the process of programmed cell death and is tightly regulated. Apoptosis is dysregulated in diseases such as cancer. A PI (sigma) and Annexin V APC (BD Pharmingen) protocol was implemented to investigate spheroid health in response to drug treatment by looking at dead, apoptotic and live cell populations. PI will increase its fluorescence (red) when the cell membrane is compromised and PI can access the DNA, therefore is a measure of dead cells. Annexin V works by binding to phosphotidylserine (PS). PS is usually expressed on the interior of the cell membrane

but when cells become apoptotic the PS is translocated to the outer membrane, in a process known as membrane flipping, allowing the Annexin V to bind (Vermes et al., 1995). Binding of annexin V is dependent on calcium so a calcium-binding buffer is required for effective staining to be observed.

If the cells within the spheroid are dead, they will stain positive for PI and annexin V. Early apoptotic cells will only stain positive for annexin V, while healthy cells will be unstained.

*3.3.9.2 **Spheroid preparation***

Spheroids were prepared as previously described (section 2.2.6) and treated with DCA from day 3 for a period of 4 days. On day 7, spheroids were harvested from the multiwell plate and transferred into Eppendorf tubes, centrifuged at 1300rpm for 10 minutes and washed twice in PBS. Following the last wash, the spheroids were centrifuged and the PBS was removed to waste. To dissociate the spheroids into single cells a number of different protocols were tested:

Protocol 1: 500µl trypsin was added and the spheroids were incubated at 37^0C for 1hr and the suspension pipetted every 10 minutes to facilitate dissociation

Protocol 2: MACS Miltenyl tumour dissociation kit was used according to manufacturer's instructions and spheroids were gently pipetted every 5 minutes over the course of an hour or until a single cells suspension was achieved

Protocol 3: Spheroids were transferred into a small petri dish and 1ml accutase was added, dishes were placed in the incubator and every 20 minutes the spheroids were pipetted until single cell suspension was achieved

3.3.9.3 Staining Protocol

Once single cells were acquired, they were centrifuged at 1300 RPM for 5 minutes. The pellet was washed in PBS and centrifuged again at 15000 RPM for 5 minutes. 1X Annexin binding buffer was prepared from a pre-prepared 10X stock (BD) and 100µl of this was added to each tube. To this 5µl of Annexin APC (BD Bioscience) and 1µl of 100µg/ml PI was added. Cells were vortexed and incubated at room temperature for 15 minutes. Following incubation 400µl of 1X binding buffer was added to each tube, mixed and centrifuged. The supernatant was removed and discarded and 500µl fresh 1 X binding buffer was added and cells were placed on ice until analysed by FACS.

3.3.9.4 Flow cytometry analysis

The flow cytometer used was a BD LSR II (BD Bioscience, Oxford, UK). This instrument is equipped with a blue laser (488nm) and a red laser (633nm). The flow cytometer is equipped with two light scatter detectors that measure the forward scatter FSC (an estimation of cell size) and side scatter SSC (an estimation of intracellular granularity). The data generated was plotted as a histogram of SSC versus FSC. The regions on these plots can be sequentially separated, based on fluorescence intensity, by creating a series of data subsets, termed "gates". A gate is a numerical or graphical boundary that can be used to define the characteristics of particles to include for further analysis. In any particular plot, discrete populations of cells (or cells with different characteristics e.g. dead/dying cells) occupy different parts of the plot. “Gating” is used to isolate these subsets of cells on the plot and is

the reason why so many controls are necessary. Single cells were gated on and 10,000 total cell events were recorded. Data was analysed using BD FACS Diva 5.0 software (BD Biosciences).

In order to set the gates the following controls were used:

1. Live cells unstained with binding buffer
2. Live cells with Annexin V, no buffer – with PBS containing 1% FBS
3. Live cells with Annexin V and binding buffer
4. Live cells with PI with binding buffer
5. Live cells with PI and Annexin V
6. Dead cells unstained with binding buffer
7. Dead cells with Annexin V, no binding buffer – with PBS containing 1% FBS
8. Dead cells with Annexin V, and binding buffer
9. Dead cells with PI
10. Dead cells with PI and Annexin V

Dead cells were created in two ways (i) treating overnight with 100µM menadione (Sigma) (menadione induces cell death that gives a PI positive response) and (ii) treating overnight with 6µM camptothecin (Sigma) (camptothecin induces apoptotic death and was necessary to assess the annexin V staining).

3.3.10 Microvesicle Analysis - Flow cytometry

Before spheroids were seeded, the media and FBS were processed to remove as many microvesicles as possible and reduce the risk of interference later on in the analysis. The FBS was filtered through a 0.1µm Whatman Anatop filter tip before being ultra-centrifuged at 29,000 rpm for 16 hours. Following ultracentrifugation, the FBS was then supplemented as normal into DMEM at a concentration of 10%. The complete media (containing ultra-filtered FBS, L-glutamine and P/S) was then filtered through a 0.1µm Millipore Stericup. The spheroids were then set up in this media and cultured for 3 days before DCA was added. On the seventh day after seeding (and after 4 days of treatment) the spheroids were harvested and processed for the PI/Annexin V staining as detailed in section 3.3.9.2.

The media was retained for microvesicle analysis. Media samples were centrifuged at 1300rpm for 20 minutes to remove any large cellular debris after which the supernatant was collected and run on the flow cytometer neat (without any pre-concentration). It is possible to concentrate the vesicles through a series of ultracentrifugation steps (Dragovic et al., 2011; Dragovic et al., 2013). The BD SLR II was used for this analysis. This instrument has been validated and optimised for use in microvesicle analysis by the forward and side scatter voltages. A gate has been set at 1µm that allows the separation of vesicles into two categories, those less than 1µm in size and those greater. Prior to running the samples, the level of background noise/contamination needed to be assessed. This was achieved by running filtered PBS through the system and acquiring data for 2 minutes. The number of PBS events was subtracted from the sample vesicle counts in order to eliminate this noise, a

media blank was also collected to get an estimation of the level of background microvesicles in the media.

In order to calculate total vesicle concentrations per volume of sample analysed BD TruCount beads (3.0 – 3.4µm) were used. Each tube contains a known amount of fluorescent beads. 500ul of filtered PBS was added to the Trucount tube and mixed well. Data was acquired for 2 minutes on the low flow rate setting giving it an approximate flow rate of 15ul/min. The TruCount beads appear on the scatter plot in a distinct region that can be gated on. The number of events collected in this gate, for a period of two minutes collection time, divided by the total number of beads (see manufacturers box) multiplied by the volume (500µl) gives the volume of sample measured in the two minute acquisition time. Knowing the precise flow rate provides a standard for calculating the absolute number of vesicles/ml in each sample. Samples were run after the beads for 2 minutes and total number vesicles/ml was calculated as described above. Data was analysed using BD Diva software version 5.03.

Flow cytometry is useful for the analysis of vesicles in excess of 290nm but there is still a large vesicles (exosome) population not detected by this method. To analyse these nano sized tiny exosomes Nanosight (NTA) was used (see 3.3.11).

3.3.11 Microvesicle analysis - Nanosight

Nanoparticle tracking analysis (NTA) is a relatively new (launched in 2006) and unique system that measures nanoparticle concentrations in solution. It uses a finely focussed laser beam, which passes through the suspension of particles via a glass prism. The beam is refracted as it passes through the sample and any particles within it are illuminated. The particles can then be visualised by the light they scatter. The light scattered by the particle is recorded in 60 second videos using a scientific digital camera and the motion of each particle is tracked from frame to frame by the specially developed software. The software can then identify individual particles and then track their Brownian motion and velocity. This allows particle size and concentration to be measured once the Stokes Einstein Equation has been applied. The limitation of flow cytometry is the 290nm vesicle cut off point. NTA complements flow cytometry because it can detect the population below this threshold and most importantly, it can resolve different sized particles within a complex mixture that is crucial when analysing samples that are biological in origin (Dragovic et al., 2011).

The NTA instrument used was the NS500. Spheroid cultured media was diluted 1:1000, the sample introduced into the inlet tube and analysed using a pre-defined 5X60second video capture method on the NS500. Particle size distribution and particle numbers were calculated and plotted in Graphpad Prism.

*3.3.12 **Statistical Analysis***

Graphs were generated using Graphpad Prism 6. Depending on the data set either a unpaired two-tailed student t-test was performed or a one-way ANOVA with Dunnett correction. $p<0.05$ *, $p<0.01$ **, $p<0.001$ ***, $p< 0.0001$ ****

3.4 Results

3.4.1 DCA is not cytotoxic to rhabdomyosarcomas cells cultured in 2D

Based on the literature surrounding DCA and its mechanism of action one would expect it to have an adverse effect on cancer cells that display a glycolytic phenotype. The toxic effects of DCA in 2D cultures was assessed using PI (Propridium iodide) and Hoechst using the plate reader platform. PI binds to exposed DNA in dead cells and as such provides information on the cytotoxicity of compounds. The dead control for the PI assay was achieved by adding 100µM menadione 12 hours (causes maximal death) before the assay was conducted. The dead control was set as 100% cytotoxic and the DCA effect was determined relative to this. The Hoechst stain binds to DNA of intact and dead cells. The protocol implements a number of wash steps following staining in order to remove the dead population so only the viable cells are analysed thus giving a measure of viability and cell number. DCA treated cells were compared to untreated cells (0mM DCA) as a negative control. RD and RH30 cells were treated with DCA for 24, 48 and 72 hours and after each time point the percentage death and percentage viability were measured. As RD cells have previously been described as being aerobic, a lack of efficacy of DCA was expected in this line. As expected in the RD cells DCA, up to a maximum concentration of 10mM, had no deleterious effect on the viability of the cells and caused no cytotoxicity Figure 3.1.

DCA treatment of RH30 cells which show a more glycolytic profile on high glucose media also showed no evidence to cytotoxicity with an unexpected significant increase in cell number after 72 hour treatment (Figure 3.2).

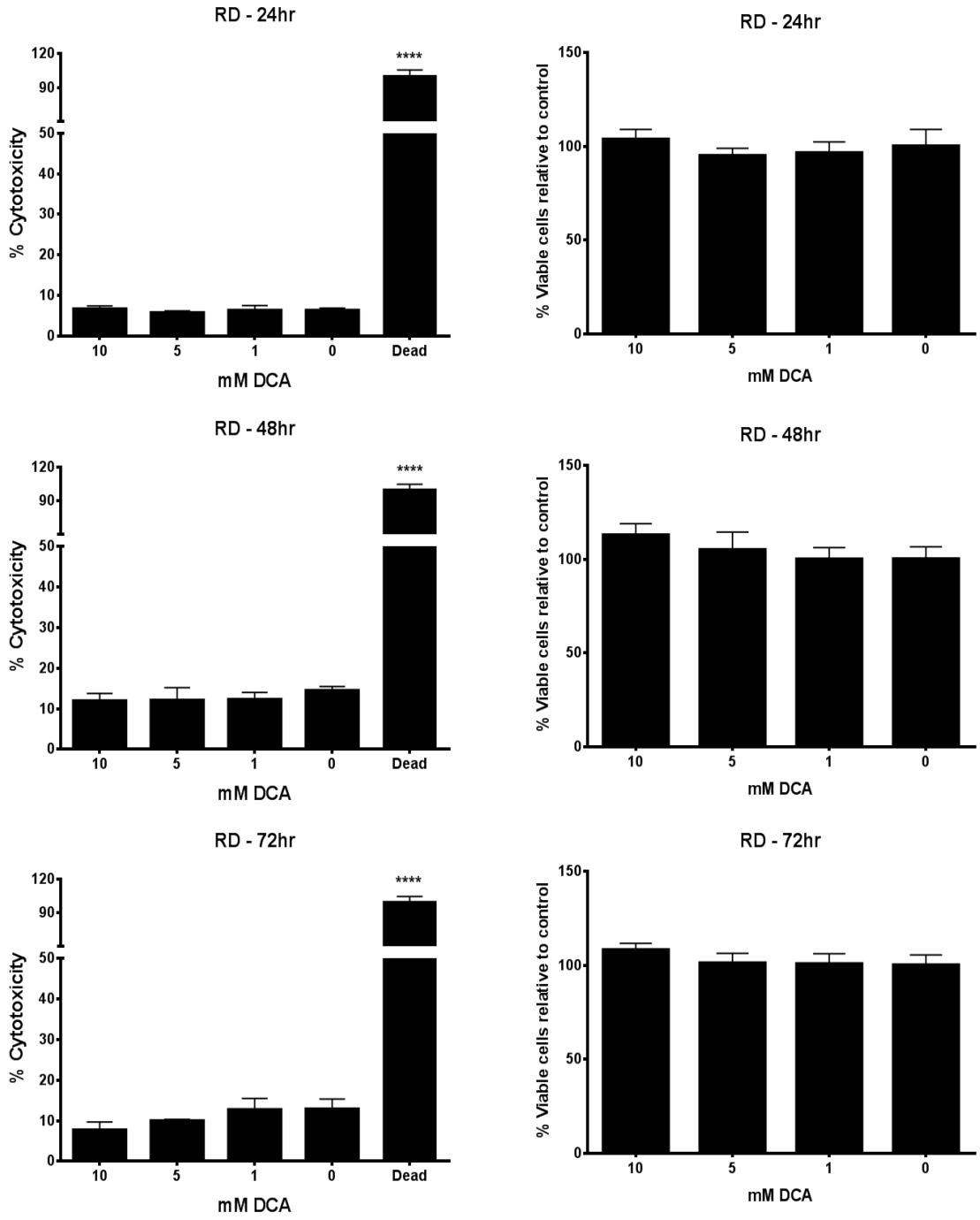

Figure 3.1: DCA does not induce death or slow proliferation in RD cells during a 72 hour treatment period. Cells were treated with various doses of DCA for either 24, 48 or 72 hours. PI assays assessing the percentage death are shown in the left hand column while Hoechst assays assessing viability and cell number are on the right hand column. N = 3 and the error bars represent the standard deviation of the mean

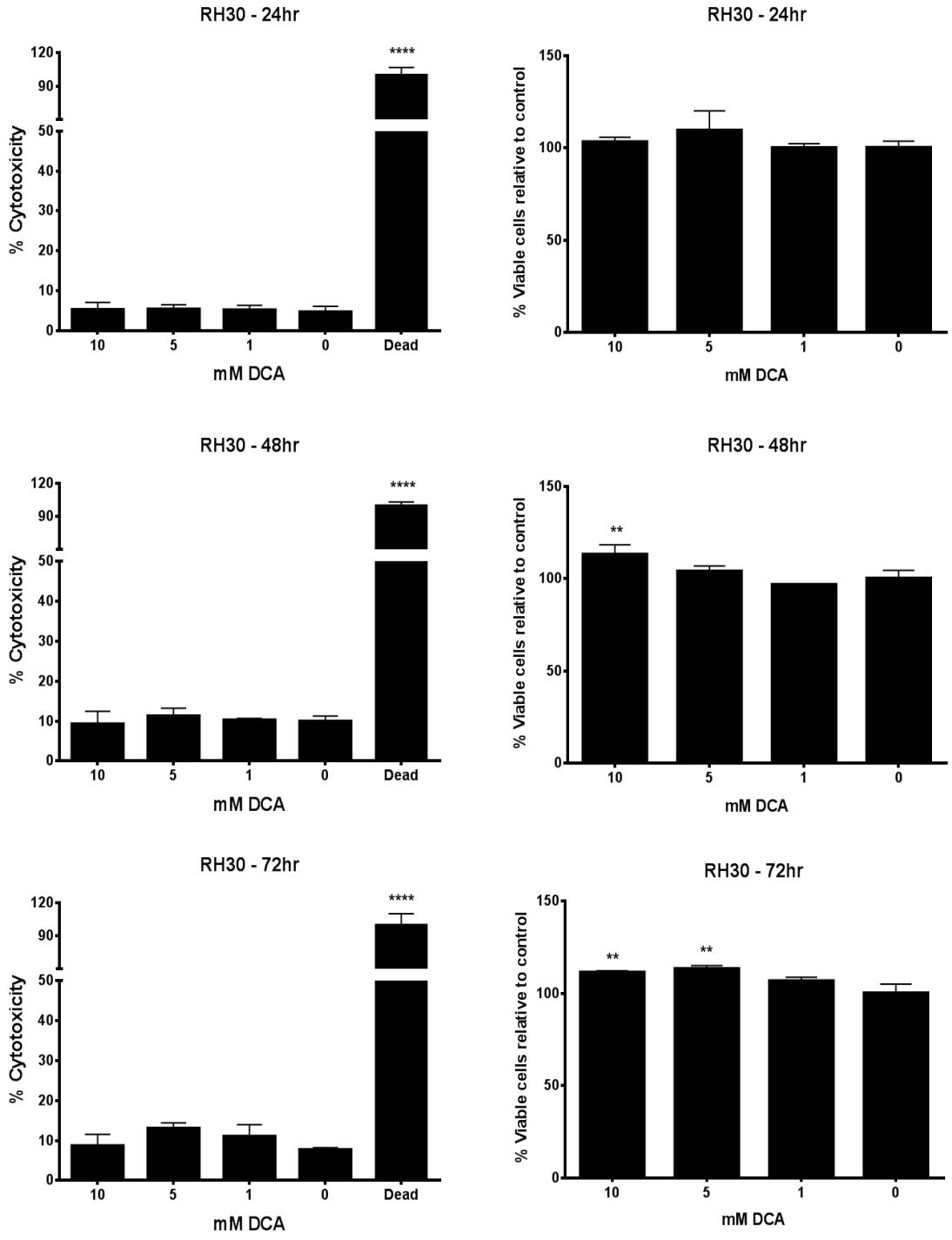

Figure 3.2: DCA does not induce death in RH30 cells but 5 & 10mM appear to increase the proliferation rates significantly after 72 hours. Cells were treated with various doses of DCA for either 24, 48 or 72 hours. PI assays assessing the % death are shown in the left hand column while Hoechst assays assessing viability and cell number are on the right hand column. N = 3 and the error bars represent the standard deviation of the mean

3.4.2 DCA increases cell proliferation in glycolytic U87MG and M059K cells in 2D

The earlier studies by Bonnet et al and Michelakis et al were among the first to identify DCA as a possible therapy for cancer (Bonnet et al., 2007; Michelakis et al., 2008). Michelakis in particular investigated the potential of the drug in the treatment and management of glioblastoma multiforme (GBM) (Michelakis et al., 2010). As U87MG and M059K cell lines were both derived from GBM tumours it was anticipated that these lines out of the cell panel tested would show sensitivity to DCA treatment.

In this study, U87MG cells in 2D culture were found to be insensitive to DCA treatment. DCA up to a maximum concentration of 10mM was unable to induce cell death or decrease cell proliferation Figure 3.3. In the long term a similar response to RH30 cells was observed with an increase in cell numbers seen the at 48hour time point. Similarly, the M059K cell line showed an increase in cell number after 48 and 72 hours coupled with no signs of significant toxicity Figure 3.4.

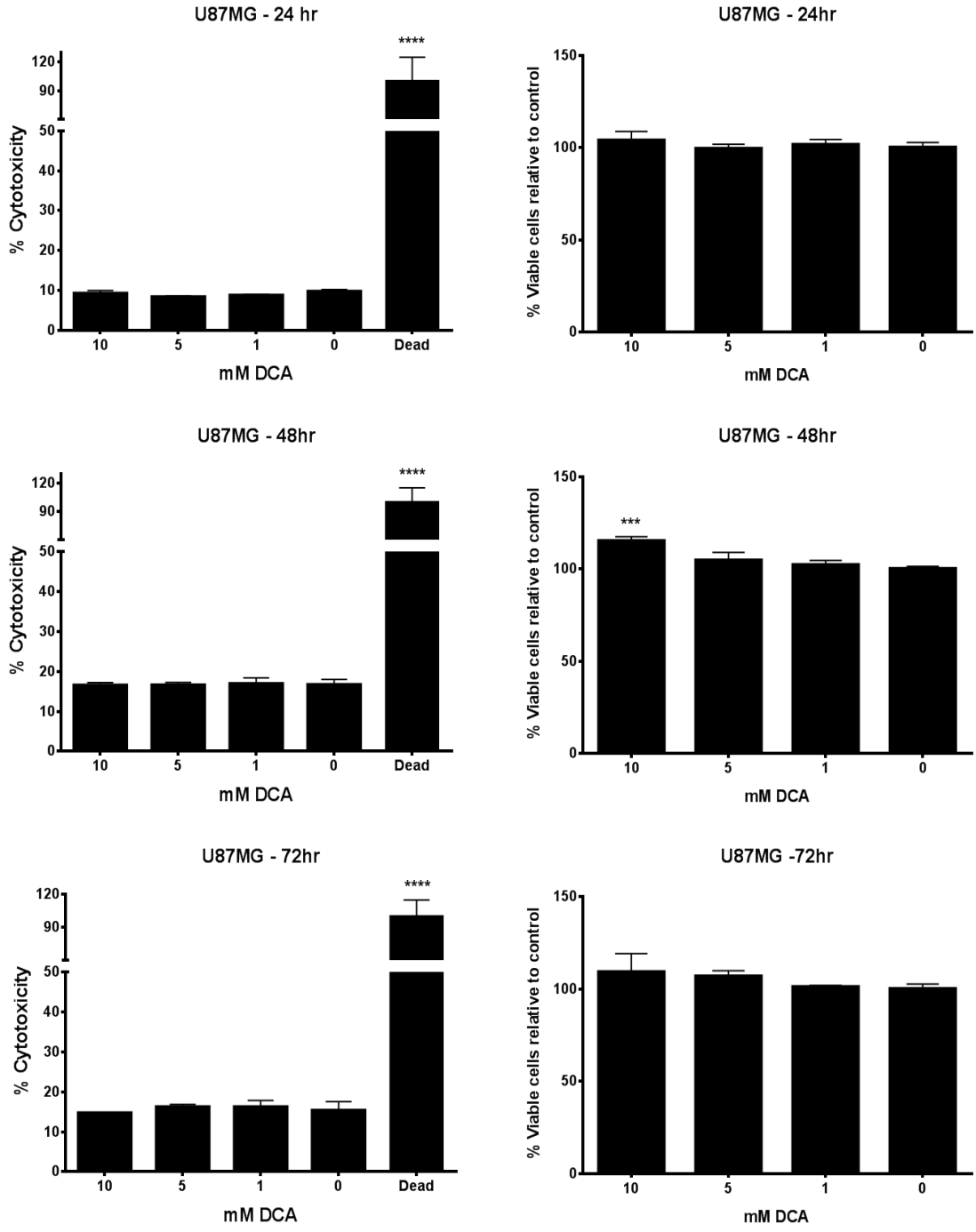

Figure 3.3: DCA does not induce death in U87MG cells 10mM appears to increase the proliferation rate significantly after 48 hours. Cells were treated with various doses of DCA for either 24, 48 or 72 hours. PI assays assessing the % death are shown in the left hand column while Hoechst assays assessing viability and cell number are on the right hand column. N = 3 and the error bars represent the standard deviation of the mean

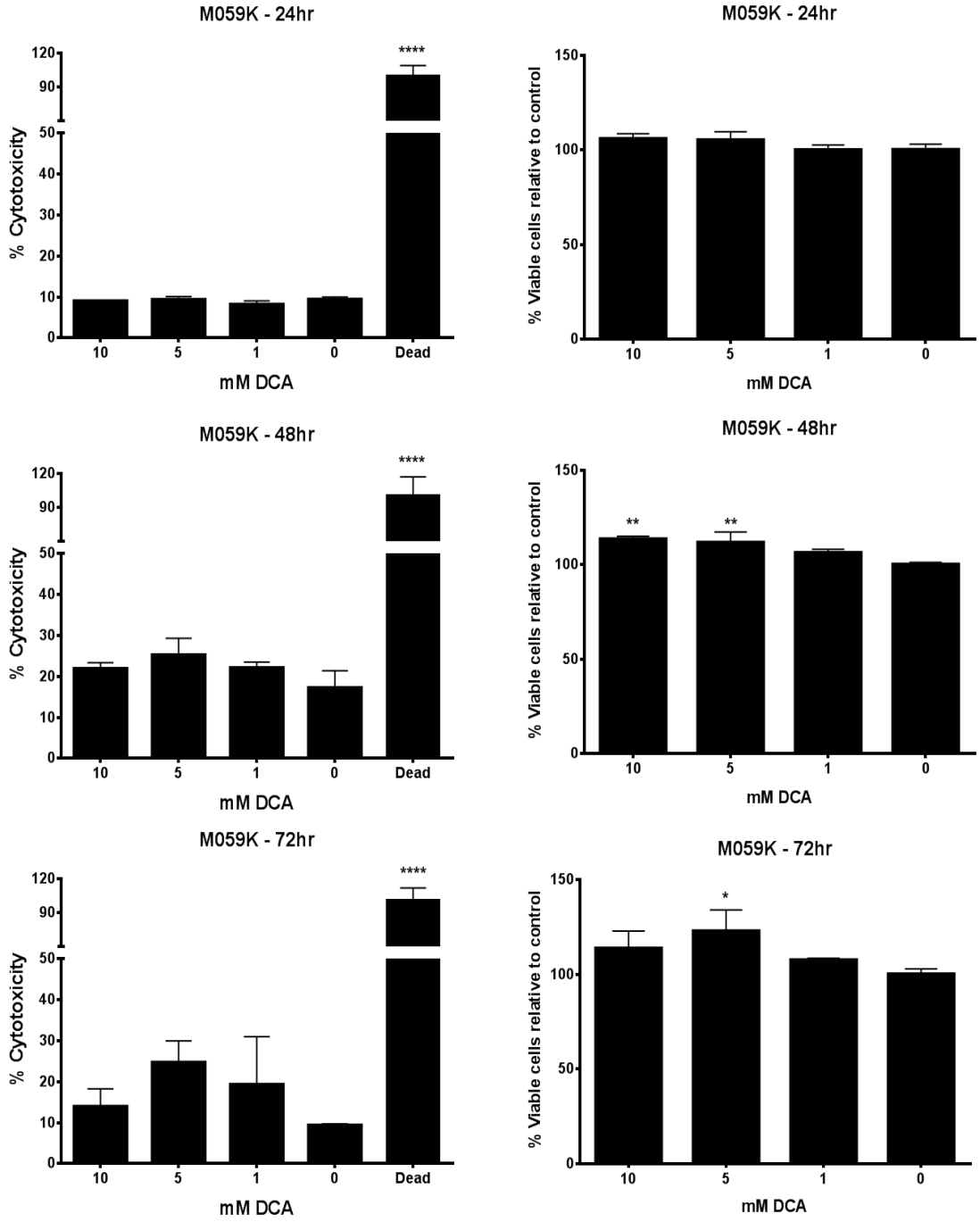

Figure 3.4: DCA does not induce death or slow proliferation in M059K cells during a 72 hour treatment period. It actually results in an increase in cell number after 48 and 72 hours. Cells were treated with various doses of DCA for either 24, 48 or 72 hours. PI assays assessing the percentage death are shown in the left hand column while Hoechst assays assessing viability and cell number are on the right hand column. N = 3 and the error bars represent the standard deviation of the mean

3.4.3 DCA decreases proliferation in the high-grade IV paediatric glioma cell lines but not the grade III glioma line in 2D culture

In the previous chapter, the high-grade glioma cell lines were shown to have a distinct metabolic profiles compared to their adult counterparts (section 2.3.1). The adult lines displayed high rates of glycolysis coupled with attenuated mitochondrial respiration when cultured on media containing 20mM glucose while the high-grade paediatric cell lines showed high rates of mitochondrial respiration. Interestingly SF188 cells while showing high oxygen consumption rates also had significant rates of glycolysis on 20mM glucose media. SF188 cell line is a glial cell and normal glial cells in-vivo are known to metabolise glucose to lactate and then export the lactate to the neurons for oxidation to water and carbon dioxide so perhaps the glycolysis rates seen in this line are expected (Itoh et al., 2003). The KNS42 and UW479 cells have enhanced mitochondrial respiration and very low glycolysis rates (Figure 2.7). As mentioned earlier KNS42 cells showed reduced ATP and reduced respiration when glucose was removed. These cells are also glial cells and glucose is very important substrate for this cell type.

If DCA has a mode of action on cancer cells as suggested by Michelakis et al 2010, that is restoring mitochondrial oxidative metabolism and increasing mROS production in glycolytic cancers, it would be expected to have a significant impact on the glycolytic cancer lines. However, this was not observed for the adult glioblastoma cell lines; U87MG and M059K (section 3.4.2). When the high-grade paediatric glioma cell lines were exposed to DCA over a 3-day period, we see small but significant impact on the rates of proliferation. The SF188 cell line showed

significant decreases in the cell number after 24 hours when exposed to 5 and 10mM DCA but this effect was no longer apparent at 48 and 72 hours Figure 3.5.

The KNS42 cells show a similar response to DCA, a significant decrease in cell number after 24 hours which although reduced over 48 and 72hrs still showed a significant decrease (Figure 3.6). There is a significant decrease in cell number when the cells were treated with 1, 5 and 10mM DCA. After 48 and 72 hours DCA exposure, while there is still a significant decrease in the number of cells the percentage decrease is not as low as the 24 hour treatment possibly due to the drug being metabolised and losing efficacy.

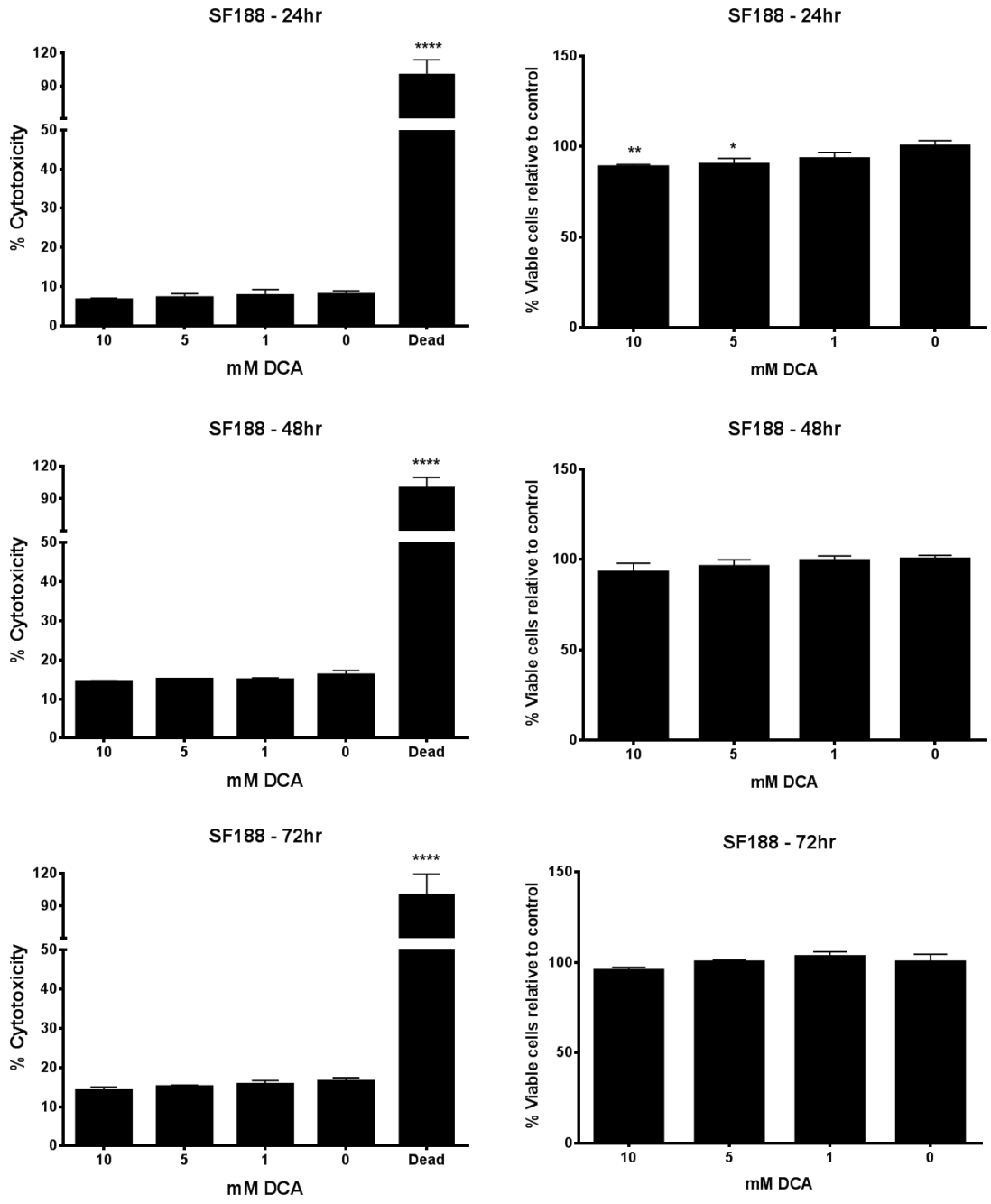

Figure 3.5: DCA does not induce death or slow proliferation in SF188 cells during a 72 hour treatment period. After 24 hours there appears to be a decrease in cell number in the cells treated with 5 and 10mM but this was not seen in the 48 or 72 hour samples. Cells were treated with various doses of DCA for either 24, 48 or 72 hours. PI assays assessing the percentage death are shown in the left hand column while Hoechst assays assessing viability and cell number are on the right hand column. N = 3 and the error bars represent the SD of the mean

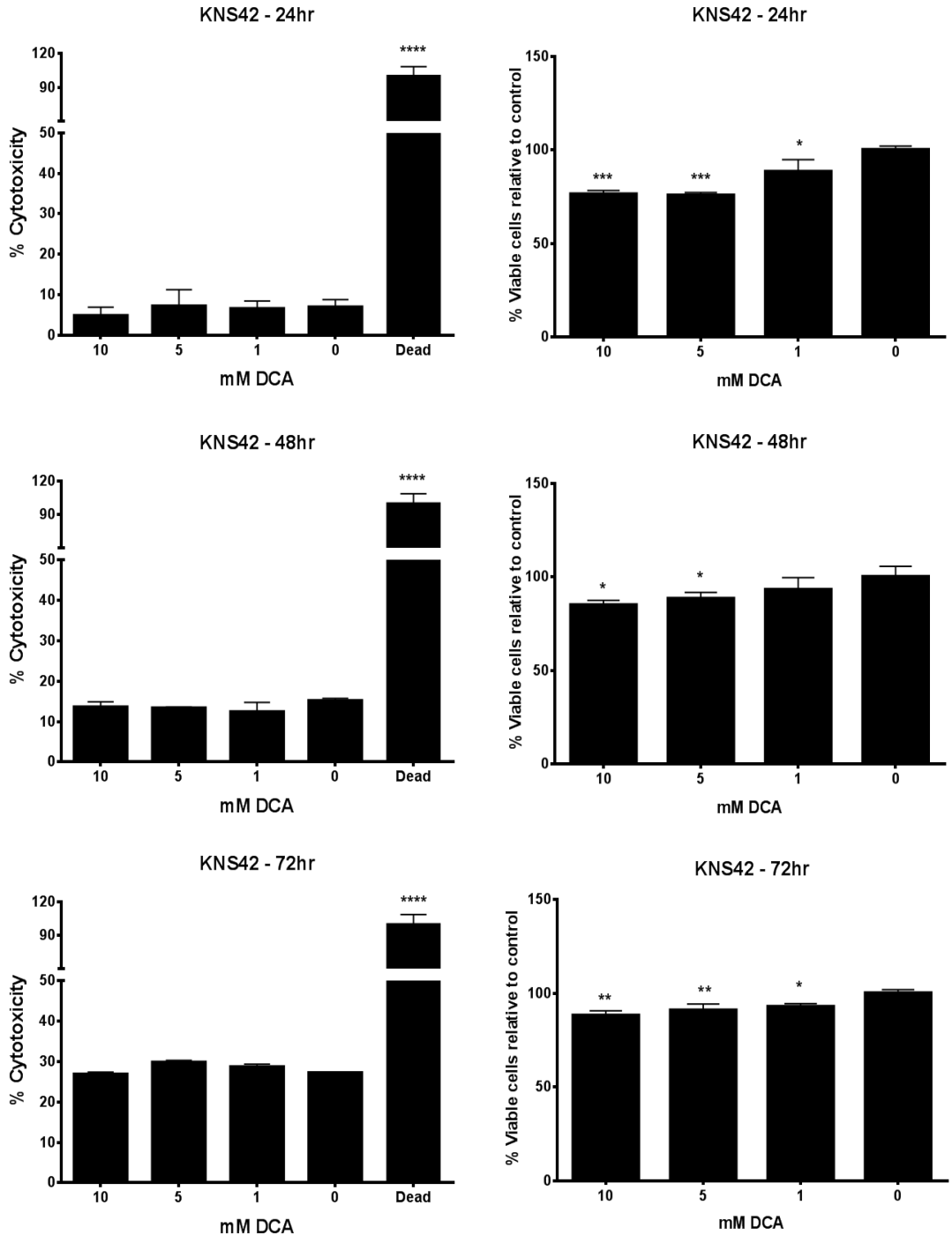

Figure 3.6: DCA does not induce death in KNS42 cells during a 72 hour treatment period. It does reduce the proliferation at all concentrations tested. The effects were more pronounced after 24 hours. Cells were treated with various doses of DCA for either 24, 48 or 72 hours. PI assays assessing the percentage death are shown in the left hand column while Hoechst assays assessing viability and cell number are on the right hand column. N = 3 and the error bars represent the standard deviation of the mean

The UW479 cells, while considered a high-grade glioma, appear very different from the adult lines and produced a similar metabolic profile to the SF188 and KNS42 GBM paediatric cell lines. In fact, UW479 had the highest basal oxygen consumption rates of all the cell types investigated. However, when we treated the UW479 cells with DCA the response seen does not resemble the SF188 and KNS42 response. DCA has no cytotoxicity and no impact on cell number (Figure 3.7). There was a huge increase in basal cytotoxicity after 72 hours for all cells including the control most likely because of over confluency after a 3-day culture period.

The glycolytic Res259 low-grade paediatric cell line showed no susceptibility to DCA (Figure 3.8). This was not surprising as all the glycolytic lines assayed up to this point were capable of tolerating the doses of DCA tested.

Overall, the DCA viability/cytotoxicity assays highlighted some interesting findings mainly the apparent susceptibility of the high-grade oxidative paediatric lines (SF188 and KNS42) and the tolerance of the glycolytic cell lines (RH30, U87MG, M059K and Res259). This was unexpected as DCA has been proposed as a potential therapy for glycolytic cancers but it showed little efficacy when tested on the glycolytic lines in this study.

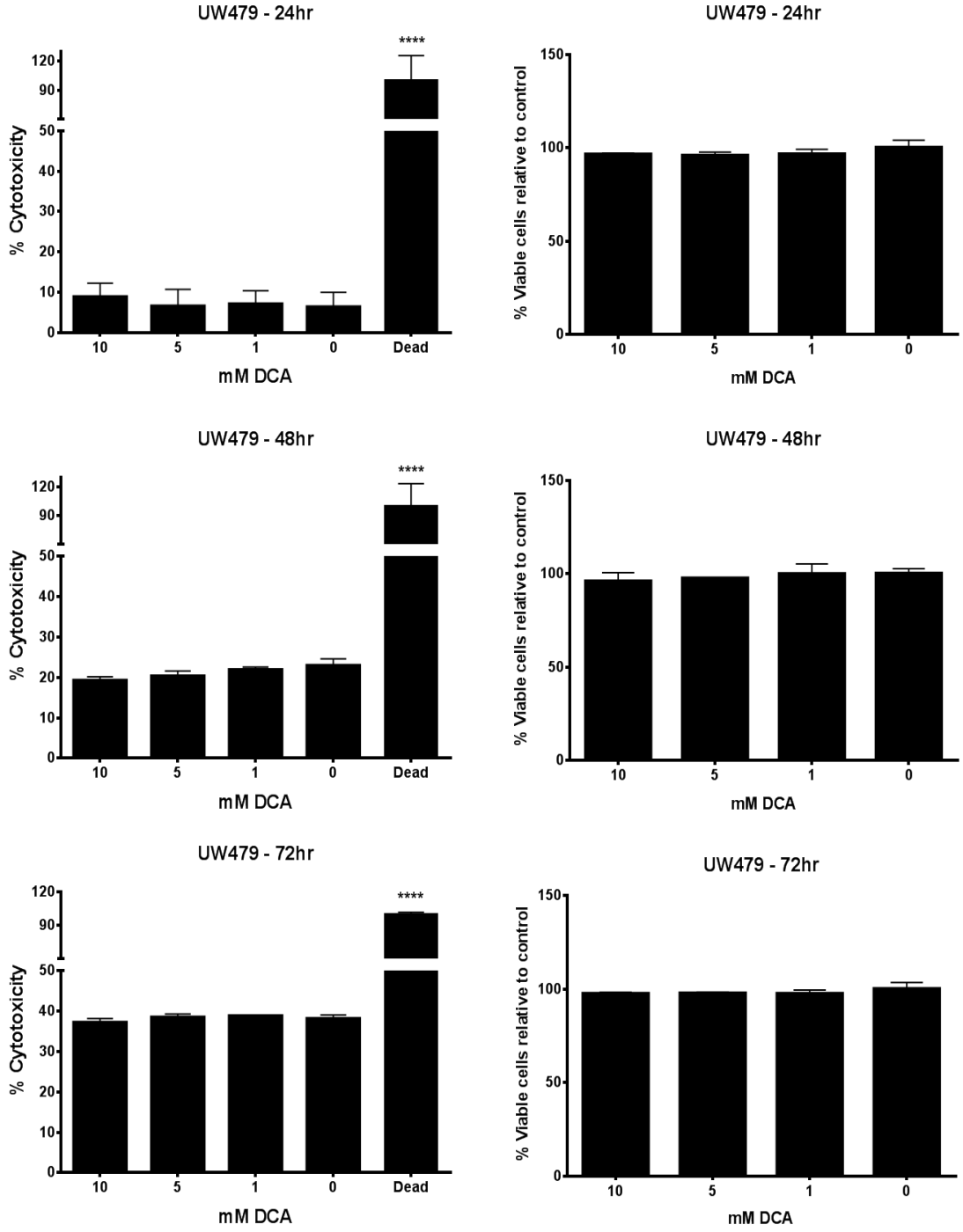

Figure 3.7: DCA does not induce death or slow proliferation in UW479 cells during a 72 hour treatment period. Cells were treated with various doses of DCA for either 24, 48 or 72 hours. PI assays assessing the percentage death are shown in the left hand column while Hoechst assays assessing viability and cell number are on the right hand column. N = 3 and the error bars represent the standard deviation of the mean

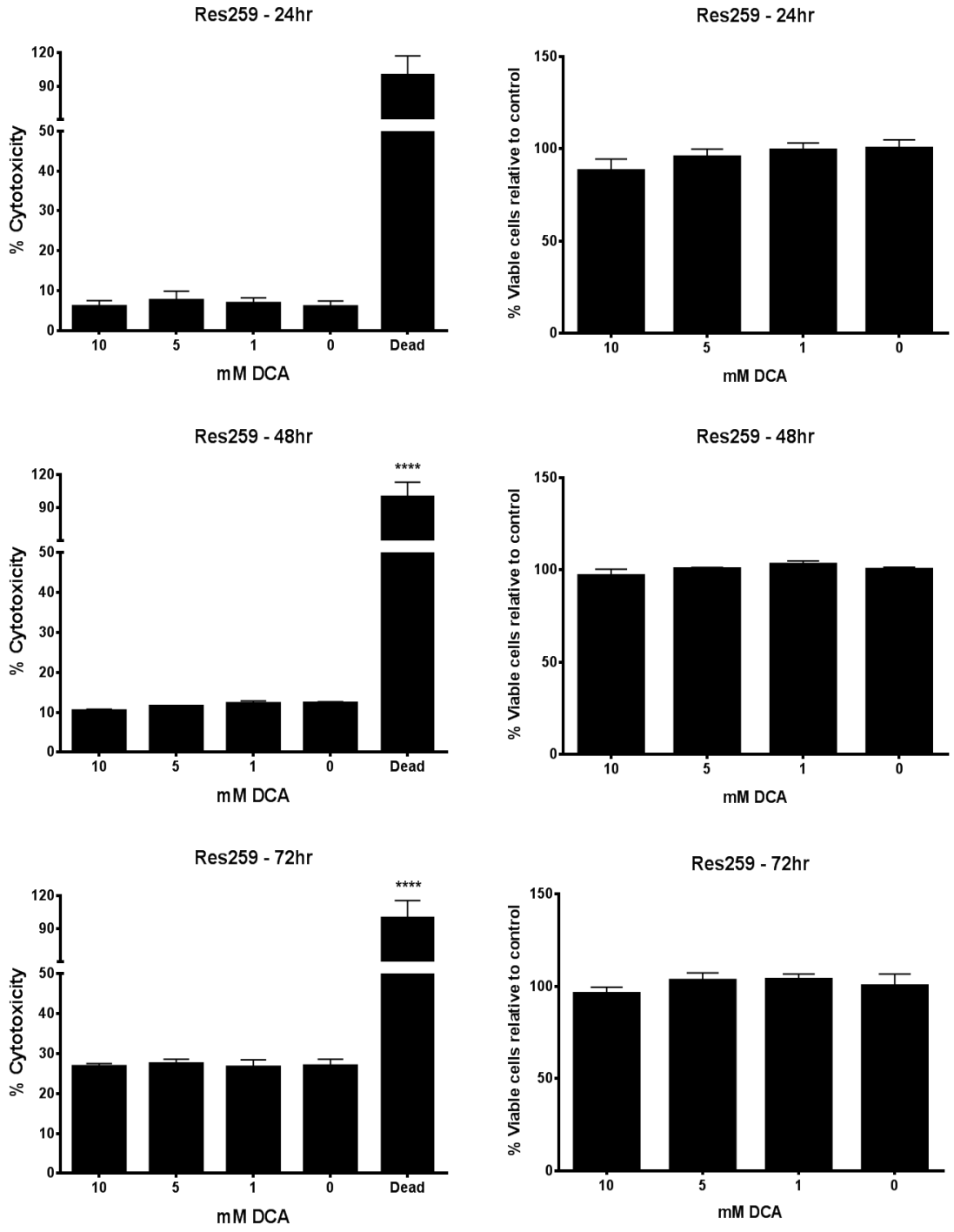

Figure 3.8: DCA does not induce death or slow proliferation in Res259 cells during a 72 hour treatment period. Cells were treated with various doses of DCA for either 24, 48 or 72 hours. PI assays assessing the percentage death are shown in the left hand column while Hoechst assays assessing viability and cell number are on the right hand column. N = 3 and the error bars represent the standard deviation of the mean

3.4.4 DCA increases oxygen consumption in glycolytic cells cultured in physiological glucose

The interest in DCA as an anticancer treatment has increased exponentially since the Bonnet et al 2007 paper with several in-vitro and pre-clinical/clinical studies published. The efficacy of DCA is quite variable and a comprehensive literature review in 2011 by Papandreou et al identified that in-vivo efficacy was greater than that observed in-vitro efficacy (Papandreou et al., 2011). So perhaps it is not surprising that DCA had limited effects on the viability of cell lines grown as 2D cultures. While DCA may not be cytotoxic to the cells it should act on them to increase cellular respiration by inhibiting PDK and allowing pyruvate entry to the mitochondria. Oxygen consumption was assessed using the methods described in Chapter 2. Cells were seeded at 30,000 cells/well allowed to adhere and then treated with either 0, 1, 5 or 10mM DCA overnight. Preliminary results showed no increase in oxygen consumption with DCA in RD, RH30, U87MG or M059K cells cultured on high glucose (20mM) (data not shown). As was demonstrated in the previous chapter the concentration of glucose can have a significant impact on the rates of mitochondrial respiration and glycolysis. To establish the effects of DCA under more physiological glucose levels we used media containing 5mM and 1mM glucose to better reflect plasma and cell /tissue glucose levels. On 1mM glucose an overnight DCA incubation had no effect on the oxygen consumption in all lines studied Figure 3.9 .This is likely due to the enhanced respiration observed at this glucose concentration preventing further enhancement of respiration by DCA. At 5mM glucose the more OXPHOS RD cells don't respond to DCA while , the glycolytic

RH30 increase respiration significantly in DCA in the low mM range (1mM) with respiration returning to control levels at the higher DCA concentrations . It was shown that 10mM (Figure 3.2) DCA does not induce death in these cells so cell loss due to death would not explain this decrease.

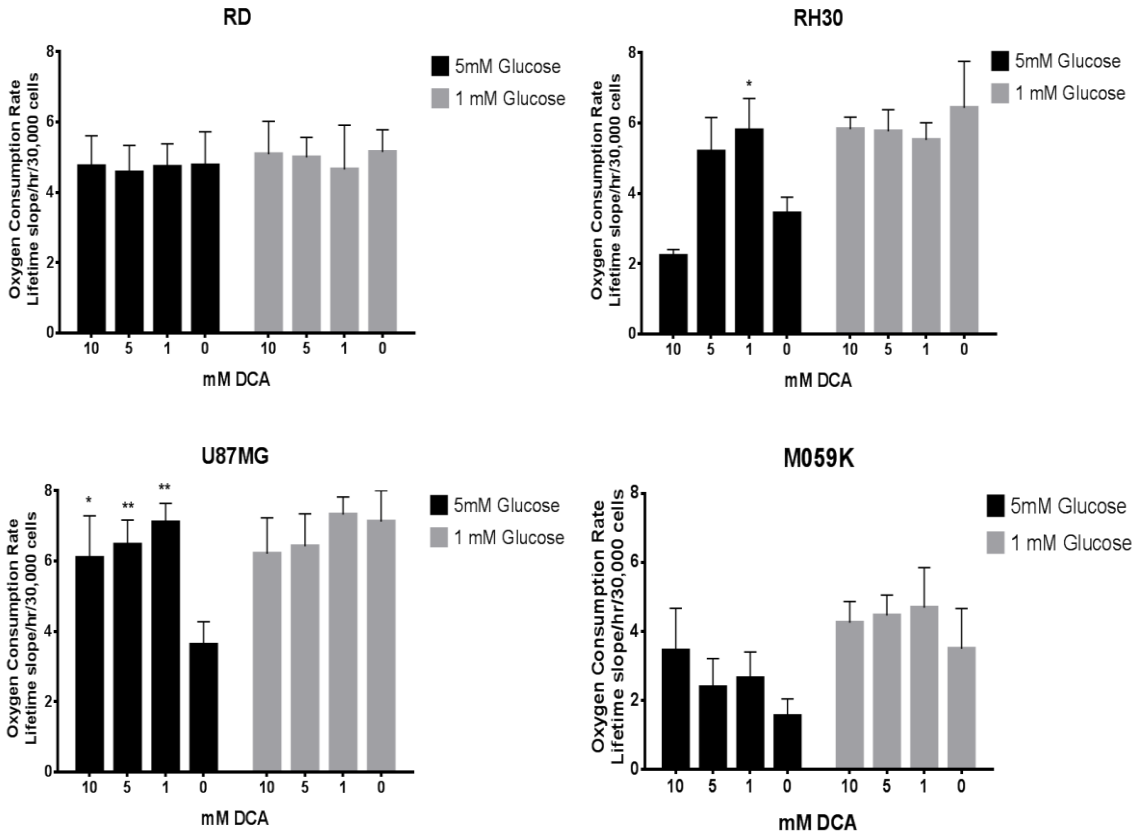

Figure 3.9: Effect of DCA on the oxygen consumption rates of RD, RH30, U87MG and M059K cells cultured on either 5mM or 1mM glucose. Cells were seeded at 30,000cells/well and treated overnight with 0, 1, 5 or 10mM DCA. N = 3 and error bars represent the standard deviation above the mean

The U87MG cell line significantly increased respiration rates on 1, 5 and 10mM DCA on 5mM glucose but on 1mM glucose DCA had no effect on respiration as the basal OCR rates were higher due to the reduced glucose concentration. M059K cells show a trend towards increasing respiration rates but were not significant.

Due to the aerobic nature of the paediatric glioma cell lines the effect of DCA on their respiration rates was not assessed as it was thought DCA would not have an impact on their already oxidative states.

3.4.5 Spheroids as model to assess drug efficacy

Spheroids are a model that better reflects the in-vivo tumour (Figure 3.10). There is a stark contrast between in-vitro culture and in-vivo. In-vitro culture as mentioned earlier there is a large excess of nutrients and oxygen and the supply likely far outweighs the demand. In-vivo tumours represent the other extreme where there is limited supply of nutrients and oxygen and inadequate removal of waste products due to the bottleneck created by poor vasculature (Vaupel, 2004). Spheroids fall between the two extremes and as such are perhaps a better model assessing compounds that affect in vivo tumour growth. Spheroids have areas of hypoxia as well as nutrient and waste gradients. Since DCA has shown potential efficacy in-vivo with less success in-vitro, 3D models might be better than 2D models to assess DCA's potential as an anti-cancer drug.

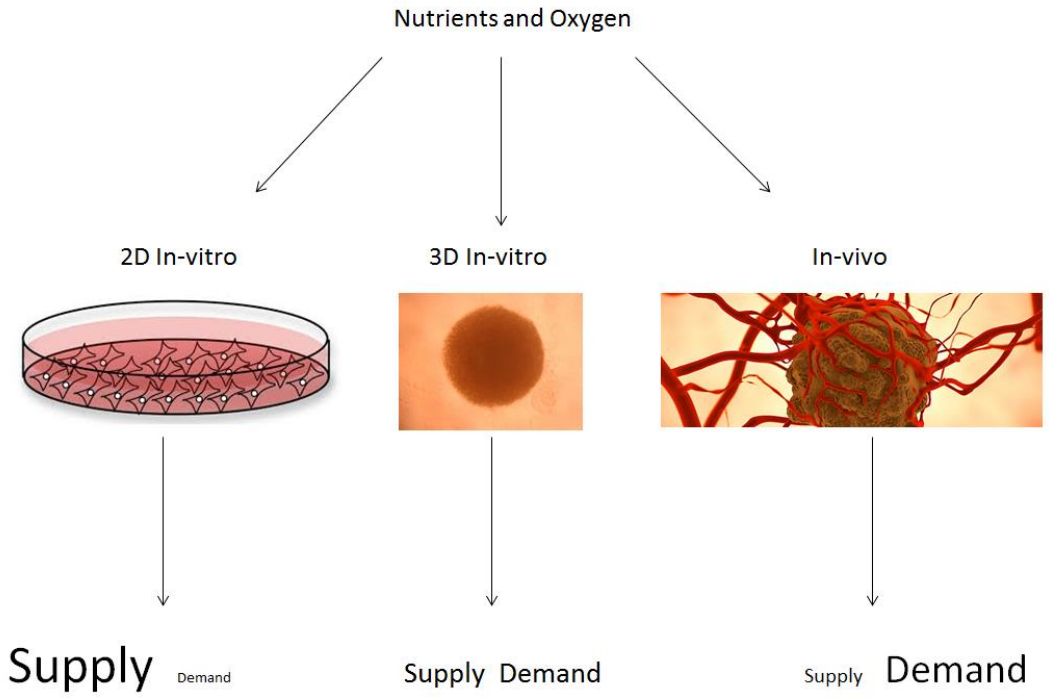

Figure 3.10: 3D in-vitro models are more relevant than 2D culture systems

3.4.6 Spheroid volume

Spheroids were cultured as described earlier and on day three treated with various doses of DCA for 96 hours. For the RD (Oxphos) line, proliferation of spheroids was not affected by DCA treatment up to 20mM. RH30 (glycolytic) spheroids treated with 5mM and 20mM DCA appeared smaller (Figure 3.11).

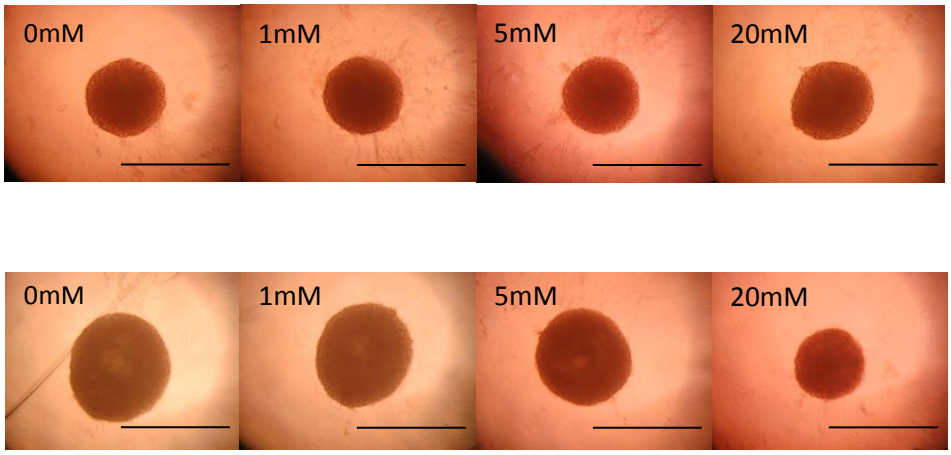

Figure 3.11: DCA does not affect spheroid volume in RD cells but high doses (20mM) DCA results in reduced spheroid volume in RH30 cells. Scale bars represent 1000µm

Old U87MG spheroids when treated with 20mM DCA were smaller and morphologically distinct from the untreated spheroids (Figure 3.12). The 5mM DCA spheroid treatment had inconsistent effects on spheroid size some spheroids were similar in size to the untreated control, others were smaller and the rest were in fact larger than the controls. The growth curve in Figure 3.12 indicates that 5mM DCA treated U87MG spheroids may be proliferating faster than the untreated control. However, the increased spheroid volume observed in the 5mM treated U87MG spheroids does not necessarily reflect enhanced proliferation. U87MG spheroids were also treated with hydrogen peroxide as a positive control and the expected result was that there would be a decrease in spheroid size over time but we observed an increase in volume (Figure 3.13). When analysed by flow cytometry the spheroids treated with H_2O_2 were completely dead despite their larger appearance. The health of the cells in the spheroid will be discussed in detail later in this chapter but these results indicate that relying on spheroid volume alone is an inadequate approach in

assessing drug treatment effects. Proliferation of M059K spheroids was reduced by 20mM DCA but not by lower concentrations (Figure 3.12).

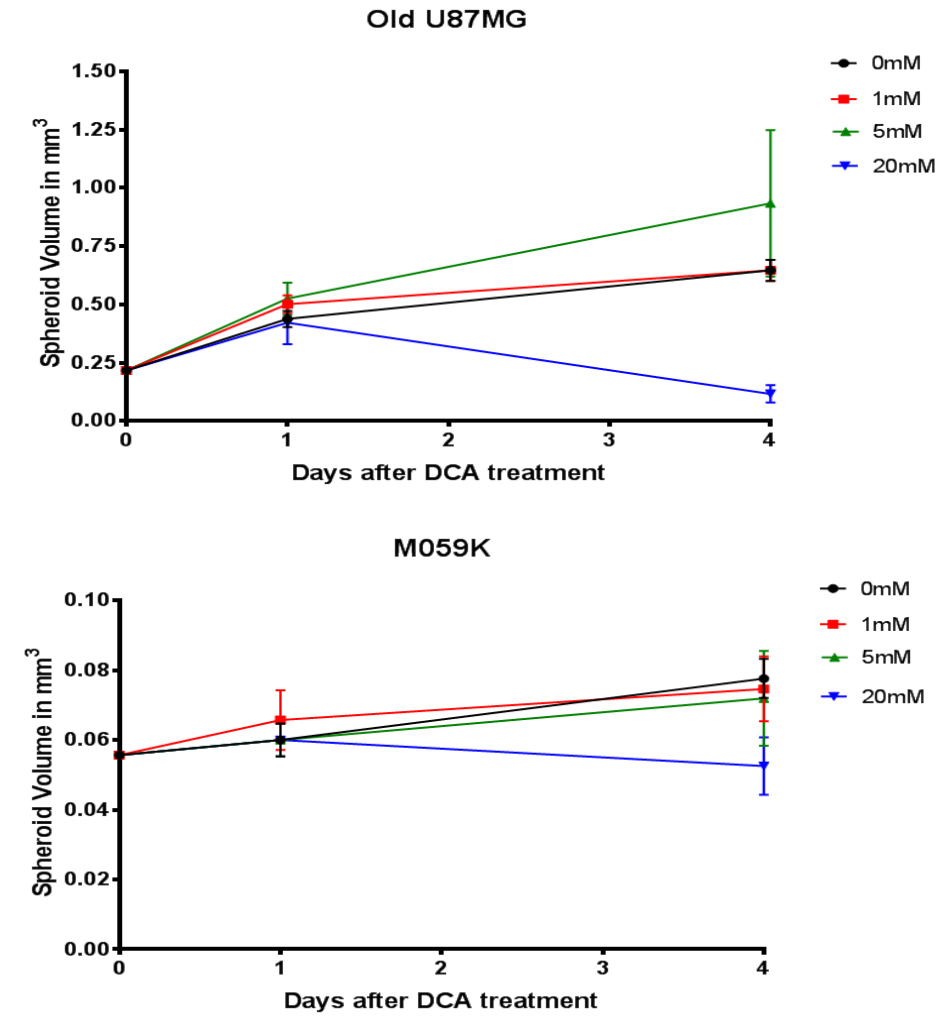

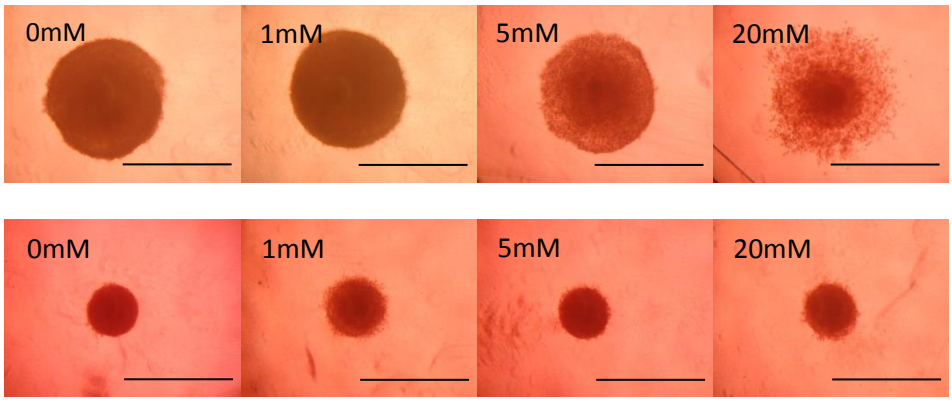

Old U87MG

M059K

Figure 3.12: 20mM DCA reduces spheroid volume in U87MG spheroids. M059K spheroids are also smaller when exposed to 20mM DCA. Scale bars represent 1000µm

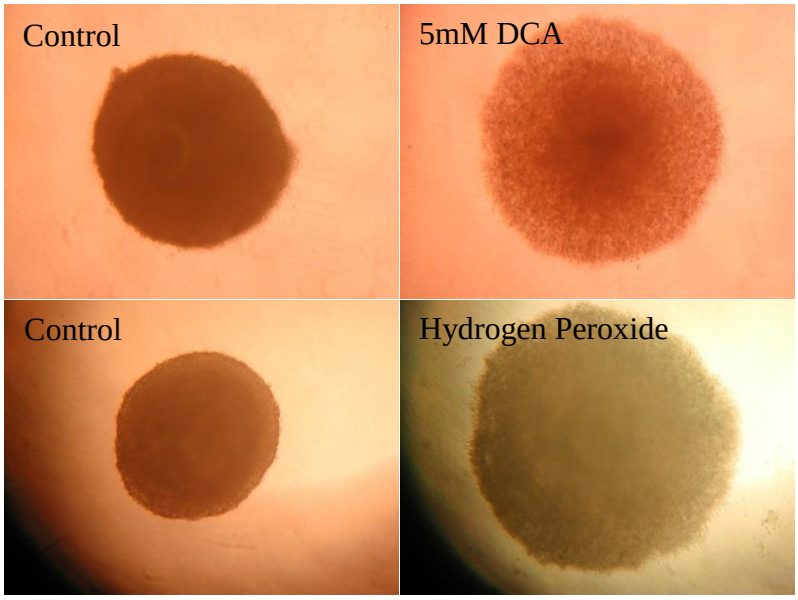

Figure 3.13: Increased spheroid volume does not always equate to increased proliferation. U87MG spheroids treated with 5mM DCA and hydrogen peroxide are bigger than the untreated controls but the cells in the spheroid treated with H2O2 are dead.

3.4.7 DCA reduced respiration rates in the GBM U87MG and KNS42 spheroids

In chapter 2, it was demonstrated that the Mito-Xpress and pH-Xtra probes are suitable for measuring oxygen consumption and acidification rates in spheroids. In this section, we use these probes to assess the downstream effects of DCA on mitochondrial respiration in RD, RH30, U87MG and KNS42 spheroids. RD spheroids showed no significant changes in either OCR or ECAR with DCA treatment (Figure 3.14). The RH30 spheroids responded with an increase OCR as DCA dose increased. Of interest, although not significant, is the RH30 ECAR response. It appears to be trending towards increased acidification on the higher doses of DCA.

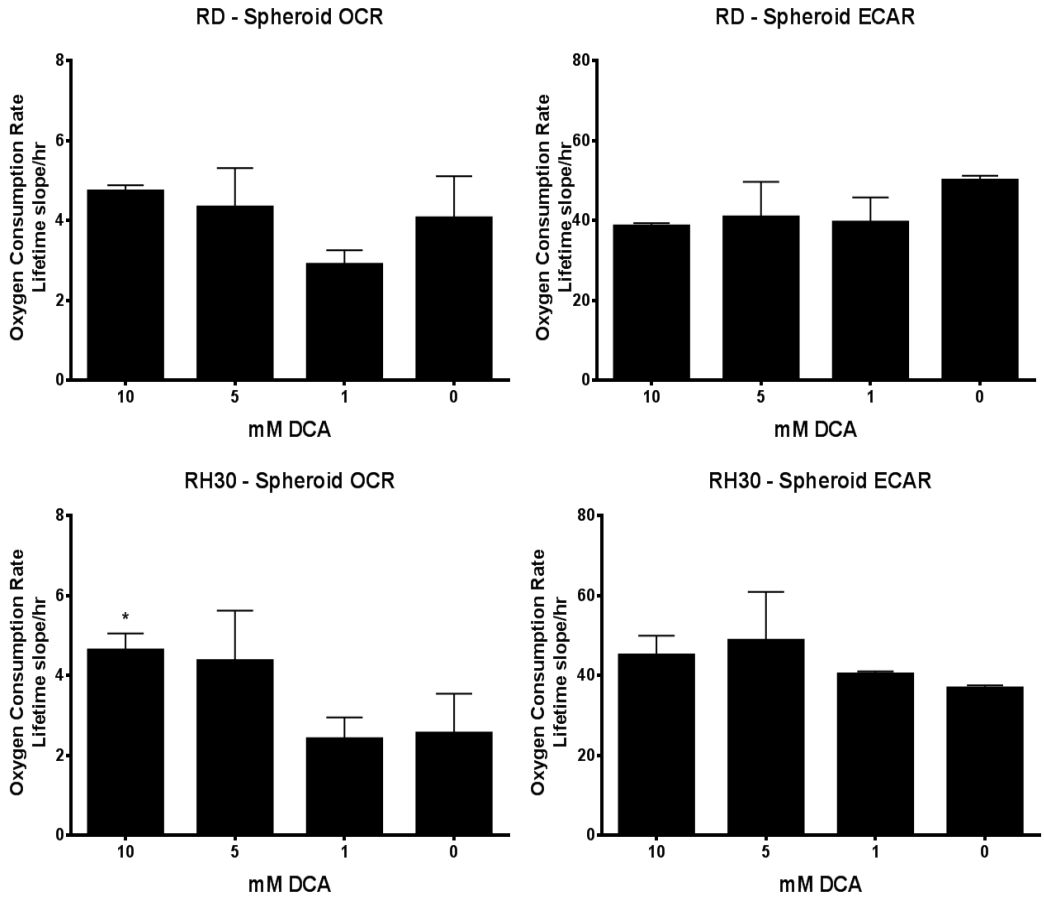

Figure 3.14: Effect of 24 hour DCA treatment on the oxygen consumption rates and acidification rates of RD and RH30 spheroids. 10mM DCA increased the respiration rates in RH30 spheroids but not RD spheroids. N=3 and error bars represent the SD. (data normalised to spheroid volume)

The OCR of the glioblastoma multiforme spheroids U87MG (adult) and KNS42 (paediatric) showed significant decreases in respiration when treated with 1, 5 and 10mM DCA (Figure 3.15). The reduced OCR rates were not coupled to alterations in the ECAR rates. The ECAR rates for both U87MG and KNS42 spheroids at all DCA doses used remained consistent.

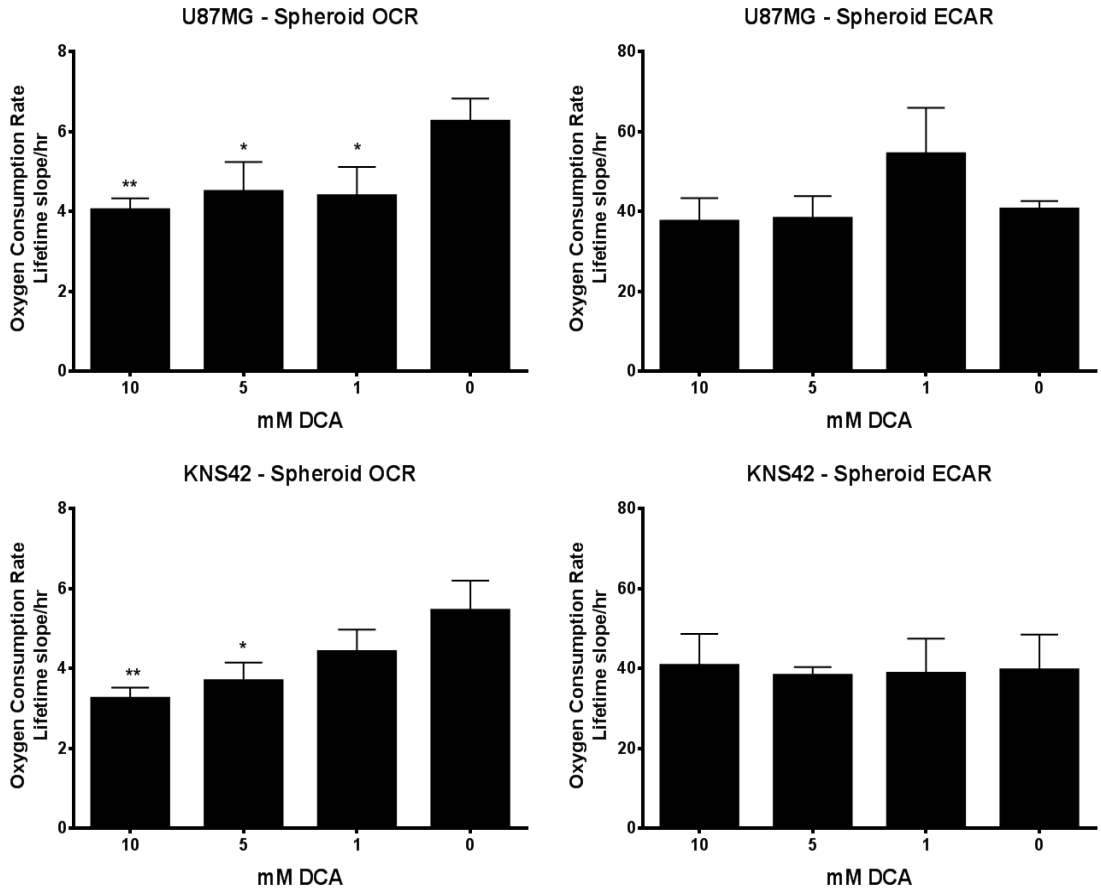

Figure 3.15: Increasing doses of DCA decrease OCR in U87MG and KNS42 spheroids but ECAR is unaffected. N = 3 and error bars represent the SD.

When using the linear portion of the ECAR plot to determine the rates of acidification DCA treatment does not appear to affect the ECAR (Figure 3.14 & Figure 3.15). However, when the raw data ECAR plots are examined clear DCA effects on ECAR can be observed (Figure 3.16). Untreated spheroids start to acidify the media after 2 hours but the DCA treated spheroids do not start to acidify the media until 6 hours (Figure 3.16). This highlights a need for better way to analyse the data.

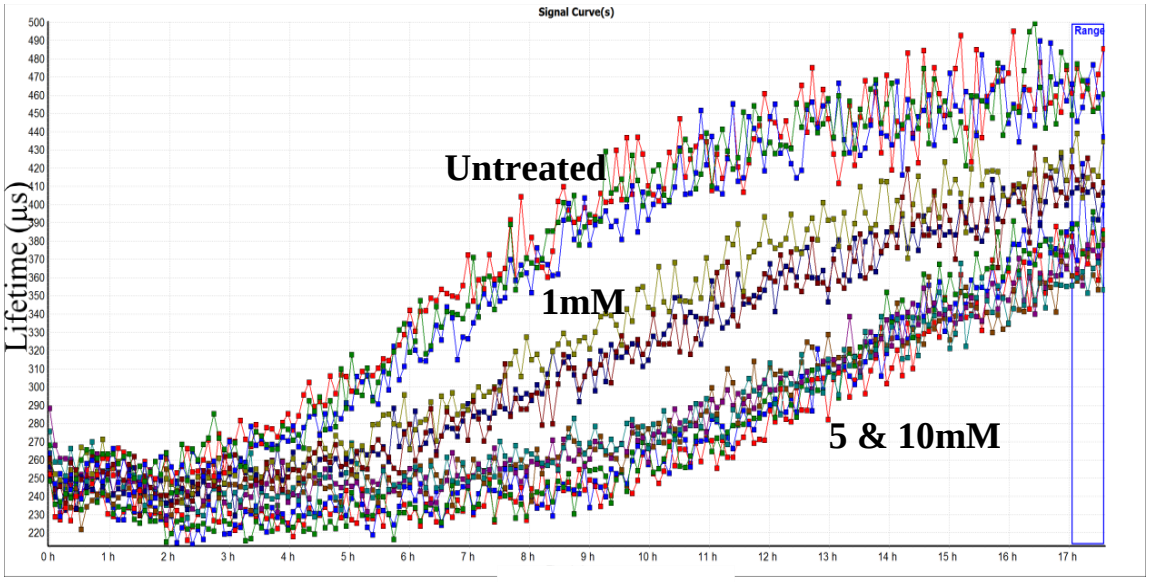

Figure 3.16: U87MG spheroids treated with 1, 5 and 10mM DCA show delayed acidification rates of the media.

3.4.8 Spheroid Viability and Apoptosis

As discussed previously, relying on changes in spheroid size does not necessarily give a true reflection of the health of the cells within the spheroid. Our results with hydrogen peroxide (Figure 3.13) suggest that larger spheroids are not necessarily an indication that a drug treatment has a) been ineffective at reducing growth or b) has improved spheroid growth. In order to gain a deeper understanding of what is happening to the cells inside the structure spheroids were dissociated and analysed for cell death (PI) and apoptosis (annexin V) (discussed earlier in section 3.3.9).

3.4.8.1 Setting up the gates

To assess the effects of drug treatment on the viability of cells in spheroids a PI/Annexin V APC staining protocol for flow cytometry was applied (see 3.3.9.3).

The protocol requires live cells, dead cells and debris to be easily discriminated during the FACS run. To do this gates are established which define the individual populations. Live and dead cells stain differently with PI and annexin V depending upon their status. Within the live population there will be normal healthy cells and possibly early apoptotic cells. Live cells will not stain with either PI or annexin V. Early apoptotic cells will stain with annexin V but not stain with PI. Within the dead population PI and annexin V, staining is observed (double staining).

Figure 3.17 is a representative example of the overall scatter plot of the cells (FSC on the x axis and SSC on the y axis). Based on their size and granularity the cells can be divided into two discrete populations, labelled P1 and P4. P4 lies to the left hand side of the scatter plot and is consistent with dead or unhealthy cells. P1 lies more to the centre of the scatter plot and is consistent with live and healthy cells. The dense black area on the bottom left of this graph is consistent with cellular debris and instrument noise.

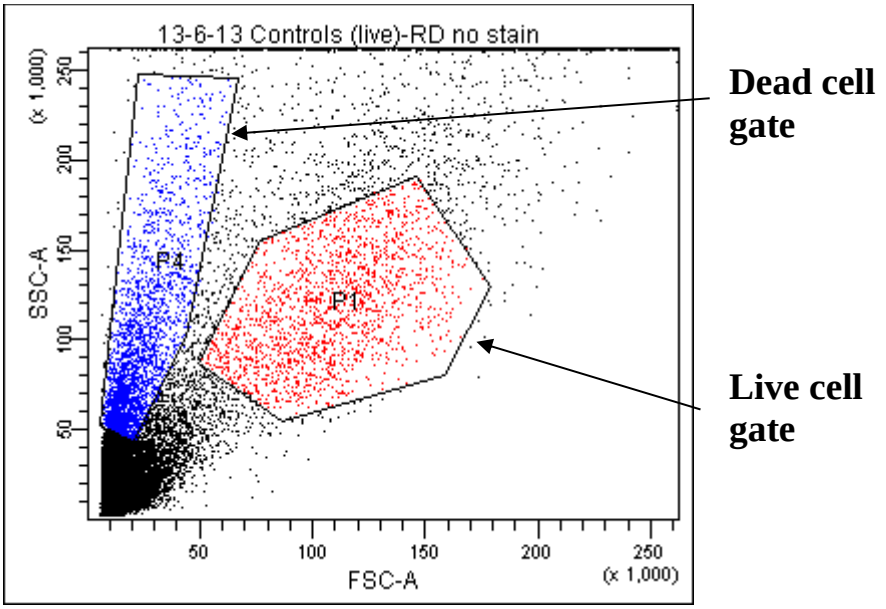

Figure 3.17: Representative flow cytometry scatter plot. P1 (red population) represents the live cell population while P4 (blue population) represents the dead cell population.

Once the live and dead cell populations have been assigned (P1&P4) cells within each of these populations can be further subdivided into PI and annexin V positive or negative (Figure 3.18). The P1 live cell population (in red) is divided into (A) P2 the cells that are in the live population but staining positive for PI and (B) P3 the portion of the live cell population that are annexin V positive (early apoptotic). The P4 dead population is also divided into (C) P5 the portion of PI positive cells in the dead population and (D) P6 the annexin positive cells in the dead population (late apoptotic). Figure 3.18E is a representative table depicting the number events recorded in any given population. This data allows percentage viable cells, PI positive cells and annexin V positive cells to be calculated and graphed.

Figure 3.18 is a representation of unstained cells therefore there were no events recorded in P2, P3, P5 or P6. Figure 3.19 and Figure 3.20 depict PI and annexin staining respectively.

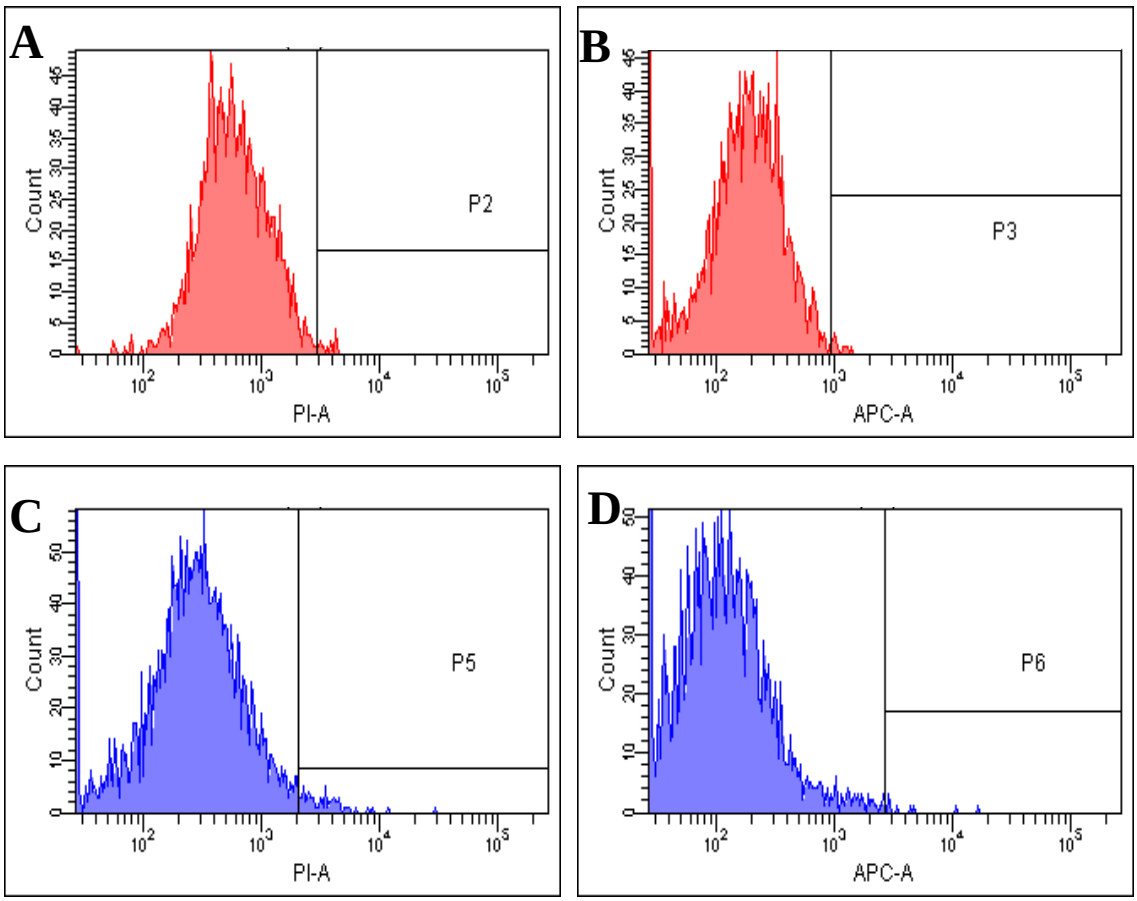

E

Population	#Events	%Parent	%Total
All Events	28,793		100.0
P1	1,772	6.2	6.2
P3	14	0.8	0.0
P2	14	0.8	0.0
P4	2,727	9.5	9.5
P5	68	2.5	0.2
P6	11	0.4	0.0

Figure 3.18: Setting the gates for PI and annexin V using unstained samples. The gates are set to the immediate right of the respective populations (indicated by black vertical lines). (A) shows the PI plot for the live population (B) is the live plot showing annexin V staining. (C) is the dead plot where PI positive results will be seen while (D) shows the annexin V positive cells in the dead population. (E) Gives the numbers of events in each gated population. In this unstained example there is no fluorescence in either the PI or annexin-APC channels.

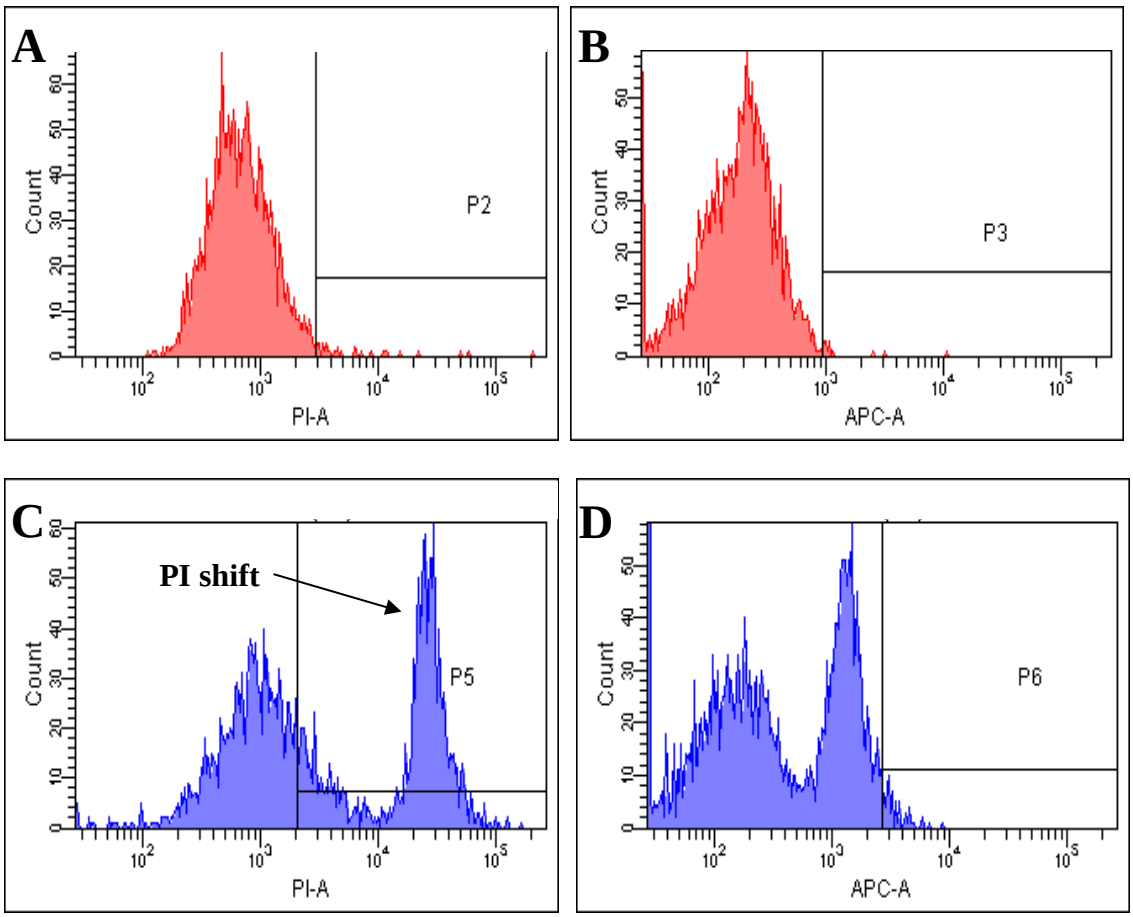

Figure 3.19: Typical profile of PI stained cells. Cells stained with PI are not detected in the live cell population (A). PI staining in (B&D) was not expected, as this is the APC channel for the annexin V. A positive population shift in (C) is characteristic of PI positive cells in the dead population.

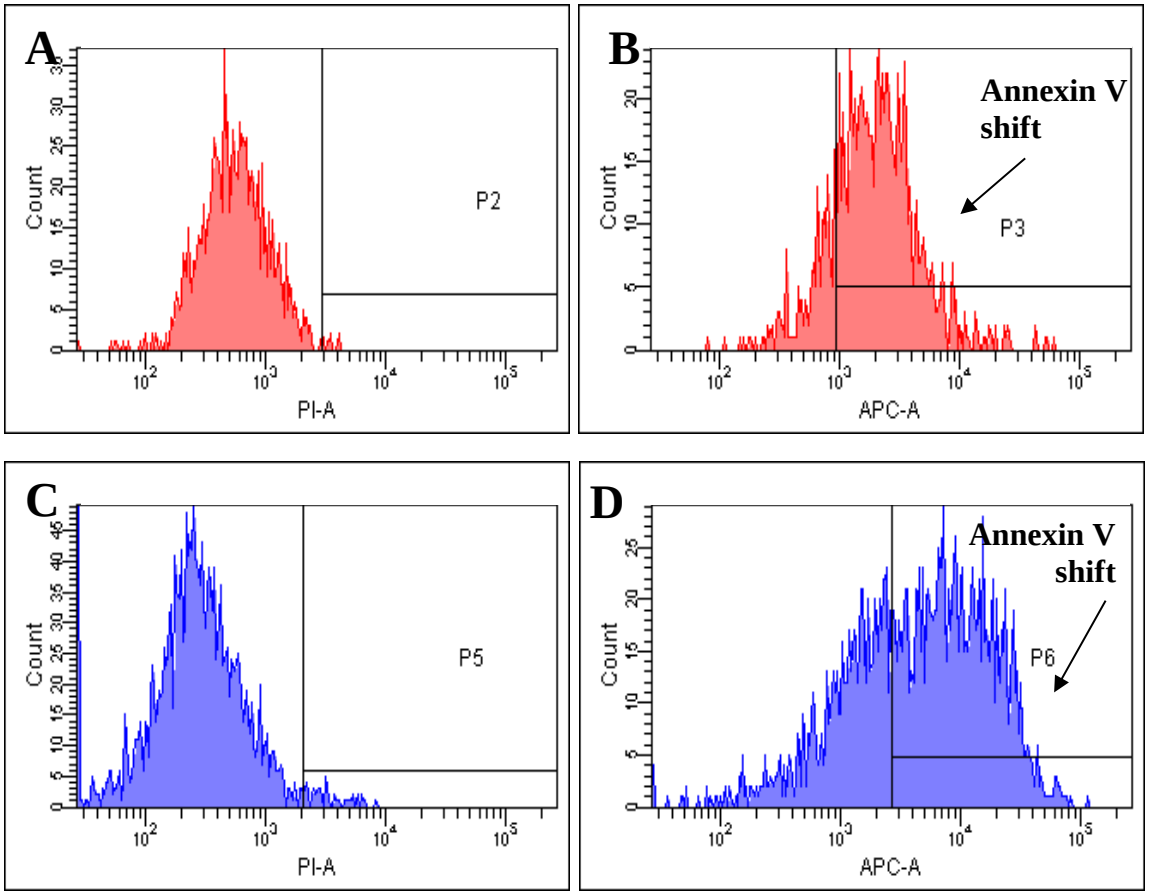

Figure 3.20: Typical profile of annexin V stained cells. Cells stained with annexin V are not detected in the live cell population (A) because this is the PI channel. Annexin staining and the associated population shift in (B&D) is expected where cells in the live and dead populations express PS. No population shift in (C) is expected, as this is the PI channel.

As an added control annexin V staining was evaluated in the absence of the calcium binding buffer to eliminate non-specific binding (Figure 3.21). This figure clearly shows that calcium binding buffer is necessary as there is no annexin signal without it.

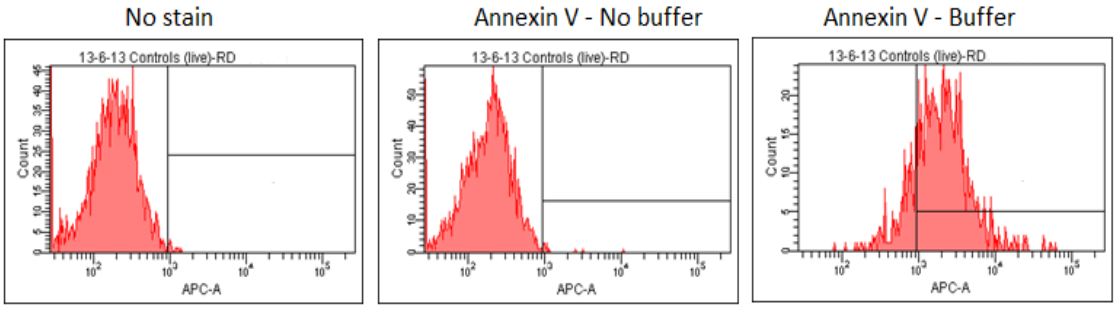

Figure 3.21: Annexin V can only bind in the presence of calcium binding buffer (right). No annexin V staining is observed in the absence of this (centre).

3.4.8.2 Spheroid Dissociation

As a means of assessing the "health" of cells in spheroids they were dissociated in a number of ways with varying degrees of success (see section 3.3.9.2 for dissociation procedures).

Trypsin dissociation of spheroids

Initially spheroids were dissociated with trypsin (following a PBS wash) however this was not successful for U87MG cells as a single cell suspension suitable for flow cytometry analysis could not be achieved (data not shown). RD and RH30 spheroids could be dissociated readily with trypsin. Figure 3.22 (A&B) shows the flow cytometry scatter plots for trypsin dissociated RD and RH30 spheroids treated with DCA. For the untreated controls of both cell types only 6% of all the events collected were in the live cell population (P1). This indicates that the majority of cells were dead in the spheroid prior to dissociation or that the trypsin dissociation process is contributing to the low levels of cell viability. Increasing doses of DCA resulted in a further reduction in the number of events collected in the P1 population (red). When

plotted there appears to be a DCA dose dependent reduction in the number of viable cells collected for both cell types (Figure 3.22 C&D). However, because the viable population in the untreated control was so low in the control spheroids (~6% for both cell types) it was difficult to determine if the effect of DCA was just an additive effect to a stressful isolation protocol.

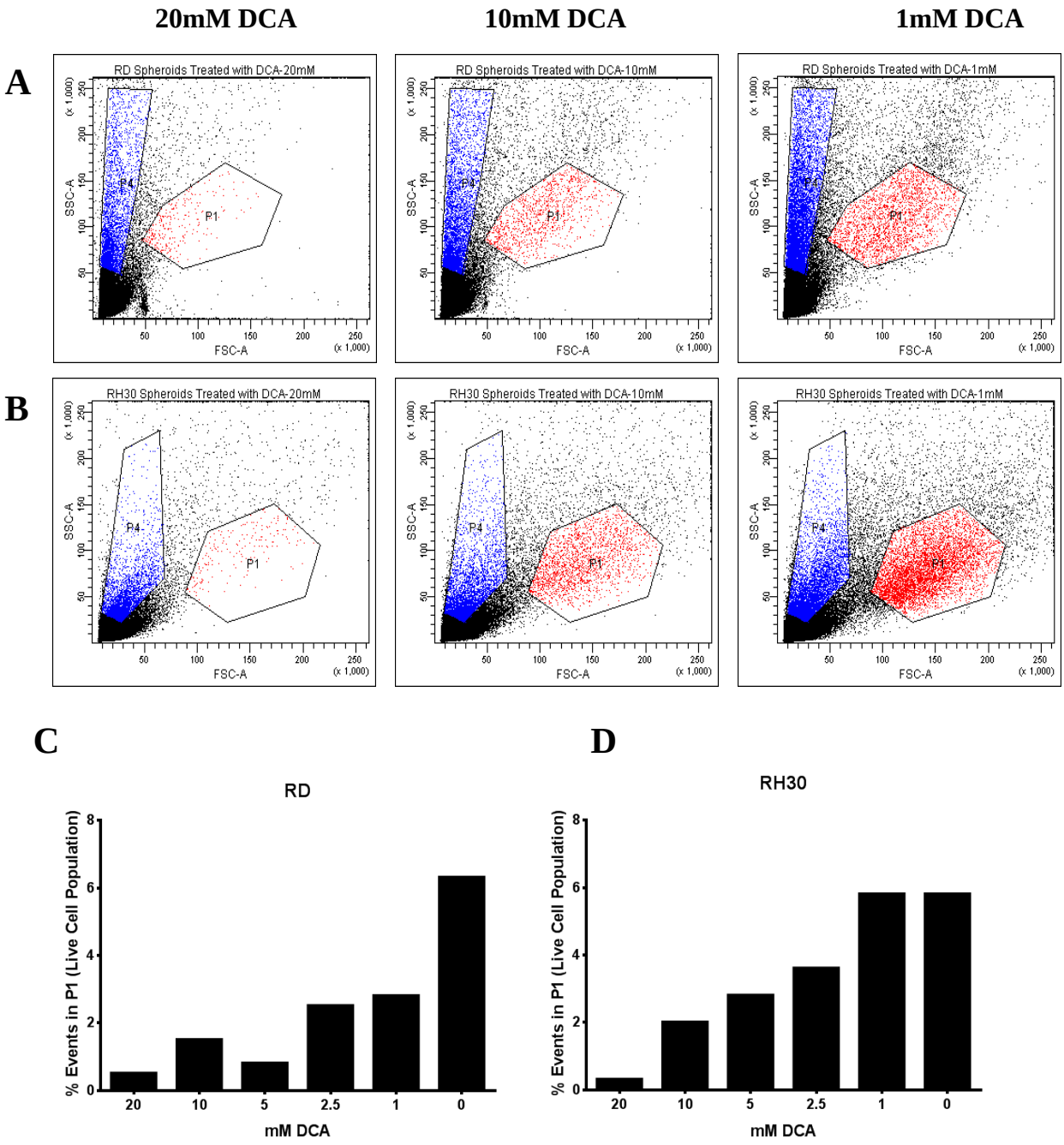

Figure 3.22: DCA decreases the number of viable cells in RD and RH30 spheroids. Spheroids dissociated with trypsin show a DCA induced dose dependent decrease in the number of viable cells (P1 red population) in RD and RH30 spheroids (A&B). Plots of the % viable cells in the RD spheroids (C) and RH30 spheroids (D). N = 1

Tumour dissociation kit (MACS Miltenyl kit)

The tumour dissociation kit was effective in providing a single cell suspension but did require excessive sample agitation (achieved through extensive pipetting) and as such the number of viable cells in each sample remained low although slightly higher than trypsin dissociation . Figure 3.23 (A&B) shows that RD spheroids when treated with 1, 5 and 10mM DCA have significantly fewer events in the live population. This was surprising as DCA in Figure 3.11 had no apparent effect on the growth rate or spheroid volume. It highlights that spheroid size and proliferation may not be the most effective means of assessing DCA in a spheroid model. Interestingly the percentage annexin staining decreased as DCA dose increased Figure 3.23(C).

A similar effect was seen in the RH30 spheroids Figure 3.24. DCA decreased the number of viable cells in the P1 population and it decreased the percentage of cells labelling positive for annexin V.

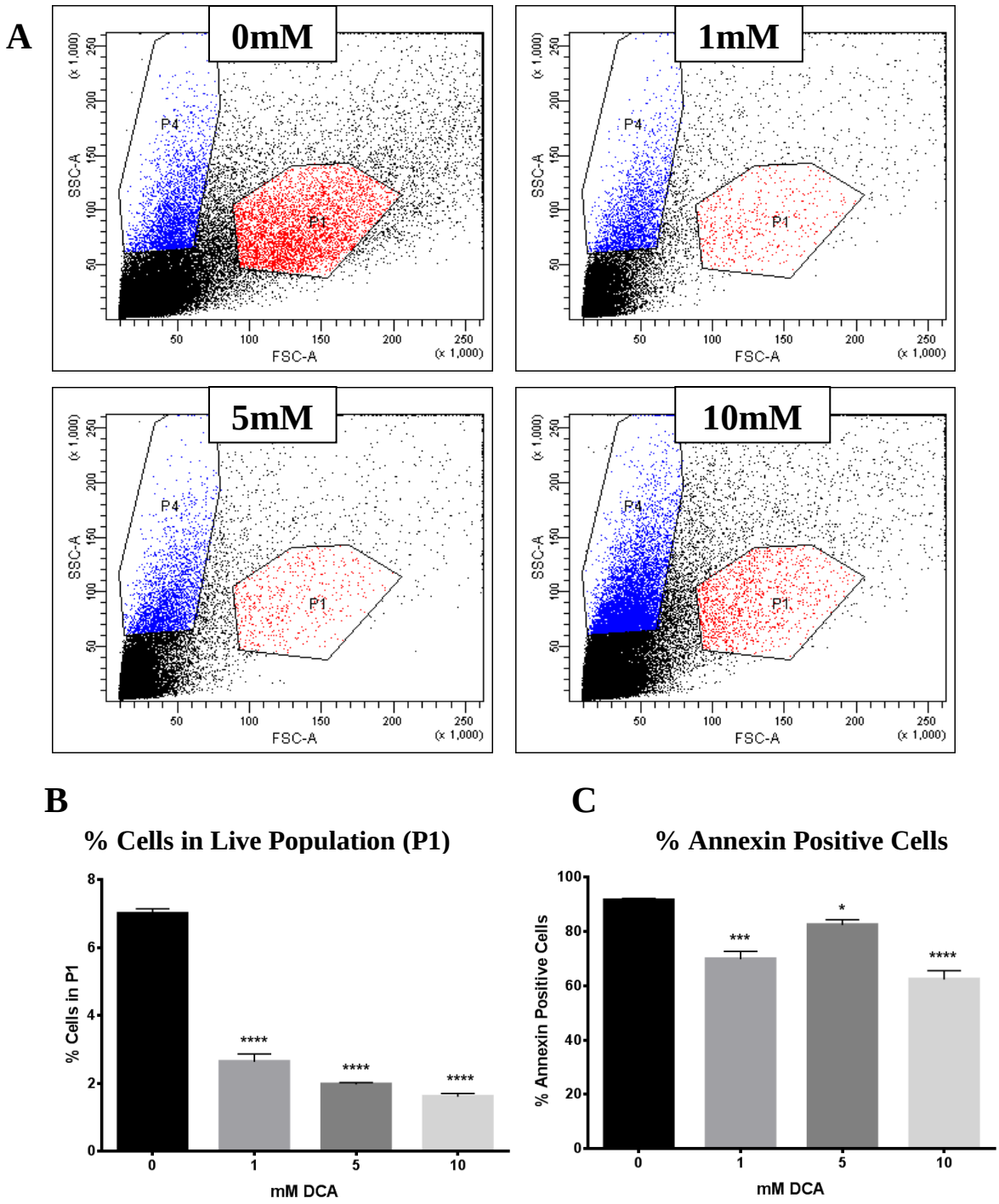

Figure 3.23: DCA decreases the number of viable cells in RD spheroids. Spheroids dissociated with MACS tumour dissociation kit show a DCA induced dose dependent decrease in the number of viable cells (P1 red population) in RD spheroids (A) and this is graphed in (B). (C) graphs the % annexin positive cells detected in P1 (P3). N = 1 (error bars represent triplicate samples)

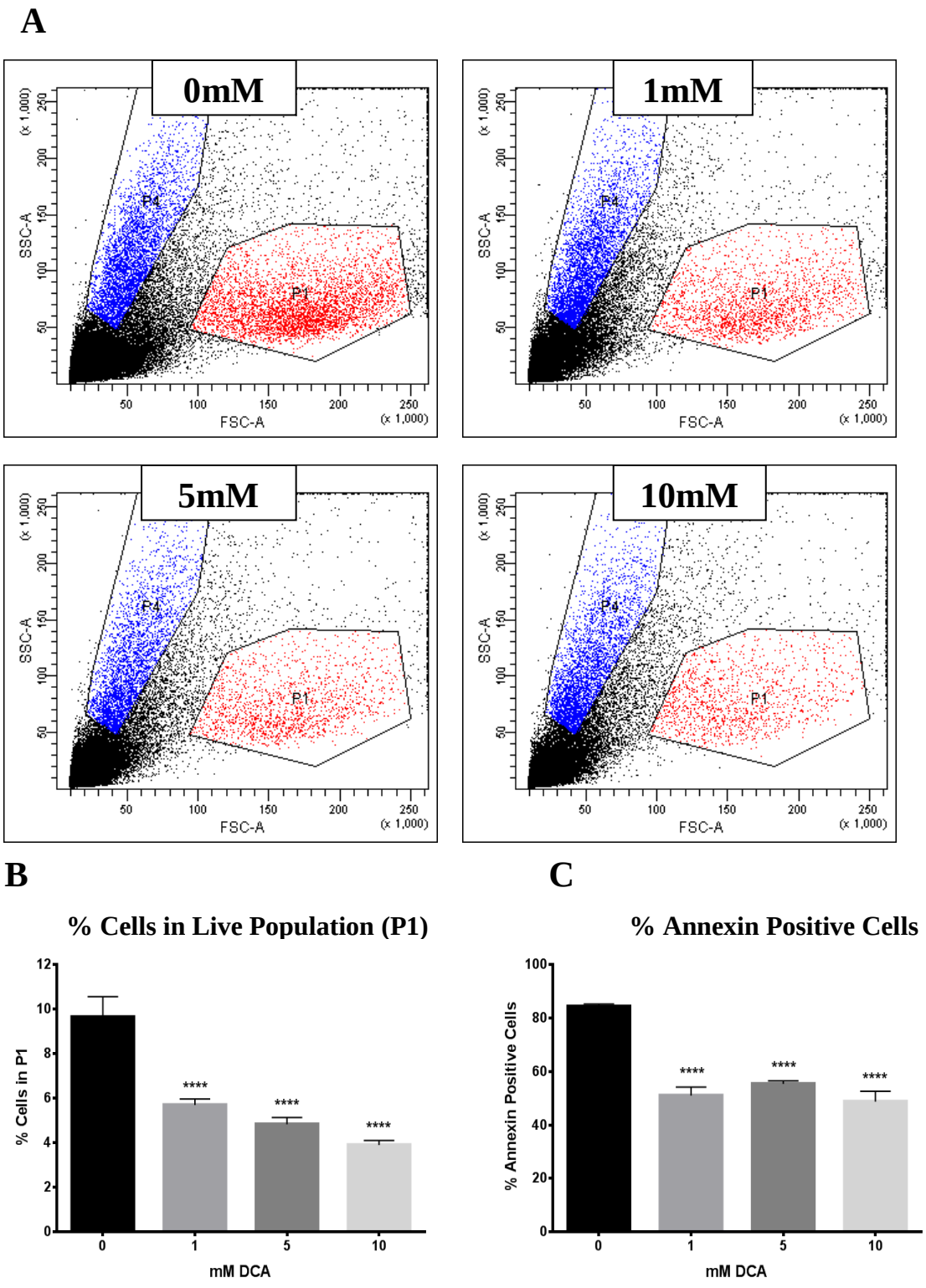

Figure 3.24: DCA decreases the number of viable cells in RH30 spheroids. Spheroids dissociated with MACS tumour dissociation kit show a DCA induced dose dependent decrease in the number of viable cells (P1 red population) in RH30 spheroids (A) and this is graphed in (B). (C) graphs the % annexin positive cells. N = 1 (error bars represent triplicate samples)

Accutase digestion

The results for accutase spheroid digestions show much cleaner FACS plots, the high debris levels observed in the other dissociation methods are greatly reduced. Using trypsin or the MACS kit cells in RD and RH30 spheroids showed only 6% of the cells to be viable. Using accutase the percentage of viable cells in P1 (red) rises to >40% for the RD and RH30 spheroids (Figure 3.26 A&B) and >30% for the U87MG and KNS42 spheroids (Figure 3.25 C&D).

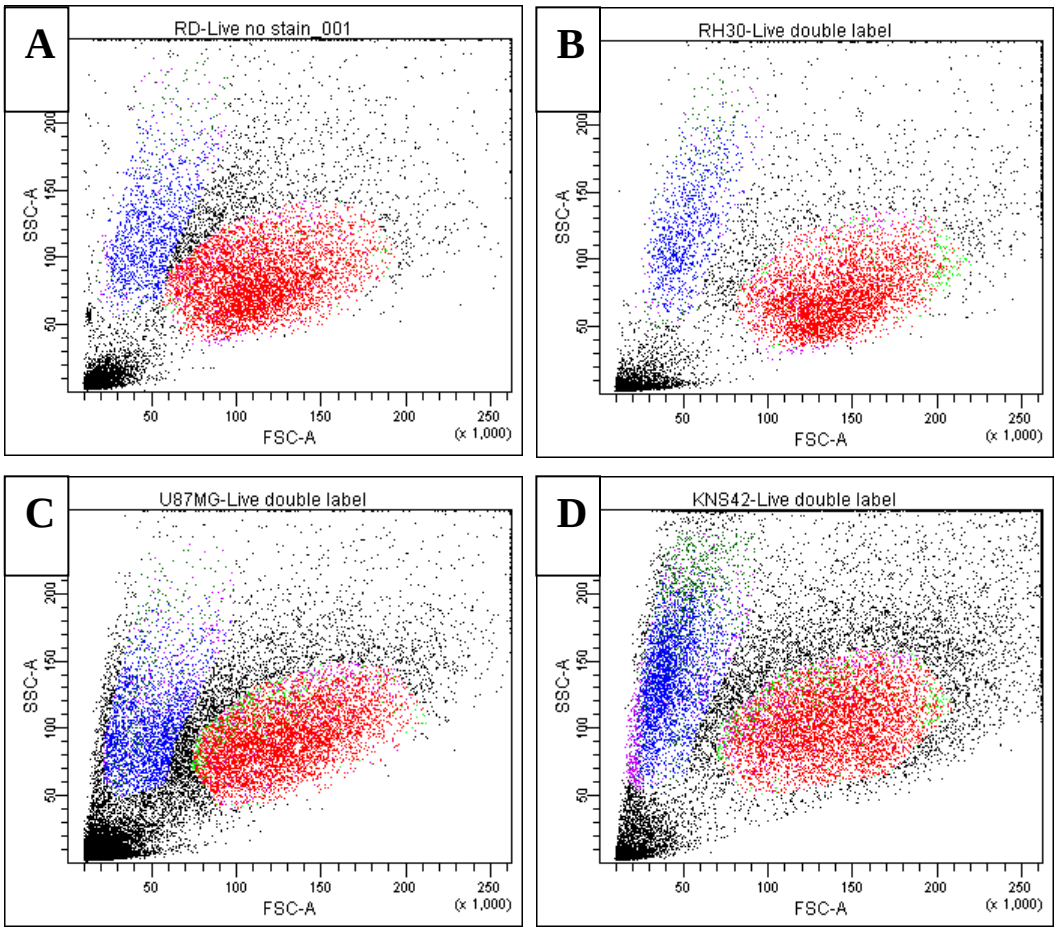

Figure 3.25: RD (A), RH30 (B), U87MG (C) and KNS42 (D) spheroids were easier to dissociate in accutase. The red population is the live population and the dead population is shown in blue.

As accutase was identified as the mildest means of dissociating the spheroids producing the lowest levels of isolation induced cell death this approach was used to assess the effect of DCA on spheroid viability. Figure 3.26C shows that 5&10mM DCA caused a reduction in the number of viable cells in P1 for the RH30 spheroids. U87MG and KNS42 spheroids also experience a decrease in the viable cell population when treated with DCA (Figure 3.27).

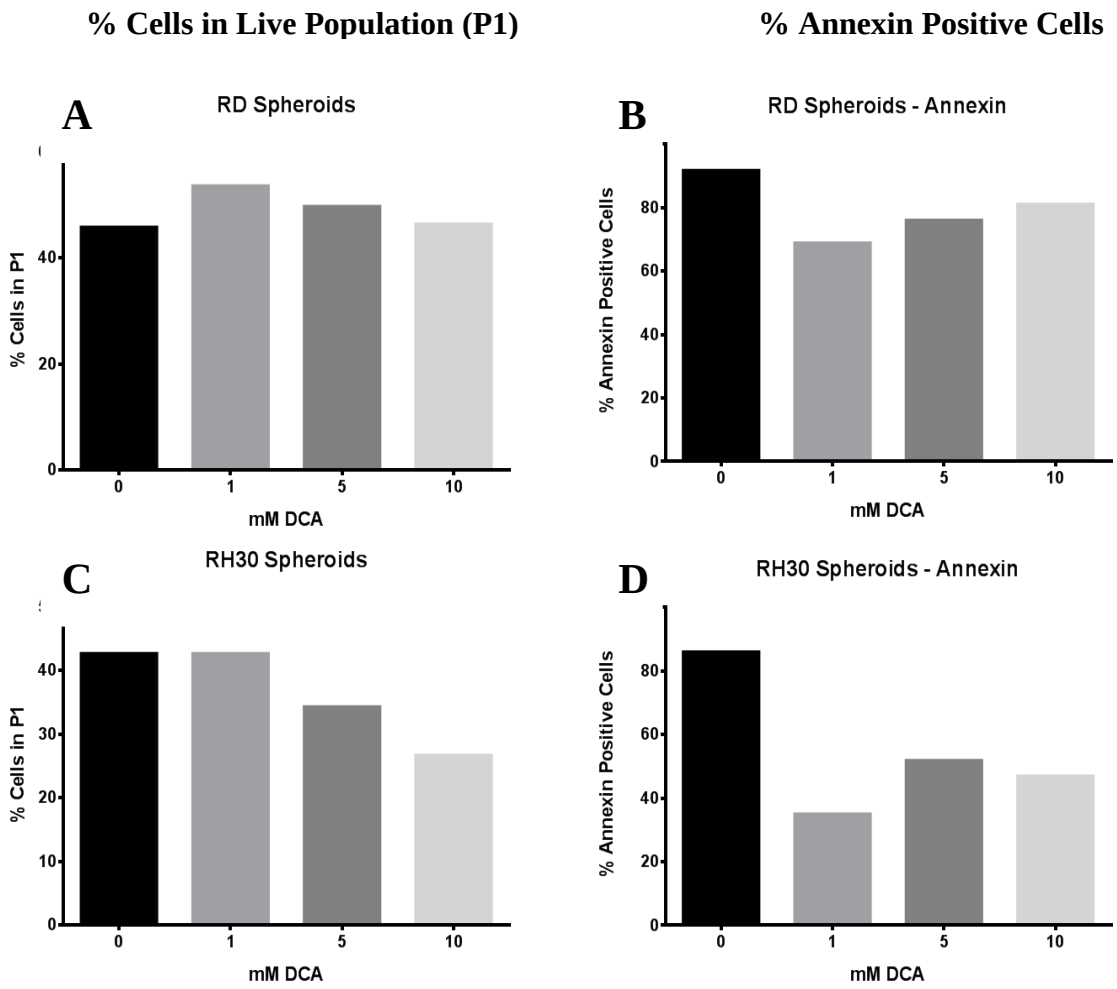

Figure 3.26: DCA appears to decrease cell viability (percentage cells in P1) in RH30 spheroids (C). Annexin positive cells are also decreased in both RD and RH30 spheroids (B&D). N = 1

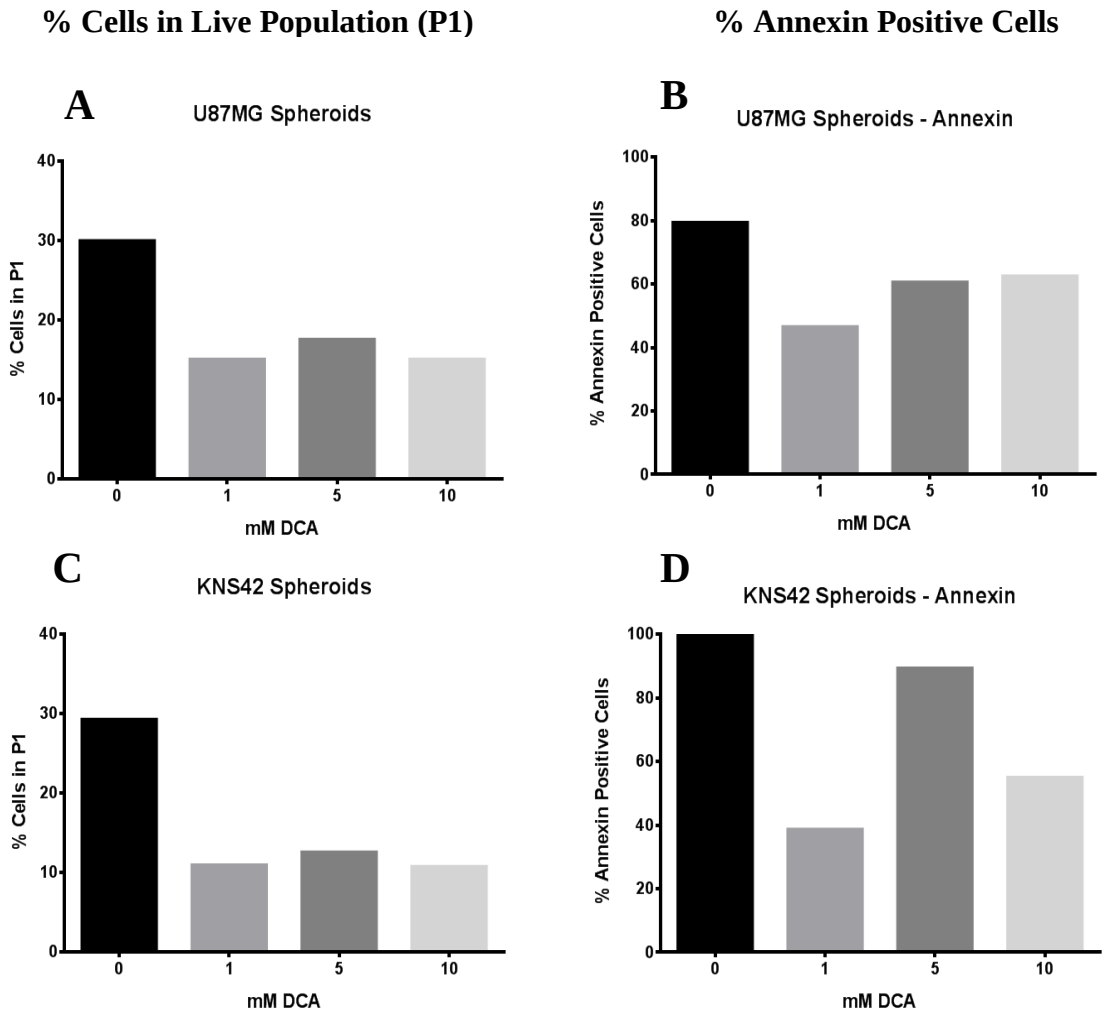

Figure 3.27: DCA appears to decrease cell viability in U87MG and KNS42 spheroids (A&C). It also decreases annexin V staining (B&D). N = 1

There was some concern over the annexin V staining in these experiments. The staining ranged from 80-96% in the untreated spheroids, implying that most of the cells were undergoing apoptosis. DCA consistently reduced the percentage staining in all spheroids examined (i.e. reducing apoptosis). Such high annexin binding (apoptosis) indicates the cells are not happy in the spheroid to begin with, which could make them unsuitable for assessing drug effects.

3.4.8.3 Annexin staining is high in cancer cells due to over expression of PS on the cell surface

To investigate the annexin staining further RD, RH30, U87MG and control fibroblasts (non-cancer control) were cultured in 2D and stained for annexin V and analysed by flow cytometry. Annexin staining was high in all the cancer cell lines and very low in the control non-cancerous line (Figure 3.28).

Recent studies indicate that the PS expression on the outside of the cell membrane is increased in cancer cells (Riedl et al., 2011). PS is cell surface marker which binds annexin V binds which potentially explains the high level of annexin V staining in the cancer cell lines (both in 2D and spheroids) and the low staining in the control fibroblasts.

In this study annexin V was selected as a parameter to determine if DCA treatment increased apoptosis in cancer cells via its up regulation of mitochondrial respiration. Therefore, it was initially puzzling that DCA consistently decreased the percentage annexin staining in spheroid models. However, in light of the finding that cancer cells have high PS while non-cancerous cells have low PS it further supports the idea that DCA is having an impact on cells cultured in 3D as it reduces the levels of PS expressed and is reverting the cells to a more primary cell "phenotype".

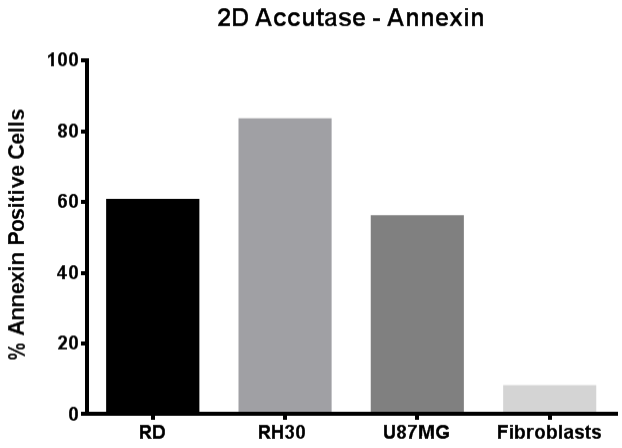

Figure 3.28: Annexin V staining is high in RD, RH30 and U87MG cancer cells due to increased levels of PS but is low in non-cancerous fibroblast cells. Level of annexin staining in fibroblasts is 7-10 fold less than in the cancer cell lines. N = 1

While dissociating the spheroids and assessing their viable/dead/apoptotic profiles has hinted at DCA efficacy it is a not a particularly high throughput means of acquiring information. It is time consuming and requires an excessive number of controls and would not be suitable as a high through put drug screening protocol. In this section, I assessed if microvesicle shedding from spheroids as a marker of cellular stress could offer a higher throughput means of assessing a spheroid drug response.

3.4.9 Microvesicle Analysis

The study of microvesicles and nanovesicles (exosomes) is a growing research area with numerous studies citing micro and nanovesicles as potential cancer biomarkers. Microvesicle and exosome secretion is an important means of cell-cell communication. Tumours cells secrete large quantities of vesicles that carry mRNA, miRNA and various proteins that are transferred to other cells where they can

influence cell signalling. It has been reported that during hypoxia when glycolysis is increased there is an upsurge in the secretion of vesicles (Martins et al., 2013). We therefore reasoned that monitoring vesicle shedding may be a useful means of assessing the response of spheroids to drug treatment.

Whilst definitions in this emerging field currently lack formality, these two classes of biological nanoparticle are distinguished by both their size ranges and their means of production. Typically, microvesicles are described as being 100 nm to 1μm, whilst exosomes are in the range 30-100 nm (Gyorgy et al., 2011). Microvesicles are typically formed by blebbing of the plasma membrane, whereas exosomes are released by exocytosis from multivesicular bodies of the endosome. Both appear involved in cell signalling, carrying a range of signalling proteins as well as messenger and microRNAs (Simak et al., 2006). Vesicles are also involved in cell to cell communication possibly by transferring functional molecules to the target cell. Circulating levels are found to be elevated in various disorders, including atherosclerosis and coronary artery disease, haematological and inflammatory diseases, diabetes and cancer (Mostefai et al., 2008).

Tumour cells are known to shed large quantities of microvesicles that can contain an "oncogenic cargo" and are sometimes referred to as oncosomes. These oncosomes can travel to other cells within the tumour or they can affect non-cancerous stromal and epithelial cells. It is thought that drug resistance, angiogenesis and metastasis can be affected by microvesicles (Camussi et al., 2011). Glioblastomas in particular shed large quantities of microvesicles into the circulation of patients. Recent reports show that microvesicles shed by GBM can be used to determine the mutations present in

the primary tumour (as vesicles are essentially "miniaturised" versions of the cell of origin) and also monitor the response to treatment (Shao et al., 2012). Ezrin et al have also studied GBM exosomes by loading tumours with fluorophores and monitoring the presence of these fluorophores incorporated into vesicles shed into the blood stream. This is the first study that demonstrates the delivery of a small molecule to a tumour that was absorbed, incorporated into vesicles and shed into the circulation in what has been termed a "liquid biopsy" (Carr & Wright 2013).

Based on this we hypothesised that microvesicle analysis might be an appropriate means of assessing the response of spheroids to DCA by analysing the levels and types of microvesicles present in the cell culture media. Total microvesicle population was assessed using flow cytometry and NTA (see methods sections 3.3.10 & 3.3.11).

3.4.9.1 Flow cytometry (FACS)

Cellular vesicles can be isolated and measured in cell culture supernatants, blood, urine and saliva (Thery et al., 2006). Flow cytometry is one technique that can detect cellular vesicles in biological fluids. Its advantages include: biological samples can be measured directly (sometimes pre-concentration is required), it is quantitative and simultaneous analysis of multiple antigens is possible. However, it is limited in only being able to detect cellular vesicles above a certain size. FACS is generally used to analyse cells but when analysing smaller vesicles it is associated with a number of technical limitations and standardisation issues (Gelderman and Simak, 2008). The BD LSRII instrument used in these experiments can measure down to 300nm but it

is only detecting a fraction of the total vesicles (Dragovic et al., 2011). Flow needs to be adjusted to analyse microvesicles namely by changing the forward scatter (FSC) and side scatter (SSC) voltages and implementing a strict instrument cleaning regime so as to minimise background contamination and improve signal to noise (S:N) ratio. Calibration beads are required in order to quantify total number of vesicles. The upper size limit of a vesicle is considered to be 1µm. This is the general agreement in the field but there is no solid evidence in the literature and it is possible that vesicles >1µm exist but for the purposes of this experiment a1µm size limit was implemented. Figure 3.29 shows a typical scatter plot from a microvesicle analysis experiment. Flow analysis of spent media from RD, RH30, U87MG and M059K spheroids (Figures 3.30 &3.31) reveal dose dependent differences in the numbers of vesicles measured.

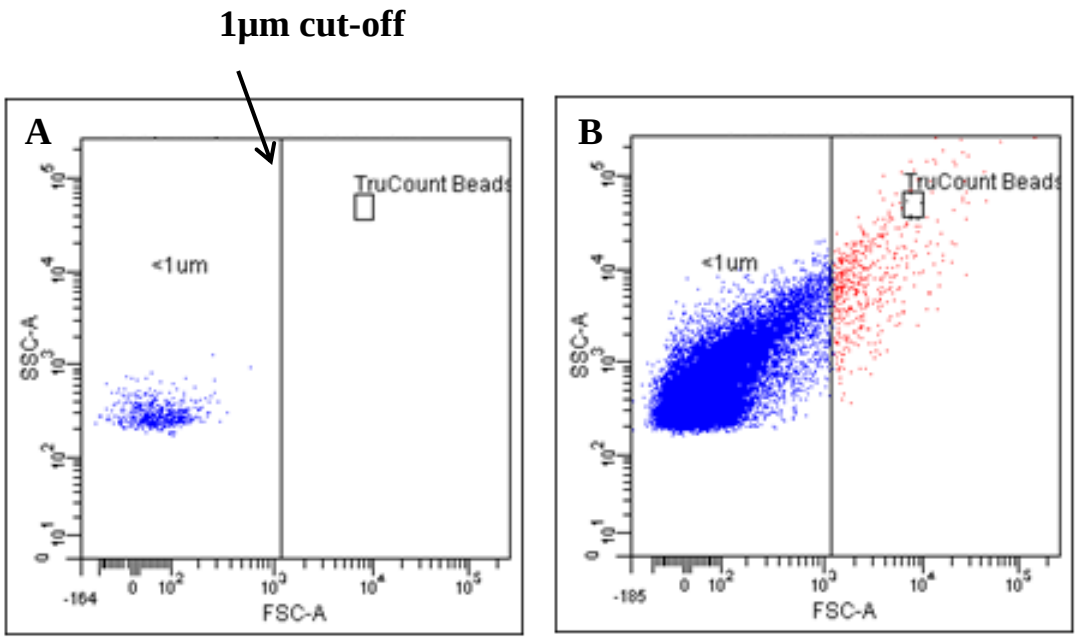

Figure 3.29: Set-up of the gates for microvesicle analysis. (A) is a PBS control showing the level of instrument noise and (B) is a typical sample plot containing microvesicles of varying sizes.

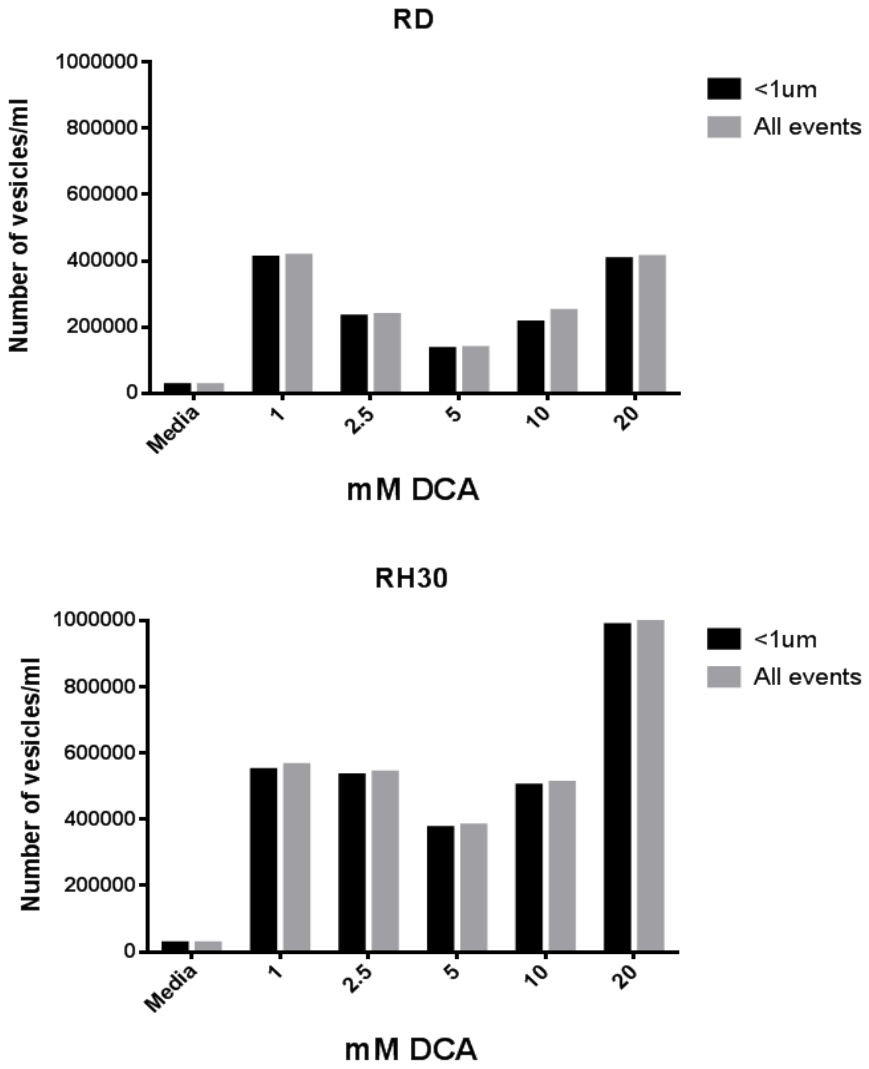

Figure 3.30: Microvesicle analysis of RD and RH30 spheroids treated with DCA and analysed using flow cytometry. Events in the size range 300nm-1000nm are in black and all events including those greater than 1000nm are in grey. DCA appears to cause dose dependent changes in the levels of microvesicles in the media. N = 1

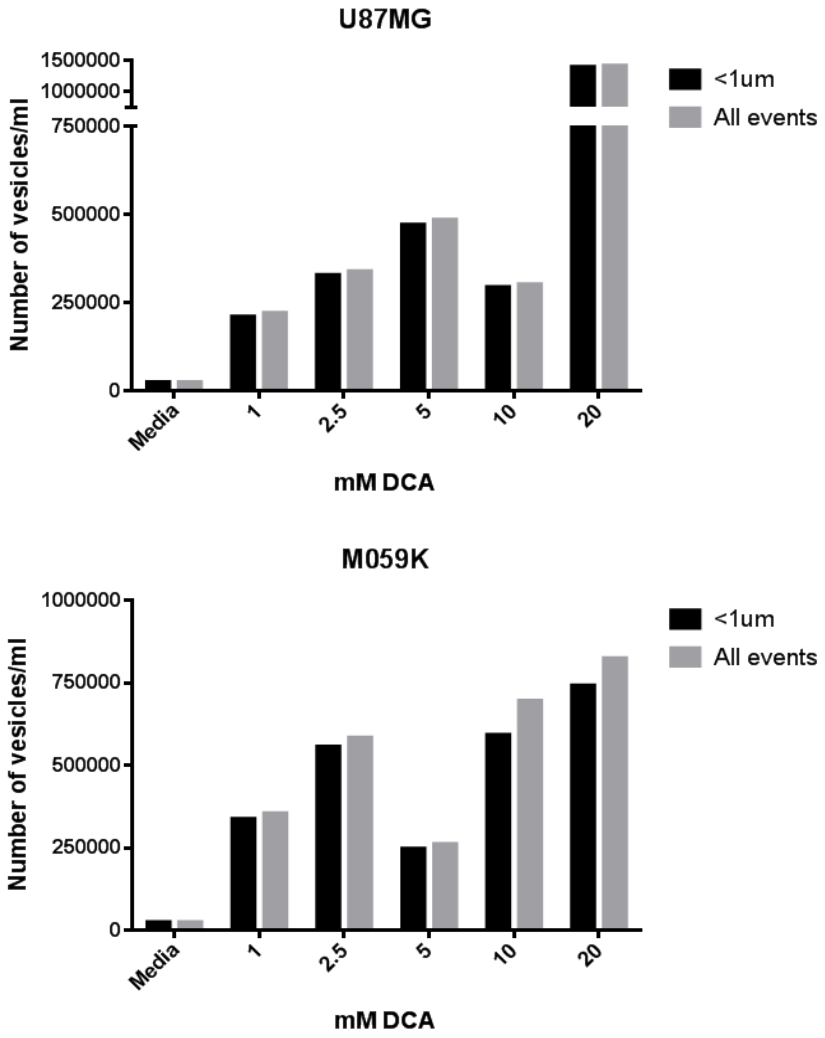

Figure 3.31: Microvesicle analysis of U87MG and M059K spheroids treated with DCA and analysed by flow cytometry. DCA concentration impacts on the number of vesicles excreted into the media. N = 1

3.4.9.2 Nanosight

As mentioned earlier sensitivity of flow, in terms of vesicle size is >290nm, therefore it can only analyse a small portion of vesicles (it completely excludes exosomes). To analyse exosomes a different technique is required. Nanosight (nanoparticle tracking analysis –NTA) is a unique system used for direct, real-time visualisation and analysis of nanoparticles in solution. To date, exosome research has been constrained

by a lack of suitable methods for characterisation but NTA addresses many of these issues.

The media from RD and RH30 DCA treated spheroids was harvested and analysed using NTA NS500 instrument and software. The instrument method was set up to record 5 X 30s recordings for each sample. The software tracks each particle in the suspension and produces a spreadsheet of particle size and concentration. Figure 3.32 shows an NS500 instrument and a typical screenshot of the analysis.

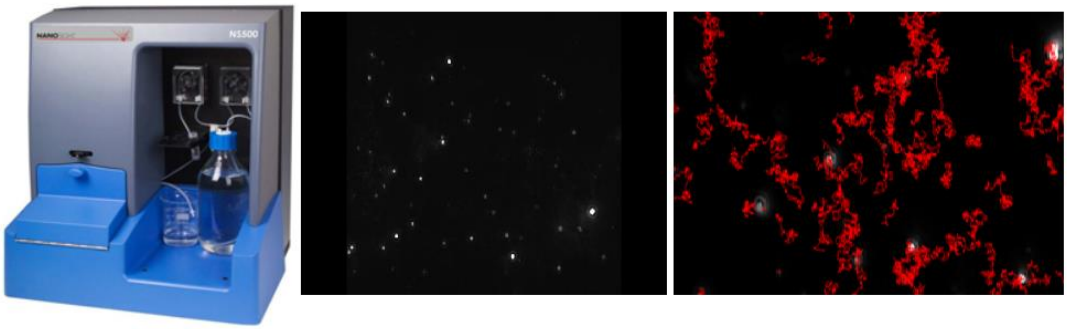

Figure 3.32: The NS500 (left) detects each particle in a fluid suspension (centre) and monitors their Brownian motion for a user defined period of time. The NTA software then tracks each particle (right) and calculates particle concentrations and sizes.

Figure 3.33 depicts the effect of DCA on RD and RH30 vesicles numbers. The media only samples in both graphs had considerable numbers of microvesicles despite having been filtered through a 0.1µm filter. Aside from this high background there is a common pattern between both sets of data. Treatment with 1mM, 2.5mM and 5mM DCA results in an apparent decrease in microvesicle concentration (even to levels below the media only background) relative to the 0mM control. The microvesicle

concentration in the 10mM and 20mM while not apparently higher than the 0mM control are higher than the lower concentrations of the drug.

Future experiments would involve looking at surface markers as well as trying to "clean up" the media probably by ultra-centrifugation of the FBS prior to addition to the media followed by a 0.1µm filtration and possible vesicle concentration step prior to analysis.

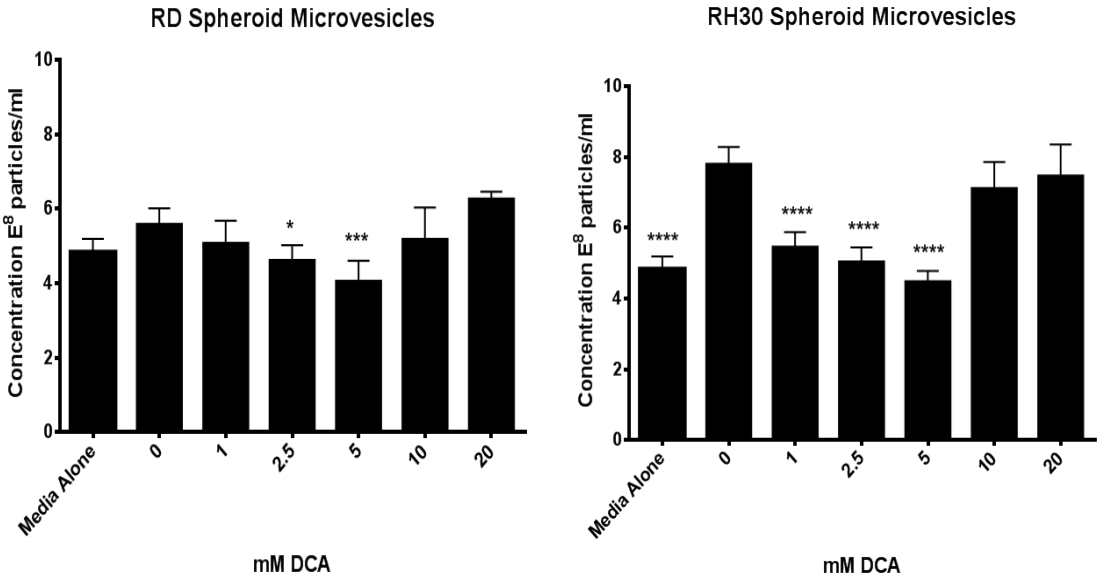

Figure 3.33: Total vesicle concentration in RD and RH30 DCA treated spheroids as analysed by Nanosight. N = 1 (5 separate replicates in the one experiment).

3.4.10 Phenformin

Metformin and phenformin are members of the biguanide family. They were developed in the 1950's and have been used to treat type II diabetes but phenformin was withdrawn in the 1970's due to its side effect of producing lactic acidosis. Metformin is still used today to treat diabetes. Biguanides also have anti-cancer

properties and retrospective studies of patients taking metformin show lower incidences of cancer (Dowling et al., 2012). The exact mechanism of their anticancer potential is still unclear but it is thought to be through complex I inhibition and subsequent AMPK activation (Dykens et al., 2008).

Metformin has been shown to reduce growth in mouse xenograft models (Algire et al., 2011). Metformin has an extensive safety profile which makes it an attractive drug to evaluate and re-purpose for cancer therapy. Phenformin is almost 50 times more potent than metformin (Dykens et al., 2008) and is capable of delaying tumours growth more than metformin.

Researchers in the Whitehead Institute in the US have been studying cell lines with mitochondrial defects and cells that are unable to utilise glucose efficiently in order to better predict the cellular response to biguanides. Birsoy et al developed a system called Nutristat to circulate low glucose media (0.75mM) around cells. They evaluated 30 cell lines of various origins (lung, pancreas, lymphoma, and thyroid). Initially they monitored the growth of these cells in their nutristat system and found that most were unaffected, some thrived while others suffered. They questioned if it is possible to exploit the cells that struggle under reduced glucose conditions which might better reflect the situation in vivo. The cancer cells that suffered under reduced glucose conditions were found to contain defects in the genes for Oxphos and glucose transport. By impairing mitochondrial function with phenformin, they found that these cancer cell lines were 5-20 fold more susceptible to the drug than the control cancer cell lines (Birsoy et al., 2014).

Similarly we hypothesised that phenformin might work well as a combination anti-cancer therapy with DCA or could be effective on its own. If glucose levels were low in tumour cells the cells would potentially rely more heavily on mitochondrial respiration as demonstrated in Chapter 2. Unfortunately, due to time constraints, we did not investigate the DCA /phenformin combination in this study. However, phenformin was evaluated as a single agent. This data is shown in the supplemental section (Figure 7.2 - Figure 7.9). In summary phenformin increased cell death in all cell lines when experiments were carried out in media containing 5mM glucose in a dose dependent manner. Interestingly, phenformin cytotoxicity was not confined to the Oxphos cell lines, the glycolytic cell lines were also susceptible to its effects. Phenformin shows promise as a single anti-cancer agent and it will be interesting in the future to explore potential synergy with DCA in different models (2D, 3D spheroid, 3D scaffold). Toxicity to normal cells and tissues needs to be considered with drugs such as DCA and phenformin which can cause toxicity with long term use.

3.5 Discussion

The last two decades have seen an explosion of interest in the area of tumour metabolism. Otto Warburg was the first to take note of the altered metabolism exhibited by tumour cells. The evident differences in how tumours metabolise substrates has initiated an interest in investigating selective therapeutic targets (Pan and Mak, 2007). One possible mechanism for the glycolytic phenotype exhibited by cancer cells is the regulation of Oxphos by hif1α transcription via pyruvate dehydrogenase kinase (PDK) activation. PDK is a target of Hif1α and under hypoxia when Hif is transcribed it induces PDK (in particular PDK1). PDK phosphorylates PDH and inactivates it leading to a blockade in the flux of pyruvate into the mitochondria and through the TCA cycle (Papandreou et al., 2006).

Dichloroacetate (DCA) is a drug that may be beneficial to treat cancer by targeting PDK. DCA's ability to inactivate PDK and increase PDH activity was first identified in 1973 using a rat heart model (Whitehouse and Randle, 1973). Since then DCA has been used to treat lactic acidosis in patients with mitochondrial disease. However, its most important application could be as an anti-cancer agent as many cancer cells have increased PDK expression coupled with increased rates of glycolysis and decreased mitochondrial function (Papandreou et al., 2011).

In 2007 Bonnet et al demonstrated DCA to have selective cytotoxic effects on an A549 cancer cells in a rat xenograft model (Bonnet et al., 2007). Numerous studies have now been published showing DCA to have varying degrees of efficacy with the

emerging pattern that DCA has better anti-cancer efficacy in-vivo compared to in-vitro models.

When starting this research there were certain expectations of what effect DCA would have on the cell lines investigated. One expectation was that DCA would be cytotoxic to the cells with a glycolytic profile. This was not observed as DCA treatment of the glycolytic cell lines RH30, U87MG, M059K and Res259 did not induce cytotoxicity or reduce proliferation rates in 2D in-vitro culture. In fact in the RH30, U87MG and M059K cells cultured in 2D we saw an increase in cell number on 10mM DCA. The very aerobic paediatric GBM lines SF188 and KNS42 lines were the only lines to exhibit a dose dependent decrease in cell number. The SF188 line only exhibited this decrease after a 24 hour treatment. No effect on cell number was observed at 48 or 72 hours for this line. The pitfall of the experimental design was that the DCA was added as a single treatment at T = 0 hours. After 24 hours, a decrease in cell number was apparent but after 48 and 72 hours, the cells on all doses of DCA were comparable. A possible reason for this is that DCA has been detoxified by the cells. The first step of DCA metabolism is the removal of the two chlorine groups by the cytochrome P450 system (Stacpoole, 1989). CYP1, 2 and 3 families are key player in drug and xenobiotic metabolism. Glial cells have been shown to have significant levels of CYP 1A1, 2B2 and 2E1, a possible safety mechanism to prevent neurotoxicity (Tripathi et al., 2013). Perhaps after 24 hours the drug has been metabolised and the cells have recovered.

DCA did appear to improve mitochondrial respiration with significant increases in oxygen consumption rates in the glycolytic RH30 and U87MG cells there was just no cytotoxicity associated with their release from their glycolytic state.

A lack of in-vitro efficacy is likely due to the un-physiological nature of 2D cell culture. Pre-clinical animal models assessing DCA have been more promising in lung cancer (Bonnet et al., 2007), pancreatic cancer (Chen et al., 2009), metastatic breast cancer (Sun et al., 2010) and colorectal cancer (Cairns et al., 2007). With this in mind, we wanted to assess DCA efficacy in a more physiologically relevant in-vitro model using 3D spheroids. High doses of DCA decreased the growth rates of RH30, U87MG and M059K spheroids but had no effect on the growth rates of the other spheroid types. However, as we demonstrated spheroid size does not necessarily relate to spheroid health. After investigating several means of dissociating the spheroids it was found that DCA decreased viability in RH30, U87MG and KNS42 spheroids (despite having no impact on spheroid size in this line). All spheroids treated with DCA experienced a reduction in the annexin V binding suggestive of a return to a more normal phenotype.

There is quite a lot of conflicting data in the literature regarding the potential of DCA as a chemotherapeutic agent. A study by Niewisch et al in 2012 treating paediatric brain tumour lines with DCA did not publish promising results. In the Niewisch et al study paediatric neuroblastoma cell viability decreased to 90% in two lines but only to 98% in the third when treated with 2mM DCA for 48hours. There was a small decrease in lactate production with DCA treatment but insignificant changes in oxygen consumption rates (Niewisch et al., 2012). The researchers therefore

dismissed DCA as a potential therapy for paediatric neuroblastoma. In another study, Vella et al reported that undifferentiated paediatric neuroblastoma cells are sensitive to DCA but only in the 5-50mM range (Vella et al., 2012). In the literature DCA has shown promise in-vitro in lung cancer (Bonnet et al., 2007) where it induced apoptosis, prostate cancer (Cao et al., 2008) where it inhibited growth, endometrial cancer (Wong et al., 2008) where it also induced apoptosis. Concentrations of DCA tested vary considerably, some studies use clinically relevant doses (0.5-1mM) while others use supra-pharmacological doses (10-100mM) (Papandreou et al., 2011). Other studies have shown no cytotoxic effect in-vitro (Cairns et al., 2009; Heshe et al., 2011; Stockwin et al., 2010; Sun et al., 2011; Sun et al., 2010).

CHAPTER 4

Measuring intracellular oxygen concentrations as a means of assessing cellular response to drugs that affect energy metabolism

4.0 Measuring intracellular oxygen concentrations

4.1 Introduction

Approximately 90% of the oxygen we consume contributes to the process of oxidative phosphorylation. This proportion of oxygen is required for the efficient oxidative metabolism of fuels like glucose and fatty acids. These substrates are metabolised into carbon dioxide, water and the high energy substrate ATP. The remaining 10% of the oxygen is used for enzymatic reactions e.g. oxidation and hydroxylation. A residual proportion of oxygen contributes to the production of reactive oxygen species (ROS) (Baynes J,W. 2009). So oxygen has an important role to play in mammalian cells for their normal functioning by providing ATP for energy, assisting in enzymatic reaction and generating ROS which is important for metabolism also (Dmitriev and Papkovsky, 2012; Dmitriev et al., 2012).There are many physiological and indeed pathophysiological requirements for oxygen especially in cancer and the adaptive response to hypoxia. Cells and tissues are exposed to different levels of oxygen. Most tissues have a partial pressure of oxygen (PO2) of 20-40mmHg but a large tumour can be severely hypoxic or anoxic with PO2 levels <0.1mmHg (Aragones et al., 2009; Semenza, 2007).

Hypoxia is present in most solid tumours with up 60% exposed to <1% oxygen (Vaupel and Mayer, 2007). Hypoxia and Hif are important in the metabolic reprogramming of cancer cells so measuring hypoxia and oxygen is essential. When it comes to measuring oxygen or assessing hypoxia it can be challenging as oxygen levels are not fixed and constant. Current methods of detecting hypoxia include:

1. Measuring oxygen with a polarographic needle electrode (Vaupel et al., 2007)
2. Performing immunohistochemistry (IHC) on biopsies to assess Hif1a and its targets (GLUT1, CAIX, and VEGF). These markers are not ideal as they can also be affected by other factors not related to hypoxia (Vaupel and Mayer, 2007)
3. Pimonidazole binds to thiol containing proteins in hypoxic cells and can be detected in biopsies by antibodies (Varia et al., 1998)
4. More recent advances in the study of hypoxia involve the use of F-18 fluoromisonidazole (FMISO) coupled with PET (Hendrickson et al., 2011)

The main limitation with the above techniques is that they do not allow the direct measurement of changes in tumour oxygenation. Cells vary in their energy needs and depending on their location within the body can be exposed to varying oxygen tensions. Epithelial cells lining the bronchi are exposed to atmospheric oxygen levels while chondrocytes are exposed to low oxygen (Chi et al., 2006).

Oxygen levels fluctuate so it is of great importance to develop and utilise tools that monitor the more subtle and transient changes in oxygen concentrations. Determining and monitoring the oxygen tension within different mammalian cell models as well as culture conditions is of great importance to allow for a deeper understanding of cellular metabolism (Kondrashina et al., 2013). Standard in-vitro cell culture conditions offer an excess of substrates and oxygen which can impact cell metabolism. Hyperoxia (as is often what is used in in-vitro culture conditions) can lead to overproduction of ROS (Zhao et al., 2012).

Oxygen concentrations and consumption rates can be difficult to monitor as there is constant diffusion between the cells and the extracellular environment and between the atmosphere and cell culture media solution (Fercher et al., 2011).Techniques to measure oxygen based on phosphorescence quenching are well established (Papkovsky, 2004) but only as an extracellular means of assessing oxygen levels and consumption rates (Hynes et al., 2009a). However, monitoring this analyte within a cell has remained problematic for years. Previous attempts to quantify intracellular oxygen have included using probes that needed to be microinjected (Schmalzlin et al., 2005), electroporation or have endocytosis induced (O'Riordan et al., 2007). Complex, time consuming and invasive methods have hindered advances in this area.

A recently developed in-vitro tool was used to investigate the level of monolayer oxygenation. MitoXpress®-Intra (Nan02) probe is an easy to use cell-penetrating phosphorescence-based oxygen sensing probe that enables the real-time quantification of oxygen within the cell monolayer using plate reader and microscopy based techniques (Kondrashina et al., 2013).

4.2 Methods

4.2.1 The MitoXpress-Intra probe

The MitoXpress®-Intra (NanO2) probe consists of cationic hydrogel nanoparticles loaded with a PtFPP (Pt(II)-5,10,15,20-tetrakis-(2,3,4,5,6-pentafluorophenyl)-porphyrin) dye (Figure 4.1). The particles are internalised *via* endocytosis (Kondrashina et al., 2013). Molecular oxygen present in the cells is able to quench the emission of the probe. More actively respiring cells will reduce the oxygen concentration resulting in an increase the fluorescence intensity. The MitoXpress-Intra probe is easy to use and does not require any specialised equipment other than a plate reader with TRF capabilities and an atmospheric control unit (ACU) would also be beneficial.

4.2.2 Probe loading

Cells are cultured to 80-90% confluency in a 96 well plate in appropriate culture media. Media is then replaced with 150µl fresh culture media containing 10µg/ml of probe. Once the probe is internalised it remains in the cells and does not leak back out of the cells over time. However, upon cell division it will become less concentrated. Maximum probe uptake generally occurs in 6-16 hours. The small particle size (<100nm) allows high penetration with minimum damage/toxicity to the cells (Fercher et al., 2011).

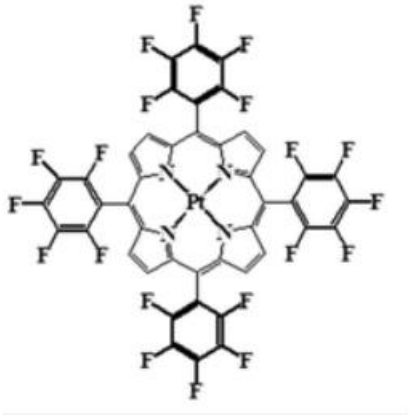

Figure 4.1: PtFPP structure.

4.2.3 Theory of the measurement and probe response

The MitoXpress®-Intra probe is measured using the same experimental set up as the MitoXpress-Xtra (discussed in chapter 2) consisting of dual delay time resolved measurements (Ex 340 - 400nm/Em640 - 660nm) on a BMG Omega plate reader with an atmospheric control unit (ACU). The delay times are 30 and 70μs and the principle for calculating the lifetime is depicted in Figure 4.2. The raw data produced is a graph of time (x-axis) versus TR-F intensity (y-axis).

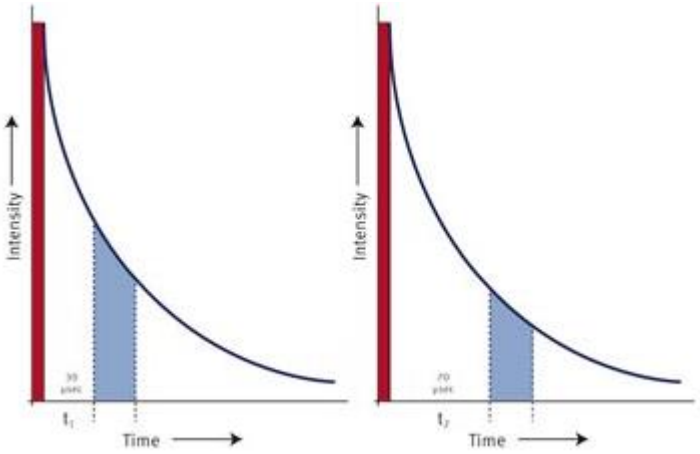

Figure 4.2: Principle for calculating the phosphorescence lifetime from ratiometric time-resolved phosphorescence intensity.

To reduce assay noise and allow the calculation of intracellular oxygen concentrations TR-F intensity signals need to be converted into phosphorescence lifetime values. Lifetime values are an important means of normalising the data from these probes as it minimises and often eliminates variables like concentration of fluorophore added or variations in the intensity of excitation. Lifetime values are calculated using the following equation: lifetime = t2-t1/ Ln (D2/D1) [t=delay time, D=measured intensity value]. Once the lifetime curves have been calculated it is possible to determine the intra-cellular oxygen levels at a particular time point using a calibration curve produced by varying the oxygen levels in the cells using the ACU unit on the BMG instrument. A stepwise reduction of oxygen concentration is performed allowing sufficient time for oxygen levels at the cell monolayer to equilibrate. Non–respiring cells are used to produce the calibration curve, which is achieved by inhibiting mitochondrial respiration with antimycin-A or rotenone. This is discussed in more detail later.

As assays with MitoXpress ®-Intra are unsealed, equilibrium is reached between oxygen consumption by the cells and back diffusion into the well from the environment. Cells will reach a “resting state “characterised by a flat signal. When cells are stimulated to consume more oxygen or inhibited from using their mitochondria a change in fluorescent signal will be observed Figure 4.3. Reduced ETC activity results in a decrease in probe signal (i.e. high cellular O_2) as a result of reduced oxygen consumption by the cells. Conversely, an increase in probe signal will be seen where there is a reduction in cellular oxygen because of stimulated respiration (i.e. increased ETC activity).

This theory of probe response was assessed using RD cells that were treated with FCCP. The initial signal represents the steady state oxygen level. Uncoupling with FCCP increases the oxygen consumption causing a reduction in the oxygen levels inside the cell (Figure 4.4).

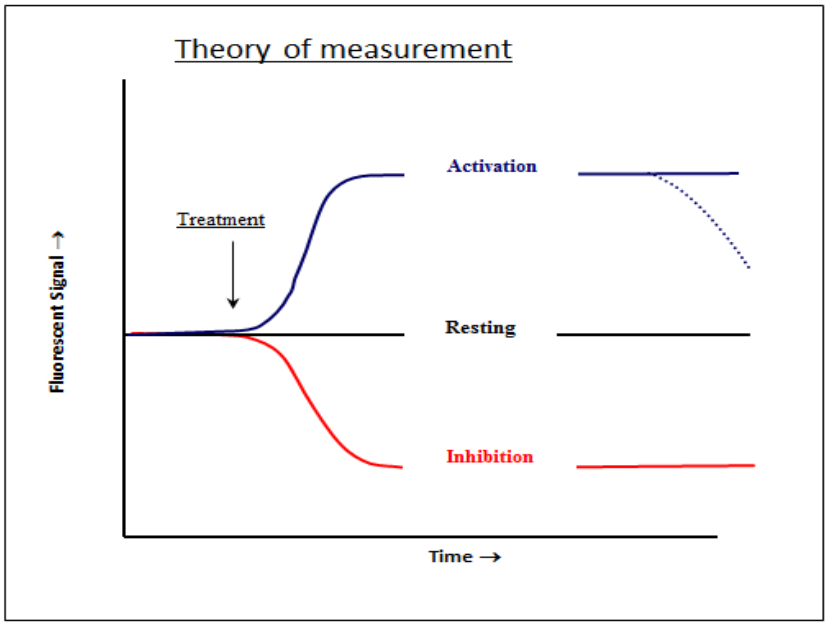

Figure 4.3: The theory behind the drug response observed with the MitoXpress-Intra probe. Diagram taken from Luxcel bioscience website

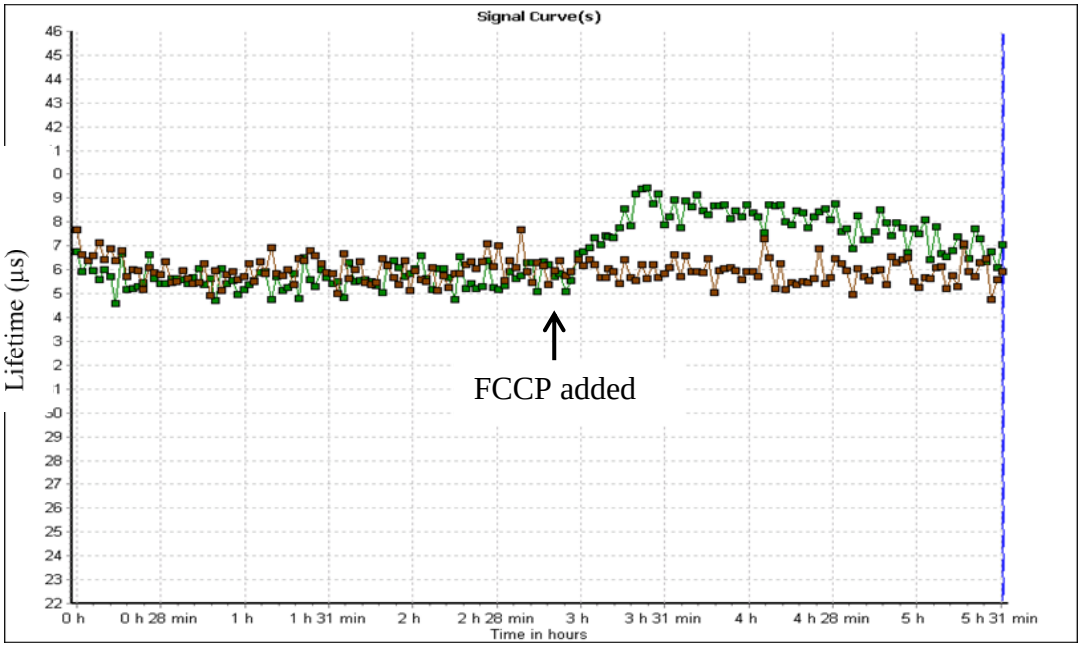

Figure 4.4: Lifetime signal of RD cells treated with FCCP (green) or untreated (brown). Increase in signal represents an increase in oxygen consumption due to uncoupling thus highlighting the theory behind the measurement.

4.3 Results

4.3.1 Probe calibration: Converting lifetime values into percentage oxygen levels

To determine intracellular oxygen levels a calibration curve was constructed which allows the conversion of measured lifetime values into the percentage oxygen. To convert life time values to intracellular oxygen levels cells loaded with MitoXpress-Intra probe were treated with either 1µM rotenone or 4µM antimycin-A. These compounds inhibit cellular respiration increasing the intracellular oxygen levels for most cell lines to environmental oxygen levels.

The BMG plate reader has an atmospheric control unit (ACU) that allows the user to control the temperature, oxygen and carbon dioxide levels in the plate chamber. CO_2 was set to 5% and the temperature was 37^0C. When the assay was started the oxygen level was set to 18% (this is the upper limit of the instrument) and allowed to run until the fluorescence equilibrated to a flat line. Once this equilibrium was reached the oxygen levels were dropped to 8% and again left until equilibrium was established. Oxygen was reduced in this stepwise manner until the 1% equilibrated state was reached (Figure 4.5). At this point glucose oxidase injected into the wells chemically de-oxygenates them by yielding the following reaction:

$$\textit{D-glucose} + H_2O + O_2 \xrightarrow{\textit{Glucose Oxidase}} \textit{D-gluconic acid} + H_2O_2$$

As oxygen in the reader is reduced, there is an increase in probe fluorescence. The fluorescence is allowed to reach a steady state before the oxygen is reduced again.

Figure 4.5 shows the time it takes for the non-respiring monolayer to equilibrate to the new O_2 concentration.

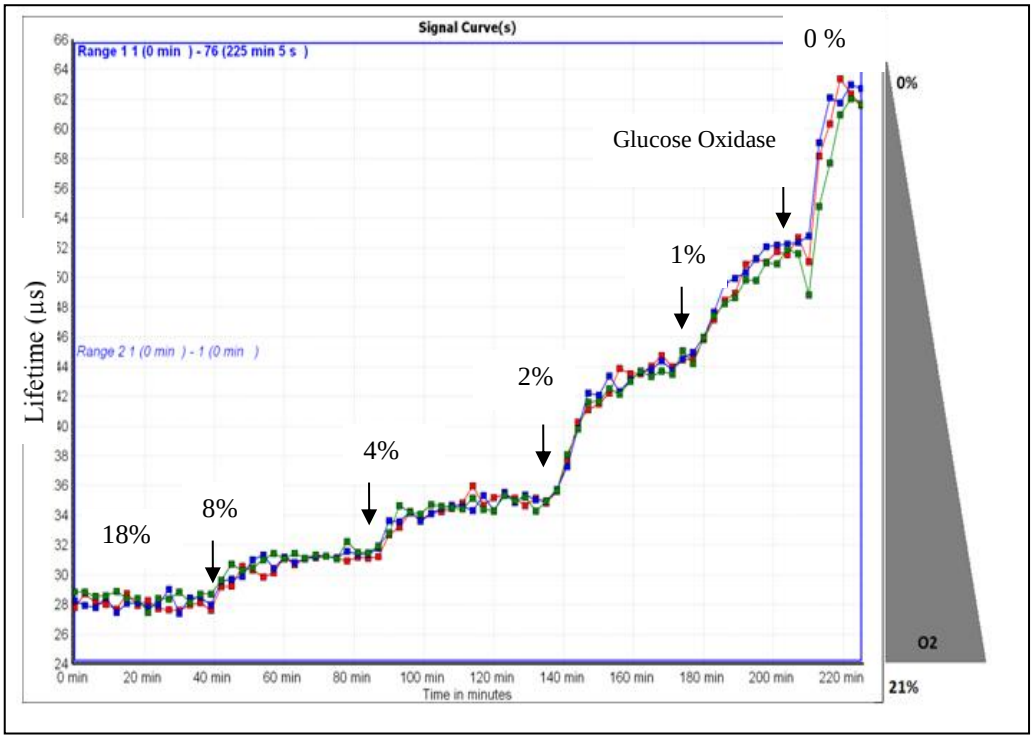

Figure 4.5: Kinetic trace of the intracellular probe showing the response of a non-respiring cell monolayer (antimycin A treated) to decreasing atmospheric oxygen concentrations. Starting atmospheric oxygen concentration was 18%, once the signal had equilibrated the oxygen was dropped to 8%, 4%, 2%, 1%. Complete de-oxygenation was achieved by the addition of glucose oxidase.

Once the kinetic trace had been generated 6 lifetime values from each oxygen concentration were averaged and plotted against their corresponding percentage oxygen to create the curve depicted in Figure 4.6. This curve allows oxygen concentration within the cell monolayer to be determined in future experiments by inputting the lifetime value into the equation of the line and solving for X (% O_2). $Y = a + \exp^{(bx + c)}$ where y is measured lifetime value, a = 30.02, b = -0.20, c = 3.55. This formula was kindly calculated by Dr. Iain Johnston, Imperial College. The

calibration curve need only be generated once and can be used to determine the oxygen concentration for that cell line for all subsequent assays. In practice, the calibration curve works for all cell lines as long as the inhibition of respiration by the respiratory chain inhibitors is almost complete.

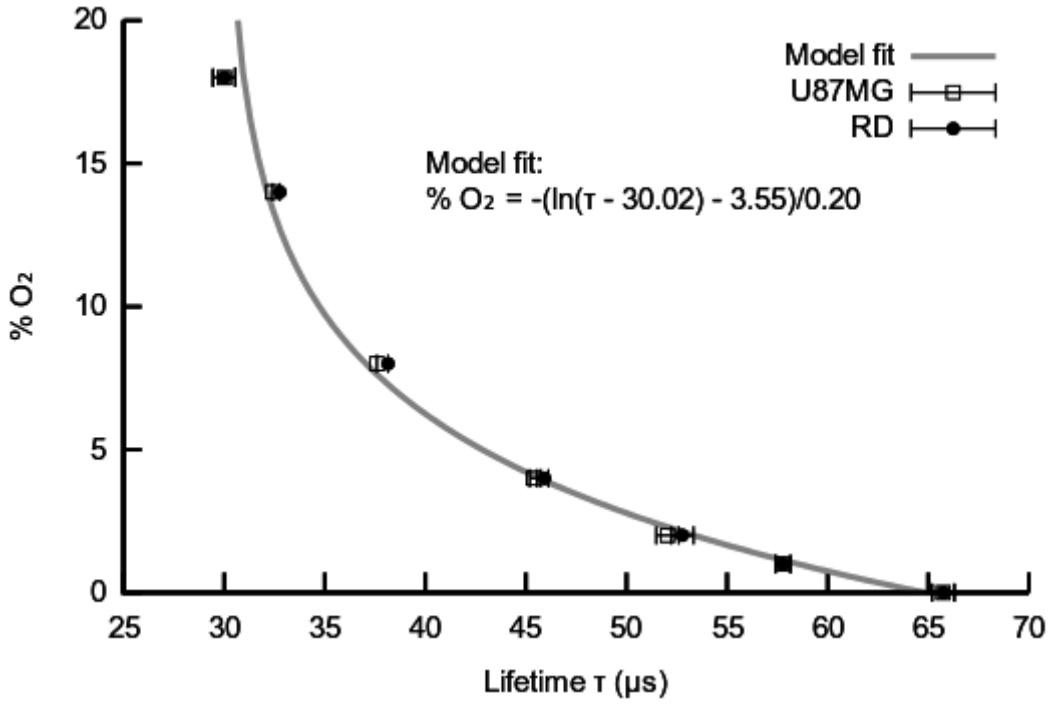

Figure 4.6: Calibration curve for the intracellular probe plotting lifetime values against percentage ambient oxygen. Values represent the mean and standard deviation of six replicates.

The importance of using antimycin-A to calibrate the curve is outlined in Figure 4.7. Here were see the response of an active aerobic line, HepG2 (and an aerobically suppressed line, U87MG, to antimycin-A, high glucose (20mM) and glucose free (0mM) media. The purple lines are the antimycin-A treated cells and the signal seen is solely due to probe response to ambient oxygen changes. In the HepG2 cells that are very oxidative the high glucose (blue line) cells show significant increases in lifetime values for any given percentage of atmospheric oxygen. Increased lifetime

equates to decreased oxygen. The difference between the purple lines and blue lines are the contribution of cellular respiration to probe response. In the glycolytic U87MG cells the difference between antimycin-A and glucose is negligible.

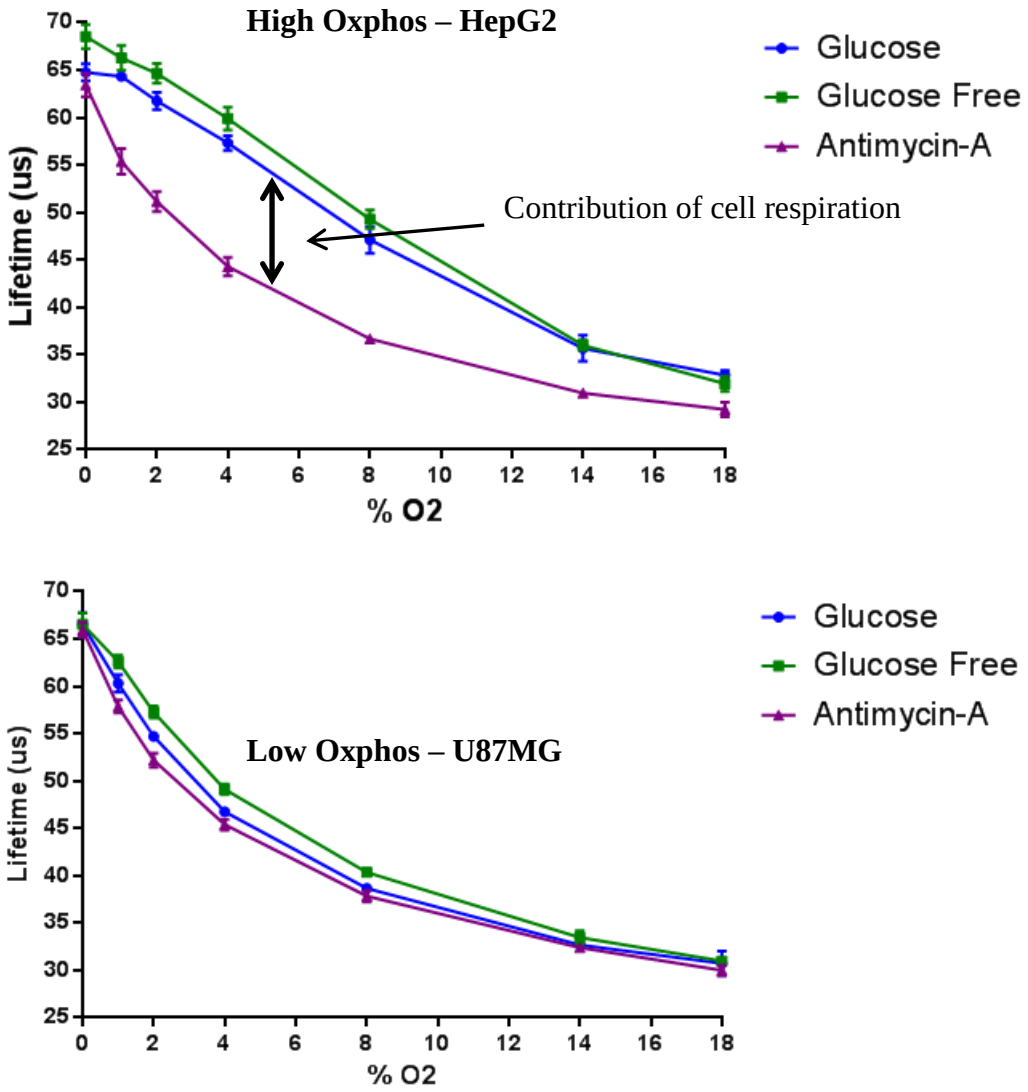

Figure 4.7: Differences between applied oxygen concentration and intracellular oxygenation in HepG2 cells (top) and U87MG cells (bottom). HepG2 cells are extremely aerobic and this is represented by the blue line. At any given applied oxygen concentration there is a significant difference in the lifetime values between the antimycin-A treated cells on the cells on glucose indicating lower than expected intracellular oxygen concentrations. The U87MG cells do not display depleted intracellular oxygen thus reinforcing the theory that they are glycolytic.

4.3.2 Level of intracellular oxygenation is significantly decreased in aerobic cells

This new tool was employed to examine the metabolism of two established cancer cell lines, RD (rhabdomyosarcoma) and U87MG (glioblastoma multiforme) under different applied oxygen concentrations and the results presented highlight some interesting findings. RD cells cultured on high glucose (20mM) do not rely solely on glycolysis for ATP production as was demonstrated in chapter 2. RD cells displayed high rates of oxygen consumption on high glucose media consistent with a cell with an aerobic phenotype. Interestingly when the intracellular oxygen levels were assessed a deeper than expected de-oxygenation was seen at all ambient concentrations evaluated (Figure 4.8, Table 4.1). When ambient oxygen is set to 18% oxygen one might assume that the cells are at 18% as it's been reported that the rate of oxygen diffusion into the cells is faster than the oxygen consumption rate (Papandreou et al., 2011). However, we see that the aerobic cells are consuming and depleting the intracellular oxygen while the glycolytic cells are not. The aerobically proficient RD cells, at ambient oxygen concentrations of 18, 10 and 5%, have intracellular levels of 13.67, 6.15 and 2.5% respectively (Figure 4.8, Table 4.1). In contrast to this are the glycolytic U87MG cells that displayed oxygen levels of 17.9, 9.65 and 4.6% (Table 4.1). When the ambient oxygen levels were 2%, the aerobic RD cells had negligible oxygen levels inside the cells (data not shown).

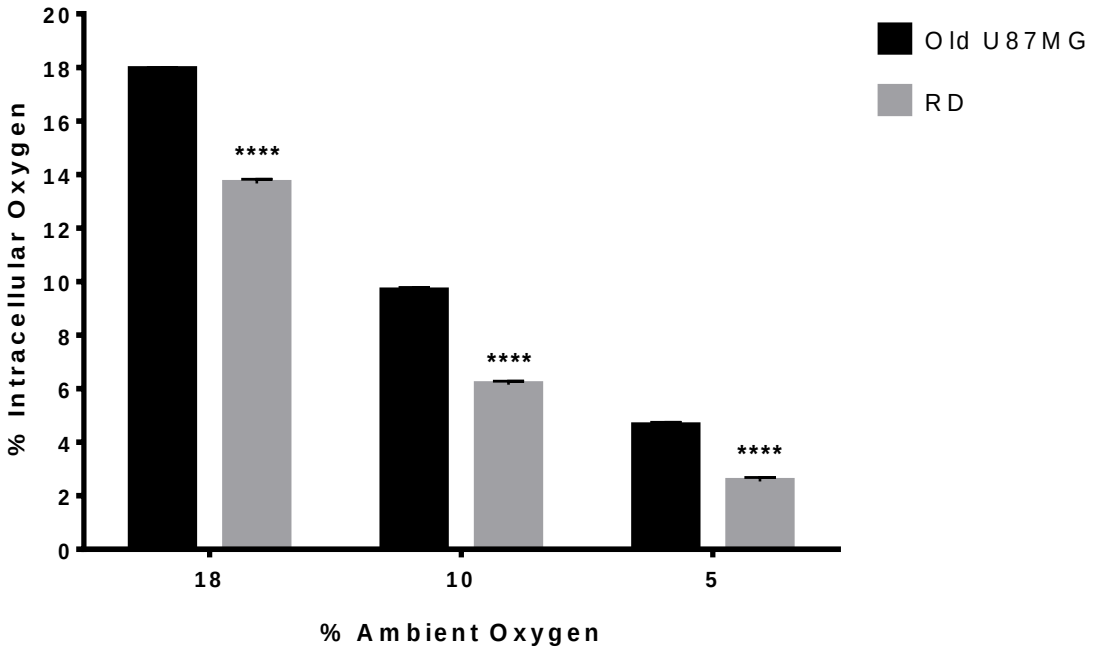

Figure 4.8: At 18% ambient oxygen RD cells were found to contain intracellular oxygen levels of 13.67% ± 0.15, thus suggesting that they are metabolically proficient cells. This gap in the level of oxygenation widens when ambient oxygen levels are dropped to more physiological levels. In contrast, U87MG cells, known for their glycolytic phenotype, had intracellular oxygen levels of 17.92% ± 0.08 at 18% ambient oxygen. Cells were cultured in high glucose (20mM).

Ambient Oxygen	18%	10%	5%
Old U87MG	17.92 ± 0.08	9.65 ± 0.13	4.6 ± 0.12
RD	13.67 ± 0.15	6.15 ± 0.13	2.5 ± 15

Table 4.1: Intracellular oxygen values in Old U87MG and RD cells at 18, 10 and 5% ambient oxygen

These results could have important implications in hypoxia studies and will be significantly affected by the levels of glucose in the culture media. It has highlighted that if aerobically competent cells are placed in a reduced oxygen environment the

intracellular oxygen levels may be considerably lower than expected and more consistent with an anoxic environment.

Not all cell types respond to hypoxia in the same way. Some cells can survive in anoxia while others will die. Chi et al investigated and found significant heterogeneity in the hypoxic responses between a variety of cell types (Chi et al., 2006). Three mechanisms underpinning the difference in hypoxia response in tumours have been proposed including (i) variations in oxygen tension in the tumours (ii) cell type specific differences in the extent/threshold of the response to hypoxia or (iii) genetic changes that result in incorrect activation of the hypoxia response (pseudohypoxia) (Chi et al., 2006). While the hypoxic response in some tumours is caused by mechanisms (ii) and (iii) such as loss of VHL in renal clear cell carcinomas the hypoxia response in most tumours is thought to lie in the variations in oxygen tension. Accurately measuring the transient changes in oxygen tension is therefore crucial for hypoxia studies and this MitoXpress-Intra probe could prove to be a valuable tool.

4.3.3 Measuring oxygen levels inside spheroid structures

Standard 2D cell culture conditions are ubiquitous in cell biology and it is well documented that these models do not accurately portray the complexity of in-vivo environments. 3D spheroids provide heterogeneous microenvironments that more accurately reflect tissue, including cell-to-cell interactions, cell-matrix interactions as well as gradients of oxygen, nutrients, waste products and drugs. The importance of

3D models and the effect of 3D culture on cellular bioenergetics have been previously discussed (Chapter 2).

MitoXpress®-Intra in 3D has the potential to further our understanding of individual oxygen concentration gradients in 3D systems and is an important area to develop. Oxygen gradients will exist in the structure that create heterogeneous sub-populations of quiescent, hypoxic and anoxic cells each of which will have distinct metabolic profiles (Dmitriev et al., 2013). Measuring oxygen consumption externally has proven to be useful but has its limitations the MitoXpress-Intra can overcome.

Initial experiments using the intra probe involved culturing the U87MG spheroids for 6 days and adding the MitoXpress-Intra probe overnight before assaying on the 7th day. In this experiment, the loading of the probe was likely confined to the periphery of the pre-formed spheroids. This is consistent with the findings of Dmitriev et al 2011 where poor probe permeation and dispersion throughout the spheroid was observed when pre-formed spheroids were used. Despite the limited probe loading when the spheroids were treated with DCA (inhibits PDK1 and increases TCA activity) there was an increase in the observed lifetime values in a dose dependent manner Figure 4.9. As lifetime and oxygen levels have an inverse relationship the higher lifetime values observed with the 2.5, 5 and 10mM DCA treated spheroids indicates that oxygen levels are lower most likely because of increased aerobic metabolism induced by the treatment. This experiment has highlighted the applicability and importance of this technique as a means of assessing drug effects on 3D structures in a real time and non-invasive manner. Traditional, methods of assessing spheroid “health” are time-consuming involving spheroid dissociation or

fixing and staining prior to sectioning and immunohistochemistry. Using the intracellular probe potentially allows the assessment of spheroid health in minutes with the ability to assess the effects of a drug screen in real time. Once the intracellular oxygen levels have been assessed the spheroids are still viable and can be used in other assay to assess added parameters using established techniques.

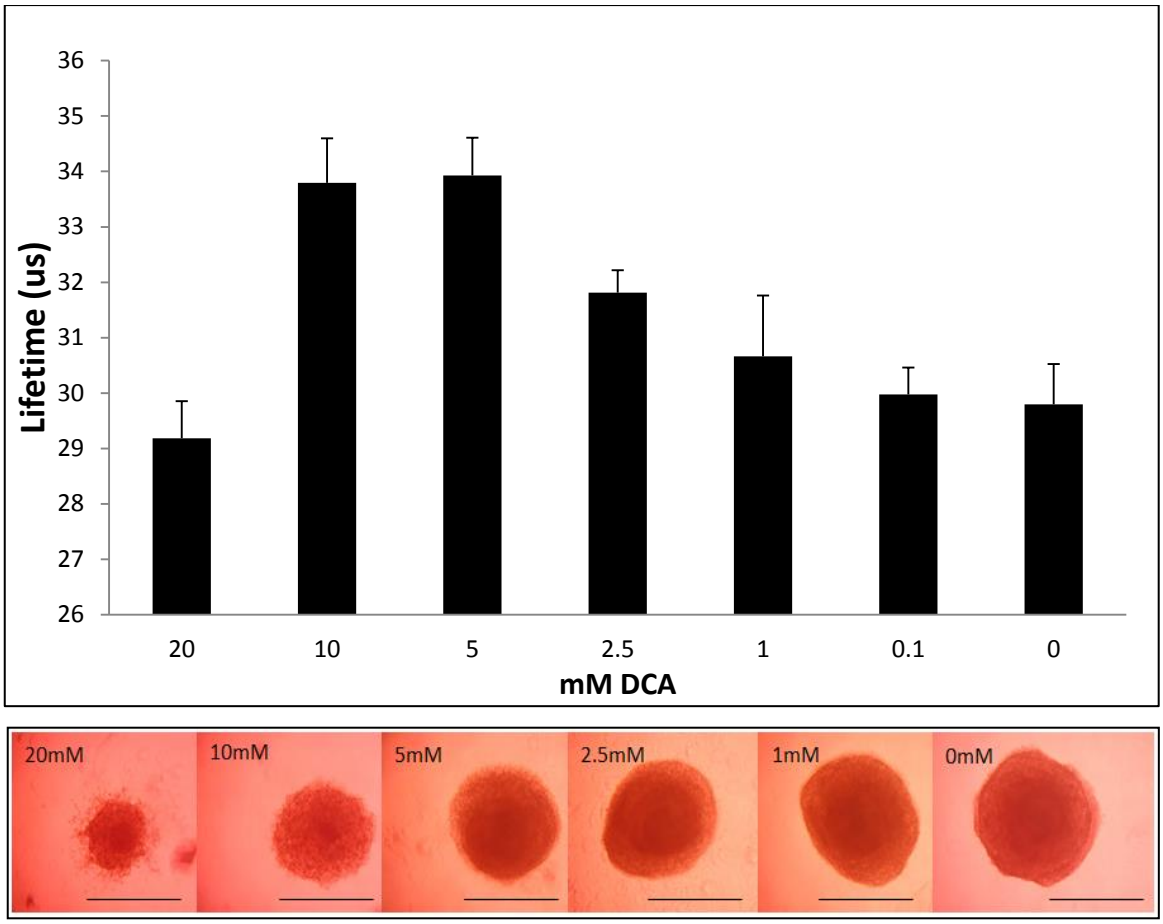

Figure 4.9: Increasing doses of DCA in U87MG spheroids led to lower intracellular levels of oxygen (depicted as higher lifetime values) resulting from enhanced oxygen consumption (top). The effect of DCA treatment on the growth of U87MG spheroids is seen below the graph. Scale bars represent 1000µm. n=2

4.3.3.1 ***Probe distribution in a 3D spheroid structure***

A problem with this probe and its 3D applicability, aside from the aforementioned loading issue, is that if a uniform probe distribution can be achieved it is not known how the probe will disperse itself upon cell division and spheroid expansion. Will it be uniformly dispersed or be confined to more localised regions of the structure. In order to achieve uniform probe loading the probe was added to the media at the time of spheroid formation and top up doses of probe were added on days 2, 4 and 6 before imaging on day 7. MitoXpress-Intra is also applicable to microscopy based techniques so wide field microscopy was used to assess the probe dispersion (according to the method detailed by Kondrashina et al 2012). Briefly, a Zeiss AxioZoom microscope equipped with temperature control and a perfusion system was utilised and the probe was excited at 405nm (20% laser power) and emission collected at 600-70nm. Figure 4.10a shows efficient staining to the interior of the spheroid. Adding the probe at this early stage of the process had no detrimental effect on the spheroids as the size and growth rate of the spheroids with and without probes was comparable (data not shown). Spheroids remained well stained up to 36 hours after the last staining Figure 4.10b. 48 hours after the last staining the probe signal remained although slightly weaker and less uniform Figure 4.10c&d.

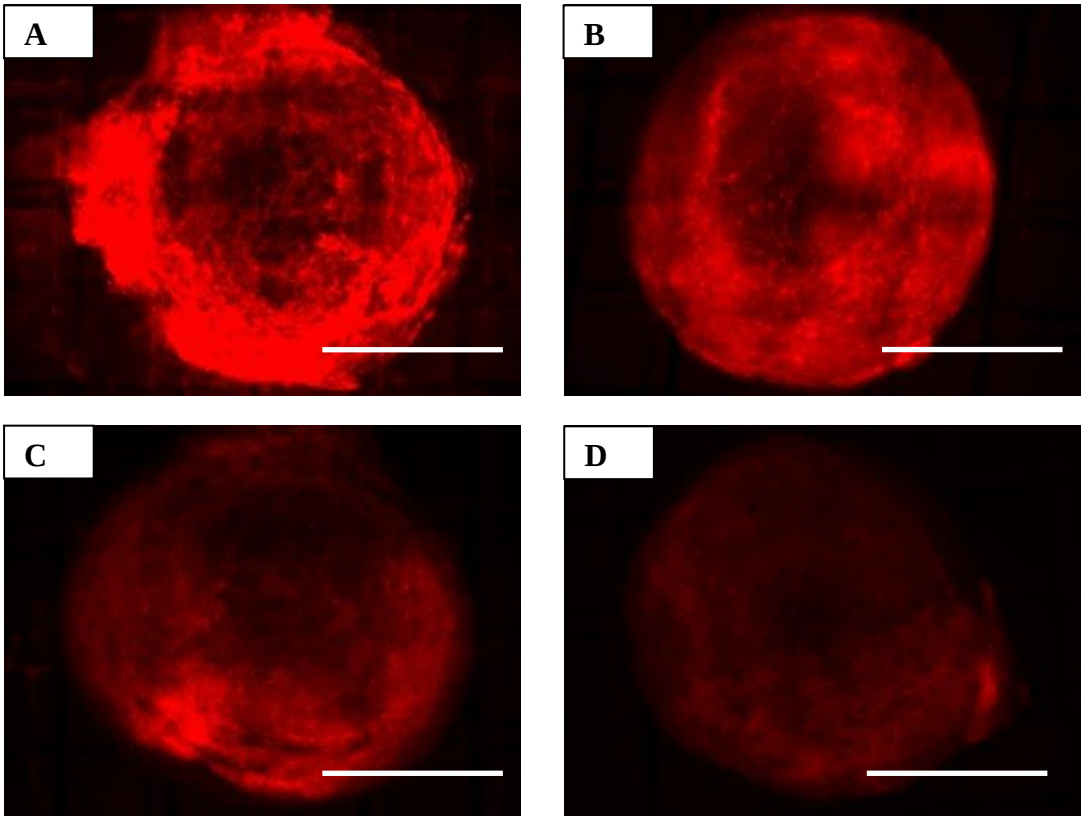

Figure 4.10: Images of the spheroids containing MitoXpress-Intra. (A) Spheroid 24 hours after last probe addition, (B) 36 hours after last probe addition and (C&D) 48 hours after last probe addition. Scale bars represent 1000µm.

This experimental set up allowed for real time monitoring of the spheroid/probe response. This was carried using a range of treatments well known to affect mitochondrial function these included using the mitochondrial substrates glutamine and pyruvate, 1mM glucose and FCCP. In order to establish the most appropriate concentration of FCCP to use in the U87MG cell line, cells cultured in 2D were treated with various doses of FCCP and their oxygen consumption rates measured using the MitoXpress-Xtra. 1 and 2 µM FCCP were shown to be the optimal in increasing mitochondrial respiration increase the OCR rates two-fold Figure 4.11.

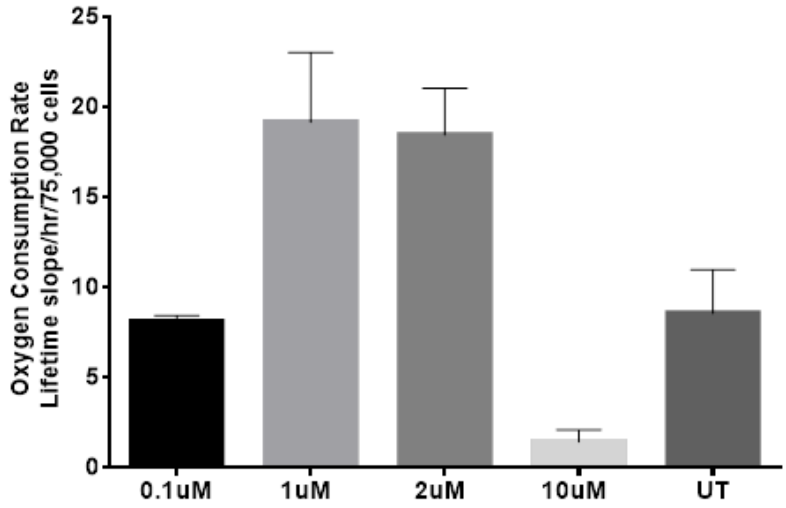

Figure 4.11: Optimum FCCP dose necessary to uncouple the mitochondria was assessed in U87MG cells cultured on high glucose in a 2D monolayer. 0.1µM had no effect on OCR, 10µM resulted in significant decrease in OCR possibly due to cell death while 1 and 2 µM resulted in significant increases in OCR.

Once an optimum FCCP concentration had been established the spheroids were prepared for imaging. They were immobilised using a fine mesh to allow for continuous perfusion of the sample. The fluorescence was measured every 15 seconds over the course of an hour according to the methods described by Kondrashina et al 2013. Once a steady state was reached the perfusion medium containing 5mM glucose was removed and a glucose free solution containing pyruvate and glutamine as the only substrates was added to the spheroids. A substantial increase in probe fluorescence is seen consistent with decreased oxygen levels due to increased oxygen consumption rates (Figure 4.12). Once the glucose was returned to the solution the fluorescence intensity returned to the basal level. As mentioned earlier FCCP concentration was optimised to allow maximum uncoupling in order to monitor the probe response. However, when FCCP was added to the perfusion solution unexpectedly there was a substantial drop in the probe

fluorescence. Zhdanov et al have studied the effect of substrates on the uncoupling response and found that depending on the substrates there can be four different responses to uncoupling: 1) deep and continuous de-oxygenation, 2) de-oxygenation followed by progressive re-oxygenation, 3) moderate, transient drop in oxygen levels and 4) no change or slow progressive increase (Zhdanov et al., 2014). This type 2 response was seen in the cells deprived of pyruvate and glutamine and may be the reason we see the decrease in fluorescence as the perfusion solution contained no pyruvate or glutamine, only glucose and FCCP. Regardless of the reason for the decrease once the FCCP is removed the effect is reversible and the fluorescence returns to basal levels.

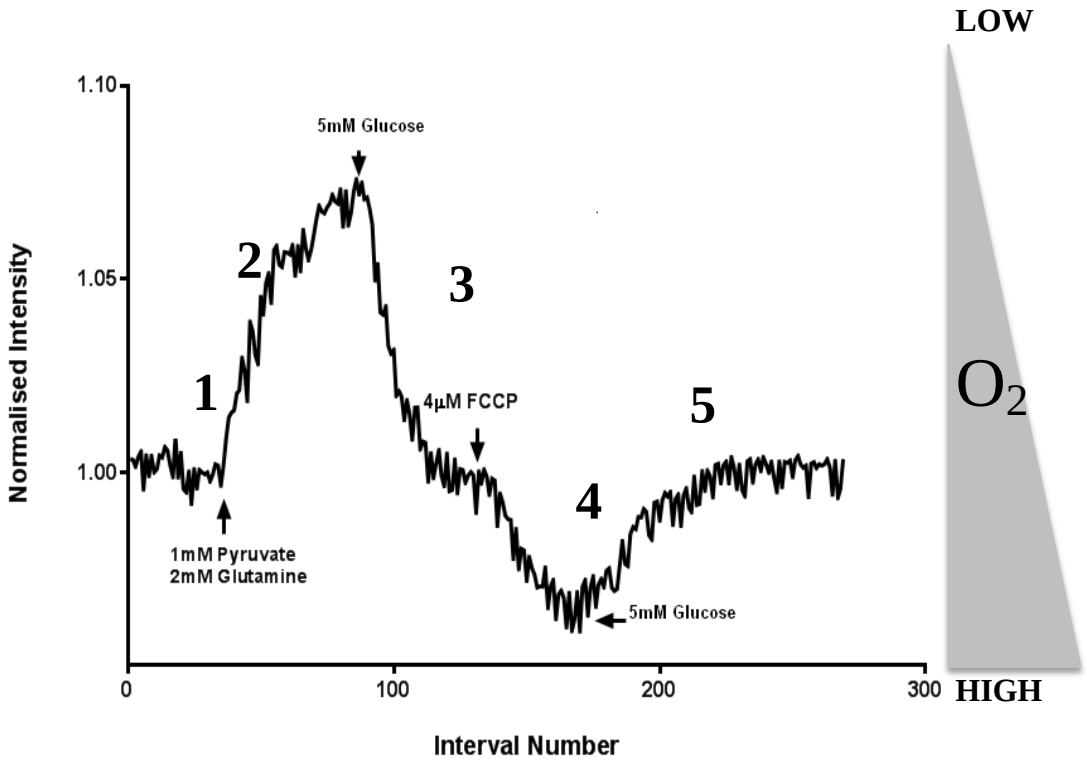

Figure 4.12: A U87MG spheroid was imaged in real time with continuous perfusion and its normalised intensity plotted. (1) buffer containing 5mM glucose was perfused through the sample until a steady state was reached, (2) when glucose was removed and replaced with pyruvate and glutamine the signal intensity increases (due to stimulated Oxphos and increased oxygen consumption) (3) upon the replacing the glucose metabolism switches back to glycolysis dropping the oxygen consumption rates and the signal once again return to baseline, (4) addition of FCCP (in the absence of glucose) caused a drop in intensity which could be reversed upon addition of glucose (5).

4.4 Discussion

Molecular oxygen has an important role in the ETC and is therefore a valuable marker of mitochondrial function and cellular metabolism. Standard cell culture protocols use hyperoxic conditions of 21%. Using more appropriate, biologically relevant conditions is important as cells may behave and react to drugs differently at different oxygen levels (Marwick et al., 2013; Vij et al., 2012). Controlling external oxygen is easily acquired using atmospheric control units, the question is how does ambient oxygen levels relate to the degree of oxygenation in a tissue/cell. Analysing extracellular oxygen levels and oxygen consumption rates is easily achieved through use of readily available and validated techniques (Hynes et al., 2009a). Intracellular oxygen monitoring is not quite as straightforward and is still in its infancy.

Luxcel Bioscience has recently released another oxygen sensitive probe that is capable of monitoring intracellular O_2. It allows for the determination of the percentage oxygen within the cell monolayer/spheroid, a critical parameter in many fields of research including hypoxia and cancer metabolism. Analysis of molecular oxygen enables the elucidation of critical biochemical pathways; including cell survival and death, mitochondrial function, the toxicological impact of compounds and metabolic alterations caused by various disease states for example cancer (Kondrashina et al 2013). Real time measurements can be recorded in a plate reader in a non-invasive and high throughput manner. The probe is taken up by endocytosis and its fluorescence is quenched in the presence of molecular oxygen. Actively respiring cells will deplete the oxygen and cause an increase in probe signal.

Monitoring the cells in a real time manner allows us to investigate more transient changes in oxygen levels. This is crucial for areas of study involving hypoxia and cancer. The added benefit of this probe is that it can be run in parallel with the pH-Xtra to monitor the effect of oxygen on lactate production.

Although the bioenergetic phenotypes of the RD and U87MG cells have already been investigated (chapter 2) monitoring the intracellular oxygen levels was beneficial for the RD cells as it highlighted a substantial level of de-oxygenation within the monolayer compared to the atmospheric levels. This data highlights that significant differences can exist between the oxygen concentration that pertain at the cell monolayer and the applied ambient oxygen concentration, a difference rarely accounted for in standard in vitro analysis. This understanding is particularly significant in hypoxic environments or samples (tumour) where metabolically active cells can display a deeper level of hypoxia. Hypoxic incubators are often kept at 1% or 0.1% oxygen, if RD cells are maintained in this environment they will be anoxic. To evaluate the effect of hypoxia on these cells it may be better to raise the oxygen levels in the incubator and have the intracellular levels at 1%/0.1%.

3D models vary significantly from 2D counterparts and knowing the level of oxygenation can be vital as it gives insight into the balance between glycolysis and Oxphos pathways. Spheroids were preloaded with probe before spheroid formation in a matrigel matrix and probe was added every two days until imaged. Adding probe after spheroid formation results in only the cells on the periphery taking it up. This dispersion issue was easily addressed by adding the probe to the spheroids at the time of formation and continually adding probe for the duration of culture. Removing the

glucose from the spheroids and up-regulating aerobic metabolism caused a deepening of the hypoxia present in the spheroids. These types of analysis will be very beneficial when it comes to evaluating spheroids and drug responses as was demonstrated by the increased respiration in the spheroids treated with DCA.

The intracellular oxygen probe is showing promise as a real time method for monitoring subtle effects on mitochondrial function as a result of toxic insult by allowing the measurement of oxygen within the cell. The equation generated from the calibration curve will be of great benefit in future experiments by allowing more accurate estimations of oxygen concentrations within the cell population. The impact of metabolic stimulation and drug effect can now be easily examined and compared under controlled oxygen concentration, more closely simulating their physiological environment.

The MM2 is a modified version of the MitoXpress-Intra probe. It retains the oxygen sensitive PtFPP but also contains the reference dye PFO (poly(9,9-dioctylfluorene). PFO acts as a FRET donor and is oxygen insensitive allowing for the ratiometric determination using one or two photon microscopy. Intensity based methods are simple and semi qualitative but ratiometric measurements are best as it combines oxygen sensitive and insensitive modalities allowing for better quantitation (Kondrashina et al., 2013).

These probes enable us to further our understanding of intracellular oxygen gradients which will be vital in studies investigating metabolic disorders and mitochondrial function.

5.0 Conclusion

Over the decades, major battles against cancer have been won but the war is ongoing. Cancer cells are very adaptable and often demonstrate extreme heterogeneity both of which hinder the performance of cancer drugs. Cancer metabolism and the Warburg effect are of significant interest at present. However, a single unified mechanism to explain cancer metabolism is unlikely given its complexity. Tumours often display heterogeneity with numerous sub-populations of cells that each may have their own distinct genotypes and metabolic phenotypes. The metabolism of a cell is highly dependent on oncogenic and tumour suppression mutations as well as external factors like hypoxia and nutrient availability. It is generally accepted there will be no "one size fits all" therapy and there is now a shift towards providing more personalised therapies. This will not only require the identification of cancer associated mutations but also a greater understanding of how the environment (eg. glucose and oxygen concentrations) impacts on cancer cell metabolism and proposed treatment regimes.

5.1.1 Key Achievements of this thesis

1) Bioenergetically profiled a panel of cancer cell lines, including five paediatric glioma cell lines whose bioenergetic phenotypes have not been reported in the literature
2) Compared energy metabolism in adult and paediatric brain tumour lines

3) Validated the use of metabolic probes for use in 3D culture systems. This approach provides models more similar to those found in vivo.
4) The intracellular oxygen monitoring system described in this thesis allows changes in oxygen levels to be monitored in real time. This monitoring can be either rapid (over minutes or hours, as with the mitochondrial inhibitor phenformin), or over several days (if the assays are run in a plate reader with an atmospheric control unit). The MitoXpress intra probe thus allows an insight into cellular oxygenation that has not previously been attainable. This new probe could be extremely useful as a tool to identify compounds or gene knockouts that modulate mitochondrial respiration in a high throughput format.
5) Identified different drug effects when using DCA in different model systems and culture conditions. This is important as a drug may be deemed an unsuitable candidate if there is a lack of efficacy of a drug in 2D. In addition, drugs affecting mitochondrial energy metabolism could be missed if screened in a 2D approach using non-physiological glucose levels.

Work from this thesis contributed to the following publications

Published: The over-expression of cell migratory genes in alveolar rhabdomyosarcoma could contribute to metastatic spread (2012). Rapa, E., Hill, S.K., Morten, K.J., Potter, M., and Mitchell, C. Clinical & experimental metastasis 29, 419-429.

Under review: Monitoring intracellular oxygen concentration - implications for hypoxia studies and real time oxygen monitoring

In preparation: Quercetin analogue LY294002 as a chemotherapeutic: Novel synthesis, in vitro testing, and metabolic sensitivity study

5.1.2 Main Limitations of this thesis

Chapter 2

Throughout this thesis, I have iterated and re-iterated the importance of controlling nutrient and substrate availability as this can have profound effects on mitochondrial metabolism and glycolysis rates. However, while I was monitoring the effect of glucose I conducted all of the experiments at 21% oxygen. Future work would involve repeating chapter 2 to include physiological oxygen as well as hypoxic conditions. Another limitation of this chapter is that the 2D and 3D comparisons were not run in parallel (i.e. the experiments were independent and not set up from the exact same cells at the same time). Due to this cell drift/variation may exist. In order to reliably compare 2D and 3D metabolism the assays should be conducted in parallel.

Chapter 3

Chapter 3 is far from an exhaustive investigation into the effects of DCA. The spheroid work was quite time consuming and I have highlighted the difficulties

encountered when attempting to dissociate and analyse them. The successful accutase dissociation giving the best cell recovery was one of the final experiments and currently has an n=1. Moving forward I would have liked to assess the effect of DCA on the spheroids N=3. The microvesicle analysis was a very crude method of assessing drug impact on the spheroids as it is a relatively non-specific means of assessing microvesicles. In the future, it would be beneficial to carry out a more in depth characterisation the vesicles.

Chapter 4

This chapter mainly demonstrates proof of principle and highlights the applicability of the MitoXpress-Intra probe. A substantial amount of time was spent optimising the conditions to just detect the probe leaving no time to apply to method to the monitoring of drug effects in real time. Now proof of principle has been determined this approach could be used to monitor the effect of DCA (and other drugs) on the oxygen concentration gradients with tumour spheroids.

5.1.3 Future work

The results presented in this thesis are far from exhaustive. Interesting research areas to follow up on in the future are outlined below. The number of cancer cell lines could be expanded to include other types of cancers (i.e. breast, colorectal and ovarian) to determine if a specific biogenetic profile relates to a particular type of cancer or whether cancers can adopt different metabolic profiles irrespective of their tissue of origin. More non-cancerous controls should be included although many of the standard models such as fibroblasts show very low rates of oxygen consumption.

1. Linking the cancer mutation status of the lines to bioenergetic phenotype would be a useful exercise. If an in vitro link can be found between a successful metabolic treatment and a particular cancer genetic profile this could be invaluable in the clinic where only the cancer genetic profile maybe known. The oncogenic mutation profile of RD (OxPhos) and old U87MG (Glycolytic) cells lines was determined by deep sequenced by NIMGenetics (supplemental Figure 7.10, Figure 7.11 and Figure 7.12) but no conclusions can be drawn from this preliminary investigation. The Sanger Institute provide extensive information regarding the mutations of numerous lines however the same cell line handled by different scientists or in different labs may not contain the same mutations. It is important to understand the exact cell line you are working with and not the ATCC equivalent. In this project sequencing the cancer mutation status of the adult and paediatric glioblastomas could be very valuable and might give insights to why these two similar types of cancers show clear differences in bioenergetics
2. A comparison between cell lines and primary tissue from patients would also be very interesting. Cell lines cultured in-vivo are subject to extensive genetic changes that may not accurately reflect the in-vivo system. Accessing patient samples would have been beneficial in this study but unfortunately did not come to fruition during my research.
3. In the absence of access to primary tumour tissue it would be beneficial to further investigate improving the spheroid/Alvetex models. Another possibility of 3D culture is to investigate perfused culture systems. We purchased a 3D perfusion system from Zyoxel, which was developed in

Oxford (Cui et al., 2007). It consists of 12 parallel perfused wells (TissueFlex®) which allow spheroids to be constantly perfused with media. Perfusion removes metabolites and replenishes nutrients at pre-determined rates. It provides a more static culture environment. Perfusion models with real time monitoring of glucose and oxygen linked to systems to regulate the two parameters to defined levels

6.0 References

Websites

http://publications.cancerresearchuk.org/downloads/Product/CS_KF_ALLCANCERS.pdf - Cancer Research UK Key Facts for All Cancers Combined January 2014 (date accessed 8-3-14)

http://www.cancerresearchuk.org/cancer-info/cancerstats/childhoodcancer/incidence/ (date accessed 8-3-14)

Books

Baynes J,W. (2009) Chapter 12 "Anaerobic Metabolism of Glucose in Red Blood Cells" in Baynes J,W. and Dominiczak M,H. (3rd edition), *Medical Biochemistry,* MOSBY Elsevier

Baynes J,W. (2009) Chapter 37 "Oxygen and Life" in Baynes J,W. and Dominiczak M,H. (3rd edition), *Medical Biochemistry,* MOSBY Elsevier.

Berg JM, Tymoczko JL, Stryer L. (2002), *"Biochemistry*", (5th edition), New York: W H Freeman.

Carr B., Wright M., (2013) Nanoparticle Tracking Analysis: A review of applications and usage.

Dominiczak H,M. (2009) Chapter 21 "Glucose Homeostasis and Fuel Metabolism" in Baynes J,W. and Dominiczak M,H. (3rd edition), *Medical Biochemistry,* MOSBY Elsevier.

Hartnett M,M. and Goodridge H,S. (2009) Chapter 21 "Glucose Homeostasis and Fuel Metabolism" in Baynes J,W. and Dominiczak M,H. (3rd edition), *Medical Biochemistry,* MOSBY Elsevier.

Helmkamp G,M. (2009) Chapter 5 "Oxygen Transport" in Baynes J,W. and Dominiczak M,H. (3rd edition), *Medical Biochemistry,* MOSBY Elsevier.

Pitt A. and Kolch W. (2009) Chapter 36 "Genomics, Proteomics and Metabolomics" in Baynes J,W. and Dominiczak M,H. (3rd edition), *Medical Biochemistry,* MOSBY Elsevier.

Rang, HP., Dale, MM., (2007) Section 5 "Drug used in the treatment of infectious diseases and cancer" (6th edition), *Pharmacology,* Churchill Livingstone Elsevier, pages 647-718.

Simons, AL., Orcutt, KP., Madsen, JM., Scarbrough, PM., Spitz, DR. (2011) Chapter 2 "The role of Akt pathway signalling in glucose metabolism and metabolic oxidative stress" , *Oxidative stress in cancer biology and therapy,* Springer.

Stillway L,W. (2009) Chapter 9 "Bioenergetics and Oxidative Metabolism" in Baynes J,W. and Dominiczak M,H. (3rd edition), *Medical Biochemistry,* MOSBY Elsevier.

Stillway L,W. (2009) Chapter 14 "Tricarboxylic Acid Cycle" in Baynes J,W. and Dominiczak M,H. (3rd edition), *Medical Biochemistry,* MOSBY Elsevier.

Thompson E, J. (2009) Chapter 41 "Neurochemistry" in Baynes J,W. and Dominiczak M,H. (3rd edition), *Medical Biochemistry,* MOSBY Elsevier.

Journals

Abe, Y., Sakairi, T., Kajiyama, H., Shrivastav, S., Beeson, C., and Kopp, J.B. (2010). Bioenergetic characterization of mouse podocytes. American journal of physiology. Cell physiology *299*, C464-476.

Aguer, C., Gambarotta, D., Mailloux, R.J., Moffat, C., Dent, R., McPherson, R., and Harper, M.-E. (2011). Galactose Enhances Oxidative Metabolism and Reveals Mitochondrial Dysfunction in Human Primary Muscle Cells. PloS one *6*, e28536.

Algire, C., Amrein, L., Bazile, M., David, S., Zakikhani, M., and Pollak, M. (2011). Diet and tumor LKB1 expression interact to determine sensitivity to anti-neoplastic effects of metformin in vivo. Oncogene *30*, 1174-1182.

Anderson, W.B., Board, P.G., and Anders, M.W. (2004). Glutathione transferase zeta-catalyzed bioactivation of dichloroacetic acid: reaction of glyoxylate with amino acid nucleophiles. Chemical research in toxicology *17*, 650-662.

Aragones, J., Fraisl, P., Baes, M., and Carmeliet, P. (2009). Oxygen sensors at the crossroad of metabolism. Cell metabolism *9*, 11-22.

Bax, D.A., Little, S.E., Gaspar, N., Perryman, L., Marshall, L., Viana-Pereira, M., Jones, T.A., Williams, R.D., Grigoriadis, A., Vassal, G., et al. (2009). Molecular and phenotypic characterisation of paediatric glioma cell lines as models for preclinical drug development. In PloS one (Paediatric Oncology, The Institute of Cancer Research, Sutton, United Kingdom.: Public Library of Science (PLoS)), p. e5209.

Birsoy, K., Possemato, R., Lorbeer, F.K., Bayraktar, E.C., Thiru, P., Yucel, B., Wang, T., Chen, W.W., Clish, C.B., and Sabatini, D.M. (2014). Metabolic determinants of cancer cell sensitivity to glucose limitation and biguanides. Nature *508*, 108-112.

Bonnet, S., Archer, S.L., Allalunis-Turner, J., Haromy, A., Beaulieu, C., Thompson, R., Lee, C.T., Lopaschuk, G.D., Puttagunta, L., Bonnet, S., et al. (2007). A mitochondria-K+ channel axis is suppressed in cancer and its normalization promotes apoptosis and inhibits cancer growth. Cancer cell *11*, 37-51.

Cairns, R.A., Bennewith, K.L., Graves, E.E., Giaccia, A.J., Chang, D.T., and Denko, N.C. (2009). Pharmacologically increased tumor hypoxia can be measured by 18F-Fluoroazomycin arabinoside positron emission tomography and enhances tumor response to hypoxic cytotoxin PR-104. Clinical cancer research : an official journal of the American Association for Cancer Research *15*, 7170-7174.

Cairns, R.A., Papandreou, I., Sutphin, P.D., and Denko, N.C. (2007). Metabolic targeting of hypoxia and HIF1 in solid tumors can enhance cytotoxic chemotherapy. Proceedings of the National Academy of Sciences of the United States of America *104*, 9445-9450.

Camussi, G., Deregibus, M.C., Bruno, S., Grange, C., Fonsato, V., and Tetta, C. (2011). Exosome/microvesicle-mediated epigenetic reprogramming of cells. American journal of cancer research *1*, 98-110.

Cao, W., Yacoub, S., Shiverick, K.T., Namiki, K., Sakai, Y., Porvasnik, S., Urbanek, C., and Rosser, C.J. (2008). Dichloroacetate (DCA) sensitizes both wild-type and over expressing Bcl-2 prostate cancer cells in vitro to radiation. The Prostate *68*, 1223-1231.

Chen, Y., Cairns, R., Papandreou, I., Koong, A., and Denko, N.C. (2009). Oxygen consumption can regulate the growth of tumors, a new perspective on the Warburg effect. PloS one *4*, e7033.

Chi, J.T., Wang, Z., Nuyten, D.S., Rodriguez, E.H., Schaner, M.E., Salim, A., Wang, Y., Kristensen, G.B., Helland, A., Borresen-Dale, A.L., et al. (2006). Gene expression programs in response to hypoxia: cell type specificity and prognostic significance in human cancers. PLoS medicine *3*, e47.

Chiaradonna, F., Moresco, R.M., Airoldi, C., Gaglio, D., Palorini, R., Nicotra, F., Messa, C., and Alberghina, L. (2012). From cancer metabolism to new biomarkers and drug targets. Biotechnology advances *30*, 30-51.

Chin, Y.W., Balunas, M.J., Chai, H.B., and Kinghorn, A.D. (2006). Drug discovery from natural sources. The AAPS journal *8*, E239-253.

Choi, H.B., Gordon, G.R., Zhou, N., Tai, C., Rungta, R.L., Martinez, J., Milner, T.A., Ryu, J.K., McLarnon, J.G., Tresguerres, M., et al. (2012). Metabolic communication between astrocytes and neurons via bicarbonate-responsive soluble adenylyl cyclase. Neuron *75*, 1094-1104.

Christakis, P. (2011). The birth of chemotherapy at Yale. Bicentennial lecture series: Surgery Grand Round. The Yale journal of biology and medicine *84*, 169-172.

Clark, L.C., Jr., Kaplan, S., Matthews, E.C., and Schwab, L. (1956). Oxygen availability to the brain during inflow occlusion of the heart in normothermia and hypothermia. The Journal of thoracic surgery *32*, 576-582.

Crabtree, H.G. (1928). The carbohydrate metabolism of certain pathological overgrowths. The Biochemical journal *22*, 1289-1298.

Crabtree, H.G. (1929). Observations on the carbohydrate metabolism of tumours. The Biochemical journal *23*, 536-545.

Cui, Z.F., Xu, X., Trainor, N., Triffitt, J.T., Urban, J.P., and Tirlapur, U.K. (2007). Application of multiple parallel perfused microbioreactors and three-dimensional stem cell culture for toxicity testing. Toxicology in vitro : an international journal published in association with BIBRA *21*, 1318-1324.

da Rocha, A.B., Lopes, R.M., and Schwartsmann, G. (2001). Natural products in anticancer therapy. Current opinion in pharmacology *1*, 364-369.

Dang, C.V. (2012). Links between metabolism and cancer. Genes & development *26*, 877-890.

Dang, C.V., Le, A., and Gao, P. (2009a). MYC-induced cancer cell energy metabolism and therapeutic opportunities. Clinical cancer research : an official journal of the American Association for Cancer Research *15*, 6479-6483.

Dang, L., White, D.W., Gross, S., Bennett, B.D., Bittinger, M.A., Driggers, E.M., Fantin, V.R., Jang, H.G., Jin, S., Keenan, M.C., et al. (2009b). Cancer-associated IDH1 mutations produce 2-hydroxyglutarate. In Nature (Agios Pharmaceuticals, Cambridge, Massachusetts 02139, USA.), pp. 739-744.

Dang, L., White, D.W., Gross, S., Bennett, B.D., Bittinger, M.A., Driggers, E.M., Fantin, V.R., Jang, H.G., Jin, S., Keenan, M.C., et al. (2010). Cancer-associated IDH1 mutations produce 2-hydroxyglutarate. In Nature, p. 966.

DeBerardinis, R.J. (2008). Is cancer a disease of abnormal cellular metabolism? New angles on an old idea. Genetics in medicine : official journal of the American College of Medical Genetics *10*, 767-777.

DeBerardinis, R.J., and Cheng, T. (2010). Q's next: the diverse functions of glutamine in metabolism, cell biology and cancer. Oncogene *29*, 313-324.

DeBerardinis, R.J., Lum, J.J., Hatzivassiliou, G., and Thompson, C.B. (2008). The biology of cancer: metabolic reprogramming fuels cell growth and proliferation. Cell metabolism *7*, 11-20.

DeBerardinis, R.J., Mancuso, A., Daikhin, E., Nissim, I., Yudkoff, M., Wehrli, S., and Thompson, C.B. (2007). Beyond aerobic glycolysis: transformed cells can engage in glutamine metabolism that exceeds the requirement for protein and

nucleotide synthesis. Proceedings of the National Academy of Sciences of the United States of America *104*, 19345-19350.

Denko, N.C. (2008). Hypoxia, HIF1 and glucose metabolism in the solid tumour. Nature reviews. Cancer *8*, 705-713.

Dhar, S., and Lippard, S.J. (2009). Mitaplatin, a potent fusion of cisplatin and the orphan drug dichloroacetate. In Proceedings of the National Academy of Sciences of the United States of America (Department of Chemistry and Koch Institute for Integrative Cancer Research, Massachusetts Institute of Technology, 77 Massachusetts Avenue, Cambridge, MA 02139, USA.), pp. 22199-22204.

Diaz-Ruiz, R., Rigoulet, M., and Devin, A. (2011). The Warburg and Crabtree effects: On the origin of cancer cell energy metabolism and of yeast glucose repression. In Biochimica et biophysica acta (Oxygen Sensing and Cancer Laboratory, Ludwig Institute for Cancer Research Ltd., Karolinska Institute, Nobels väg 3, SE-171 77 Stockholm, Sweden.: Elsevier Science), pp. 568-576.

Dmitriev, R.I., and Papkovsky, D.B. (2012). Optical probes and techniques for O2 measurement in live cells and tissue. Cellular and molecular life sciences : CMLS *69*, 2025-2039.

Dmitriev, R.I., Zhdanov, A.V., Jasionek, G., and Papkovsky, D.B. (2012). Assessment of cellular oxygen gradients with a panel of phosphorescent oxygen-sensitive probes. Analytical chemistry *84*, 2930-2938.

Dmitriev, R.I., Zhdanov, A.V., Nolan, Y.M., and Papkovsky, D.B. (2013). Imaging of neurosphere oxygenation with phosphorescent probes. Biomaterials *34*, 9307-9317.

Dowling, R.J., Niraula, S., Stambolic, V., and Goodwin, P.J. (2012). Metformin in cancer: translational challenges. Journal of molecular endocrinology *48*, R31-43.

Dragovic, R.A., Gardiner, C., Brooks, A.S., Tannetta, D.S., Ferguson, D.J., Hole, P., Carr, B., Redman, C.W., Harris, A.L., Dobson, P.J., et al. (2011). Sizing and phenotyping of cellular vesicles using Nanoparticle Tracking Analysis. Nanomedicine *7*, 780-788.

Dragovic, R.A., Southcombe, J.H., Tannetta, D.S., Redman, C.W., and Sargent, I.L. (2013). Multicolor flow cytometry and nanoparticle tracking analysis of extracellular vesicles in the plasma of normal pregnant and pre-eclamptic women. Biology of reproduction *89*, 151.

Dunbar, E.M., Coats, B.S., Shroads, A.L., Langaee, T., Lew, A., Forder, J.R., Shuster, J.J., Wagner, D.A., and Stacpoole, P.W. (2013). Phase 1 trial of dichloroacetate (DCA) in adults with recurrent malignant brain tumors. Investigational new drugs.

Dykens, J.A., Jamieson, J., Marroquin, L., Nadanaciva, S., Billis, P.A., and Will, Y. (2008). Biguanide-induced mitochondrial dysfunction yields increased lactate production and cytotoxicity of aerobically-poised HepG2 cells and human hepatocytes in vitro. Toxicology and applied pharmacology *233*, 203-210.

Ertel, A., Verghese, A., Byers, S.W., Ochs, M., and Tozeren, A. (2006). Pathway-specific differences between tumor cell lines and normal and tumor tissue cells. Molecular cancer *5*, 55.

Fan, T.W., Kucia, M., Jankowski, K., Higashi, R.M., Ratajczak, J., Ratajczak, M.Z., and Lane, A.N. (2008). Rhabdomyosarcoma cells show an energy producing anabolic metabolic phenotype compared with primary myocytes. Molecular cancer *7*, 79.

Fan, T.W., Lane, A.N., Higashi, R.M., Bousamra, M., 2nd, Kloecker, G., and Miller, D.M. (2009). Metabolic profiling identifies lung tumor responsiveness to erlotinib. Experimental and molecular pathology *87*, 83-86.

Fercher, A., Borisov, S.M., Zhdanov, A.V., Klimant, I., and Papkovsky, D.B. (2011). Intracellular O2 sensing probe based on cell-penetrating phosphorescent nanoparticles. ACS nano *5*, 5499-5508.

Frezza, C., and Gottlieb, E. (2009). Mitochondria in cancer: not just innocent bystanders. Seminars in cancer biology *19*, 4-11.

Gao, P., Tchernyshyov, I., Chang, T.C., Lee, Y.S., Kita, K., Ochi, T., Zeller, K.I., De Marzo, A.M., Van Eyk, J.E., Mendell, J.T., et al. (2009). c-Myc suppression of miR-23a/b enhances mitochondrial glutaminase expression and glutamine metabolism. Nature *458*, 762-765.

Garber, K. (2010). Oncometabolite? IDH1 discoveries raise possibility of new metabolism targets in brain cancers and leukemia. Journal of the National Cancer Institute *102*, 926-928.

Garcia-Cao, I., Song, M.S., Hobbs, R.M., Laurent, G., Giorgi, C., de Boer, V.C., Anastasiou, D., Ito, K., Sasaki, A.T., Rameh, L., et al. (2012). Systemic elevation of PTEN induces a tumor-suppressive metabolic state. Cell *149*, 49-62.

Gatenby, R.A., and Gillies, R.J. (2004). Why do cancers have high aerobic glycolysis? Nature reviews. Cancer *4*, 891-899.

Gatenby, R.A., and Gillies, R.J. (2007). Glycolysis in cancer: a potential target for therapy. The international journal of biochemistry & cell biology *39*, 1358-1366.

Gelderman, M.P., and Simak, J. (2008). Flow cytometric analysis of cell membrane microparticles. Methods in molecular biology *484*, 79-93.

Gillet, J.P., Calcagno, A.M., Varma, S., Marino, M., Green, L.J., Vora, M.I., Patel, C., Orina, J.N., Eliseeva, T.A., Singal, V., et al. (2011). Redefining the relevance of

established cancer cell lines to the study of mechanisms of clinical anti-cancer drug resistance. Proceedings of the National Academy of Sciences of the United States of America *108*, 18708-18713.

Gogvadze, V., Orrenius, S., and Zhivotovsky, B. (2008). Mitochondria in cancer cells: what is so special about them? Trends in cell biology *18*, 165-173.

Gohil, V.M., Sheth, S.A., Nilsson, R., Wojtovich, A.P., Lee, J.H., Perocchi, F., Chen, W., Clish, C.B., Ayata, C., Brookes, P.S., et al. (2010). Nutrient-sensitized screening for drugs that shift energy metabolism from mitochondrial respiration to glycolysis. Nature biotechnology *28*, 249-255.

Griguer, C.E., and Oliva, C.R. (2011). Bioenergetics pathways and therapeutic resistance in gliomas: emerging role of mitochondria. Current pharmaceutical design *17*, 2421-2427.

Grover-McKay, M., Walsh, S.A., Seftor, E.A., Thomas, P.A., and Hendrix, M.J. (1998). Role for glucose transporter 1 protein in human breast cancer. Pathology oncology research : POR *4*, 115-120.

Gstraunthaler, G., Seppi, T., and Pfaller, W. (1999). Impact of culture conditions, culture media volumes, and glucose content on metabolic properties of renal epithelial cell cultures. Are renal cells in tissue culture hypoxic? Cellular physiology and biochemistry : international journal of experimental cellular physiology, biochemistry, and pharmacology *9*, 150-172.

Gupta, S.C., Sung, B., Prasad, S., Webb, L.J., and Aggarwal, B.B. (2013). Cancer drug discovery by repurposing: teaching new tricks to old dogs. Trends in pharmacological sciences *34*, 508-517.

Gurib-Fakim, A. (2006). Medicinal plants: traditions of yesterday and drugs of tomorrow. Molecular aspects of medicine *27*, 1-93.

Gyorgy, B., Szabo, T.G., Pasztoi, M., Pal, Z., Misjak, P., Aradi, B., Laszlo, V., Pallinger, E., Pap, E., Kittel, A., et al. (2011). Membrane vesicles, current state-of-the-art: emerging role of extracellular vesicles. Cellular and molecular life sciences : CMLS *68*, 2667-2688.

Hanahan, D., and Weinberg, R.A. (2000). The hallmarks of cancer. Cell *100*, 57-70.

Hanahan, D., and Weinberg, R.A. (2011). Hallmarks of cancer: the next generation. Cell *144*, 646-674.

Harper, M.E., Antoniou, A., Villalobos-Menuey, E., Russo, A., Trauger, R., Vendemelio, M., George, A., Bartholomew, R., Carlo, D., Shaikh, A., et al. (2002). Characterization of a novel metabolic strategy used by drug-resistant tumor cells. FASEB journal : official publication of the Federation of American Societies for Experimental Biology *16*, 1550-1557.

Hendrickson, K., Phillips, M., Smith, W., Peterson, L., Krohn, K., and Rajendran, J. (2011). Hypoxia imaging with [F-18] FMISO-PET in head and neck cancer: potential for guiding intensity modulated radiation therapy in overcoming hypoxia-induced treatment resistance. Radiotherapy and oncology : journal of the European Society for Therapeutic Radiology and Oncology *101*, 369-375.

Heshe, D., Hoogestraat, S., Brauckmann, C., Karst, U., Boos, J., and Lanvers-Kaminsky, C. (2011). Dichloroacetate metabolically targeted therapy defeats cytotoxicity of standard anticancer drugs. In Cancer chemotherapy and pharmacology (Department of Paediatric Haematology and Oncology, University Children's Hospital, Muenster, Germany.), pp. 647-655.

Higgins, S.C., and Pilkington, G.J. (2010). The in vitro effects of tricyclic drugs and dexamethasone on cellular respiration of malignant glioma. Anticancer research *30*, 391-397.

Hirayama, A., Kami, K., Sugimoto, M., Sugawara, M., Toki, N., Onozuka, H., Kinoshita, T., Saito, N., Ochiai, A., Tomita, M., et al. (2009). Quantitative metabolome profiling of colon and stomach cancer microenvironment by capillary electrophoresis time-of-flight mass spectrometry. Cancer research *69*, 4918-4925.

Hirschhaeuser, F., Menne, H., Dittfeld, C., West, J., Mueller-Klieser, W., and Kunz-Schughart, L.A. (2010). Multicellular tumor spheroids: an underestimated tool is catching up again. Journal of biotechnology *148*, 3-15.

Hu, J., Bianchi, F., Ferguson, M., Cesario, A., Margaritora, S., Granone, P., Goldstraw, P., Tetlow, M., Ratcliffe, C., Nicholson, A.G., et al. (2005). Gene expression signature for angiogenic and nonangiogenic non-small-cell lung cancer. Oncogene *24*, 1212-1219.

Hynes, J., Natoli, E., Jr., and Will, Y. (2009a). Fluorescent pH and oxygen probes of the assessment of mitochondrial toxicity in isolated mitochondria and whole cells. Current protocols in toxicology / editorial board, Mahin D. Maines *Chapter 2*, Unit 2 16.

Hynes, J., O'Riordan, T.C., Zhdanov, A.V., Uray, G., Will, Y., and Papkovsky, D.B. (2009b). In vitro analysis of cell metabolism using a long-decay pH-sensitive lanthanide probe and extracellular acidification assay. Analytical biochemistry *390*, 21-28.

Icard, P., and Lincet, H. (2012). A global view of the biochemical pathways involved in the regulation of the metabolism of cancer cells. Biochimica et biophysica acta *1826*, 423-433.

Ishiguro, T., Ishiguro, M., Ishiguro, R., and Iwai, S. (2012). Cotreatment with dichloroacetate and omeprazole exhibits a synergistic antiproliferative effect on malignant tumors. Oncology letters *3*, 726-728.

Itoh, Y., Esaki, T., Shimoji, K., Cook, M., Law, M.J., Kaufman, E., and Sokoloff, L. (2003). Dichloroacetate effects on glucose and lactate oxidation by neurons and astroglia in vitro and on glucose utilization by brain in vivo. Proceedings of the National Academy of Sciences of the United States of America *100*, 4879-4884.

Ivan, M., Haberberger, T., Gervasi, D.C., Michelson, K.S., Gunzler, V., Kondo, K., Yang, H., Sorokina, I., Conaway, R.C., Conaway, J.W., et al. (2002). Biochemical purification and pharmacological inhibition of a mammalian prolyl hydroxylase acting on hypoxia-inducible factor. Proceedings of the National Academy of Sciences of the United States of America *99*, 13459-13464.

Jeong, J.C., Kim, J.W., Kwon, C.H., Kim, T.H., and Kim, Y.K. (2011). Fructus ligustri lucidi extracts induce human glioma cell death through regulation of Akt/mTOR pathway in vitro and reduce glioma tumor growth in U87MG xenograft mouse model. Phytotherapy research : PTR *25*, 429-434.

Jose, C., Bellance, N., and Rossignol, R. (2011). Choosing between glycolysis and oxidative phosphorylation: a tumor's dilemma? Biochimica et biophysica acta *1807*, 552-561.

Katsetos, C.D., Anni, H., and Draber, P. (2013). Mitochondrial dysfunction in gliomas. Seminars in pediatric neurology *20*, 216-227.

Kaufmann, S.H. (2008). Paul Ehrlich: founder of chemotherapy. Nature reviews. Drug discovery *7*, 373.

Khaitan, D., Chandna, S., Arya, M.B., and Dwarakanath, B.S. (2006). Establishment and characterization of multicellular spheroids from a human glioma cell line; Implications for tumor therapy. Journal of translational medicine *4*, 12.

Kim, J.-w., Tchernyshyov, I., Semenza, G.L., and Dang, C.V. (2006). HIF-1-mediated expression of pyruvate dehydrogenase kinase: a metabolic switch required for cellular adaptation to hypoxia. In Cell metabolism (Graduate Program of Pathobiology, Johns Hopkins University School of Medicine, Baltimore, Maryland 21205, USA.: Cell Press), pp. 177-185.

Knight, E., Murray, B., Carnachan, R., and Przyborski, S. (2011). Alvetex(R): polystyrene scaffold technology for routine three dimensional cell culture. Methods in molecular biology *695*, 323-340.

Knoechel, T.R., Tucker, A.D., Robinson, C.M., Phillips, C., Taylor, W., Bungay, P.J., Kasten, S.A., Roche, T.E., and Brown, D.G. (2006). Regulatory roles of the N-terminal domain based on crystal structures of human pyruvate dehydrogenase kinase 2 containing physiological and synthetic ligands. Biochemistry *45*, 402-415.

Kondrashina, A.V., Papkovsky, D.B., and Dmitriev, R.I. (2013). Measurement of cell respiration and oxygenation in standard multichannel biochips using phosphorescent O2-sensitive probes. The Analyst *138*, 4915-4921.

Kroemer, G., and Pouyssegur, J. (2008). Tumor cell metabolism: cancer's Achilles' heel. Cancer cell *13*, 472-482.

Lai, J.H., Jan, H.J., Liu, L.W., Lee, C.C., Wang, S.G., Hueng, D.Y., Cheng, Y.Y., Lee, H.M., and Ma, H.I. (2013). Nodal regulates energy metabolism in glioma cells by inducing expression of hypoxia-inducible factor 1alpha. Neuro-oncology *15*, 1330-1341.

Li, W., James, M.O., McKenzie, S.C., Calcutt, N.A., Liu, C., and Stacpoole, P.W. (2011). Mitochondrion as a novel site of dichloroacetate biotransformation by glutathione transferase zeta 1. The Journal of pharmacology and experimental therapeutics *336*, 87-94.

Lin, R.Z., and Chang, H.Y. (2008). Recent advances in three-dimensional multicellular spheroid culture for biomedical research. Biotechnology journal *3*, 1172-1184.

Liu, J., and Feng, Z. (2012). PTEN, energy metabolism and tumor suppression. Acta biochimica et biophysica Sinica *44*, 629-631.

Lunt, S.Y., and Vander Heiden, M.G. (2011). Aerobic glycolysis: meeting the metabolic requirements of cell proliferation. Annual review of cell and developmental biology *27*, 441-464.

Luo, W., and Semenza, G.L. (2012). Emerging roles of PKM2 in cell metabolism and cancer progression. Trends in endocrinology and metabolism: TEM *23*, 560-566.

Marin-Valencia, I., Yang, C., Mashimo, T., Cho, S., Baek, H., Yang, X.L., Rajagopalan, K.N., Maddie, M., Vemireddy, V., Zhao, Z., et al. (2012). Analysis of tumor metabolism reveals mitochondrial glucose oxidation in genetically diverse human glioblastomas in the mouse brain in vivo. Cell metabolism *15*, 827-837.

Marroquin, L.D., Hynes, J., Dykens, J.A., Jamieson, J.D., and Will, Y. (2007). Circumventing the Crabtree effect: replacing media glucose with galactose increases susceptibility of HepG2 cells to mitochondrial toxicants. Toxicological sciences : an official journal of the Society of Toxicology *97*, 539-547.

Martin-Requero, A., Ayuso, M.S., and Parrilla, R. (1986). Rate-limiting steps for hepatic gluconeogenesis. Mechanism of oxamate inhibition of mitochondrial pyruvate metabolism. The Journal of biological chemistry *261*, 13973-13978.

Martin, M., Beauvoit, B., Voisin, P.J., Canioni, P., Guerin, B., and Rigoulet, M. (1998). Energetic and morphological plasticity of C6 glioma cells grown on 3-D support; effect of transient glutamine deprivation. Journal of bioenergetics and biomembranes *30*, 565-578.

Martins, V.R., Dias M.S., Hainaut P., (2013). Tumor-cell-derived microvesicles as carriers of molecular information. Current Opinion Oncology *25*, 66-75

Marwick, J.A., Dorward, D.A., Lucas, C.D., Jones, K.O., Sheldrake, T.A., Fox, S., Ward, C., Murray, J., Brittan, M., Hirani, N., et al. (2013). Oxygen levels determine the ability of glucocorticoids to influence neutrophil survival in inflammatory environments. Journal of leukocyte biology *94*, 1285-1292.

Mathupala, S.P. (2011). Metabolic targeting of malignant tumors: small-molecule inhibitors of bioenergetic flux. Recent patents on anti-cancer drug discovery *6*, 6-14.

Mathupala, S.P., Ko, Y.H., and Pedersen, P.L. (2006). Hexokinase II: cancer's double-edged sword acting as both facilitator and gatekeeper of malignancy when bound to mitochondria. Oncogene *25*, 4777-4786.

Mathupala, S.P., Ko, Y.H., and Pedersen, P.L. (2009). Hexokinase-2 bound to mitochondria: cancer's stygian link to the "Warburg Effect" and a pivotal target for effective therapy. Seminars in cancer biology *19*, 17-24.

Mayer, A.M., Glaser, K.B., Cuevas, C., Jacobs, R.S., Kem, W., Little, R.D., McIntosh, J.M., Newman, D.J., Potts, B.C., and Shuster, D.E. (2010). The odyssey of marine pharmaceuticals: a current pipeline perspective. Trends in pharmacological sciences *31*, 255-265.

McDonald, P.C., Winum, J.Y., Supuran, C.T., and Dedhar, S. (2012). Recent developments in targeting carbonic anhydrase IX for cancer therapeutics. Oncotarget *3*, 84-97.

Mehta, G., Hsiao, A.Y., Ingram, M., Luker, G.D., and Takayama, S. (2012). Opportunities and challenges for use of tumor spheroids as models to test drug delivery and efficacy. Journal of controlled release : official journal of the Controlled Release Society *164*, 192-204.

Michelakis, E.D., Sutendra, G., Dromparis, P., Webster, L., Haromy, A., Niven, E., Maguire, C., Gammer, T.-L., Mackey, J.R., Fulton, D., et al. (2010). Metabolic modulation of glioblastoma with dichloroacetate. In Science translational medicine (Department of Medicine, University of Alberta, Edmonton, Alberta, Canada. em2@ualberta.ca), p. 31ra34.

Michelakis, E.D., Webster, L., and Mackey, J.R. (2008). Dichloroacetate (DCA) as a potential metabolic-targeting therapy for cancer. British journal of cancer *99*, 989-994.

Moreno-Sanchez, R., Rodriguez-Enriquez, S., Marin-Hernandez, A., and Saavedra, E. (2007). Energy metabolism in tumor cells. The FEBS journal *274*, 1393-1418.

Mostefai, H.A., Andriantsitohaina, R., and Martinez, M.C. (2008). Plasma membrane microparticles in angiogenesis: role in ischemic diseases and in cancer. Physiological research / Academia Scientiarum Bohemoslovaca *57*, 311-320.

Myung, J.K., Cho, H.J., Park, C.K., Kim, S.K., Phi, J.H., and Park, S.H. (2012). IDH1 mutation of gliomas with long-term survival analysis. Oncology reports *28*, 1639-1644.

Nicholls, D.G., and Budd, S.L. (2000). Mitochondria and neuronal survival. Physiological reviews *80*, 315-360.

Niewisch, M.R., Kuci, Z., Wolburg, H., Sautter, M., Krampen, L., Deubzer, B., Handgretinger, R., and Bruchelt, G. (2012). Influence of dichloroacetate (DCA) on lactate production and oxygen consumption in neuroblastoma cells: is DCA a suitable drug for neuroblastoma therapy? Cellular physiology and biochemistry : international journal of experimental cellular physiology, biochemistry, and pharmacology *29*, 373-380.

Nirmalanandhan, V.S., Duren, A., Hendricks, P., Vielhauer, G., and Sittampalam, G.S. (2010). Activity of anticancer agents in a three-dimensional cell culture model. Assay and drug development technologies *8*, 581-590.

Nobili, S., Lippi, D., Witort, E., Donnini, M., Bausi, L., Mini, E., and Capaccioli, S. (2009). Natural compounds for cancer treatment and prevention. Pharmacological research : the official journal of the Italian Pharmacological Society *59*, 365-378.

O'Riordan, T.C., Fitzgerald, K., Ponomarev, G.V., Mackrill, J., Hynes, J., Taylor, C., and Papkovsky, D.B. (2007). Sensing intracellular oxygen using near-infrared phosphorescent probes and live-cell fluorescence imaging. American journal of physiology. Regulatory, integrative and comparative physiology *292*, R1613-1620.

Ohh, M. (2006). Ubiquitin pathway in VHL cancer syndrome. Neoplasia *8*, 623-629.

Oliveira, P.A., Colaco, A., Chaves, R., Guedes-Pinto, H., De-La-Cruz, P.L., and Lopes, C. (2007). Chemical carcinogenesis. Anais da Academia Brasileira de Ciencias *79*, 593-616.

Ordys, B.B., Launay, S., Deighton, R.F., McCulloch, J., and Whittle, I.R. (2010). The role of mitochondria in glioma pathophysiology. Molecular neurobiology *42*, 64-75.

Ortega-Molina, A., and Serrano, M. (2013). PTEN in cancer, metabolism, and aging. Trends in endocrinology and metabolism: TEM *24*, 184-189.

Ostrovsky, O., Bengal, E., and Aronheim, A. (2002). Induction of terminal differentiation by the c-Jun dimerization protein JDP2 in C2 myoblasts and rhabdomyosarcoma cells. The Journal of biological chemistry *277*, 40043-40054.

Owicki, J.C., and Parce, J.W. (1992). Biosensors based on the energy metabolism of living cells: the physical chemistry and cell biology of extracellular acidification. Biosensors & bioelectronics *7*, 255-272.

Pan, J.G., and Mak, T.W. (2007). Metabolic targeting as an anticancer strategy: dawn of a new era? Science's STKE : signal transduction knowledge environment *2007*, pe14.

Papandreou, I., Cairns, R.A., Fontana, L., Lim, A.L., and Denko, N.C. (2006). HIF-1 mediates adaptation to hypoxia by actively downregulating mitochondrial oxygen consumption. Cell metabolism *3*, 187-197.

Papandreou, I., Goliasova, T., and Denko, N.C. (2011). Anticancer drugs that target metabolism: Is dichloroacetate the new paradigm? International journal of cancer. Journal international du cancer *128*, 1001-1008.

Papkovsky, D.B. (2004). Methods in optical oxygen sensing: protocols and critical analyses. Methods in enzymology *381*, 715-735.

Parsons, D.W., Jones, S., Zhang, X., Lin, J.C., Leary, R.J., Angenendt, P., Mankoo, P., Carter, H., Siu, I.M., Gallia, G.L., et al. (2008). An integrated genomic analysis of human glioblastoma multiforme. Science *321*, 1807-1812.

Petros, J.A., Baumann, A.K., Ruiz-Pesini, E., Amin, M.B., Sun, C.Q., Hall, J., Lim, S., Issa, M.M., Flanders, W.D., Hosseini, S.H., et al. (2005). mtDNA mutations increase tumorigenicity in prostate cancer. Proceedings of the National Academy of Sciences of the United States of America *102*, 719-724.

Pezzella, F., Pastorino, U., Tagliabue, E., Andreola, S., Sozzi, G., Gasparini, G., Menard, S., Gatter, K.C., Harris, A.L., Fox, S., et al. (1997). Non-small-cell lung carcinoma tumor growth without morphological evidence of neo-angiogenesis. The American journal of pathology *151*, 1417-1423.

Phelps, M.E., and Barrio, J.R. (2010). Correlation of brain amyloid with "aerobic glycolysis": A question of assumptions? Proceedings of the National Academy of Sciences of the United States of America *107*, 17459-17460.

Ramirez-Peinado, S., Alcazar-Limones, F., Lagares-Tena, L., El Mjiyad, N., Caro-Maldonado, A., Tirado, O.M., and Munoz-Pinedo, C. (2011). 2-deoxyglucose induces Noxa-dependent apoptosis in alveolar rhabdomyosarcoma. Cancer research *71*, 6796-6806.

Rang, H.P. (2006). The receptor concept: pharmacology's big idea. British journal of pharmacology *147 Suppl 1*, S9-16.

Rapa, E., Hill, S.K., Morten, K.J., Potter, M., and Mitchell, C. (2012). The over-expression of cell migratory genes in alveolar rhabdomyosarcoma could contribute to metastatic spread. Clinical & experimental metastasis *29*, 419-429.

Riedl, S., Rinner, B., Asslaber, M., Schaider, H., Walzer, S., Novak, A., Lohner, K., and Zweytick, D. (2011). In search of a novel target - phosphatidylserine exposed by non-apoptotic tumor cells and metastases of malignancies with poor treatment efficacy. Biochimica et biophysica acta *1808*, 2638-2645.

Sakashita, M., Aoyama, N., Minami, R., Maekawa, S., Kuroda, K., Shirasaka, D., Ichihara, T., Kuroda, Y., Maeda, S., and Kasuga, M. (2001). Glut1 expression in T1 and T2 stage colorectal carcinomas: its relationship to clinicopathological features. European journal of cancer *37*, 204-209.

Schmalzlin, E., van Dongen, J.T., Klimant, I., Marmodee, B., Steup, M., Fisahn, J., Geigenberger, P., and Lohmannsroben, H.G. (2005). An optical multifrequency phase-modulation method using microbeads for measuring intracellular oxygen concentrations in plants. Biophysical journal *89*, 1339-1345.

Schulze, A., and Harris, A.L. (2012). How cancer metabolism is tuned for proliferation and vulnerable to disruption. Nature *491*, 364-373.

Schutte, M., Fox, B., Baradez, M.O., Devonshire, A., Minguez, J., Bokhari, M., Przyborski, S., and Marshall, D. (2011). Rat primary hepatocytes show enhanced performance and sensitivity to acetaminophen during three-dimensional culture on a polystyrene scaffold designed for routine use. Assay and drug development technologies *9*, 475-486.

Semenza, G.L. (2007). Life with oxygen. Science *318*, 62-64.

Shao, H., Chung, J., Balaj, L., Charest, A., Bigner, D.D., Carter, B.S., Hochberg, F.H., Breakefield, X.O., Weissleder, R., and Lee, H. (2012). Protein typing of circulating microvesicles allows real-time monitoring of glioblastoma therapy. Nature medicine *18*, 1835-1840.

Simak, J., Gelderman, M.P., Yu, H., Wright, V., and Baird, A.E. (2006). Circulating endothelial microparticles in acute ischemic stroke: a link to severity, lesion volume and outcome. Journal of thrombosis and haemostasis : JTH *4*, 1296-1302.

Singh, D., Banerji, A.K., Dwarakanath, B.S., Tripathi, R.P., Gupta, J.P., Mathew, T.L., Ravindranath, T., and Jain, V. (2005). Optimizing cancer radiotherapy with 2-deoxy-d-glucose dose escalation studies in patients with glioblastoma multiforme. Strahlentherapie und Onkologie : Organ der Deutschen Rontgengesellschaft ... [et al] *181*, 507-514.

Soga, T. (2013). Cancer metabolism: key players in metabolic reprogramming. Cancer science *104*, 275-281.

Stacpoole, P.W. (1989). The pharmacology of dichloroacetate. Metabolism: clinical and experimental *38*, 1124-1144.

Stacpoole, P.W., Henderson, G.N., Yan, Z., Cornett, R., and James, M.O. (1998a). Pharmacokinetics, metabolism and toxicology of dichloroacetate. Drug metabolism reviews *30*, 499-539.

Stacpoole, P.W., Henderson, G.N., Yan, Z., and James, M.O. (1998b). Clinical pharmacology and toxicology of dichloroacetate. Environmental health perspectives *106 Suppl 4*, 989-994.

Stockwin, L.H., Yu, S.X., Borgel, S., Hancock, C., Wolfe, T.L., Phillips, L.R., Hollingshead, M.G., and Newton, D.L. (2010). Sodium dichloroacetate selectively targets cells with defects in the mitochondrial ETC. In International journal of cancer. Journal international du cancer (Biological Testing Branch, Developmental Therapeutics Program, SAIC-Frederick Inc., NCI-Frederick, Frederick, MD 21702, USA.), pp. 2510-2519.

Stubbs, M., and Griffiths, J.R. (2010). The altered metabolism of tumors: HIF-1 and its role in the Warburg effect. Advances in enzyme regulation *50*, 44-55.

Sudhakar, A. (2009). History of Cancer, Ancient and Modern Treatment Methods. Journal of cancer science & therapy *1*, 1-4.

Sun, R.C., Board, P.G., and Blackburn, A.C. (2011). Targeting metabolism with arsenic trioxide and dichloroacetate in breast cancer cells. Molecular cancer *10*, 142.

Sun, R.C., Fadia, M., Dahlstrom, J.E., Parish, C.R., Board, P.G., and Blackburn, A.C. (2010). Reversal of the glycolytic phenotype by dichloroacetate inhibits metastatic breast cancer cell growth in vitro and in vivo. In Breast cancer research and treatment (Molecular Genetics Group, John Curtin School of Medical Research, Australian National University, P.O. Box 334, Canberra, 2601, Australia.), pp. 253-260.

Sutendra, G., Dromparis, P., Kinnaird, A., Stenson, T.H., Haromy, A., Parker, J.M., McMurtry, M.S., and Michelakis, E.D. (2013). Mitochondrial activation by inhibition of PDKII suppresses HIF1a signaling and angiogenesis in cancer. Oncogene *32*, 1638-1650.

Sutendra, G., and Michelakis, E.D. (2013). Pyruvate dehydrogenase kinase as a novel therapeutic target in oncology. Frontiers in oncology *3*, 38.

Szakacs, G., Paterson, J.K., Ludwig, J.A., Booth-Genthe, C., and Gottesman, M.M. (2006). Targeting multidrug resistance in cancer. Nature reviews. Drug discovery *5*, 219-234.

Tennant, D.A., Duran, R.V., and Gottlieb, E. (2010). Targeting metabolic transformation for cancer therapy. Nature reviews. Cancer *10*, 267-277.

Thery, C., Amigorena, S., Raposo, G., and Clayton, A. (2006). Isolation and characterization of exosomes from cell culture supernatants and biological fluids. Current protocols in cell biology / editorial board, Juan S. Bonifacino ... [et al.] *Chapter 3*, Unit 3 22.

Tong, J., Xie, G., He, J., Li, J., Pan, F., and Liang, H. (2011). Synergistic antitumor effect of dichloroacetate in combination with 5-fluorouracil in colorectal cancer. Journal of biomedicine & biotechnology *2011*, 740564.

Tripathi, V.K., Kumar, V., Singh, A.K., Kashyap, M.P., Jahan, S., Kumar, D., and Lohani, M. (2013). Differences in the expression and sensitivity of cultured rat brain

neuronal and glial cells toward the monocrotophos. Toxicology international *20*, 177-185.

Tulp, M., and Bohlin, L. (2004). Unconventional natural sources for future drug discovery. Drug discovery today *9*, 450-458.

Vander Heiden, M.G., Cantley, L.C., and Thompson, C.B. (2009). Understanding the Warburg effect: the metabolic requirements of cell proliferation. Science *324*, 1029-1033.

Varia, M.A., Calkins-Adams, D.P., Rinker, L.H., Kennedy, A.S., Novotny, D.B., Fowler, W.C., Jr., and Raleigh, J.A. (1998). Pimonidazole: a novel hypoxia marker for complementary study of tumor hypoxia and cell proliferation in cervical carcinoma. Gynecologic oncology *71*, 270-277.

Vaupel, P. (2004). Tumor microenvironmental physiology and its implications for radiation oncology. Seminars in radiation oncology *14*, 198-206.

Vaupel, P., Hockel, M., and Mayer, A. (2007). Detection and characterization of tumor hypoxia using pO2 histography. Antioxidants & redox signaling *9*, 1221-1235.

Vaupel, P., and Mayer, A. (2007). Hypoxia in cancer: significance and impact on clinical outcome. Cancer metastasis reviews *26*, 225-239.

Vella, S., Conti, M., Tasso, R., Cancedda, R., and Pagano, A. (2012). Dichloroacetate inhibits neuroblastoma growth by specifically acting against malignant undifferentiated cells. International journal of cancer. Journal international du cancer *130*, 1484-1493.

Vergani, L., Malena, A., Sabatelli, P., Loro, E., Cavallini, L., Magalhaes, P., Valente, L., Bragantini, F., Carrara, F., Leger, B., et al. (2007). Cultured muscle cells display defects of mitochondrial myopathy ameliorated by anti-oxidants. Brain : a journal of neurology *130*, 2715-2724.

Vermes, I., Haanen, C., Steffens-Nakken, H., and Reutelingsperger, C. (1995). A novel assay for apoptosis. Flow cytometric detection of phosphatidylserine expression on early apoptotic cells using fluorescein labelled Annexin V. Journal of immunological methods *184*, 39-51.

Vij, A.G., Kishore, K., and Dey, J. (2012). Effect of intermittent hypobaric hypoxia on efficacy & clearance of drugs. The Indian journal of medical research *135*, 211-216.

Vousden, K.H., and Ryan, K.M. (2009). p53 and metabolism. Nature reviews. Cancer *9*, 691-700.

Walenta, S., Chau, T.V., Schroeder, T., Lehr, H.A., Kunz-Schughart, L.A., Fuerst, A., and Mueller-Klieser, W. (2003). Metabolic classification of human rectal

adenocarcinomas: a novel guideline for clinical oncologists? Journal of cancer research and clinical oncology *129*, 321-326.

Wallace, D.C. (2012). Mitochondria and cancer. Nature reviews. Cancer *12*, 685-698.

Warburg, O. (1956). On respiratory impairment in cancer cells. Science *124*, 269-270.

Warburg, O., Wind, F., and Negelein, E. (1927). The Metabolism of Tumors in the Body. The Journal of general physiology *8*, 519-530.

Ward, P.S., and Thompson, C.B. (2012a). Metabolic reprogramming: a cancer hallmark even warburg did not anticipate. Cancer cell *21*, 297-308.

Ward, P.S., and Thompson, C.B. (2012b). Signaling in control of cell growth and metabolism. Cold Spring Harbor perspectives in biology *4*, a006783.

Weinhouse, S. (1967). Hepatomas. Science *158*, 542-543.

Weinhouse, S., Shatton, J.B., Criss, W.E., and Morris, H.P. (1972). Molecular forms of enzymes in cancer. Biochimie *54*, 685-693.

Wenner, C.E. (2012). Targeting mitochondria as a therapeutic target in cancer. Journal of Cellular Physiology *227*, 450-456.

Whitehouse, S., and Randle, P.J. (1973). Activation of pyruvate dehydrogenase in perfused rat heart by dichloroacetate (Short Communication). The Biochemical journal *134*, 651-653.

Winau, F., Westphal, O., and Winau, R. (2004). Paul Ehrlich--in search of the magic bullet. Microbes and infection / Institut Pasteur *6*, 786-789.

Wolf, A., Agnihotri, S., Micallef, J., Mukherjee, J., Sabha, N., Cairns, R., Hawkins, C., and Guha, A. (2011). Hexokinase 2 is a key mediator of aerobic glycolysis and promotes tumor growth in human glioblastoma multiforme. In The Journal of experimental medicine (The Arthur and Sonia Labatt Brain Tumor Research Centre, Hospital for Sick Children Research Institute, University of Toronto, Toronto, Ontario, Canada.), pp. 313-326.

Wong, J.Y., Huggins, G.S., Debidda, M., Munshi, N.C., and De Vivo, I. (2008). Dichloroacetate induces apoptosis in endometrial cancer cells. Gynecologic oncology *109*, 394-402.

Wong, N., De Melo, J., and Tang, D. (2013). PKM2, a Central Point of Regulation in Cancer Metabolism. International journal of cell biology *2013*, 242513.

Wu, M., Neilson, A., Swift, A.L., Moran, R., Tamagnine, J., Parslow, D., Armistead, S., Lemire, K., Orrell, J., Teich, J., et al. (2007). Multiparameter metabolic analysis

reveals a close link between attenuated mitochondrial bioenergetic function and enhanced glycolysis dependency in human tumor cells. American journal of physiology. Cell physiology *292*, C125-136.

Xie, J., Wang, B.-S., Yu, D.-H., Lu, Q., Ma, J., Qi, H., Fang, C., and Chen, H.-Z. (2011). Dichloroacetate shifts the metabolism from glycolysis to glucose oxidation and exhibits synergistic growth inhibition with cisplatin in HeLa cells. In International journal of oncology (Department of Pharmacology and Biostatistics, Institute of Medical Sciences, Shanghai Jiao Tong University School of Medicine, Shanghai 200025, PR China.), pp. 409-417.

Yamada, K.M., and Cukierman, E. (2007). Modeling tissue morphogenesis and cancer in 3D. Cell *130*, 601-610.

Yan, H., Parsons, D.W., Jin, G., McLendon, R., Rasheed, B.A., Yuan, W., Kos, I., Batinic-Haberle, I., Jones, S., Riggins, G.J., et al. (2009). IDH1 and IDH2 mutations in gliomas. In The New England journal of medicine (Department of Pathology, Pediatric Brain Tumor Foundation Institute, Duke University Medical Center, Durham, NC 27710, USA. yan00002@mc.duke.edu), pp. 765-773.

Zhang, J., Khvorostov, I., Hong, J.S., Oktay, Y., Vergnes, L., Nuebel, E., Wahjudi, P.N., Setoguchi, K., Wang, G., Do, A., et al. (2011). UCP2 regulates energy metabolism and differentiation potential of human pluripotent stem cells. The EMBO journal *30*, 4860-4873.

Zhao, H.W., Ali, S.S., and Haddad, G.G. (2012). Does hyperoxia selection cause adaptive alterations of mitochondrial electron transport chain activity leading to a reduction of superoxide production? Antioxidants & redox signaling *16*, 1071-1076.

Zhao, Y., Butler, E.B., and Tan, M. (2013). Targeting cellular metabolism to improve cancer therapeutics. Cell death & disease *4*, e532.

Zhdanov, A.V., Waters, A.H., Golubeva, A.V., Dmitriev, R.I., and Papkovsky, D.B. (2014). Availability of the key metabolic substrates dictates the respiratory response of cancer cells to the mitochondrial uncoupling. Biochimica et biophysica acta *1837*, 51-62.

Zu, X.L., and Guppy, M. (2004). Cancer metabolism: facts, fantasy, and fiction. Biochemical and biophysical research communications *313*, 459-465.

7.0 Appendices

7.1 Limitations of established cancer cell lines

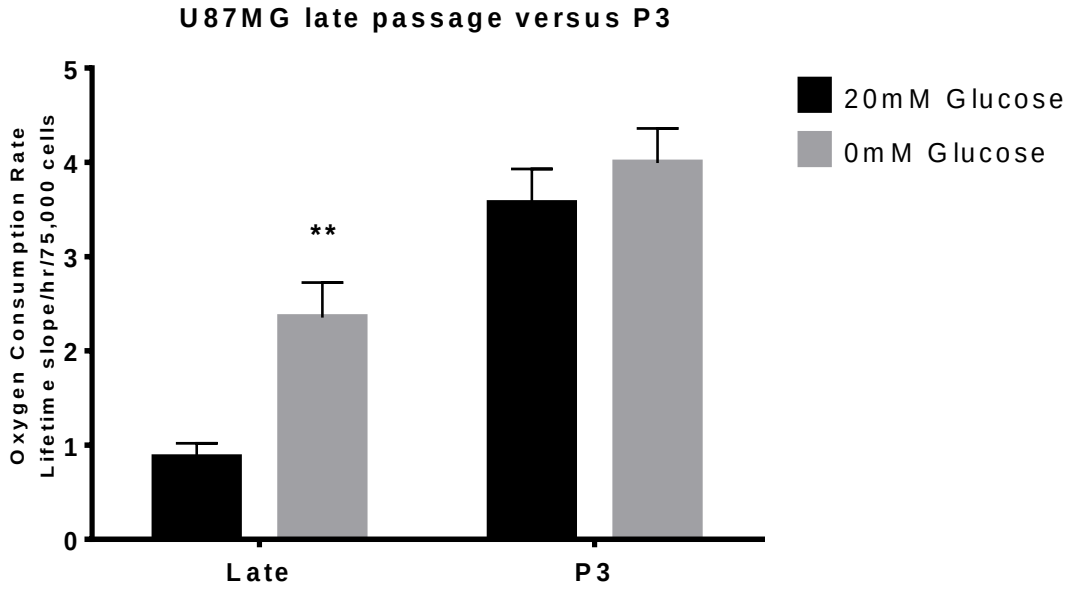

Figure 7.1: Cancer cell lines can change their metabolic profile during prolonged culture periods. Early and late passage U87MG were profiled using MitoXpress and the late passage (>p40) cells were glycolytic on high glucose while the early passage (p3) U87MG were far more oxidative.

7.2 Phenformin

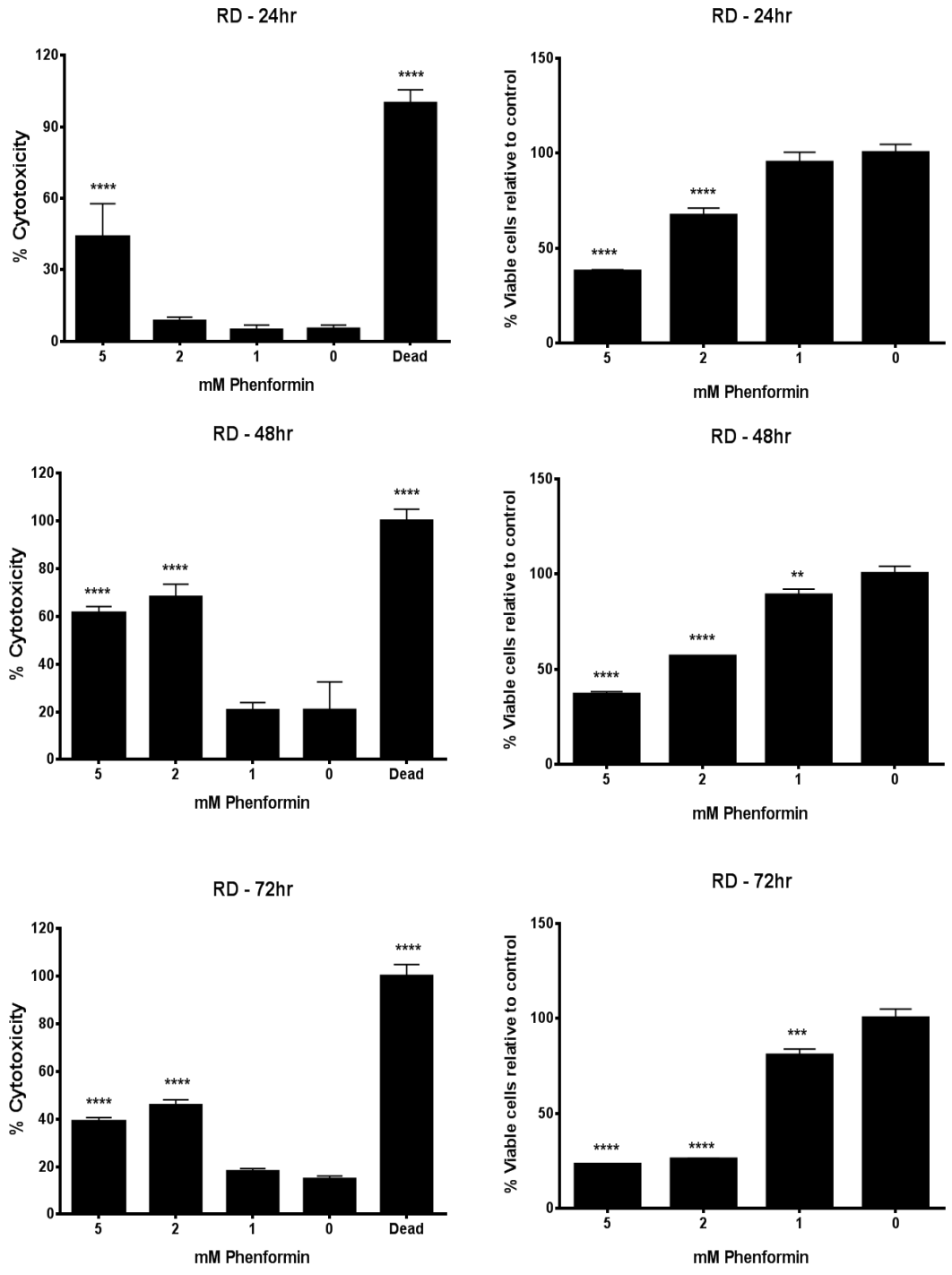

Figure 7.2: High doses of phenformin induced death and reduced cell numbers in RD cells over a 72 hour period. N = 1 and the error bars represent the standard deviation of triplicate wells.

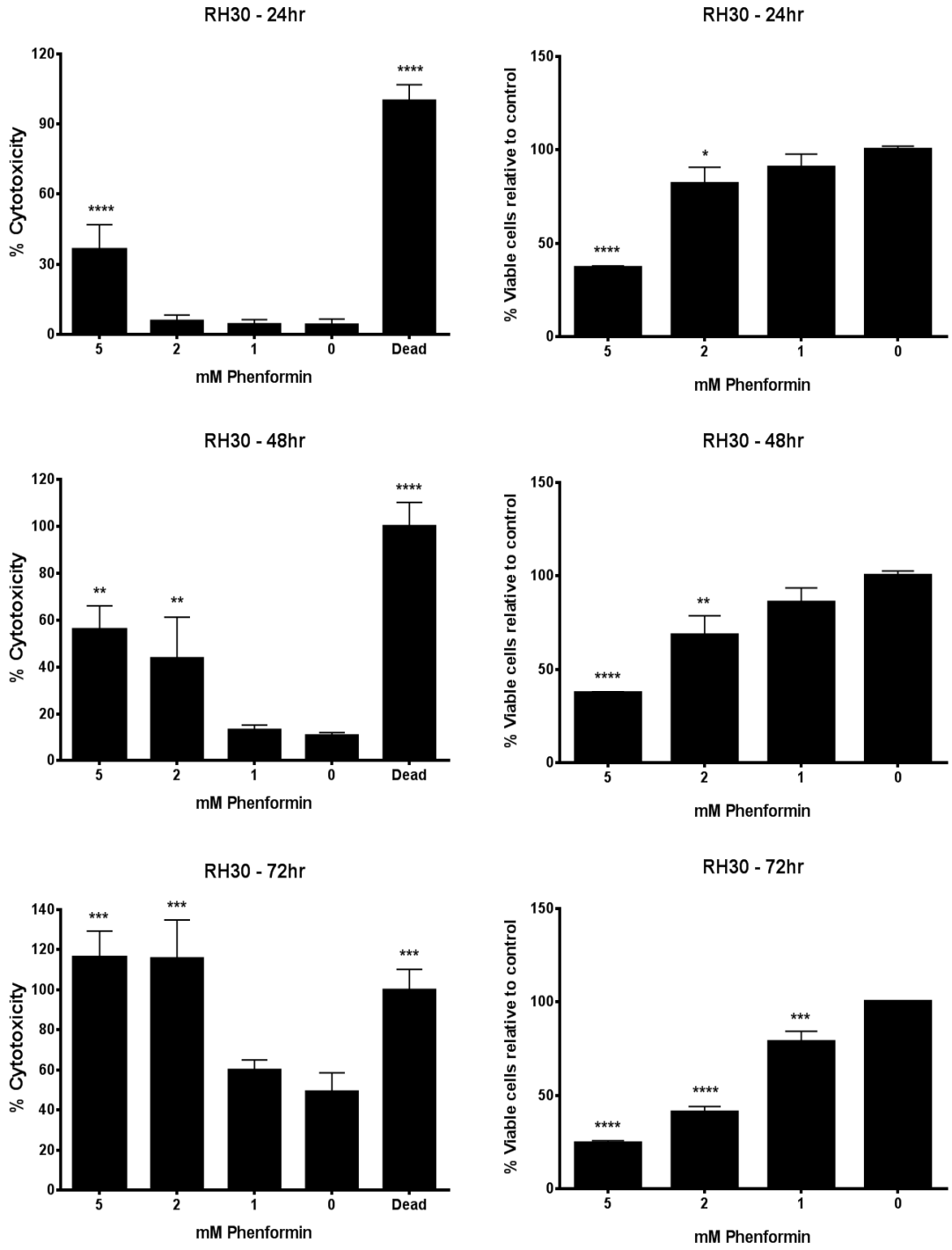

Figure 7.3: High doses of phenformin induced death and reduced cell numbers in RH30 cells over a 72 hour period. N = 1 and the error bars represent the standard deviation of triplicate wells.

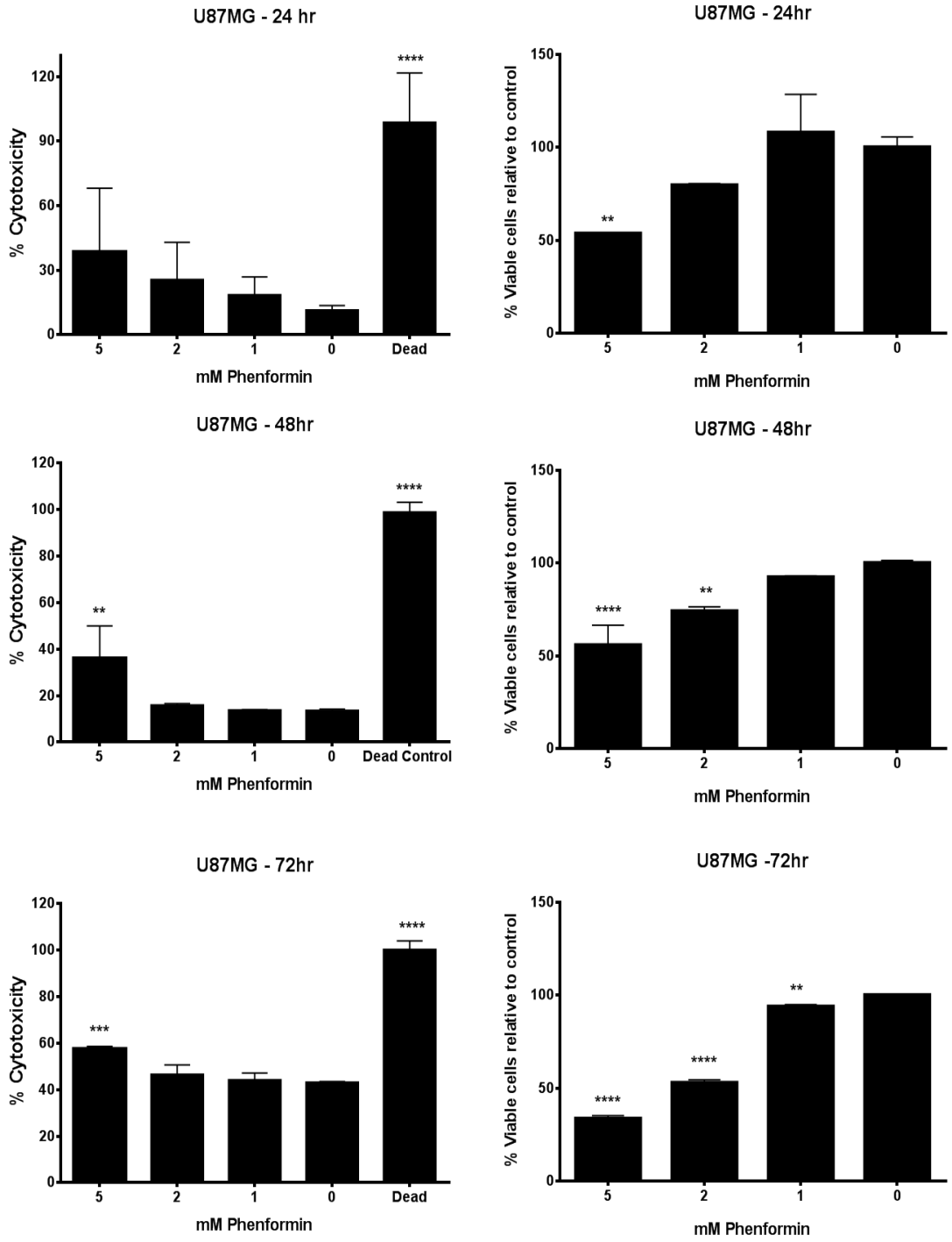

Figure 7.4: High doses of phenformin induced death and reduced cell numbers in U87MG cells over a 72 hour period. N = 1 and the error bars represent the standard deviation of triplicate wells.

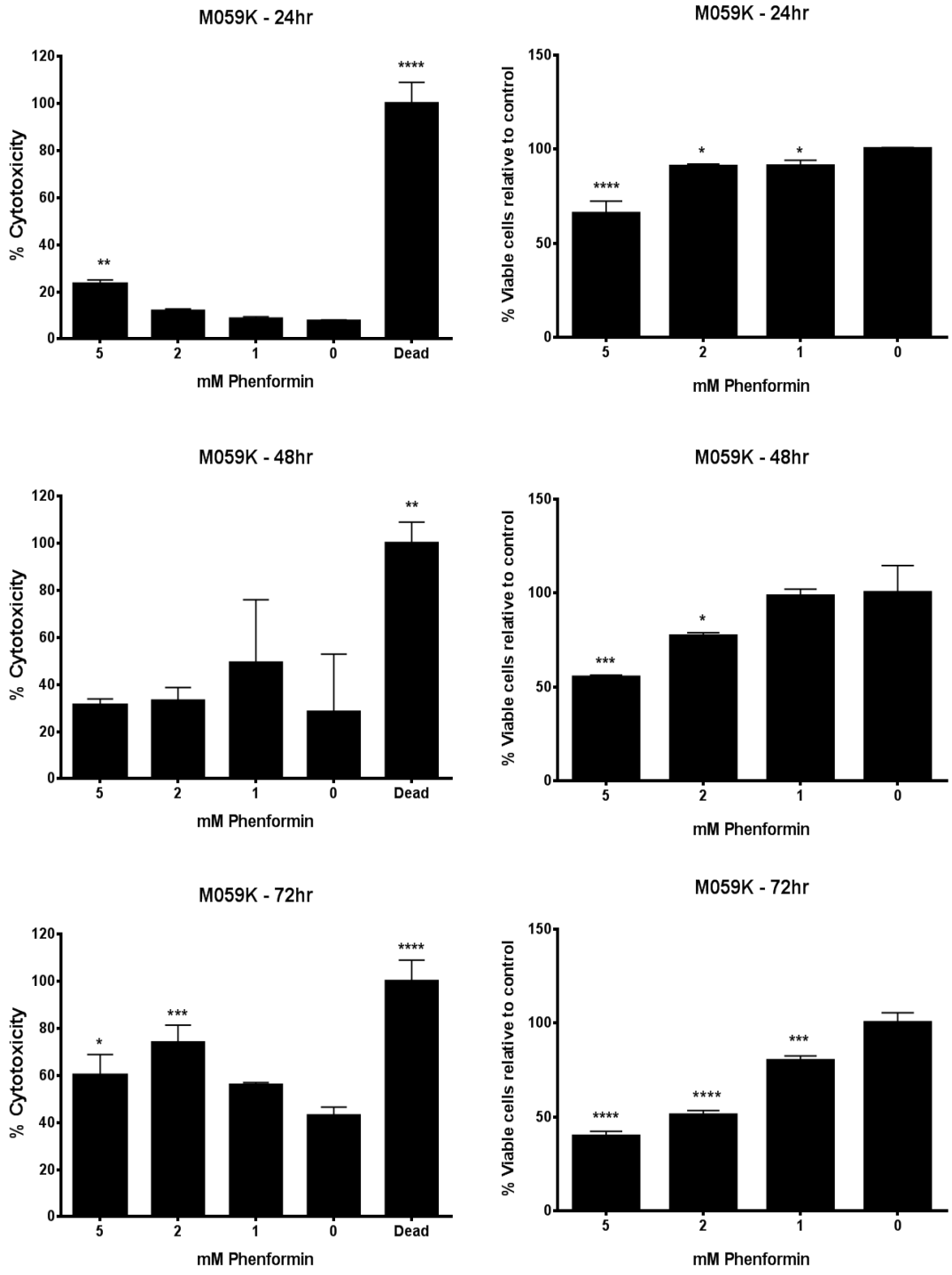

Figure 7.5: High doses of phenformin induced death and reduced cell numbers in M059K cells over a 72 hour period. N = 1 and the error bars represent the standard deviation of triplicate wells.

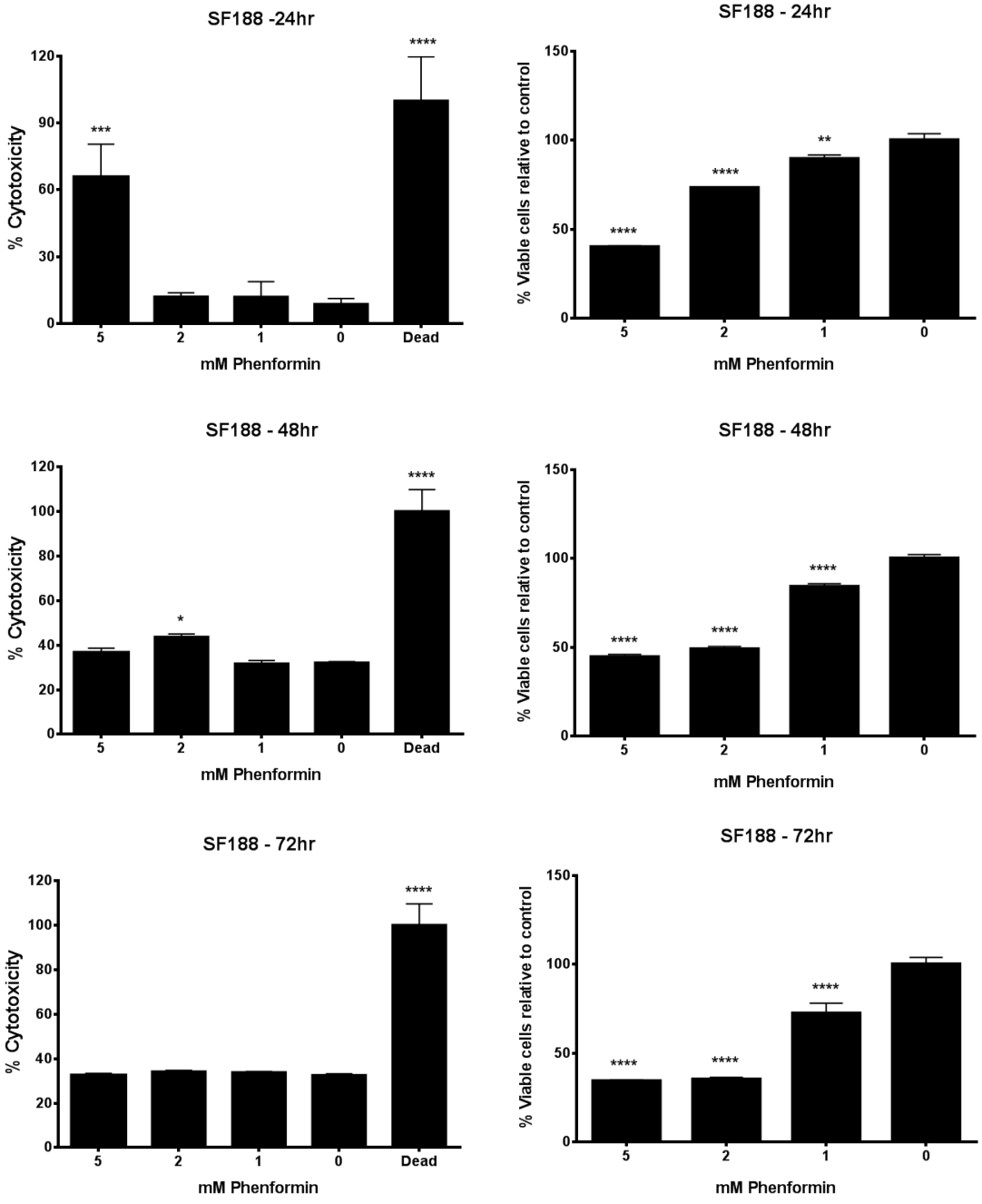

Figure 7.6: High doses of phenformin reduced the number of viable SF188 cells over a 72 hour period. N = 1 and the error bars represent the standard deviation of triplicate wells.

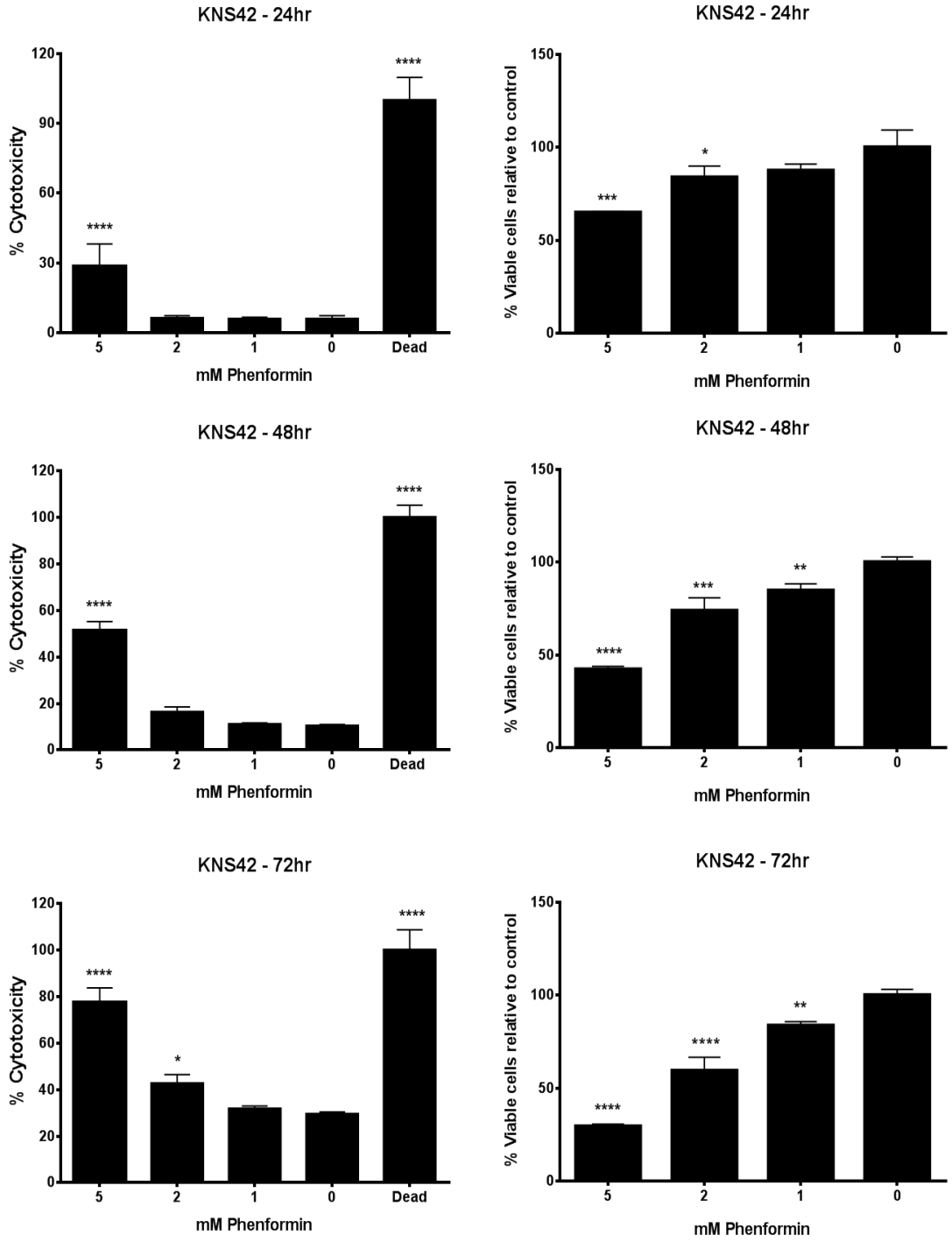

Figure 7.7: High doses of phenformin induced death and reduced cell numbers in KNS42 cells over a 72 hour period. N = 1 and the error bars represent the standard deviation of triplicate wells.

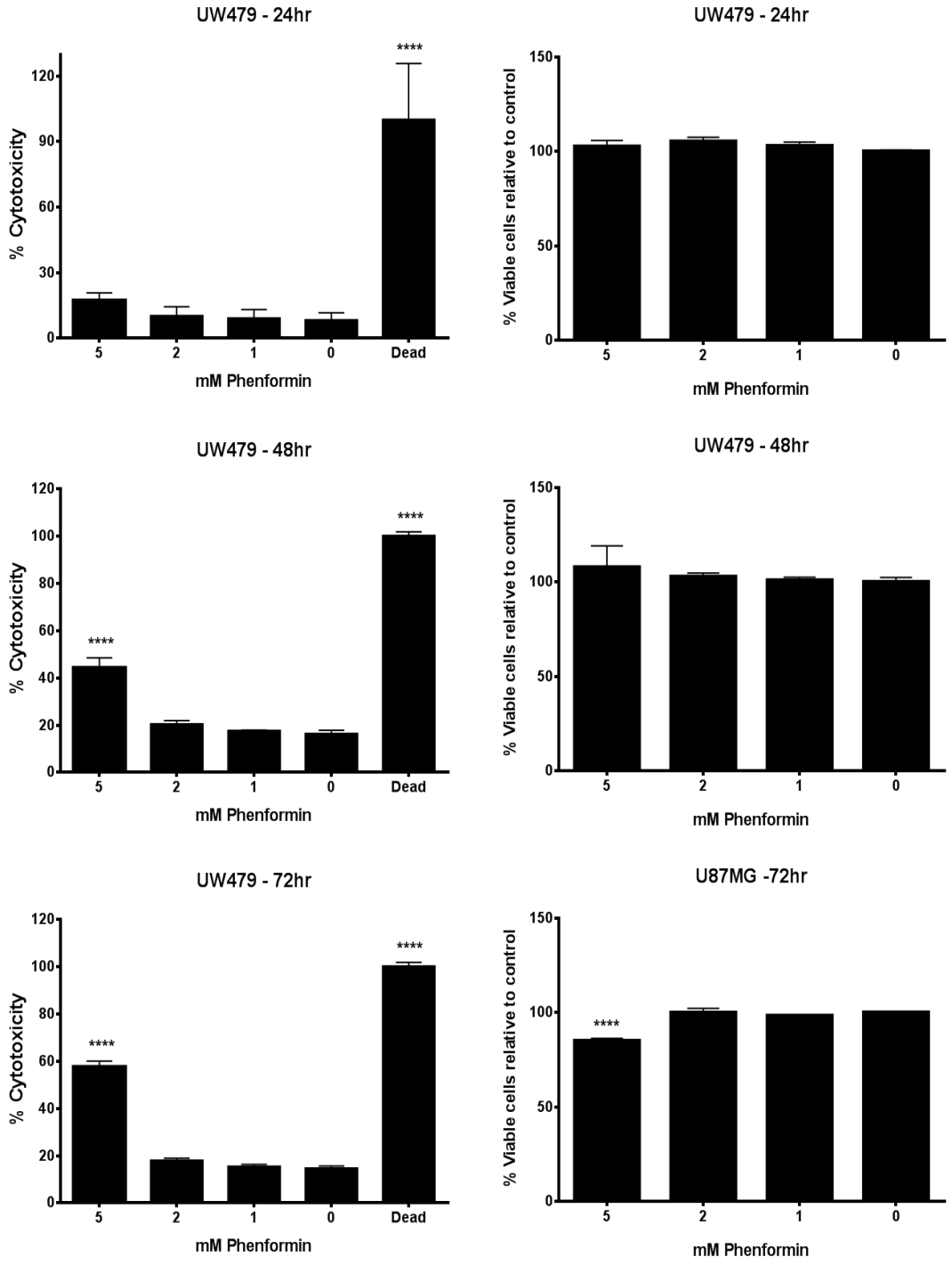

Figure 7.8: High doses of phenformin induced death but had little effect on cell numbers in UW479 cells over a 72 hour period. N = 1 and the error bars represent the standard deviation of triplicate wells.

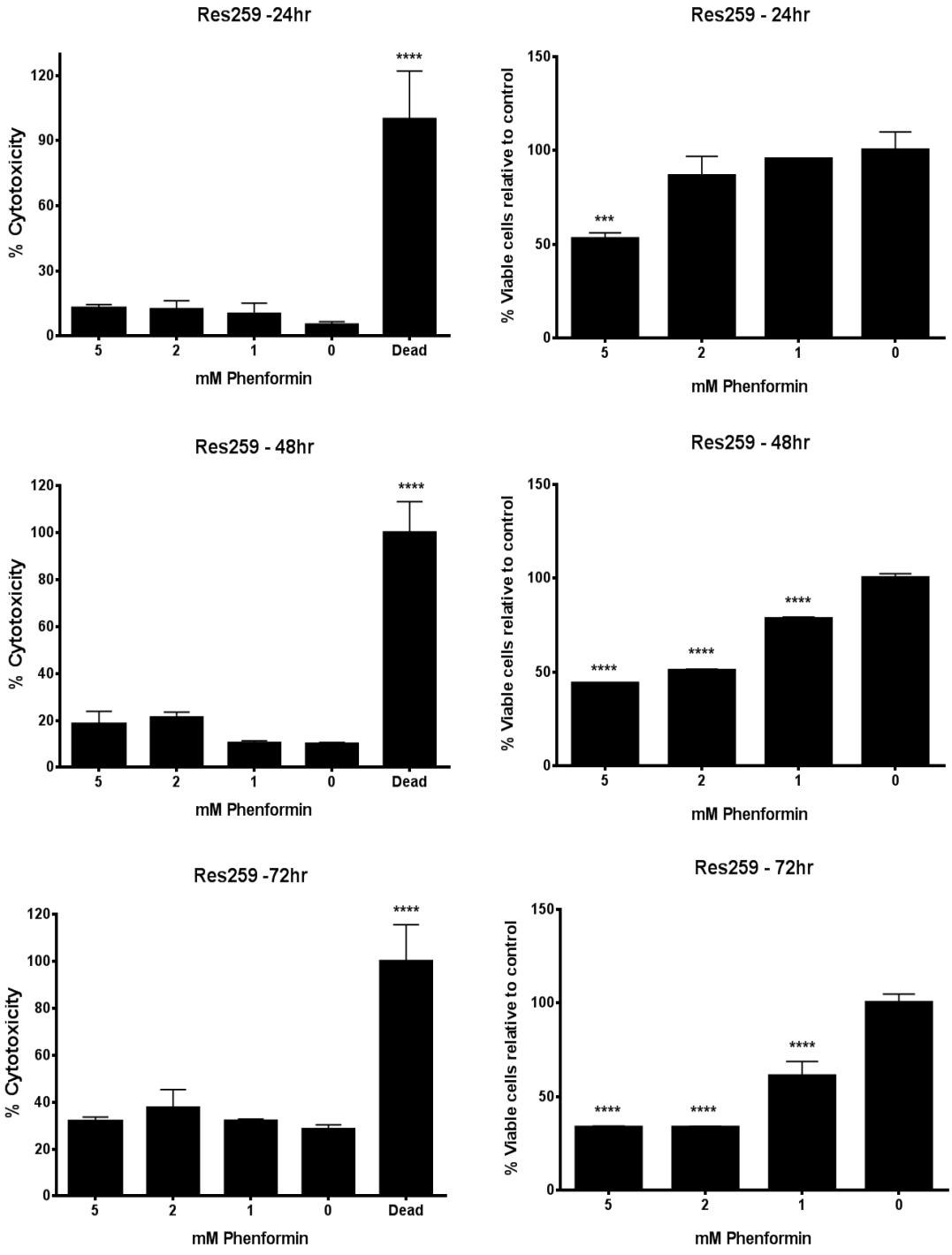

Figure 7.9: High doses of phenformin reduced cell numbers in Res259 cells without any obvious cytotoxicity over a 72 hour period. N = 1 and the error bars represent the standard deviation of triplicate wells.

7.3 Sequencing data

ABL1	CDKN2A	FBXW7	GNAS	KDR	NPM1	RET	VHL
AKT1	CSF1R	FGFR1	HNF1A	KIT	NRAS	SMAD4	
ALK	CTNNB1	FGFR2	HRAS	KRAS	PDGFRA	SMARCB1	
APC	EGFR	FGFR3	IDH1	MET	PIK3CA	SMO	
ATM	ERBB2	FLT3	IDH2	MLH1	PTEN	SRC	
BRAF	ERBB4	GNA11	JAK2	MPL	PTPN11	STK11	
CDH1	EZH2	GNAQ	JAK3	NOTCH1	RB1	TP53	

Figure 7.10: List of the tumours suppressor and oncogenes included in the test

Chr.	Position	Gene	Nucleotide Change	Amino acide Change	Var Freq	P-value	Cov.
1	115256528	NRAS	c.183A>T	p.Gln61His	62.29	14296.6	1994
17	7577539	TP53	c.742C>T	p.Arg248Trp	100.00	31855.6	1992
22	24145491	SMARCB1	c.510C>T	p.Asp170Asp	41.75	7619.91	1995

Figure 7.11: RD cells were found to contain mutations in NRAS, TP53 and SMARCB1

Chr.	Position	Gene	Nucleotide Change	Amino acide Change	Var Freq	P-value	Cov.
10	89685315	PTEN	c.209+1G>T	-	100.00	18559.6	1166

Figure 7.12: U87MG cells were found to contain a PTEN mutation.